# Measuring Salinity Changes in the Vadose Zone Using Downhole Electromagnetic Induction

**by**

**Laila M. Hall**

**Submitted in Partial Fulfillment**
**of the Requirements for the**

**Masters of Science in Hydrology**

**New Mexico Institute of Mining and Technology**
**Department of Earth and Environmental Science**

**Socorro, NM**

**May 2003**

## Abstract

To improve our ability to measure and predict quantities such as moisture content and soil water conductivity in the unsaturated, or vadose zone, an infiltration experiment was monitored with a dense array of geophysical and hydrological instrumentation. The geology of the site, as described from four continuous core samples, is fairly continuous layers of unconsolidated alluvial deposits, consisting primarily of fine sands but also containing a significant cobbly clay layer at 4-6 m depth. The infiltrometer consisted of a finely controlled irrigation system, which delivered local tap water to the surface at a flux of 2.7 cm $d^{-1}$ over a 3 m by 3 m area. After approximately 1100 days of regular infiltration events, a 6.9 g $L^{-1}$ concentration of NaCl was added to the infiltration water, increasing the irrigation water conductivity from 80 mS $m^{-1}$ to 1300 mS $m^{-1}$.

The focus of this thesis was subsurface soil electrical conductivity measurements, collected weekly during the infiltration of the salt pulse with an EM39 probe (Geonics LTD., Mississauga, ON, Canada). Data was collected in a 16 m by 16 m area surrounding the infiltrometer, in 13 boreholes reaching an average depth of 12 m. 3D images created from these measurements showed structures of salt distribution related to the stratigraphy of the field site and to the shape of the wetted area directly under the infiltrometer. To quantify how well the EM39 was capturing the extent of the salt plume, a mass balance approach was used to compare a calculated soil water salt mass to the known mass of salt infiltrated at the surface. Following models designed primarily for agricultural soils, the measured bulk soil conductivity ($EC_a$) was converted to soil water conductivity ($EC_w$) using estimates of the volumetric water content ($\theta_w$) from monthly neutron probe measurements, and the percent clay of the soil as determined by lab

analysis of the continuous core samples. The result of these calculations was a close fit ($r^2 = 0.98$) between the calculated mass of salt in the soil water and the known mass of salt infiltrated at the surface.

The low water content (<15% by volume) and low bulk soil conductivity (<100 mS $m^{-1}$) measured at the test site present more resistive conditions than previous studies of this type and were a cause for uncertainty in the calculated $EC_w$ results. Sensitivity analysis results show that due to the low measured water content at the site, the calculated $EC_w$ is strongly dependent on the chosen limit between immobile and mobile water content, or threshold water content, but determination of the value was possible through lab analysis of soils from the site. Errors in the calculated mass also arise during periods when the overall $EC_w$ is low, such as during the initial stages if the salt pulse infiltration and during a tap water flush following the end of the salt pulse. Calculations were shown to be less sensitive to soil temperature and percent clay estimates. The results of this study indicate that downhole EM39 methods show much promise for characterizing water and solute distribution in the vadose zone.

## Acknowledgements

I would like to thank Joel Bensing, Kathleen Boyer, Jim Brainard, Doug McGhee, Talon Newton, Silversun Sturgis, and Jeff Sproul for enduring the sandstorms, sunburns, and frostbite to collect data with me for this project. I would especially like to thank Jim Brainard for his friendship, support and guidance during these past 3 years. A special thank you to Melissa Stubben for the countless hours spent interpolating raw data into 3D and the patience to answer all my questions about Tecplot. I would also like to thank my advisors Dr. Robert Bowman, Jim Brainard, Dr. Jan Hendrickx, and Dr. Harold Tobin. I would like to thank Zach Barnes for lending his time to write a Lab View program to expedite the processing of the TDR data.

Funding for this research is provided through the U.S. Department of Energy (DOE) under the Environmental Management Science Program, project # 70267. Sandia National Laboratories is a multiprogram laboratory operated by Sandia Corporation, a Lockheed Martin Company, for the United States Department of Energy under contract DE-Ac04-94AL85000. I would also like to thank Doug LaBrecque and MultiPhase Technologies for partially funding the completion of this thesis.

# Table of Contents

# List of Figures

# List of Tables

## List of Notation

$EC_a$ Electrical Conductivity of Soil (or Bulk Conductivity)

$EC_{25}$ Electrical Conductivity of Soil, corrected to 25 degrees Celsius

$EC_s$ Electrical Conductivity of Soil Particles

$EC_e$ Electrical Conductivity of Soil Paste Extract (or Soil Salinity)

$EC_w$ Electrical Conductivity of Soil Water

$EC_{ws}$ Electrical Conductivity of Immobile Component of the Soil Water

$EC_{wc}$ Electrical Conductivity of Mobile Component of the Soil Water

$EC_{ss}$ Electrical Conductivity of Immobile Component of the Soil Particles

$EC_{sc}$ Electrical Conductivity of Mobile Component of the Soil Particles

$\theta_w$ Volumetric Water Content

$\theta_{ws}$ Volumetric Immobile Water Content

$\theta_{wc}$ Volumetric Mobile Water Content

$\theta_s$ Volumetric Soil Content

$\theta_t$ Threshold Volumetric Water Content (Immobile/Mobile Water Content Limit)

SP Saturation Percentage

$\rho_b$ Bulk Density of the Soil

$\rho_s$ Average Density of the Soil Particles (assumed to be 2.65 g $cm^{-3}$)

T Soil Temperature in degrees Celsius

# I. Introduction

Flow in the unsaturated, or vadose, zone between the surface and the groundwater table is usually difficult to measure or predict. Better understanding, and ultimately better predictive modeling, of flow and transport mechanisms in this zone is vital in many aspects of hydrology. Due to the close relationship between soil salinity and crop yield, quick, reliable methods of assessing soil water content and soil salinity are also especially important in agriculture. Risk assessment of surface contamination to groundwater also requires accurate predictions of flow rates and pathways through the vadose zone. The difficulty with modeling flow in the unsaturated zone is that it often follows preferential pathways through root traces, cracks, and along smooth surfaces such as rocks and man made objects like pipes. In addition, preferential flow can occur across textural boundaries. This complex distribution of soil water can make it difficult to capture flow patterns from point soil measurements, or to accurately upscale these measurements to model scale. To improve the ability to characterize flow and transport in the vadose zone using a variety of geophysical techniques, the Department of Energy (DOE) has funded a constant flux experiment. The experiment was conducted in Socorro, NM, at the New Mexico and Institute of Mining and Technology campus, and designed to monitor the movement of pulses of water at various conductivities through the deep (12 m) vadose zone.

The history of the infiltration experiment included approximately 2 years of city tap water infiltration before introduction of a low conductivity salt solution to one third of the infiltrated area, followed by a tap water flush. A second higher concentration solution was also infiltrated to one third of the infiltrated area and followed by a tap water flush.

The various geophysical techniques used to monitor this infiltration experiment included downhole electromagnetic induction (EM39), cross borehole ground penetrating radar (GPR), electrical resistivity tomography (ERT), and time domain reflectometry (TDR). GPR is one of the more common techniques used today in downhole imaging of the subsurface, and was the focus of overall data collection at this site. GPR has the potential to calculate soil water content, as well as bulk soil conductivity, by measuring the attenuation of a signal as it passes through the soil. GPR data collection is very time consuming however, and collecting data in just 5 of the 13 boreholes to 8 m depth usually took an entire day and required fairly experienced personnel. Processing of the GPR data for soil water content and salinity is equally time consuming.

The ERT data technique determines soil resistivity (inverse of conductivity) by measuring how an applied voltage decreases as it passes through a series of electrodes buried in the subsurface. The ERT showed many distinct advantages over GPR, with data collection and processing managed almost entirely by a computer program. The ERT electrodes were installed at a variety of depths and locations around the infiltrometer, providing a much more complete description of the conditions at the site than the GPR. Data collection with the ERT was also time consuming however, and required a minimum 30 hours to collect a complete data set.

Data collection with the TDR probes proved the quickest of the techniques used at the site, with measurements of soil water content and salinity collected from all 24 probes in just a few minutes. Unlike the GPR, waveform analysis for signal attenuation and data processing can be completed quickly with a simple computer program. Although the TDR probes provided very quick measurements, the poor location of the TDR probes

relative to the wetted area exemplifies the drawbacks of this technique, which can provide only point measurements. Results of the TDR are discussed in the Appendix only.

The data collected with an electromagnetic induction probe (EM39) was the focus of this thesis. Downhole EM measurements are primarily used in well logging to determine stratigraphy by measuring changes in bulk soil conductivity, and the use of this technique to measure changes in soil water conductivity is only recently emerging. Data collection and processing with the EM39 was quick and straightforward and soil conductivity measurements could be made in all 13 boreholes (up to 13 m depth) in less than 3 hours. Unlike GPR, where the transmitter and receiver are manually lowered down separate boreholes, the EM39 transmitter and receiver are contained within the same probe and can be lowered quickly down the borehole with a motorized winch.

The goal of this thesis was to monitor the infiltration of the high conductivity salt pulse, the following tap water flush, and the decline of the wetted area after infiltration ended. A second objective of this thesis was to correlate these measurements of the salt pulse to the actual mass of salt infiltrated at the surface using a mass balance approach, and a model developed by Rhoades et al. (1990) to calculate soil water conductivity ($EC_w$). Implementation of this model required estimates of the soil water content, which were based on monthly neutron probe measurements, and soil percent clay estimates, based on four continuous core sample descriptions. Due to the different measurement locations for each of these parameters, the data was first interpolated into a 3D volume and the series of calculations were then performed on each cell in the volume.

Correlation between the calculated and known mass of salt in the soil water was good ($r^2 = 0.98$) even though the very dry conditions at the site present significantly different conditions than the saturated agricultural soils the Rhoades et al. (1990) model was developed for. Sensitivity analysis results suggest that the limit of the Rhoades model at low levels of water content was site specific soil analysis to determine the limit between immobile and mobile water content and not an inability of the model to describe electrical flow in the soil in these conditions.

# II. Theory

When we measure the bulk conductivity of a soil, we are actually measuring the combined conductance of the various components contained within that soil. A model developed by Rhoades et al. (1976), Shainberg et al. (1980), and others, assumes that the main pathways for electrical current through soil are the liquid phase and the solid phase. The following equation describes this relationship, assuming that the pathways are analogous to two conductors in parallel:

$$EC_a = EC_s + T\theta_w EC_w \quad [1]$$

In this equation the bulk soil conductivity ($EC_a$) is the combined conductivity of the soil particles ($EC_s$) and the soil water ($EC_w$). The $\theta_w$ term is the volumetric water content of the soil, and T is a transmission coefficient envisioned to compensate for tortuosity. It was shown, however, that this relation between $EC_a$ and $EC_w$ becomes curvilinear at levels of $EC_w$ below about 400 mS $m^{-1}$. To compensate for this, Rhoades et al. (1989) introduced a more complete model, which recognizes a third pathway for conductance, which is a very thin film of water that adheres to the soil particles at low water contents. Rhoades et al. (1989) defined the three pathways for conductance as: 1) the alternating layers of soil particles and interstitial soil solution (a solid-liquid coupled element), 2) the surfaces of soil particles in contact with each other (a solid element), and 3) the soil pore water (a liquid element). All were assumed to act in parallel. A schematic diagram representing the model is shown in Figure 1.

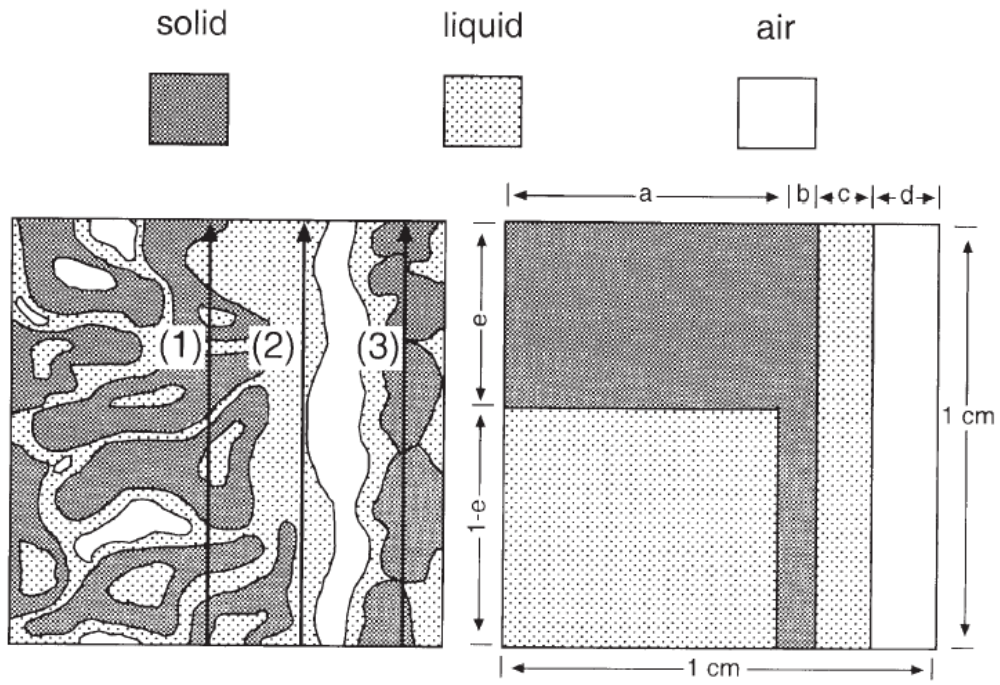


**Figure 1: Schematic diagram showing the three conceptual pathways for conductance through the soil (Rhoades et al., 1989)**

Rhoades et al (1989) then created a simplified soil model diagram, Figure 1, which is the basis for the following derivation. The parameters of the soil model a, b, and c are the representative cross sectional areas of each of the three main elements; d is the fractional cross sectional area of the void space (conductivity of air is assumed to be zero); e is the length parameter of the solid particles; and (1-e) is the soil water coupled with the soil particles. Using this model, the bulk soil electrical conductivity is described as:

$$EC_a = \frac{(a)EC_{ws}EC_{ss}}{(e)EC_{ws} + (1-e)EC_{ss}} + (b)EC_{sc} + (c)EC_{wc} \qquad [2]$$

where $EC_{ws}$ and $EC_{wc}$ are the specific electrical conductivities of the soil water that is in series-coupling with the solid particles and in the separate continuous conductance phase, respectively, and $EC_{ss}$ and $EC_{sc}$ are analogous terms for the electrical conductivity of the solid phase in these two elements respectively. Hereafter $EC_{ss}$ and $EC_{sc}$ are assumed equal since soil particle conductivity is not expected to vary dependent on contact with interstitial water or with another soil particle. From Figure 1 it can be seen that ae + b = $\theta_s$, b = $\theta_{sc}$, ae = $\theta_{ss}$, a(1-e) +c = $\theta_w$, a(1-e) = $\theta_{ws}$, and c = $\theta_{wc}$. Substitution of these identities into Eq. [2] leads to Eq. [3] below, assuming that direct particle-to-particle contact in most soil structures does not provide a continuous pathway for current:

$$EC_a = \left[ \frac{(\theta_s + \theta_{ws})^2 EC_{ws} EC_s}{\theta_s EC_{ws} + \theta_{ws} EC_s} \right] + (\theta_w - \theta_{ws}) EC_{wc} . \qquad [3]$$

In this model, the total water content of the soil is separated into mobile ($\theta_{wc}$) and immobile ($\theta_{ws}$) components as described by Eq. [4] below. Rhoades et at (1988, 1990) determined by soil saturation experiments and sensitivity analysis that the other parameters in Eq. [3] are described as:

$$\theta_{ws} = 0.639(\theta_w) + 0.011 \qquad [4]$$

$$EC_s = 0.023(\%Clay) - 0.021 \qquad [5]$$

$$\theta_s = \rho_b/\rho_s, \text{ where } \rho_s \text{ is assumed to be } 2.65 \text{ g/cm}^3 \qquad [6]$$

$$\rho_b = 1.73 - 0.0067(SP) \qquad [7]$$

$$SP = 0.76(\%Clay) + 27.25 \qquad [8]$$

The notation in Eqs. 4- 8 is defined as: SP is saturation percentage, $\rho_b$ is bulk density, $\theta_s$ is volumetric content of soil, and $EC_s$ is the electrical conductivity of the soil particles. The results of that Rhoades et al (1989) analysis show that that the exact relationship

between $EC_a$ and $EC_w$ is dependent on soil structure and clay content, and it was suggested by that similar saturation extract experiments would be useful when applying this equation to a specific site.

The electrical conductivity of the soil water, $EC_{w,}$ is obtained from the solution of Eq. [3], assuming $EC_{ws} = EC_{wc}$ (hence $EC_w\theta_w = EC_{ws}\theta_{ws} + EC_{wc}\theta_{wc}$). This is a source of error in the model, because $EC_{ws}$ and $EC_{wc}$ cannot always be assumed equal, since water in the continuous phase, or "mobile" water does not have to have the same composition as "immobile" water trapped in the fine pores, unless under conditions where diffusion equilibrium has had time to occur (Rhoades, 1989). This may be an especially poor assumption in conditions where a solution is being irrigated to the soil, such as at our site. $EC_w$ is defined in Eqs. [9-12]:

$$EC_w = \frac{-B \pm \sqrt{B^2 - 4AC}}{2A} \quad [9]$$

$$A = -\left[\theta_s(\theta_w - \theta_{ws})\right] \quad [10]$$

$$B = \left[\theta_s EC_a - EC_s(\theta_s + \theta_{ws})^2 - (\theta_w - \theta_{ws})(\theta_{ws} EC_s)\right] \quad [11]$$

$$C = \theta_{ws} EC_s EC_a \quad [12]$$

The focus of the model and sensitivity analysis by Rhoades et al (1989) was to relate the measured $EC_a$ of agricultural soils to the conductivity of a solution extracted from a saturated soil paste, $EC_e$:

$$EC_e = EC_w\left(\frac{\theta_w}{\rho_b}\frac{100}{SP}\right). \quad [13]$$

Rhoades et al. (1989) showed that Eq. [13] worked well to determine $EC_w$ and $EC_e$ when the soil was near "field capacity," but the relation between $EC_a$ and $EC_w$ was

found to be nonlinear at levels of $EC_w$ below 400 mS $m^{-1}$ (the first term in Eq. [3] is dominant at low levels of $EC_w$). It is important to note that Eq. [9] is a calculation of the only the mobile soil water conductivity ($EC_{wc}$), and as mentioned above, the immobile water ($EC_{ws}$) is then assumed to have the same conductivity. If the soil water content is considered to be entirely immobile water (i.e., $\theta_w = \theta_{ws}$), Eq, [10] becomes zero and Eq. [9] can not be solved. This critical value needed in the calculation of $EC_w$ is the threshold water content limit $\theta_t$, or limit between mobile and immobile water contents, below which measurements of $EC_a$ cannot be made (Rhoades et al. 1976). The solution of Eq. [4] shows that the minimum mobile water content that can be calculated (i.e. $\theta_w = \theta_{ws} = \theta_t$) is 3.5% volumetrically, Rhoades (1990) however, suggests a minimum of 10% to perform the calculation of $EC_w$. The actual threshold water content limit is dependent on soil structure, and in the same 1976 study, it was found to vary from 5% in a sandy soil to 12% in a clay rich soil. Calculations were made in this report using a range between 4% and 10% as threshold water content limits. The choice of threshold water content strongly influences the $EC_w$ calculation since the major part of the electrical current flow at normal levels of $\theta_w$ is primarily via $\theta_{wc}$, which means that $EC_a$ is primarily a measurement of "mobile salt" content of the soil. Lab analysis (saturation/drainage experiments) by Baker (2001) shows that estimates between 3 and 12% $\theta_t$ are appropriate for our site, with many samples having an average $\theta_t$ close to 6%.

Although the conductivity of the soil water often has the strongest influence on the soil bulk conductivity, the clay content of the soil also has an effect. Due to the high cation exchange capacity of clay minerals, the electrical conductivity of a soil solution from a sandy or silty soil can be greatly increased with a small addition of clay particles.

Rhoades et al. (1990) shows that very precise experiments must be carried out to obtain accurate values of $EC_s$, but that reasonable estimates of clay content are sufficient for most soils.

Since temperature plays a large role in the conductivity of a material, it is necessary to standardize field measured $EC_a$ values to an equivalent electrical conductivity at a reference temperature of 25°C. Sheets and Hendrickx (1995) fit a curve to a conversion table given by the U.S. Department of Agriculture (1954) to give the following temperature standardization equation:

$$EC_{25} = EC_a * \left[ 0.4470 + 1.4034 e^{-\left(T/26.815\right)} \right] \qquad [14]$$

where $EC_{25}$ is the standardized $EC_a$ and T is the soil temperature in degrees Celsius.

In this thesis, downhole EM39 measurements were converted to temperature corrected soil water conductivity measurements using this series of equations by Rhodes et al (1989, 1990), and Sheets and Hendrickx (1995). The calculation of $EC_w$ requires estimates of soil water content, clay content, and temperature at each location the equation is applied. Integration of these different parameters is more straightforward when all the measurements are taken at the surface, however, since the EM39 is a downhole measurement technique, data varies not only with location at the surface, but with depth. Since the different parameters represent data collected at different locations, the EM39, neutron probe, thermocouple, and continuous core (percent clay) data were first interpolated, using identical kriging options, into a three dimensional grid. $EC_w$ was then calculated for each of the cells in the grid.

To verify the calculated values of $EC_w$ a comparison could be made with the EC of the infiltration water and possibly with the EC of soil solutions measured with other

techniques at the test site, such as the suction lysimeters. Since the infiltration water conductivity may vary with location (as will be discussed later), but the actual mass of salt infiltrated is known, a mass balance approach is a more useful than a direct comparison of $EC_w$ in our situation.

The mass of salt in the soil water is calculated by converting $EC_w$ in mS $m^{-1}$ to concentration of NaCl in g $L^{-1}$ for each cell in the 3D volume. Due to the nonlinear nature of this relationship, especially at low values of $EC_w$, the most accurate way to convert from conductivity to salt concentration is to refer to a graph, such as in the United States Salinity Laboratory Agricultural Handbook (1954). Fortunately, most of the calculated soil water conductivities fall on the linear portions of that trend, where the slope is approximately 5.5 mg $L^{-1}$/ mS $m^{-1}$. The volume of water in each cell is then calculated using the interpolated volumetric water content of each cell and the cell dimensions. The calculated concentration and volume of water for each cell are then multiplied to arrive at a mass of NaCl for each cell. The total mass calculated in the 3D volume was then compared to the know mass infiltrated.

# III. Research Site

This study was conducted at the Sandia-Tech Vadose Zone Test Site (STVZ), which is located at the New Mexico Institute of Mining and Technology campus in Socorro, New Mexico. The geology of the site was characterized by Brainard (2003), Paprocki (2000), and Baker (2001), and consists of discontinuous layers of unconsolidated, unsaturated ancestral Rio Grande deposits ranging in particle size from clay to large cobbles, but is predominantly fine sand. This test site was chosen for many reasons, including its similarity to other DOE vadose remediation sites, the large distance to groundwater, and the growing interest in better characterization of Rio Grande deposits. During site preparation, the top half meter of soil were removed to level the study site and to remove plants, minimizing the affect of plant transpiration through the root zone. A plastic tarp was then buried across the site under approximately 6" of soil to further minimize the affects of precipitation and evaporation.

## Geology

The following descriptions of the continuous core collection, access borehole installation, and the geologic interpretation of those samples are based mainly on the upublished work of Brainard et al (2002), less detailed summaries are found in Baker (2001) and Paprocki (2000). Rodgers and Company (Albuquerque, NM) was contracted to auger boreholes while collecting continuous core samples from the subsurface. A CME 75 high torque drill rig was used to auger the holes. Eight sections of 6 ¼" ID by 5 ft long split spoon samplers were inserted into a hollow stem wire line auger with a 10 ½"

bit to collect core samples from four boreholes located within the instrumentation pad. The descriptions of these core samples are found in Appendix 4.

The field site deposits are mapped as part of the Sierra Ladrones Formation, Upper Santa Fe Group consisting of fine to coarse grained, poorly consolidated, ancestral Rio Grande axial-river deposits with intermittent layers of debris flow sediments and sedimentary layers of eolian sands. The axial-river deposits range from approximately 300-800 meters in thickness between the Socorro Basin and the Socorro Mountain block. Hydraulic mapping of the basin indicates that the water table within the vicinity of the infiltration site is located from 20-30 meters below the ground surface (Anderholm, 1983).

The geology of the test site was generalized by alternating, layers of sand, silt, gravel and clay. The main stratigraphic units identified in each of the four continuous core samples are shown in Figure 4. The upper 2 meters consists of coarse sand and gravel and is followed by 1.5 meters of fine sand. A poorly sorted silt, sand and clay nodule layer varies in thickness across the site but is generally found between 3.5 to 5 meters depth, Unit 7. Discontinuous layers of fine sand and clay-matrix supported conglomerate are found between 5 and 6 meters. A thick layer of fine sand occurs from 6 to 13 meters depth, Unit 8, and is shown in Figure 2.

**Figure 2: Fine to medium grained sands and gravels exposed in nearby sand pit. (Baker, 2001).**

**Figure 3: Close up of a small gravel layer in Figure 2, lens cap shows scale of images. (Baker, 2001)**

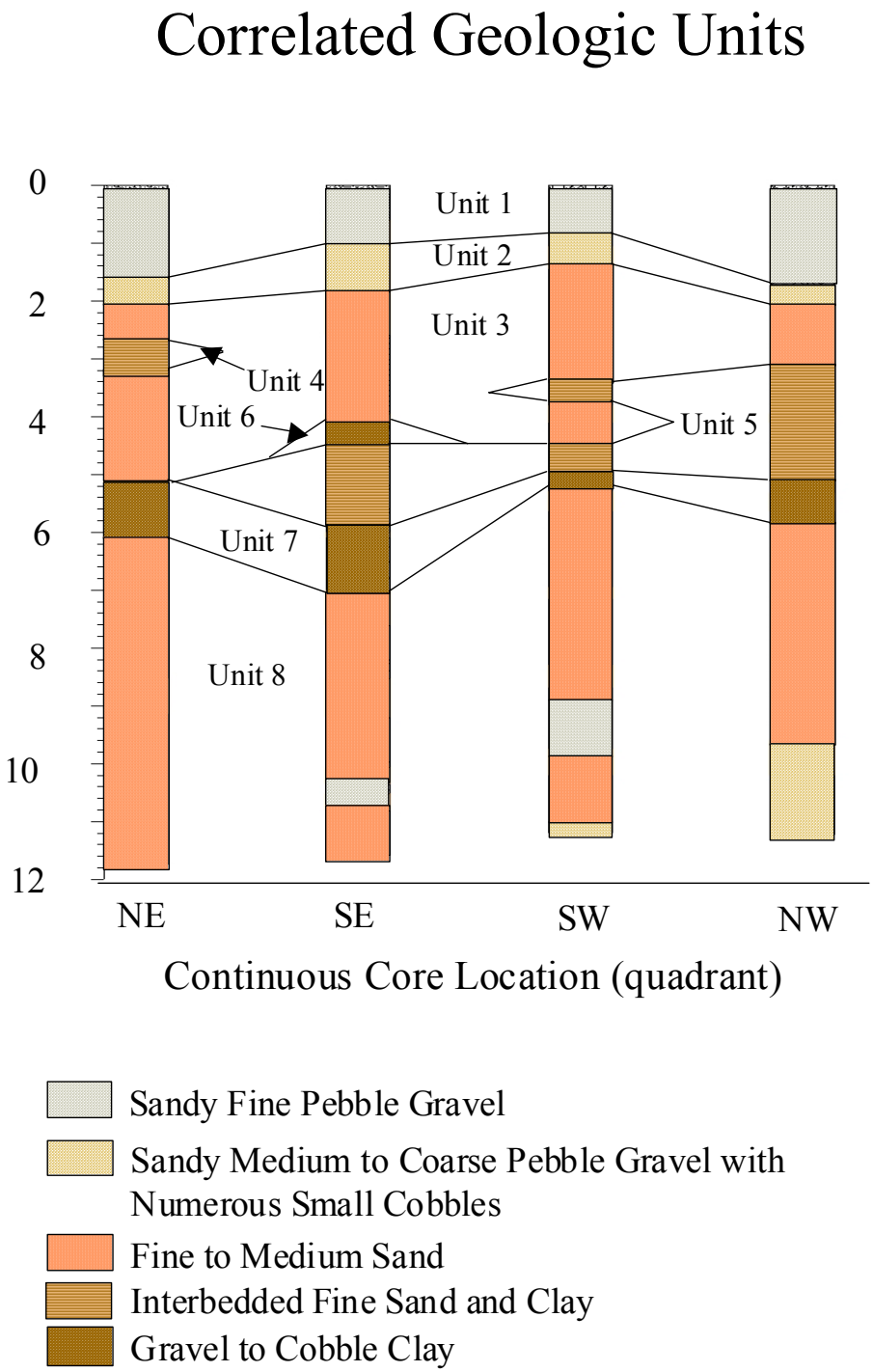


**Figure 4: Correlated geologic stratigraphic columns of the subsurface sedimentary deposits below the STVZ infiltration pad. (Brainard et al. 2002, Baker 2001, Paprocki 2000)**

**Table 1: Percent silt and clay estimates from NW core sample analysis.**

| Sample ID | Depth (m bags) | Description | % Silt and Clay |
|---|---|---|---|
| NW1 | 0.30 | coarse sand | 0.70 |
| NW2 | 0.61 | coarse sand | 1.00 |
| NW4 | 1.52 | coarse sand | 0.40 |
| NW5 | 1.81 | gravel | 3.20 |
| NW6 * | 2.72 | silty sand | 10.00 |
| NW7 | 3.05 | fine sand | 1.50 |
| NW8 | 3.35 | fine sand | 1.90 |
| NW9 | 3.66 | fine sand | 2.70 |
| NW10 | 4.27 | fine sand | 3.10 |
| NW11 | 4.57 | silty sand | 3.40 |
| NW12 | 4.88 | silty sand | 2.10 |
| NW13 * | 5.18 | sandy clay | 10.00 |
| NW14 * | 5.79 | pebbly clay | 10.00 |
| NW15 * | 6.10 | clay | 30.00 |
| NW16 | 6.40 | fine sand | 2.00 |
| NW17 | 6.71 | fine sand | 1.70 |
| NW18 | 7.32 | fine sand | 1.10 |
| NW19 | 7.62 | fine sand | 9.10 |
| NW20 | 7.92 | fine sand | 0.80 |
| NW21 | 8.23 | fine sand | 1.00 |
| NW22 | 8.84 | silty sand | 2.20 |
| NW23 | 9.14 | fine-coarse sand | 2.30 |
| NW24 | 9.75 | fine-coarse sand | 2.80 |
| NW25 | 10.36 | fine-coarse sand | 2.00 |
| NW27 | 10.97 | fine-coarse sand | 0.40 |
| * denotes estimate from hydrometer data | | | |

Table 1 is a summary of particle size analysis from a combination of sieve method analysis by Baker 2001, and hydrometer analysis presented in Appendix 4 of samples from the North West continuous core sample..

**Instrumentation**

The following description of the installation of the 13 boreholes and other instrumentation is a compilation of descriptions by Brainard (2002), Baker (2001), and Paprocki (2000). All instrumentation at the site was installed within a 15 by 15 square meter area in an axisymmetric pattern around a 3 m by 3 m infiltrometer located at the center of the site. Figures 5 and 6 are photographs (taken by Jim Brainard) of the site showing the infiltrometer and instrumentation. The actual infiltrometer was covered with multiple layers of waterproof white plastic sheeting to minimize evaporation and precipitation effects.

**Figure 5: View of the test site looking west. Infiltrometer, covered with white plastic sheeting, pictured in the center. Data loggers and supply tanks are housed in the small building to the north (Brainard et al. 2002, Baker 2001, Paprocki 2000).**

Thirteen PVC cased access tubes were installed around the infiltrometer to a depth of 12 to 13 meters. One borehole was placed in the center of the infiltrometer, with the four closest boreholes placed approximately 3 m away, see Figure 7. These access tubes were used to take neutron probe (water content) measurements, electromagnetic conductivity (EM39) data, and cross borehole ground penetrating radar (XBGPR) data. A network of 32 surface electrodes and nine vertical electrical resistivity tomography (ERT) strings were installed to a depth of 12 to 13 meters, with a 0.75 meter spacing between electrodes, to measure soil resistivity. A total of eighty tensiometers were installed to measure changes in soil water pressure. Suction lysimeters and time domain reflectometry (TDR) probes were nested with the tensiometers at 24 locations across the site (at 3.5, 6, and 8 m depth). Sixty thermocouples were also installed both above and below ground to monitor temperature changes.

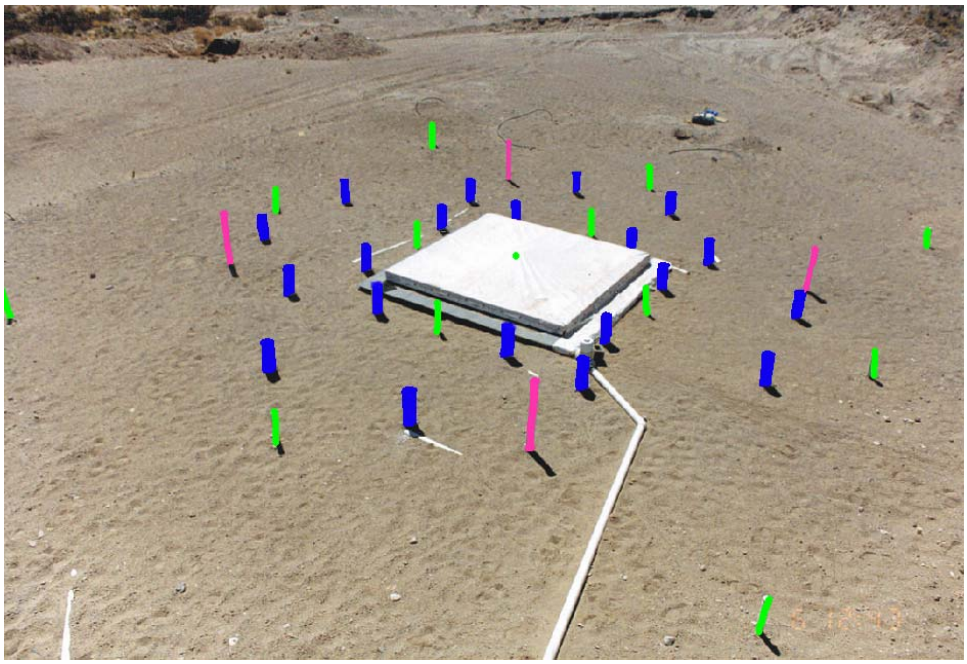

**Figure 6: View of the test site looking south. The access boreholes are colored green (center borehole hidden by infiltrometer cover), TDR/Suction Lysimeter/Thermocouple locations are colored blue, continuous core sample locations are pink.**

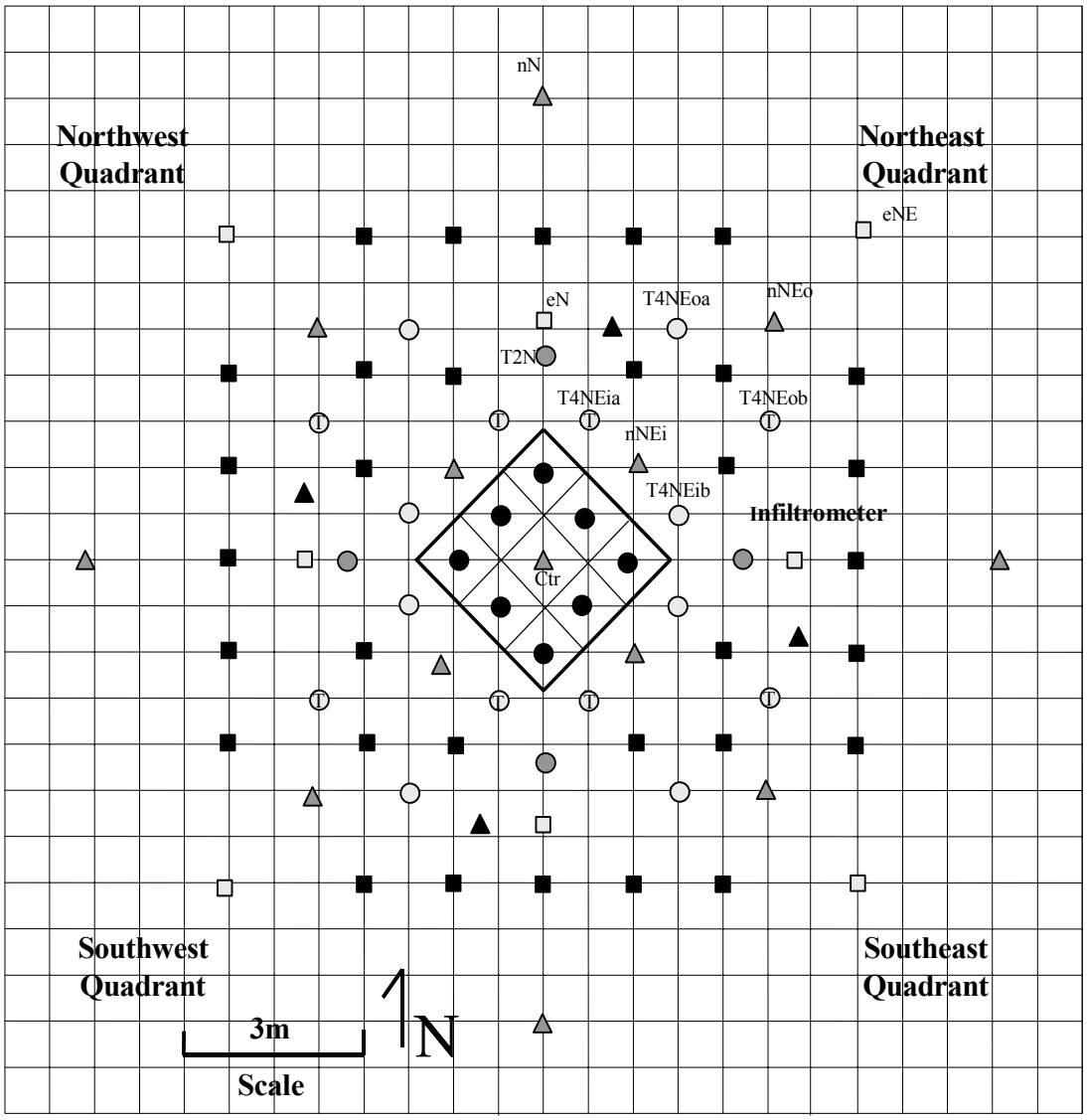


The nomenclature for identifying instrument and access tube locations is given for the NE array. Location identifiers for the other arrays are obtained by rotating the NE quadrant array 90 degrees about the center access tube and changing the quadrant abbreviation to specify the new quadrant.

○ Four-Nested Tensiometer Locations (T4 ID prefix). The tensiometer porous cups are approximately 2, 4, 6, and 8 meters below the ground surface/datum. A TDR probe is installed at the bottom of each hole with a suction lysimeter immediately above. The TDR probe/suction lysimeter pair is located just below deepest tensiometer porous cup. Ⓣ T4 nests where thermocouples are installed within 10 cm of each tensiometer porous cup.

● Two-Nested Tensiometer Locations (T2 prefix). Each hole has two instrument clusters consisting of a tensiometer, a suction lysimeter, and a TDR probe (listed from top to bottom). The clusters are approximately 3.5 and 6 meters below the ground surface/datum.

● Infiltrometer Tensiometers. The tensiometer porous cups are installed approximately 0.5 and 1 meter below the surface

△ PVC Cased Wells (n prefix). Used for collecting neutron, GPR data, electrical conductivity and gamma data.

□ ERT electrode string (e Prefix) ■ ERT surface electrode ▲ Continuous Core Sample Locations

**Figure 7: Plan view of instrumentation layout, drawn to scale (Brainard et al., 2002).**

The New Mexico Bureau of Mines and Mineral Resources drilled the 13 access boreholes using 4“ and 6“ drill bits. The 6” auger was only used for the upper 3 m to penetrate the gravel layer. The drill rig that was used had difficulty drilling through a gravel layer at approximately 1.5 m depth. The borehole deviated from vertical as boulders deflected the bit. Two-inch PVC tubes were installed in the boreholes and the annulus was backfilled with sifted sand. The upper 3 meters of the annulus was backfilled with gravels to imitate the surrounding stratigraphy. The top 1 m of the center borehole annulus was backfilled with a 20% bentonite mix to minimize preferential flow along the sides of the access tube.

The infiltrometer system was designed to deliver a constant flux of water to the soil surface, with 5 minute irrigation events occurring every 12 hours at a flow rate of approximately 2.6 L $min^{-1}$, or a flux of 2.7 cm $day^{-1}$. The irrigation system inside the 3 m by 3 m infiltrometer was divided into 9 arrays, each 1 m square in area and controlled with a separate flowmeter. An even distribution of water was achieved in each array by forcing the water through 100 syringe needles suspended 4-6” above the soil surface. The infiltrometer was insulated with thick Styrofoam sheets and two layers of waterproof plastic to minimize the effects of evaporation and precipitation. Infiltration events were timer controlled and information such as flow rates and tank levels were monitored with a series of data loggers to ensure a constant flux rate was achieved, see Brainard et al. (2002) for more details on the water supply system and instrumentation specifics.

The irrigation water was supplied by two 720-L tanks housed in the small building visible in Figure 5. The tanks were filled biweekly with city tap water, which had an approximate conductivity of 80 mS $m^{-1}$. A third supply tank was later added to

hold the salt (NaCl) solution. To ensure that the solution in the salt water tank was well mixed, it is circulated with a submersible pump for 5 minutes before each infiltration event. For each of the two salt pulse events (see timeline of events), the salt water was only supplied to three of the nine arrays, which are depicted in red in Figures 8 and 9. The blue lines indicate the two transects with the most closely spaced boreholes (approximately 3 m apart).

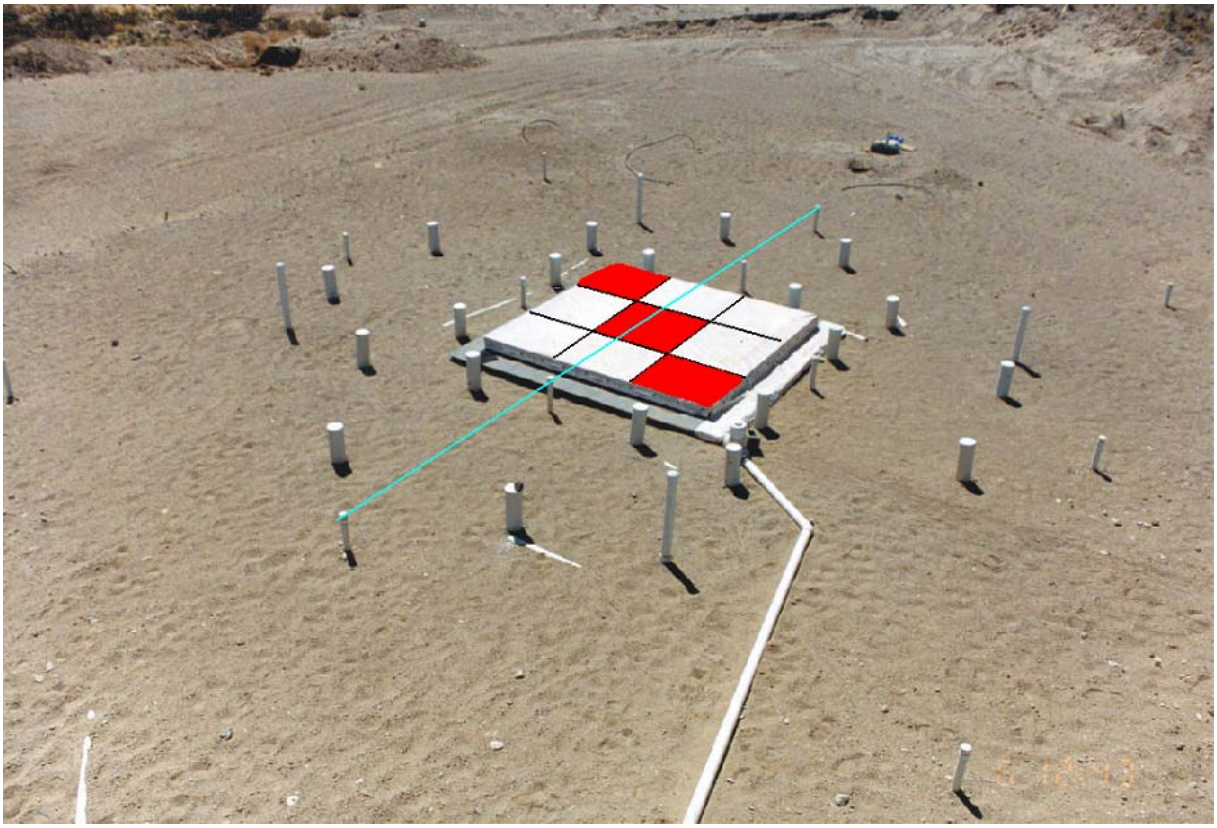

**Figure 8: The red cells indicate those that received saline water during the first salt pulse and the blue line denotes the 5 access boreholes used to collect GPR data.**

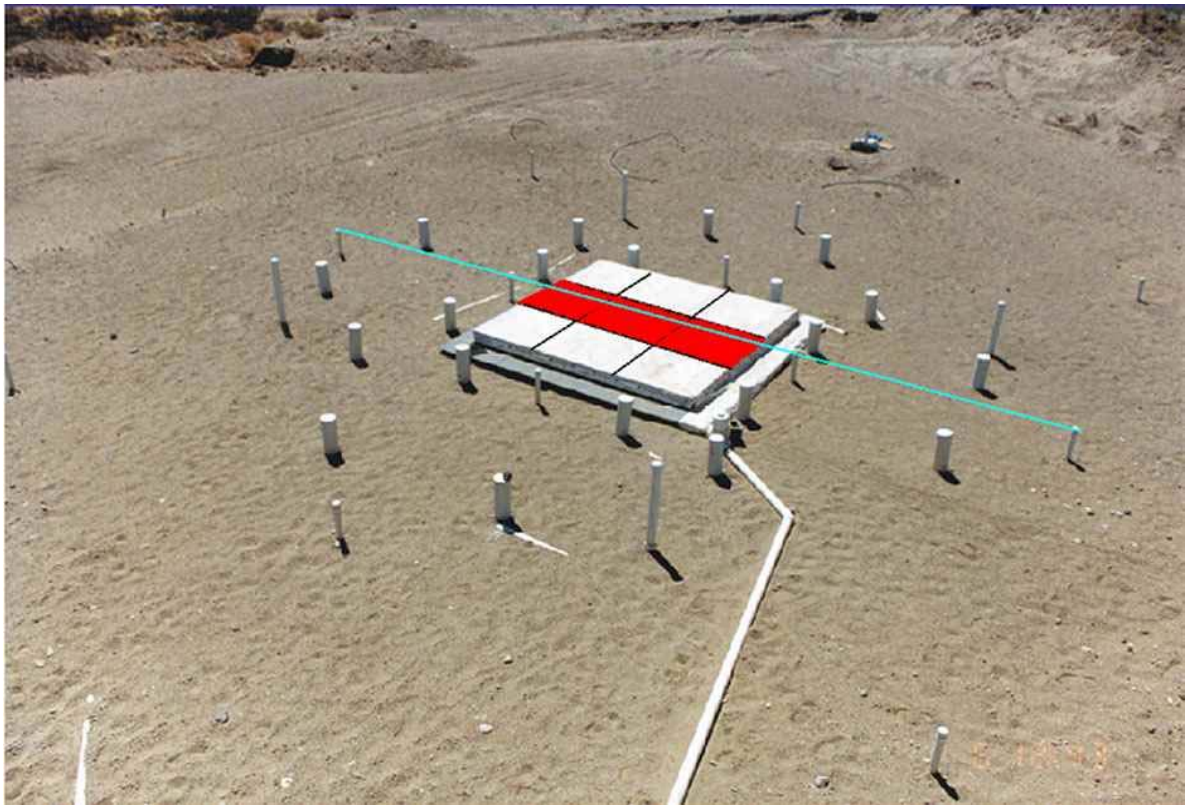

**Figure 9: The red cells indicate those that received saline water during the second pulse and the blue line denotes the 5 access boreholes inline with this injection.**

**Timeline of Events**

Infiltration with tap water began March 11, 1999. This day is considered Day 0 in Time Relative to Start of Infiltration (TRSI), which is a labeling system used during most of the data collection. Five-min irrigation events with tap water occurred every 12 hrs, at an average flux of 2.7 cm $d^{-1}$ for approximately 1237-d, when, without changing flow rates, a salt solution was supplied to the three arrays shown in Figure 6. A concentration of 1.024 g $L^{-1}$ of NaCl was added to the regularly infiltrated tap water (approximate conductivity water 80 mS $m^{-1}$) to increase the conductivity to 275 mS $m^{-1}$. The first salt pulse lasted 226-d and ended on Day 1042. For 53 days, the entire array was once again fed completely with city tap water. On Day 1095, the three arrays shown in Figure 8

were supplied with salt water at an approximate conductivity of 1,300 mS $m^{-1}$ (6.9 g $L^{-1}$ of NaCl was added to the water). The second salt pulse, lasting approximately 85-d, was stopped on Day 1180. City tap water was supplied to all nine arrays for an additional 57-d, until the last infiltration event on Day 1237. Data was collected at the site for 21-d after infiltration ended to measure the change in the wetted area. Figures 10 and 11 are timelines showing the approximate conductivity of the infiltrating water and the dates that EM39 data was collected. Figure 11 is a close-up of Figure 10, showing just the EM39 data used in the mass balance calculations. Dates that EM39 data was collected are marked with a + sign. Infiltration stopped on Day 1237, so the two data sets collected after this day are plotted at 0 mS $m^{-1}$ for infiltrating water conductivity. Since only the data collected during the second salt pulse is analyzed here, all data will now be presented as Time Relative to the Start of the Pulse in days, see Figure 11.

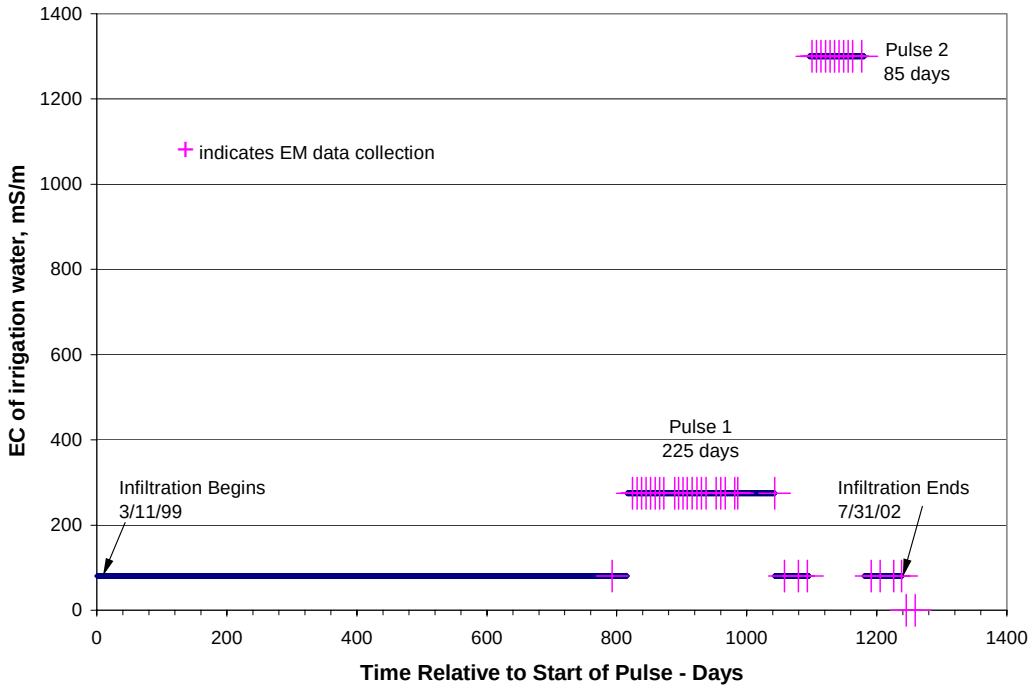


**Figure 10: Timeline showing infiltration duration and conductivity. Dates EM data was collected are marked with a +.**

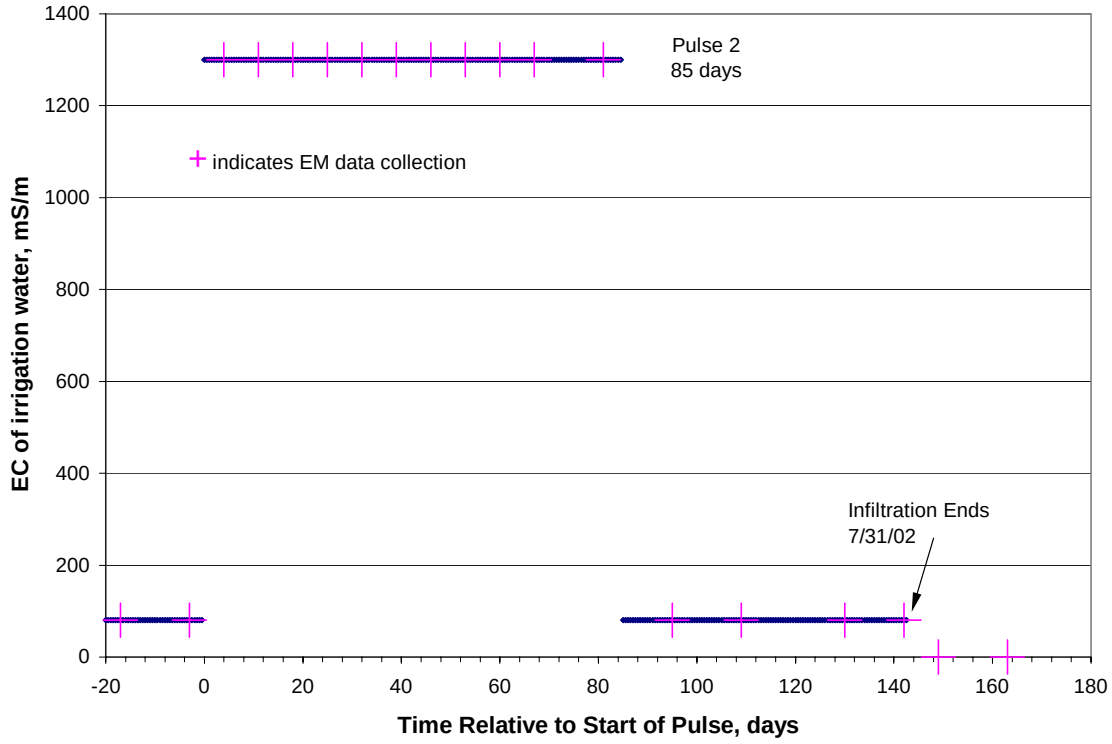


**Figure 11: Timeline showing EM data sets used in the $EC_w$ calculations. Dates EM data was collected are marked with a +.**

# IV. Methods and Materials

## Data Collection

Data for this study was collected with an EM39 down-borehole probe. The Geonics EM39 probe is a slimmer version of their more commonly used surface probes (EM31 and EM38), and can be lowered down access boreholes (minimum 2" ID). An electromagnetic (EM) probe works by sending a current through a coil of wire (a transmitter), which generates a magnetic field. A secondary magnetic field is created in the surrounding material and measured with a passive wire coil (a receiver), see Figure 12. The strength of the secondary field is controlled by the conductance of the soil, which is a combination of many factors including the soil water and clay contents, and temperature. The conductivity measurement range was set at 0-100 mS $m^{-1}$ during each data collection. Repeatability of the data was below to the reported noise level of 0.5 mS $m^{-1}$ and the measurement precision is 5% at 30 mS $m^{-1}$ (McNeill 1990).

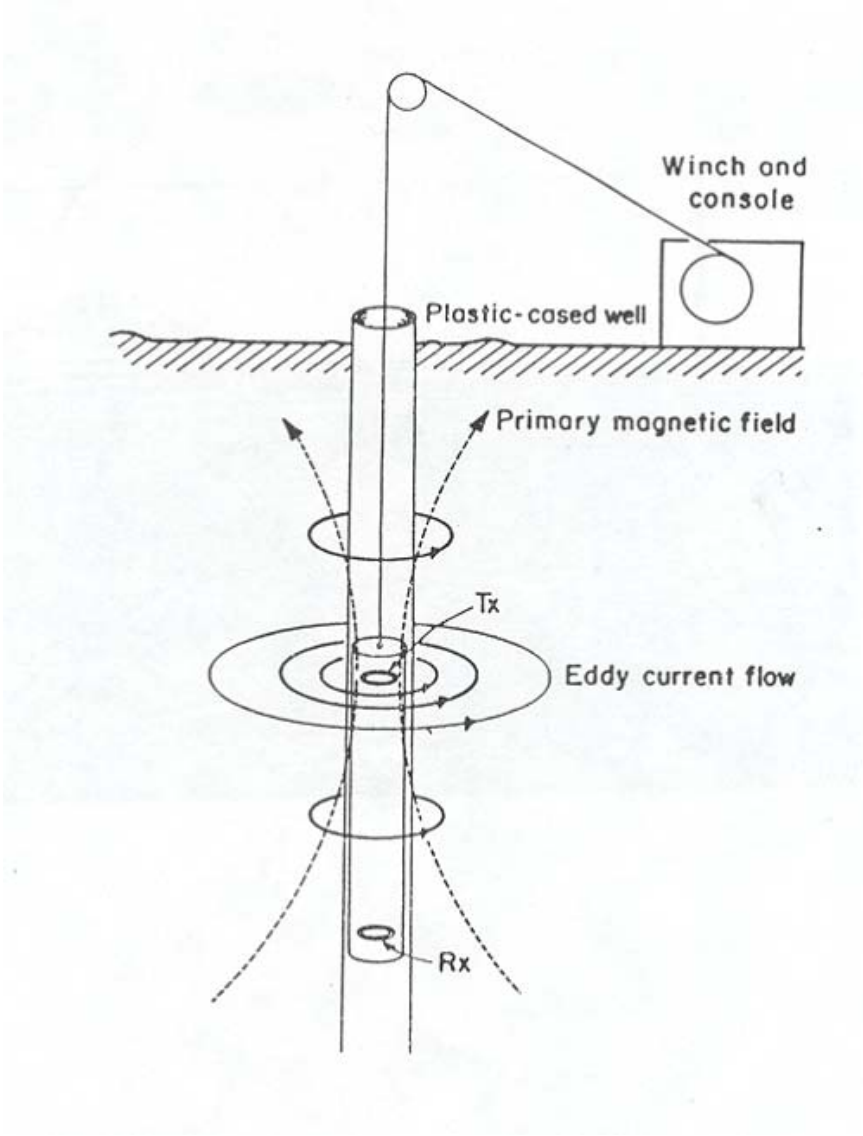


**Figure 12: Conceptual diagram of EM39 probe (McNeill 1990).**

The measurement volume and sensitivity of the probe depends on the strength of the initial magnetic field and the distance between the coils. The probe used in this study has an operating frequency of 39.2 kHz and an intercoil spacing of 50 cm. The EM39 probe was designed to measure the apparent soil conductivity in boreholes both above and below the water table. To minimize the influence of the borehole fluid on the soil conductivity reading, the probe is most sensitive to material at a radial distance of 30 cm from the probe center and has almost zero response to material within 5 cm of the axis,

see Figure 13. The vertical response of the probe is similar, but somewhat asymmetrical due to the use of a focusing coil, see Figure 14.

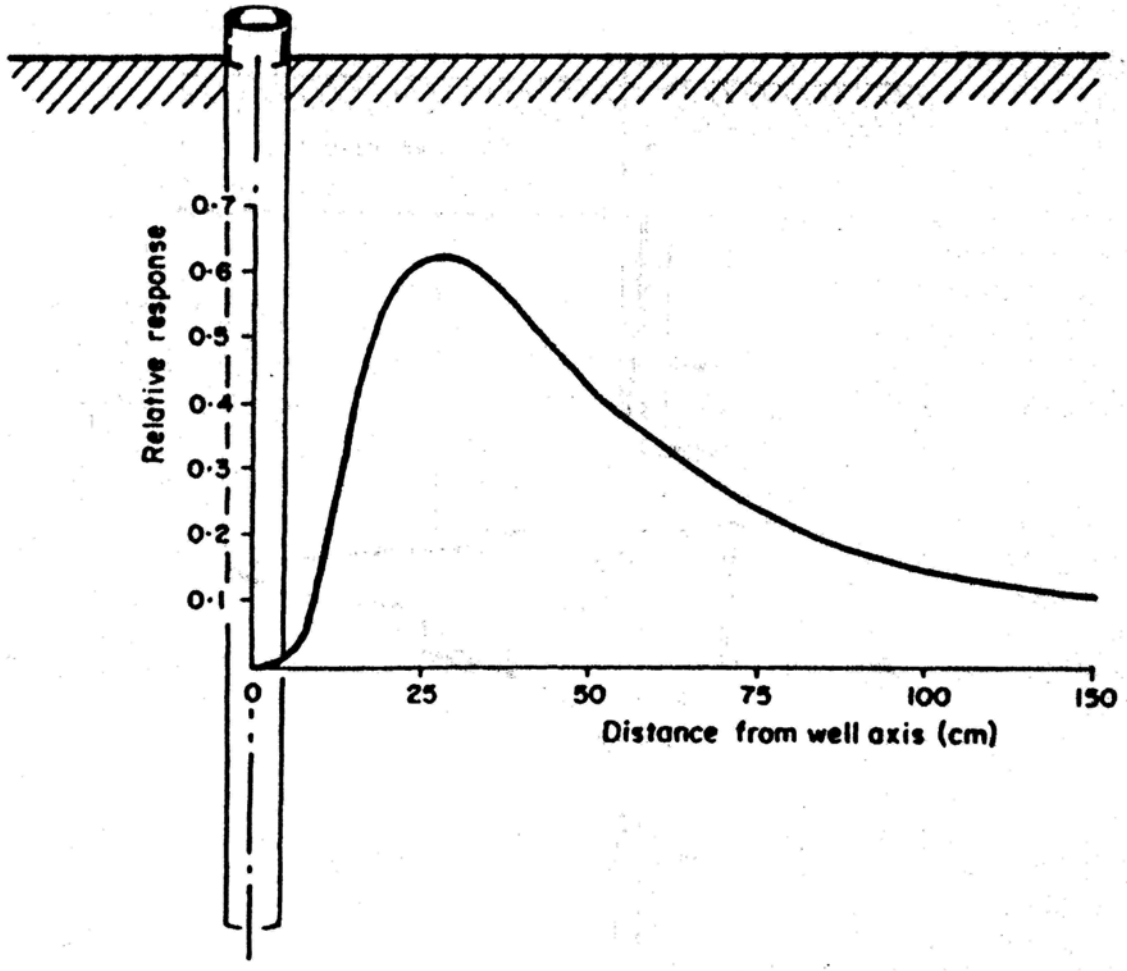


**Figure 13: Relative response of the probe with axial distance (McNeill 1990).**

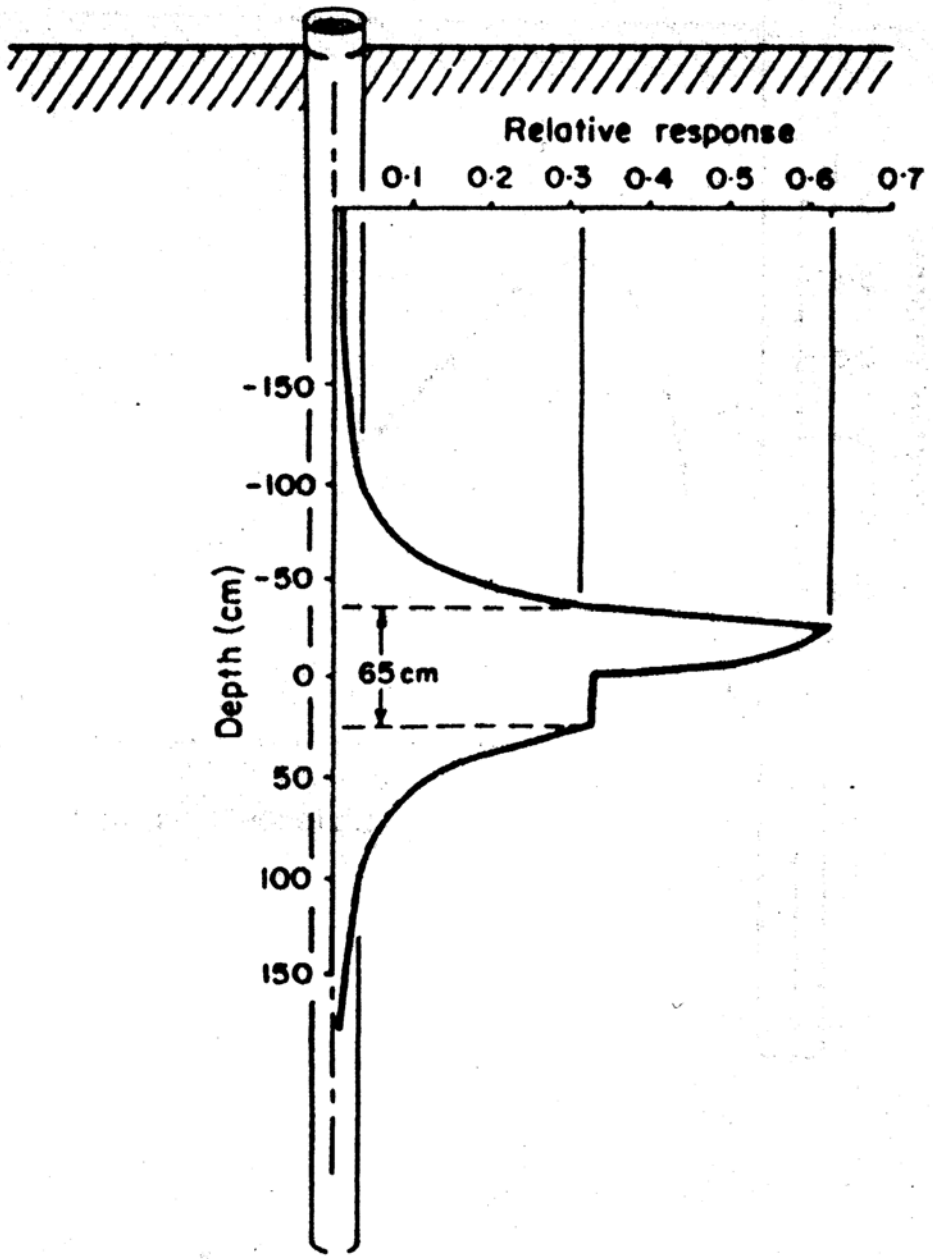


**Figure 14: Relative response of the probe with vertical distance (McNeill, 1990).**

Data was collected in each of the thirteen boreholes every 0.10 m while the probe was lowered down the borehole with a winch. The speed of logging was 0.100 m $s^{-1}$, with a ±0.010 m $s^{-1}$ error due to inconsistencies with the winch motor. Data collection in all 13 boreholes, including equipment set-up and take down, took between 2½ and 3 hours. Data was collected weekly during the early stages of each pulse but then reduced to biweekly collection as conditions approached steady state. Data collection also usually occurred at the same time of day for each data set.

Due to inconsistencies in the speed of logging and calibration of the EM probe during the infiltration of the first pulse, only the data from the second, higher conductivity pulse will be analyzed and presented here (see Appendix 1 and the following section for more details).

Soil water content was measured monthly with the neutron probe in all thirteen boreholes to a depth of 12 m with readings taken at 0.25-m intervals, see Appendix 2. Temperature was monitored hourly with thermocouples at 60 locations across the site both above and below ground, see Appendix 3.

**EM39 Calibration**

Data collected during the first salt pulse showed a consistent pattern with depth, but varied greatly in magnitude. It was determined that the cause of this drift was most likely differences in the probe temperature from one calibration to the next. This was a slightly surprising result, since the EM39 probe is designed to compensate for temperature changes and consequently the operating manual does not mention a need to temperature-equilibrate the probe before use. The temperature variations were most

likely due to the fact that the EM39 equipment was stored at the site in a metal shed with no insulation and no precautions were taken to cool the probe to subsurface temperatures before taking readings. Thus, the probe was constantly undergoing temperature changes during calibration and logging. To correct the temperature equilibration problem for readings taken during the second salt pulse, the probe was left at the bottom of the east borehole for an hour before use. Extra care was taken during data collection to minimize the temperature fluctuations felt by the probe. Specific operating procedures are detailed in Appendix 1.

The EM39 manual suggests calibrating the probe before the logging of each borehole. Calibration procedures require lifting the probe above your head while adjusting the settings to ensure that the probe is measuring zero conductivity. Unfortunately, since the probe was very likely at a different temperature for each calibration during the first salt pulse, the zero conductivity readings were often false. It is also difficult to find a zone of zero conductivity by holding the probe above your head (due to power lines or other nearby metallic objects). To minimize error introduced by the additional calibrations, the probe was also only calibrated once for each data set (all 13 boreholes), and calibrated in the same location each time. For each calibration the probe was held in place (with a small section of PVC pipe) on the top of a 1.5m wooden fence post, ensuring that people and equipment were at a safe distance away. The conductivity measured at this calibration location does not necessary represent the location of zero conductivity at the site, but the conductivity at that location should remain constant throughout the experiment (unless affected by temperature).

To ensure that the drift problems had been corrected, the first and last measurements of each data set were always taken in the East borehole (the same one used for the temperature equilibration period). Comparisons of these two readings show that the drift problem was almost completely eliminated after temperature-stabilizing the probe. Data taken 3 days before the salt pulse began (used in later calculations of pre-salt pulse conductivity) is shown Figure 15, and is representative of most of the repeatability measurements taken for all 18 data sets. The repeatability of these measurements ensures that temperature fluctuations of the probe were minimized during the 2-3 hrs of data collection, these comparisons do not give any information on the repeatability of the calibration on different days however. Included on the plot is an average of all the readings from the East borehole collected in the period of –3 to 163 days TRSP (approximately 36 readings, 2 for each of the 18 days data was collected), to ensure that the probe was calibrated the same each day. Comparison to an average assumes that conductivity and temperature changes during the time period were negligible. This is not a bad assumption, as the temperature remains near 18 C at the bottom of the borehole during this time, see Figure 16. The comparison to an average conductivity value is most valid below 8 m, where conductivity and temperature change with time was negligible. All of the conductivity data from the East borehole is shown in Appendix 1.

Figure 17 is a good example of how temperature fluctuations were kept at a minimum during data collection (i.e., the early and late measurements for that day show little drift), but the calibrated zero value varied from average on this day. The data in Figure 17 was collected 7-d after infiltration had ended and shows little drift on that day, but does not fit well with the average conductivity measured, which is noticed in the mass

calculations later. This suggests that the probe was kept at a constant temperature during data collection, but the actual probe temperature had varied from average.

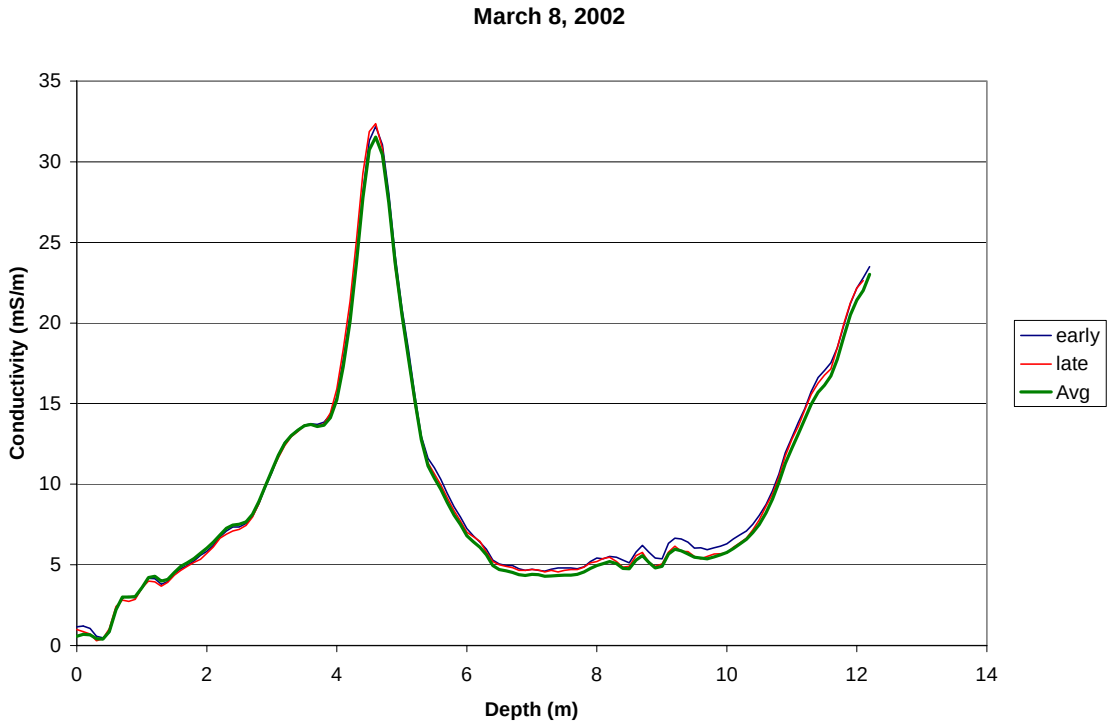


**Figure 15: Readings taken in the East borehole at the beginning and end of the data set collected 3 days before the pulse began. The Avg line is the average of all "early" and "late" measurements taken between –3 and 163D TRSP.**

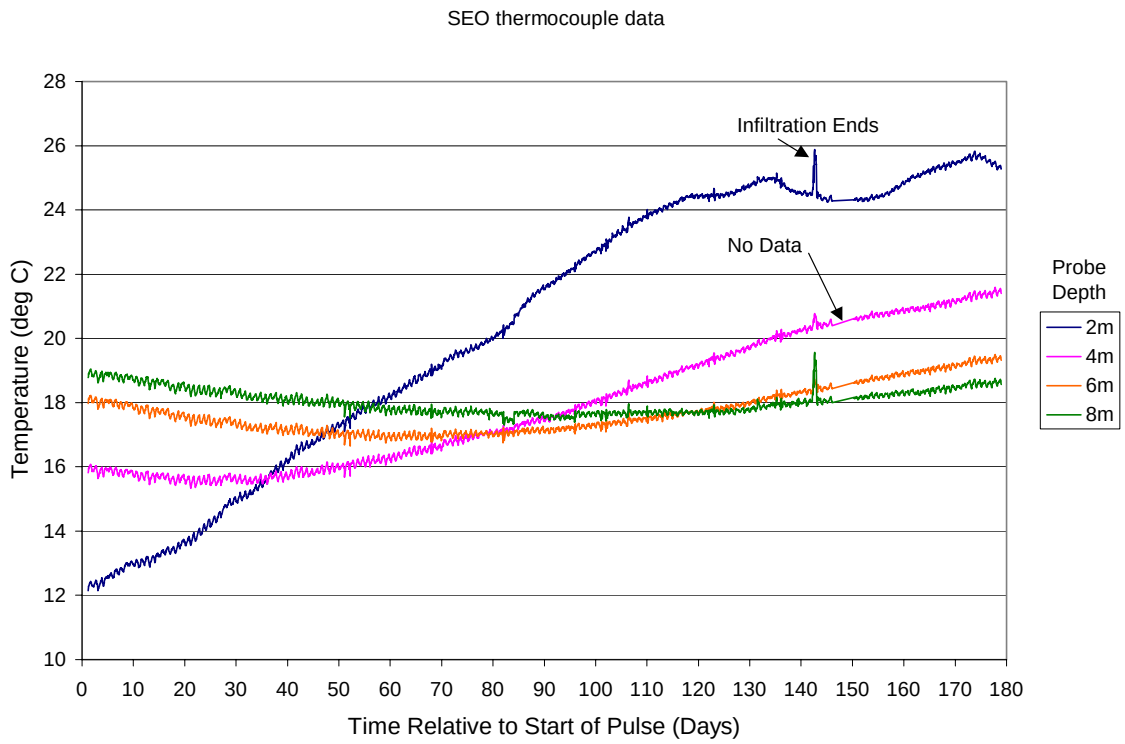


**Figure 16: Thermocouple data collected from the SEO location at 2, 4, 6 and 8m depth.**

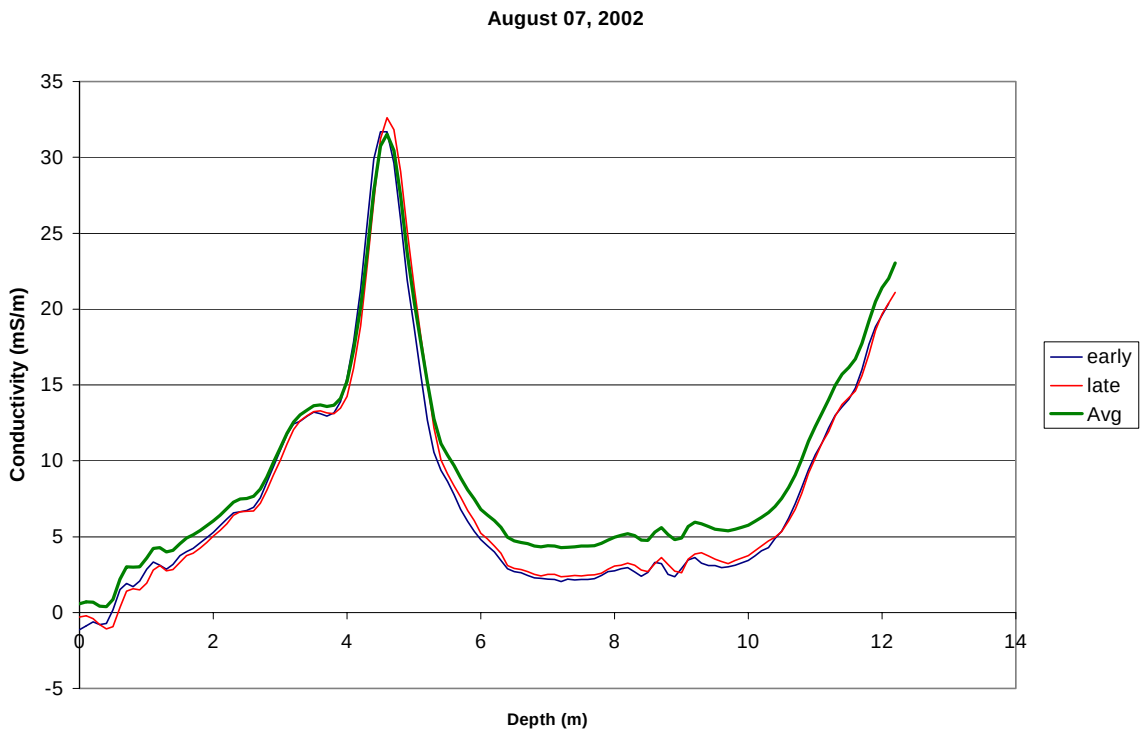


**Figure 17: Readings taken in the East borehole at the beginning and end of the data set collected 7 days after infiltration ended. The Avg line is the average of all "early" and "late" measurements taken between –3 and 163D TRSP.**

Table 2 shows the amount of drift seen during each data set (expressed as the average of the late reading minus the early reading for each depth on that day, so a positive drift means the conductivity readings were increasing since calibration). The average drift of all the data sets is 0.4 mS $m^{-1}$, which is below the instrument noise level of 0.5 mS $m^{-1}$. The other problem with the data collected during the first salt pulse was inconsistent speed of logging resulting in smeared data and loss of resolution. Another consequence of varying probe speed is offset in the total depth measured with the probe (i.e., if the probe is lowered to fast some of the readings are skipped and the total depth of the borehole may be recorded to vary as much as 30-40cm). A comparison of the depth measured is also given to ensure a consistent speed of logging. A value of zero in the

Depth Error column of Table 2 represents a day where the early and late reading were recorded at the same speed and the total number of readings was the same. As is clear from Table 2, speed of logging errors were insignificant during the second salt pulse.

| TRSP | Avg Diff | Avg Depth | Error +/- |
|---|---|---|---|
| **Days** | **mS/m** | **m** | **m** |
| **-17** | -1.25 | 12.15 | 0.05 |
| **-3** | -0.34 | 12.15 | 0.05 |
| **4** | -1.63 | 12.25 | 0.05 |
| **11** | -1.29 | 12.2 | 0 |
| **18** | -1.02 | 12.2 | 0 |
| **25** | -0.50 | 12.2 | 0.1 |
| **32** | | | |
| **39** | -0.42 | 12.2 | 0 |
| **46** | 0.53 | 12.2 | 0 |
| **53** | -0.85 | 12.15 | 0.05 |
| **60** | -0.63 | 12.2 | 0 |
| **67** | -0.09 | 12.15 | 0.05 |
| **81** | -0.28 | 12.2 | 0 |
| **95** | -1.12 | 12.2 | 0 |
| **109** | 0.39 | 12.1 | 0 |
| **130** | -0.11 | 12.2 | 0 |
| **142** | 0.85 | 12.2 | 0 |
| **149** | 0.27 | 12.15 | 0.05 |
| **163** | 0.19 | 12.2 | 0 |
| **AVG** | **-0.41** | **12.18** | **0.02** |

**Table 2: The average difference between the two readings taken in the east borehole during each data set. Repeatability measurements were not taken on Day 32.**

# V. Results

Figure 18 shows the measured conductivity of solution samples from the 6.9 g $L^{-1}$ NaCl solution that was infiltrated to one third of the infiltrometer. Samples of the tap water fed to the other two thirds of the array were not routinely collected, but had an average conductivity of 80 mS $m^{-1}$ as measured during TDR lab experiments (Appendix 7). The conductivity of the salt solution was measured periodically by collecting samples from the supply tank and testing the conductivity with an Orion Conductivity Meter (Model 150 Conductivity Cell: 012210). The low conductivity measurement at 14 days was collected before the salt solution in the supply tank had become well mixed and does not represent a mistaken amount of salt added to the tank (as later calculations of mass added over time show to be very consistent). The other variations in salt tank conductivity are most likely due to sampling error, and not to fluctuating salt solution concentration. Possible causes for the sampling error include poor calibration of the probe, evaporation from a poorly sealed containers (occurred in at least one of the samples tested for repeatability over a period of several months), or collecting samples from a poorly mixed solution.

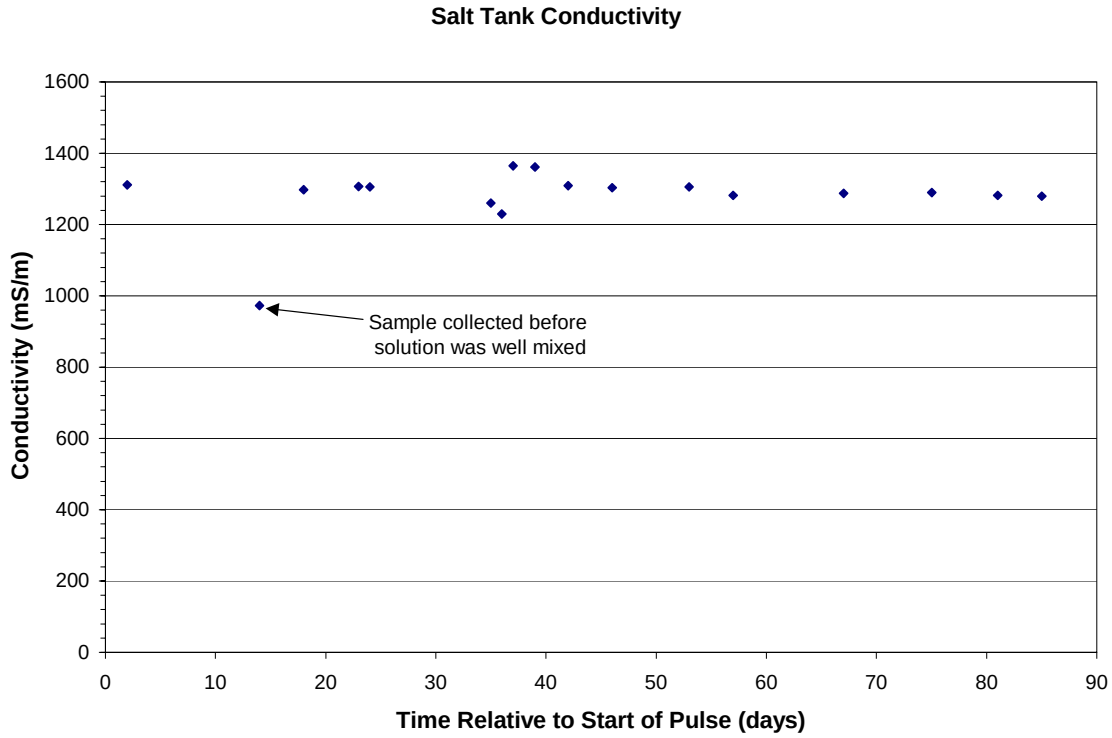


**Figure 18: Measured solution conductivity of samples collected from the salt solution supply tank. Tap water conductivity approximately 80 mS $m^{-1}$.**

The raw data collected with the EM39 device is simply a bulk soil conductivity measurement at a given depth, as shown in Figure 19, from the center access borehole. As would be expected, the data collected in the center borehole showed the largest increase in conductivity after the start of the salt pulse. Noticeable increases in conductivity were also measured in the SE inner and outer, SW inner and outer, and NW inner boreholes. Figures 20-22 show the inner lysimeters during the application of the salt pulse. The slow movement of the salt pulse is seen in Figure 21, where the measured conductivity is still increasing 28 days after the salt pulse ended. The data in Figures 19-22 show similar trends of slowly increasing mass, especially between 4 and 6m depth. The remaining 7 boreholes showed very little change during the data collection period and are found in Appendix 1.

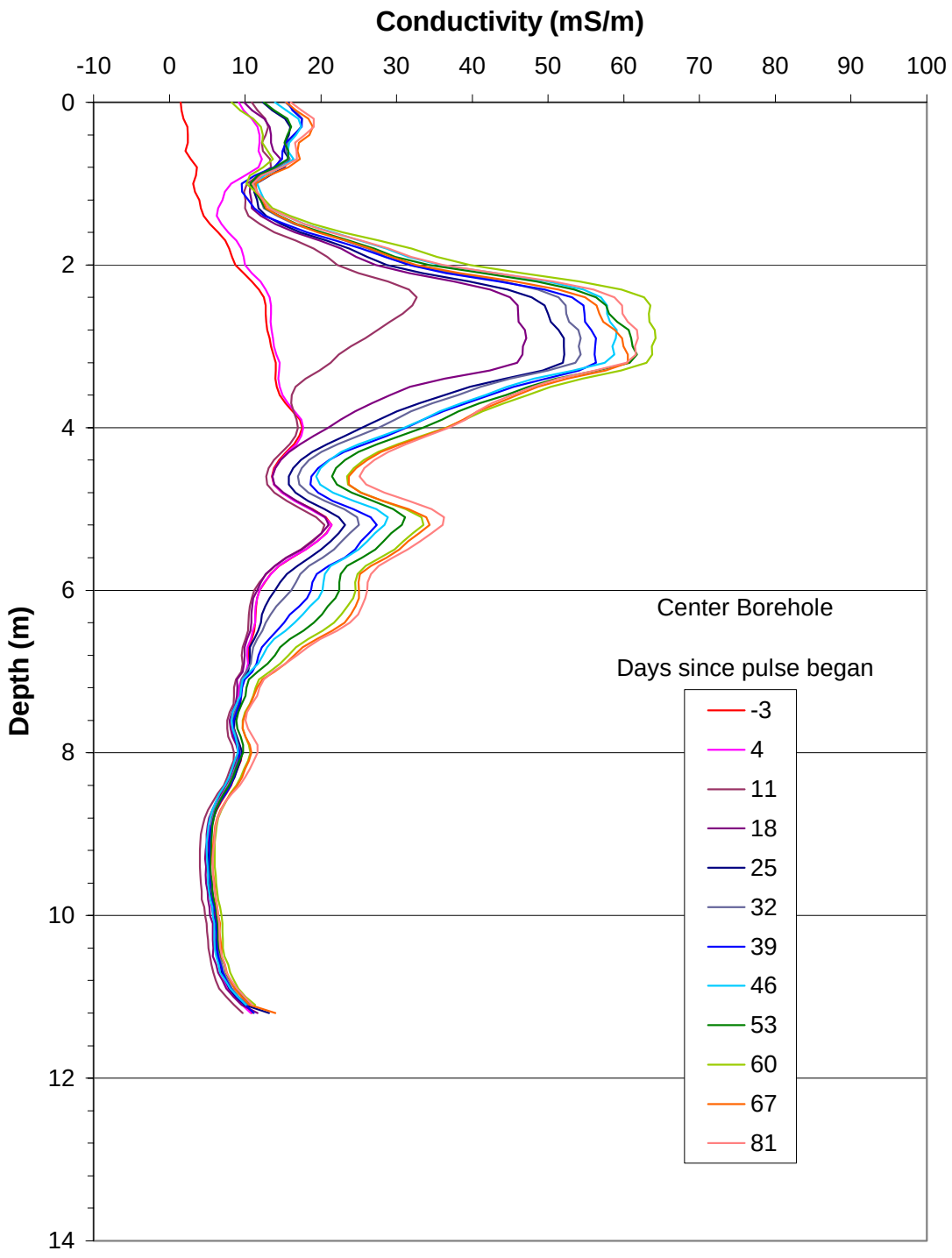


**Figure 19: Raw EM39 data, in mS $m^{-1}$, from the center borehole during the application of the second salt pulse (pulse ended Day 85).**

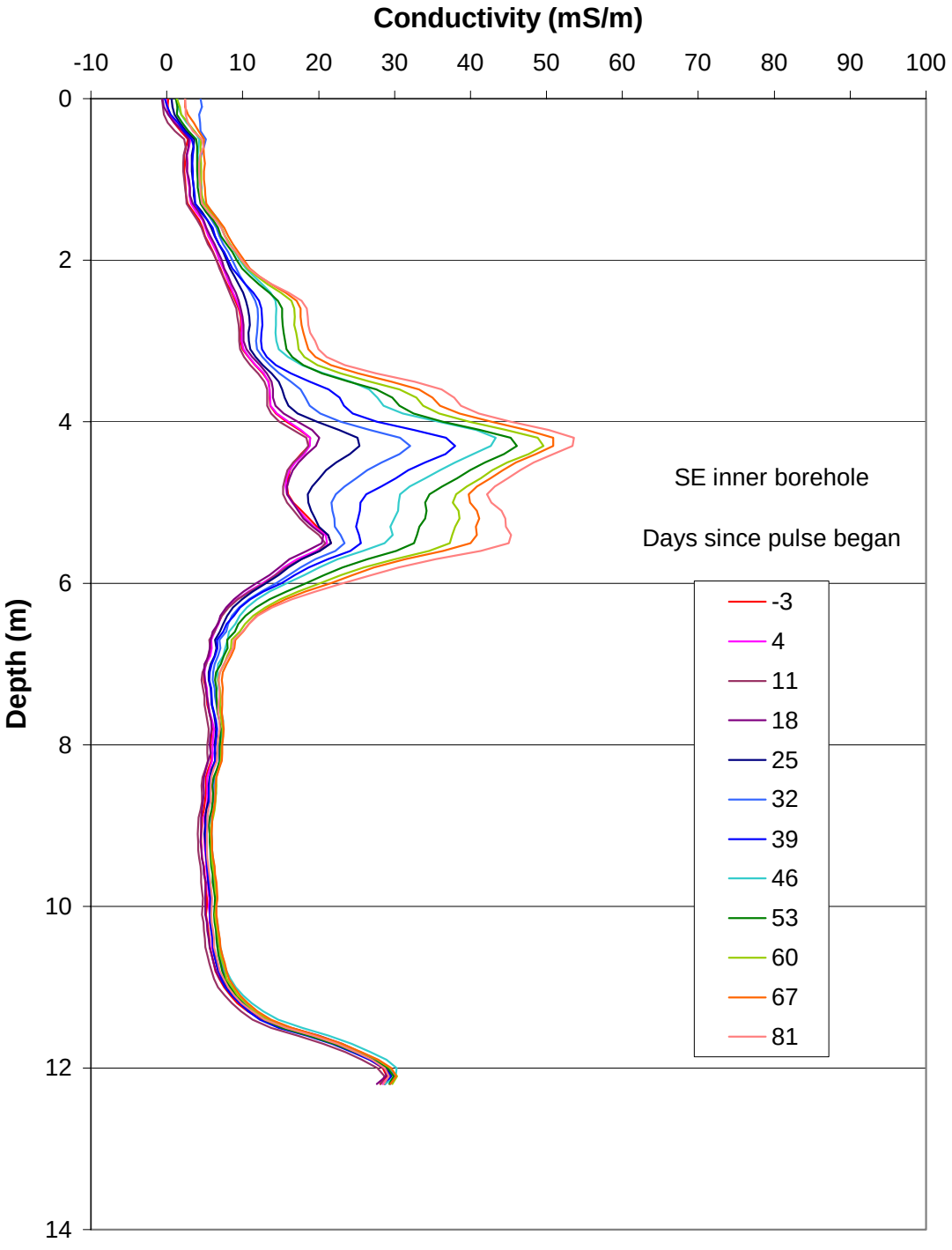


**Figure 20: EM39 readings from the SE inner borehole during the infiltration of the second salt pulse (pulse ended Day 85).**

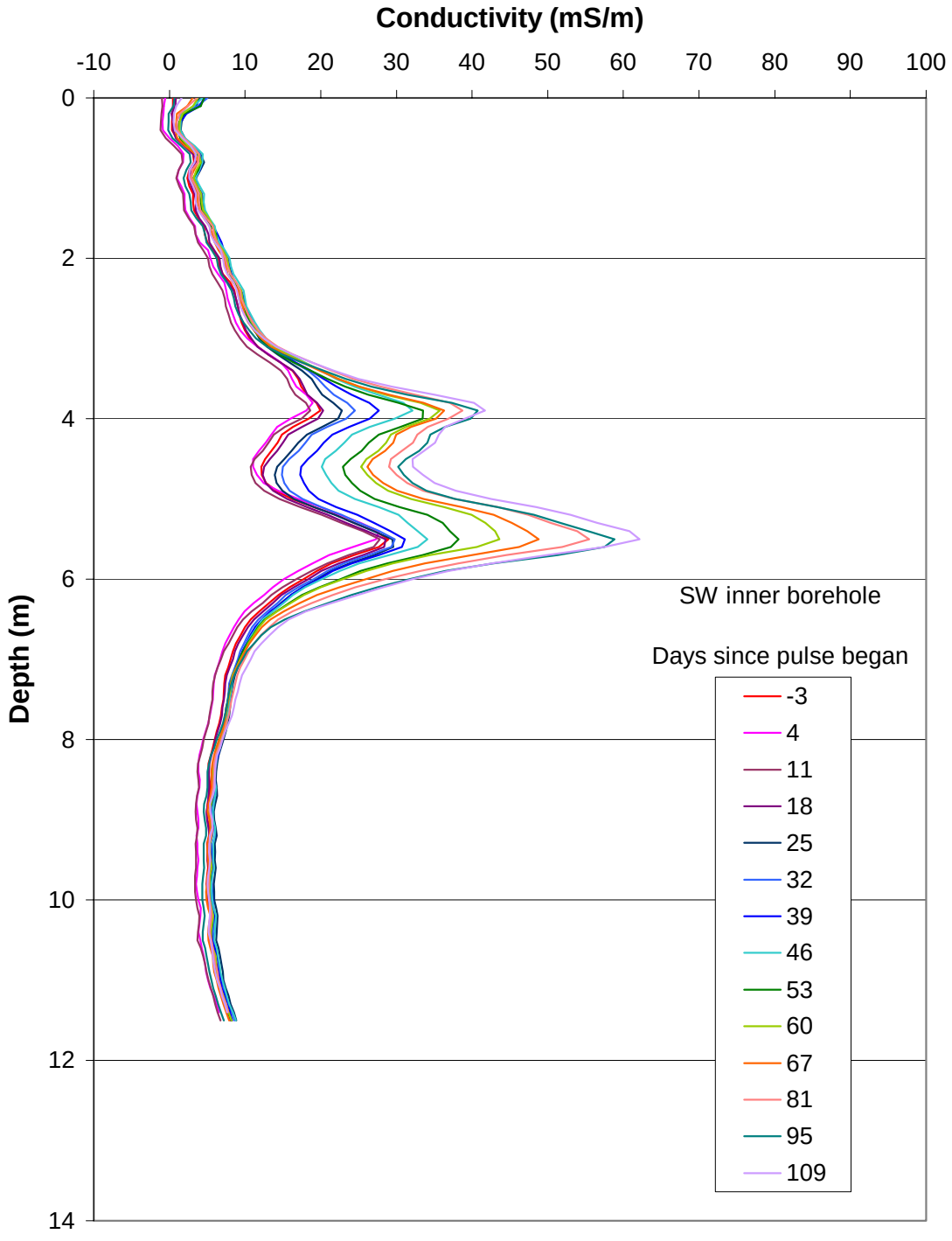


**Figure 21: Raw EM39 data from the SW inner borehole collected during the first salt pulse (pulse ended Day 85, but conductivity is still increasing at Day 109).**

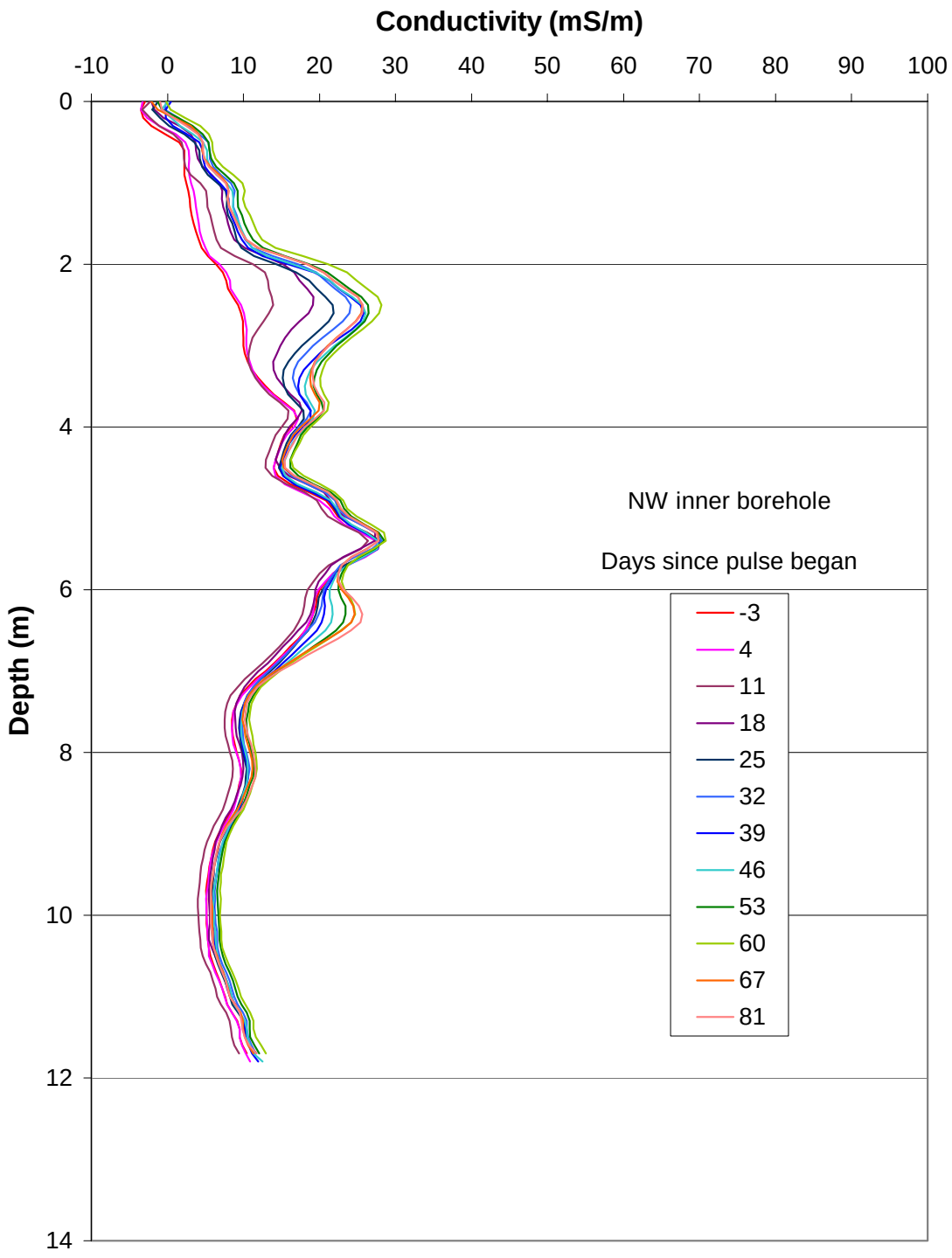


**Figure 22: Raw EM39 data from the NW inner borehole collected during the second salt pulse (pulse ended Day 85).**

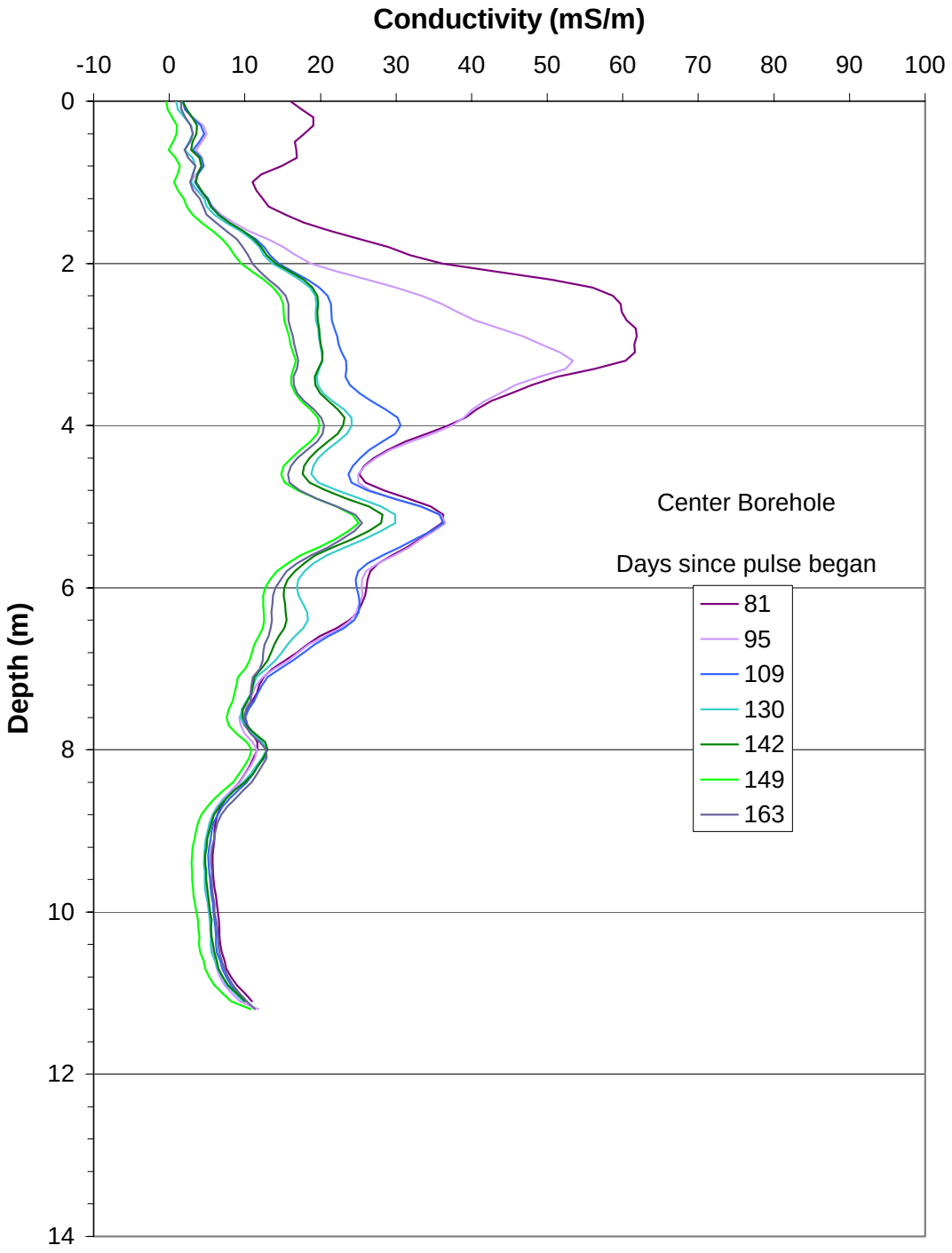


**Figure 23: Decrease in mass during the tap water flush and after infiltration ended on Day 142.**

Data collected with the EM39 during the 57-d tap water flush following the pulse and after infiltration ended, measured a decrease in conductivity as the salt plume was first rinsed away by the tap water, and measured a second decrease as the wetted area shrank. Figure 23 shows the EM data collected in the center borehole after the salt pulse had ended, see Appendix 1 for more images of the conductivity decrease with time.

A comparison of the standard deviation of all readings (between –3 and 163 days TRSP) at each depth interval for each borehole is seen in Figure 24. The standard deviation graph quickly tells us which boreholes measured any noticeable change in conductivity after the application of the tracer, and the depths that the increase was measured. The center borehole is the only location where a conductivity increase was measured near the surface, but the strongest increase was measured at approximately 3-m depth in this borehole. Conductivity increases in SEI, SEO, and SWI were measured most strongly between 3-7 m. Very little change in conductivity was detected in any of the boreholes below approximately 8 m depth, and the standard deviation between 8-12 m is approximately or less than the repeatability level of the instrument, 0.5 mS $m^{-1}$.

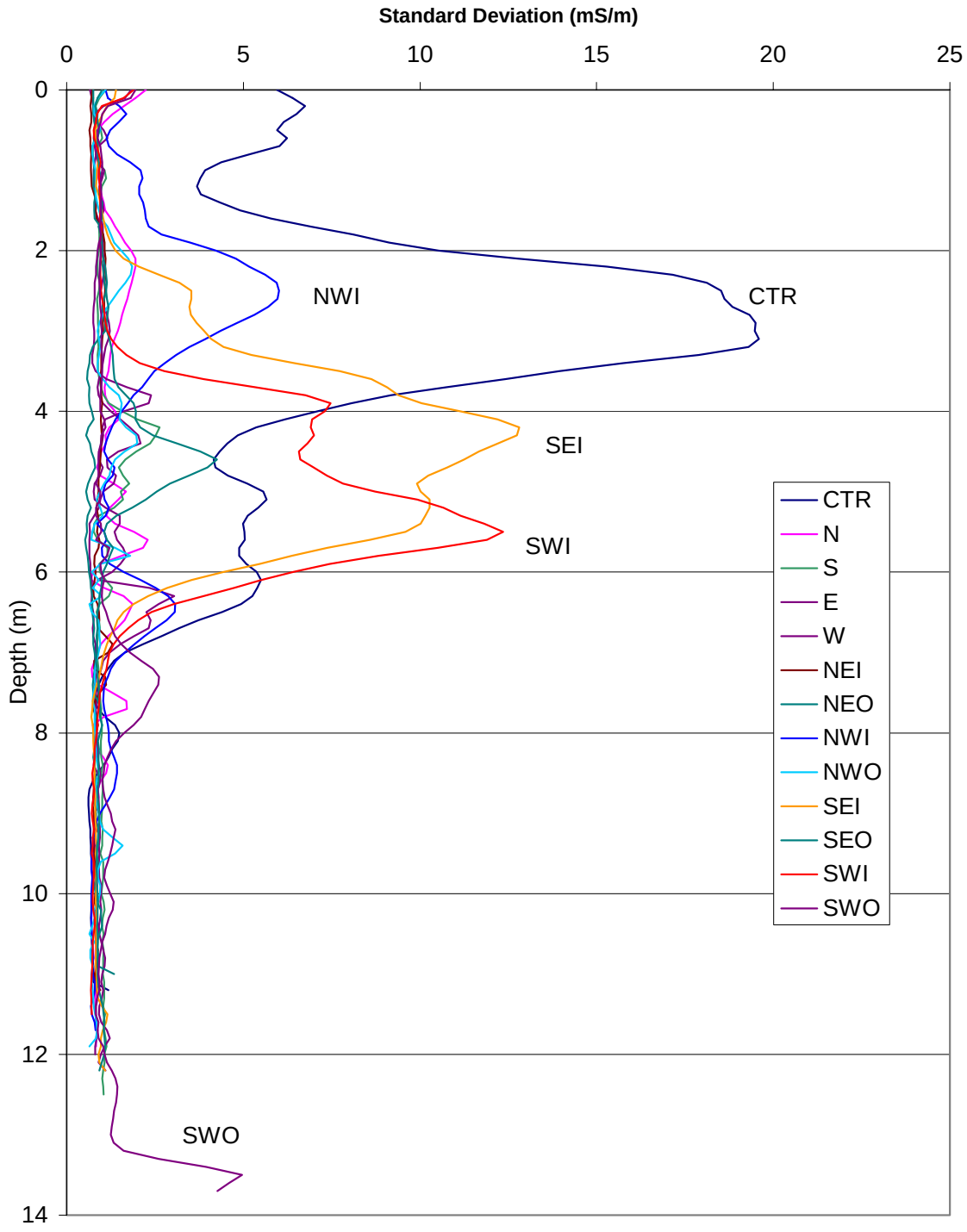


**Figure 24: Standard deviation of all readings, at each depth, for data sets taken between –3 and 163 days TRSP.**

The southwest outer borehole reaches 1.5 m deeper than most of the boreholes, to a depth of 13.7 m, see Appendix 1. Conductivity readings from the last 30 cm of this borehole were usually near 100 mS $m^{-1}$, which is almost double the conductivity measured anywhere else at the site. This zone of high conductivity could be due to a more saturated zone just below the base of the boreholes. A depth of 13.7 m is probably too shallow to attribute the high conductivity readings to the water table, but a large clay layer could have caused a perched water table at this depth. It is difficult to verify the cause of this high conductivity zone since none of the other measurements techniques collected data this deep.

**3D Interpolation**

Rhoades et al. (1988) determined by sensitivity analysis that reliable determinations of soil salinity could be obtained from measurements of bulk electrical conductivity ($EC_a$) with reasonable estimates of other model parameters such soil water content and clay content. In this thesis, estimates of the percent clay in the soil were based on particle size analysis of samples from one (NW) of the four continuous core samples (Baker (2001)), see instrumentation figures for core locations. The particle size analysis performed on these samples included sieving and hydrometer techniques. The analysis of the hydrometer testing was not completed by Baker however, and these calculations are presented in Appendix 4. Percent clay was estimated in the other three continuous core samples by correlating their stratigraphy to the NW core. Estimates of soil water content were based on monthly neutron probe readings. Due to the differences in sample location, measurement volume, etc, the different parameters required to

calculate $EC_w$ were first interpolated into the same 3D volume using Tecplot v.9.0 (Amtec Engineering Inc.). Different choices of 3D volumes, cell size and interpolation, or kriging options were tried, and will be discussed later.

The 3D volume used in this analysis is shown in Figure 25, the individual cells are outlined in blue. The dimensions of the analyzed volume are 15.75 m by 15.75 m wide and 13 m deep, which is divided into 42 by 42 by 34 cells. Each cell is approximately 0.375m by 0.375 m by 0.382 m in size, and has a volume of 0.0536 $m^3$. Figure 26 shows that the chosen volume covers the entire instrumented area around the infiltrometer.

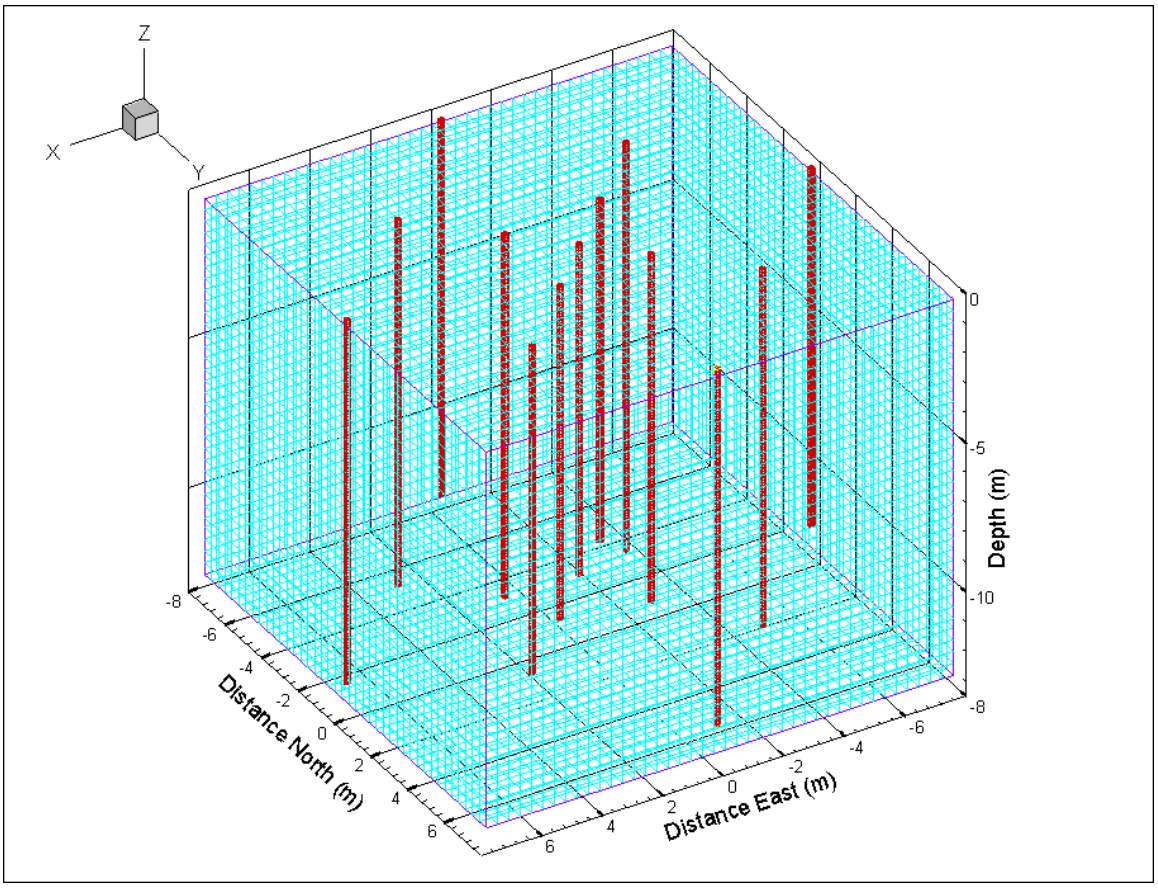


**Figure 25: 3D grid used in mass balance analysis, looking southwest.**

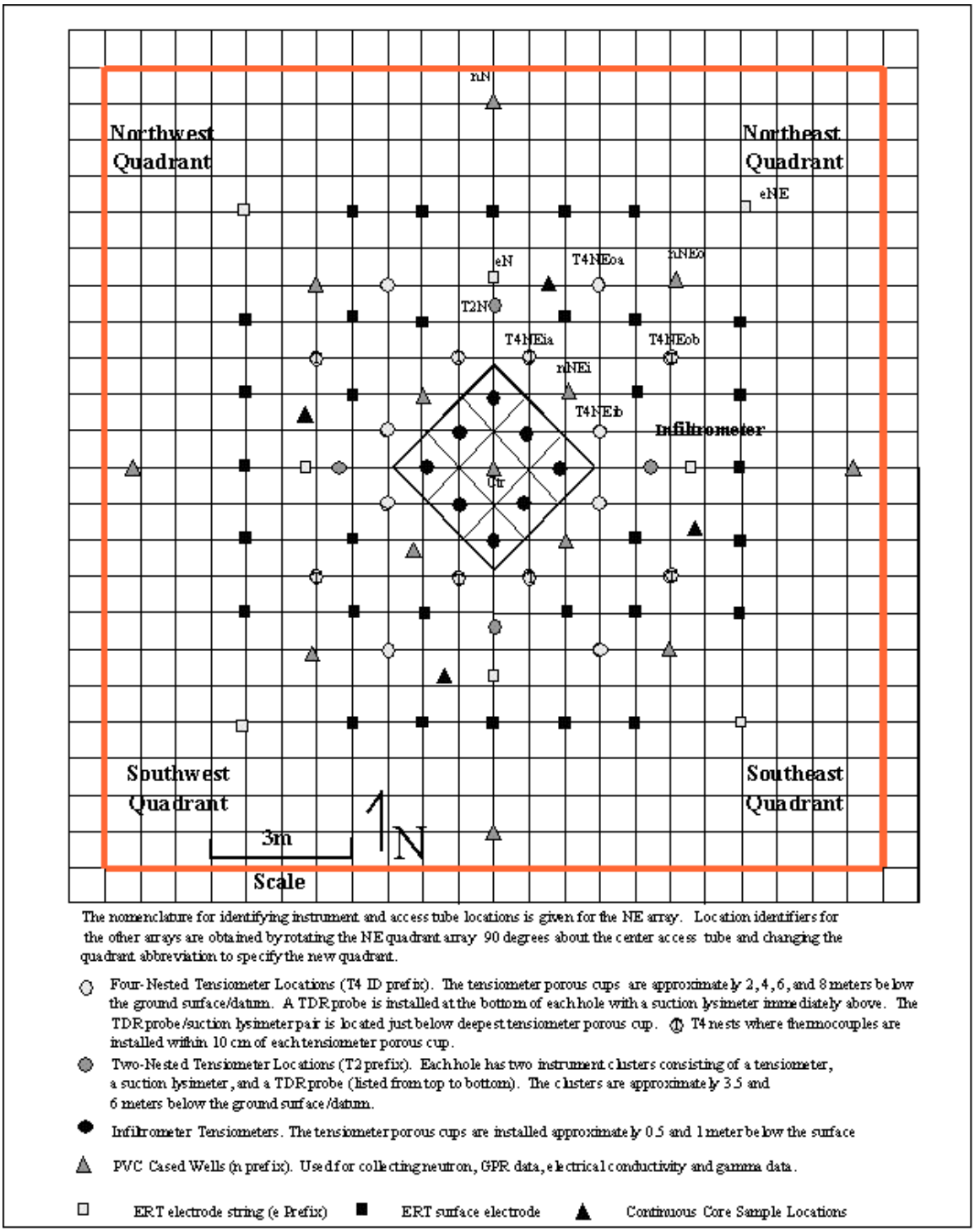


**Figure 26: The thick border shows the volume used in the mass balance calculations, relative to the instrumented area.**

The actual images of water content, soil conductivity and temperature varied on slightly between the difference calculated scenarios of the following sensitivity analysis, so only one set of images is presented here. The data are plotted to show the three-dimensional surface of each contour interval, or iso-surface (except for the temperature data, which varied most significantly with depth). Figures 27-29 are representative of the complete set of conductivity, water content, and temperature images found in Appendix 2, 3 and 4 respectively.

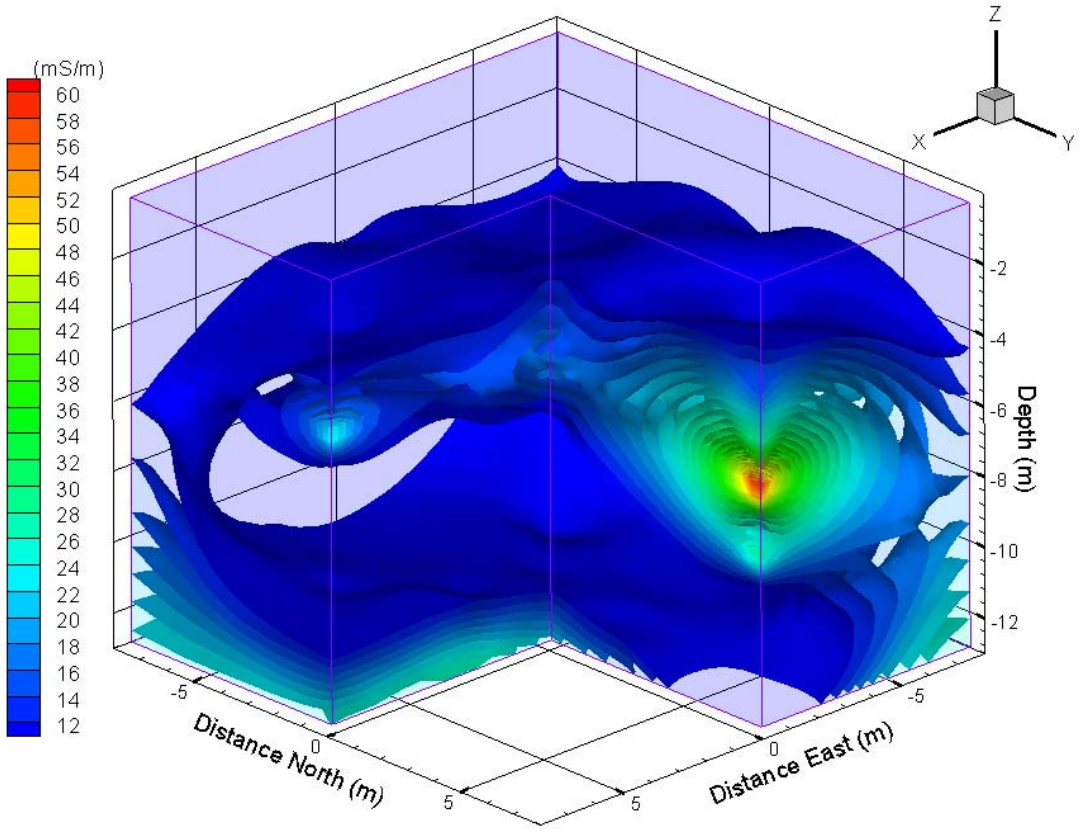


**Figure 27: EM39 data collected 3 days before the salt pulse began.**

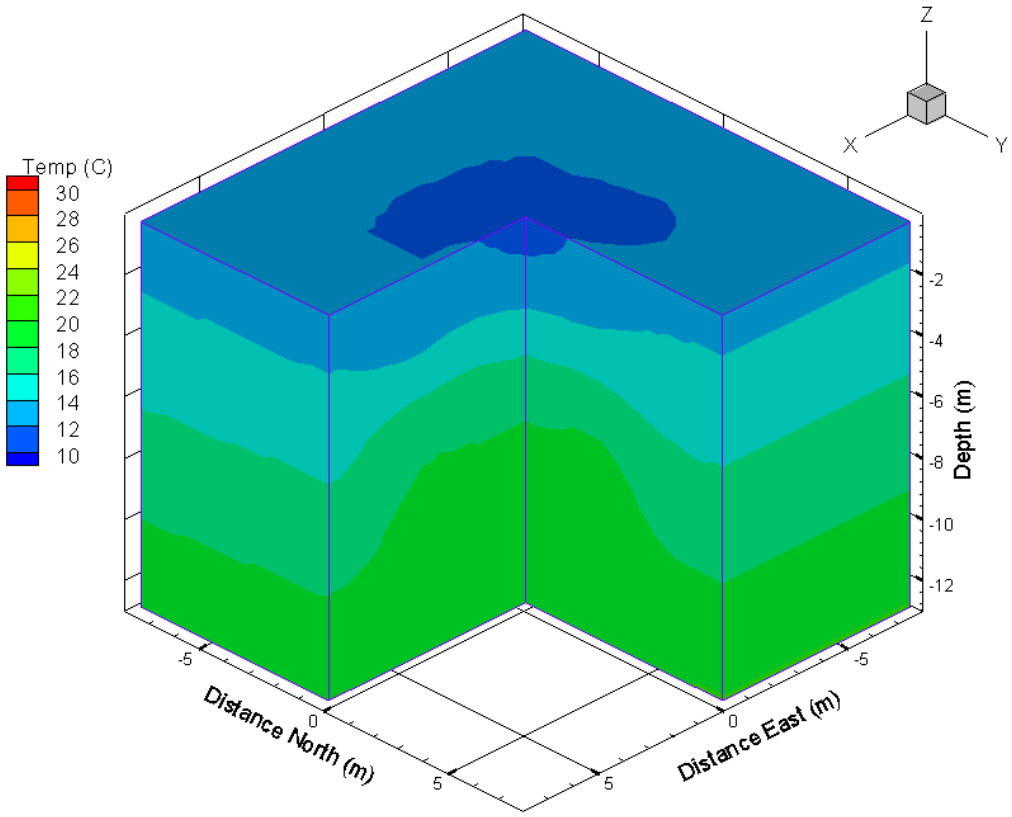


**Figure 28: Temperature data collected 3 days before the salt pulse began.**

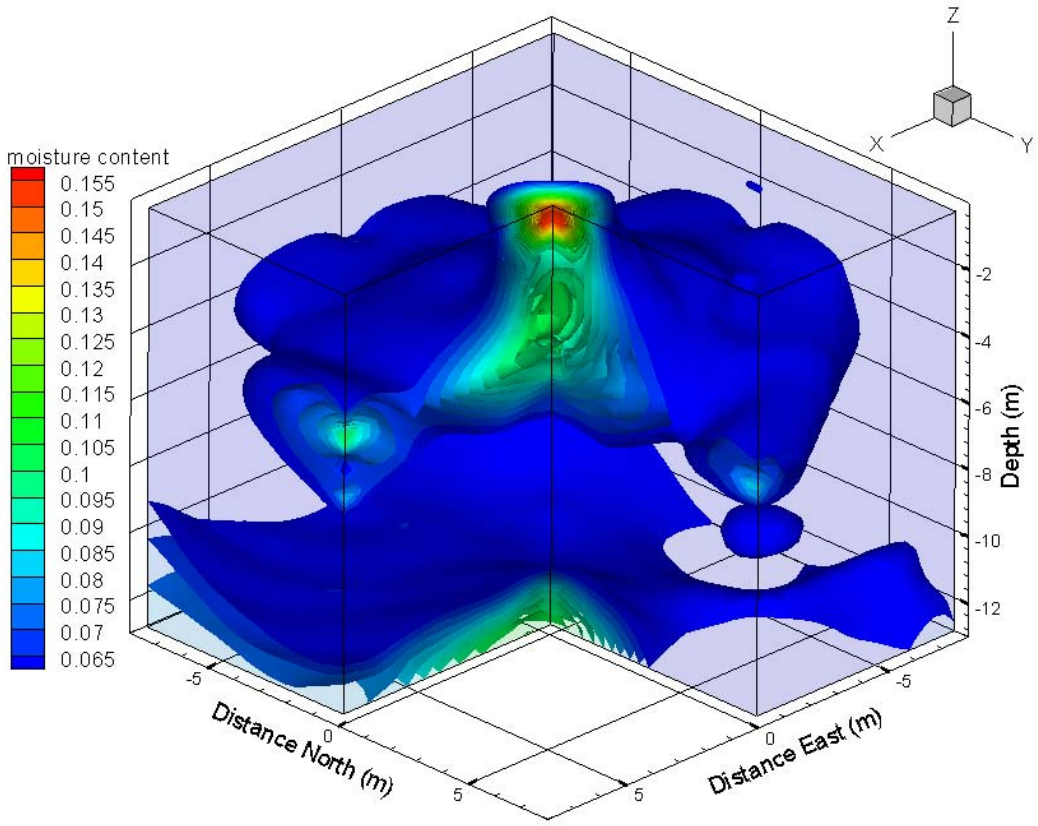


**Figure 29: Neutron probe data collected 17 days before the salt pulse began.**

The EM39 data shows a zone 2-5 m directly below the infiltrometer, which increases in conductivity in an almost spherical shape during the application of the salt pulse. The pulse quickly shrinks after the pulse ends, and again after infiltration ends

The temperature images are based on 39-point measurements at various depths across the site. Temperature distribution appears to be largely controlled by depth, but also by the temperature of the infiltration water. The water and salt solutions supplied to the infiltrometer were stored in supply tanks in a small building that was subject to large diurnal temperature fluxes. The infiltrated water was very cold in the spring (approximately 10 ˚C) and warm in the summer (approximately 30 ˚C). The average

temperature between 6 and 12 m remained near 18 ˚C however, during the 6 months of data presented here.

The water content images show that the shape and extent wetted area did not change significantly during the infiltration of the second salt pulse and closely follows the stratigraphy. Stability of the wetted area was expected, since infiltration had been occurring regularly for almost 1100 days prior to the infiltration of the salt pulse. Figures 30-32 show the raw water content data collected 17 days before the pulse began, and 8 and 21 days after infiltration ended respectively. Figure 30 is representative of water content conditions during the salt pulse, Figures 31 and 32 show a very slight decrease in water content due to the end of infiltration, but are remarkably similar to Figure 26.

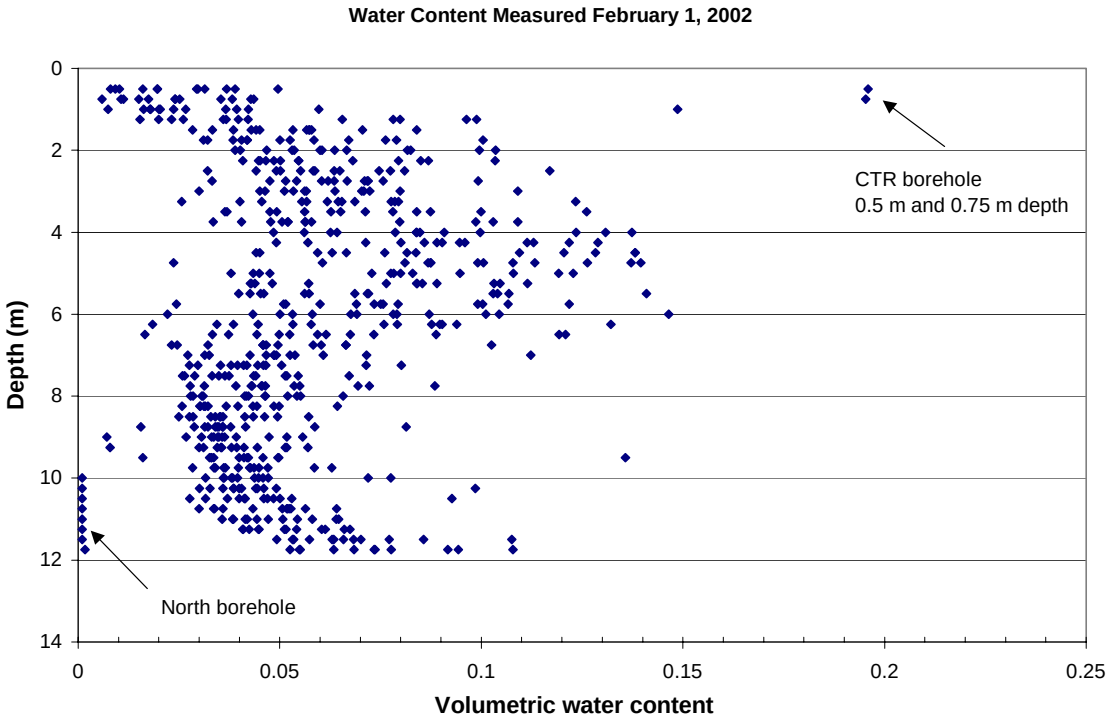


**Figure 30: Raw water content data measured 17 days before the pulse began in all 13 boreholes.**

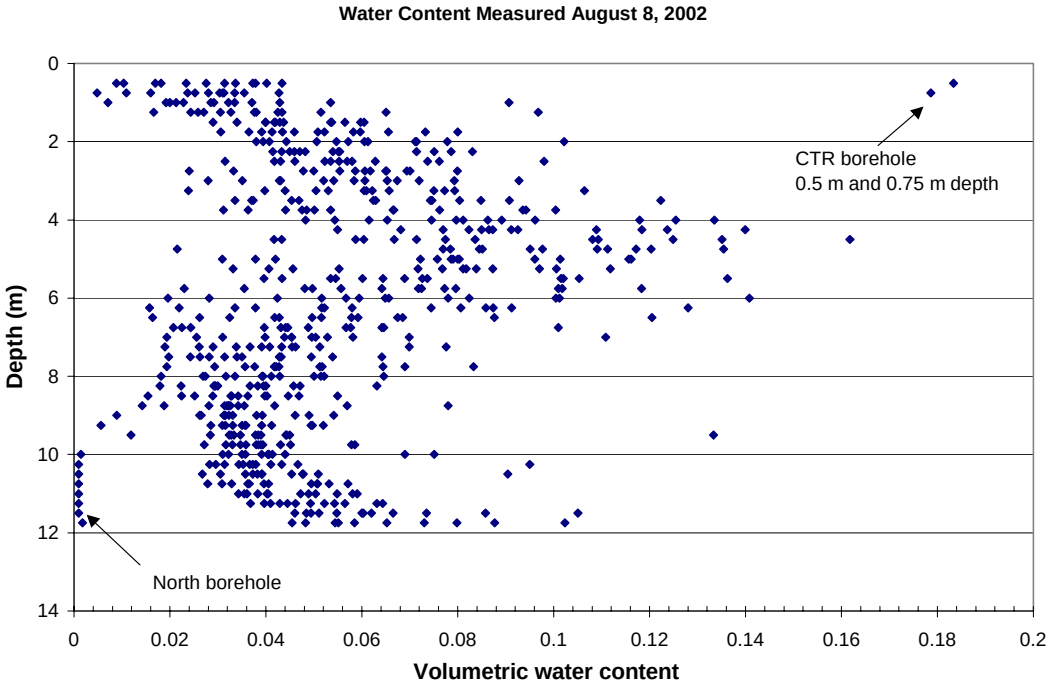


**Figure 31: Raw water content data measured 8 days after infiltration ended in all 13 boreholes.**

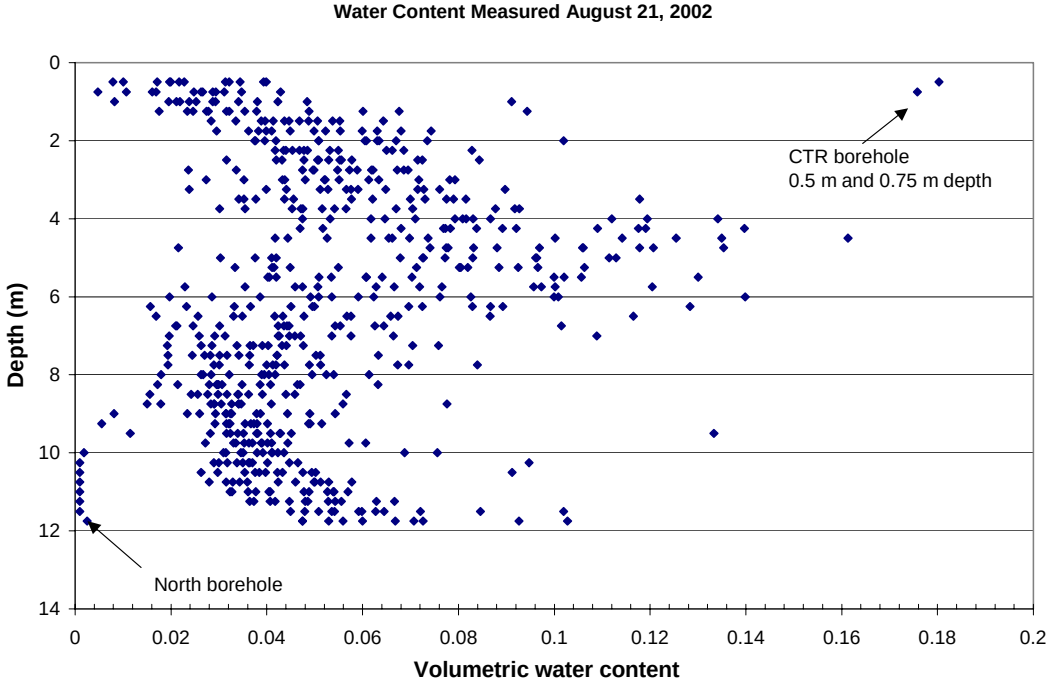


**Figure 32: Raw water content data measured 21 days after infiltration ended in all 13 boreholes.**

A distinct decrease in the wetted area directly below the infiltrometer (but above 4m depth) is measured after infiltration events ended on Day 142 TRSP. Figures 33 and 34 show the images produced from the raw data shown in Figures 31 and 32. It is interesting to note that a zone of higher water content remains near the surface directly below the infiltrometer, which is most likely due to a clay plug surrounding the center borehole from 0-1.5m depth. The extremely low evaporation rates directly below the infiltrometer could also be a cause for this zone of high water content. Both the neutron and EM images show a zone of low conductivity/water content, or discontinuity of the wetted area between the clay layer at 2-3 m depth and directly below the infiltrometer. This low conductivity zone is most likely due to a gravel and cobble layer at this depth, which retains low moisture content and probably contains many small, fast flowpaths, which are poorly imaged with this technique.

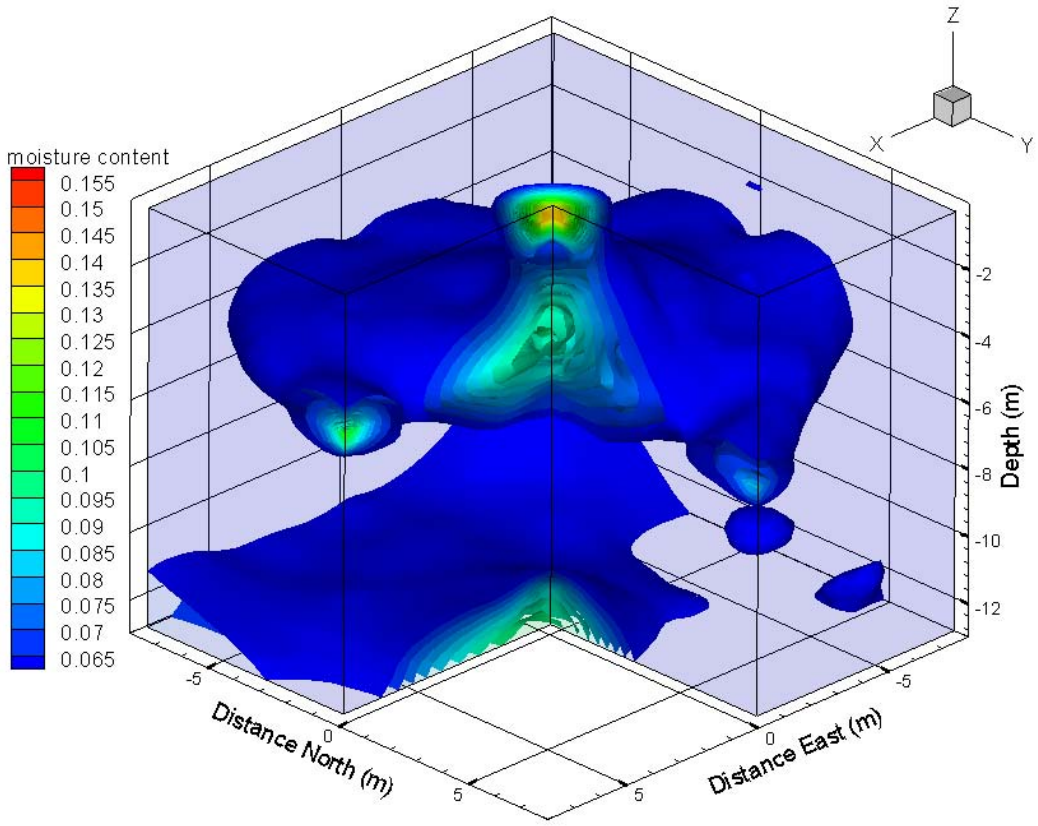


**Figure 33: 3D image of neutron probe data collected 7 days after infiltration ended.**

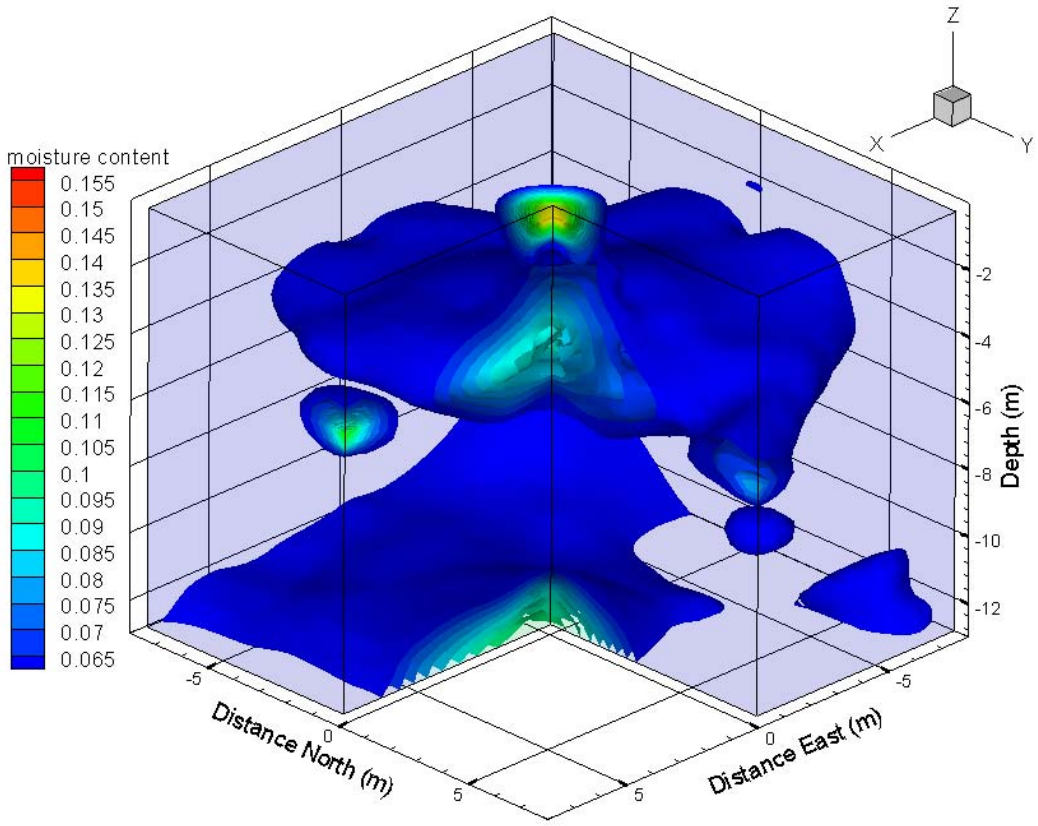


**Figure 34: 3D image of neutron probe data collected 21 days after infiltration ended.**

Figure 35 shows the percent silt and clay estimates made with the hydrometer and sieve data. This 3D image was created using the percent clay estimates for the 4 continuous core samples.

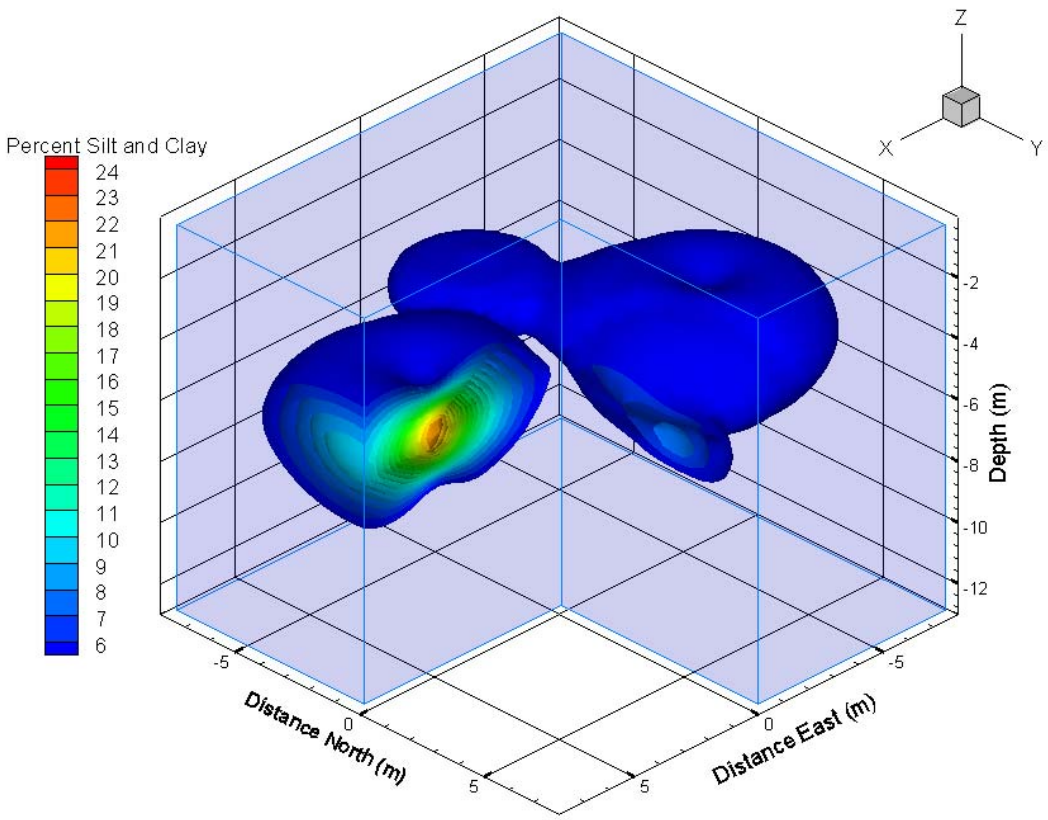


**Figure 35: Percent silt and clay estimated from correlation of 4 continuous core samples.**

To better visualize the shape of the salt pulse, the EM39 data was also plotted as a series of 3D images showing just the increase in conductivity from 3 days before the start of the salt pulse. Figures 36-46 is a series of difference images clearly showing a plume of increased conductivity growing directly under the infiltrometer. The plume appears to grow in an almost spherical shape until 25 days after the start of the pulse, Figure 39, when it begins to slowly spread laterally at 4-6m depth until the pulse ends.

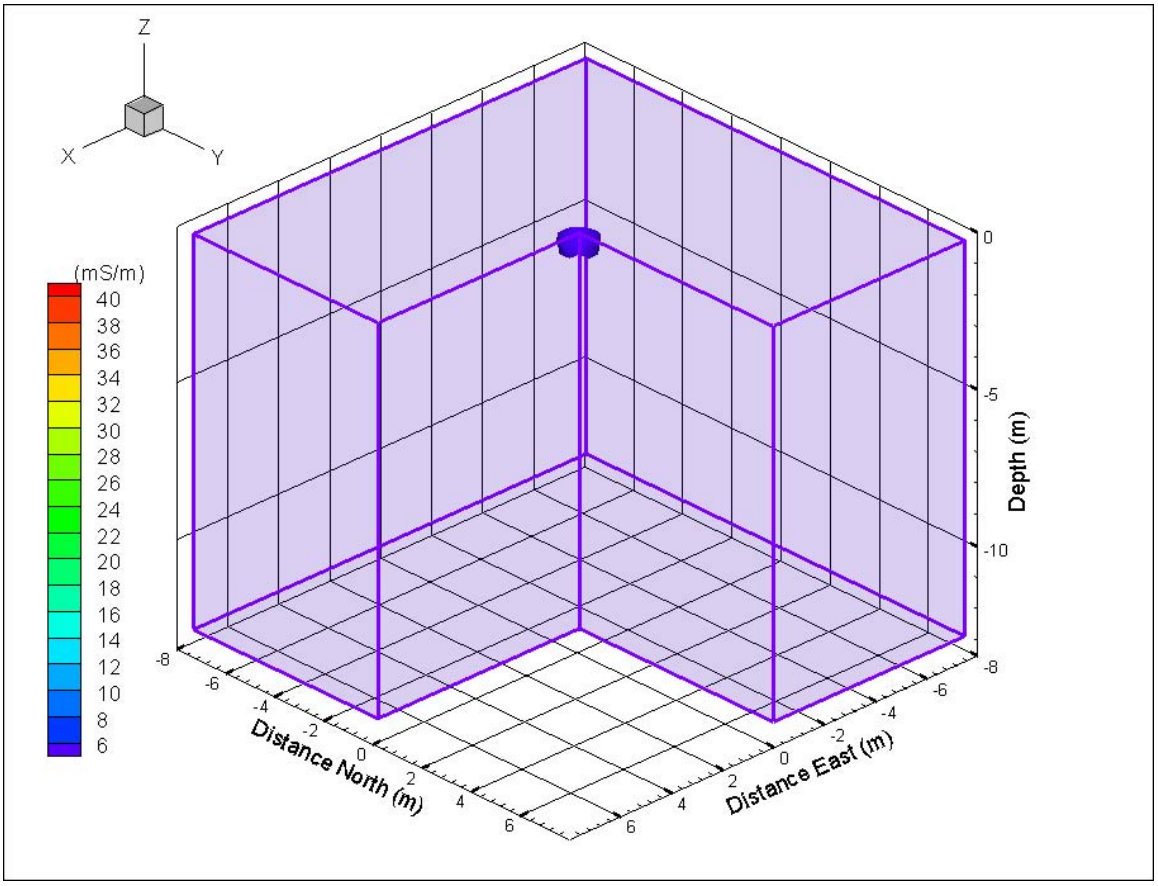


**Figure 36: Increase in conductivity (mS $m^{-1}$) from 3 days before the salt pulse began, measured 4 days after the salt pulse started.**

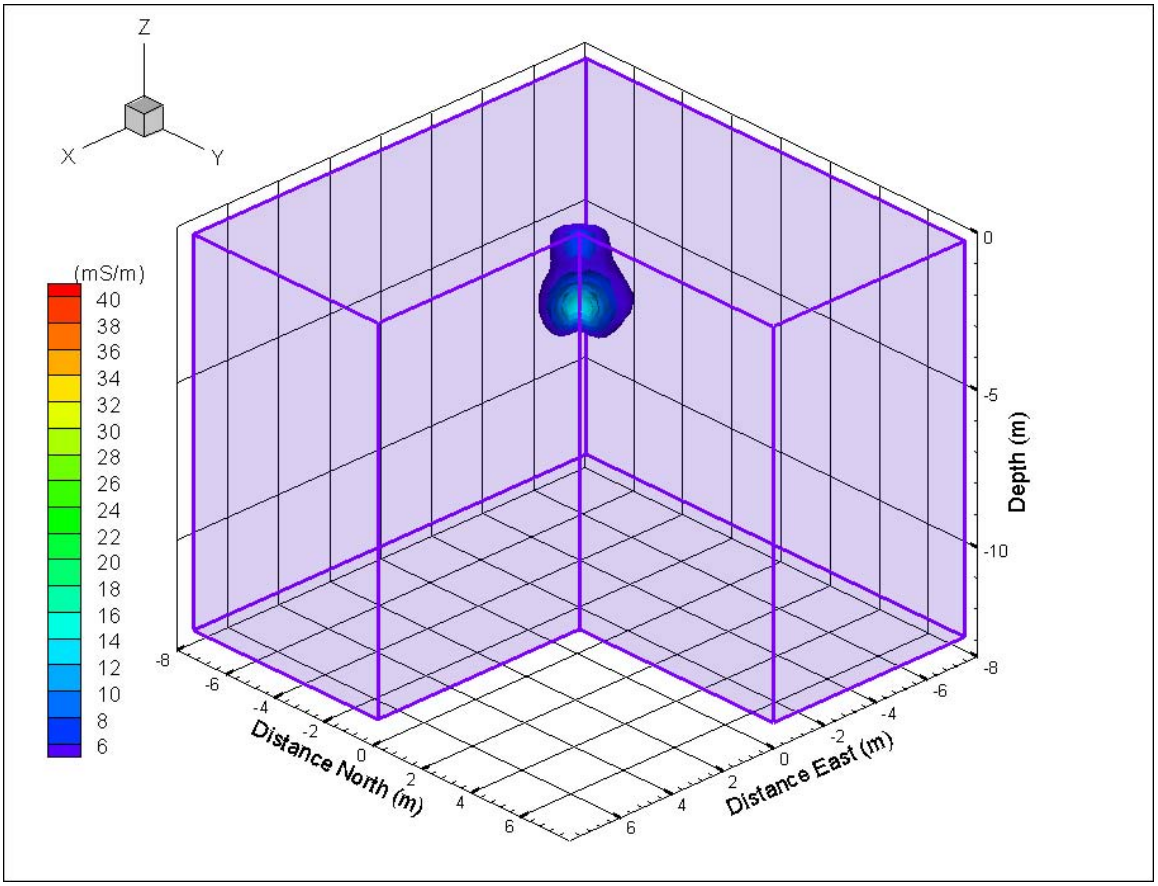


**Figure 37: Increase in conductivity (mS $m^{-1}$) from 3 days before the pulse began, measured 11 days after the salt pulse started.**

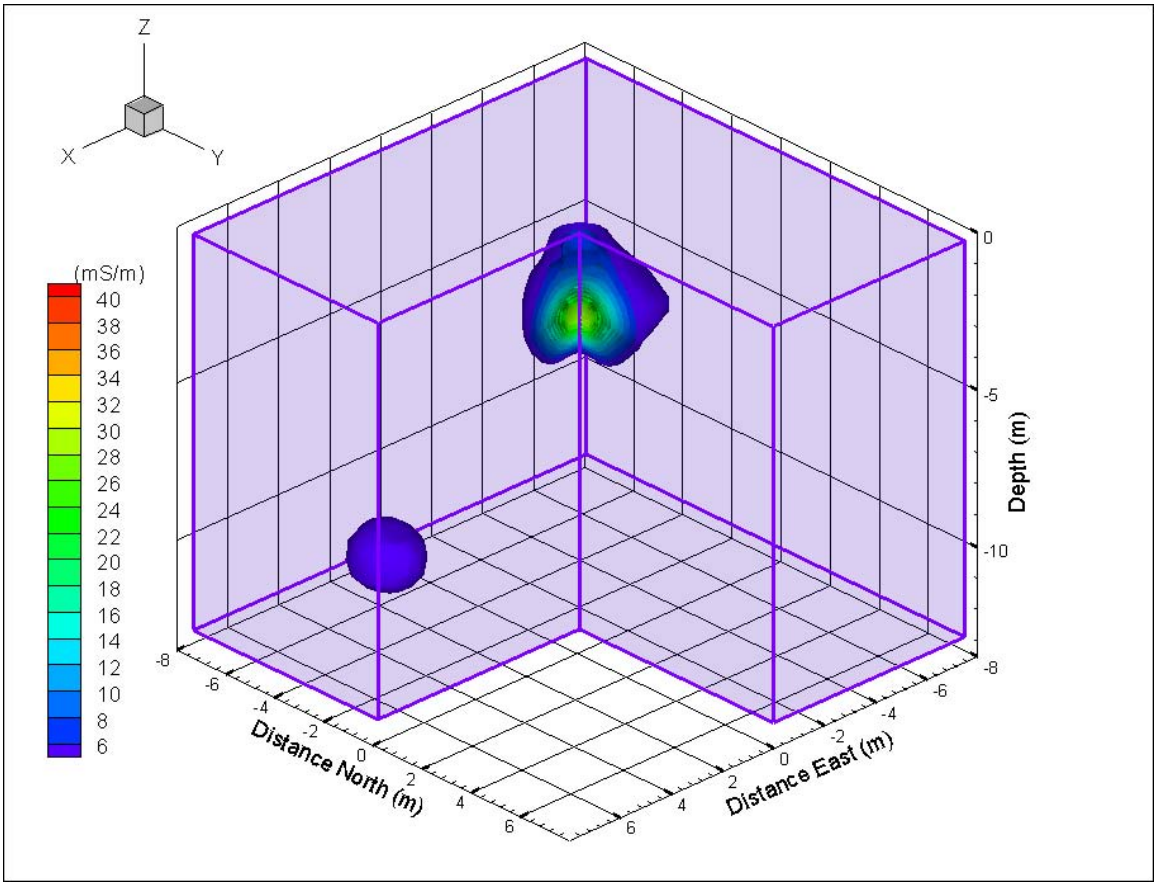


**Figure 38: Increase in conductivity (mS $m^{-1}$) from 3 days before the pulse began, measured 18 days after the salt pulse started.**

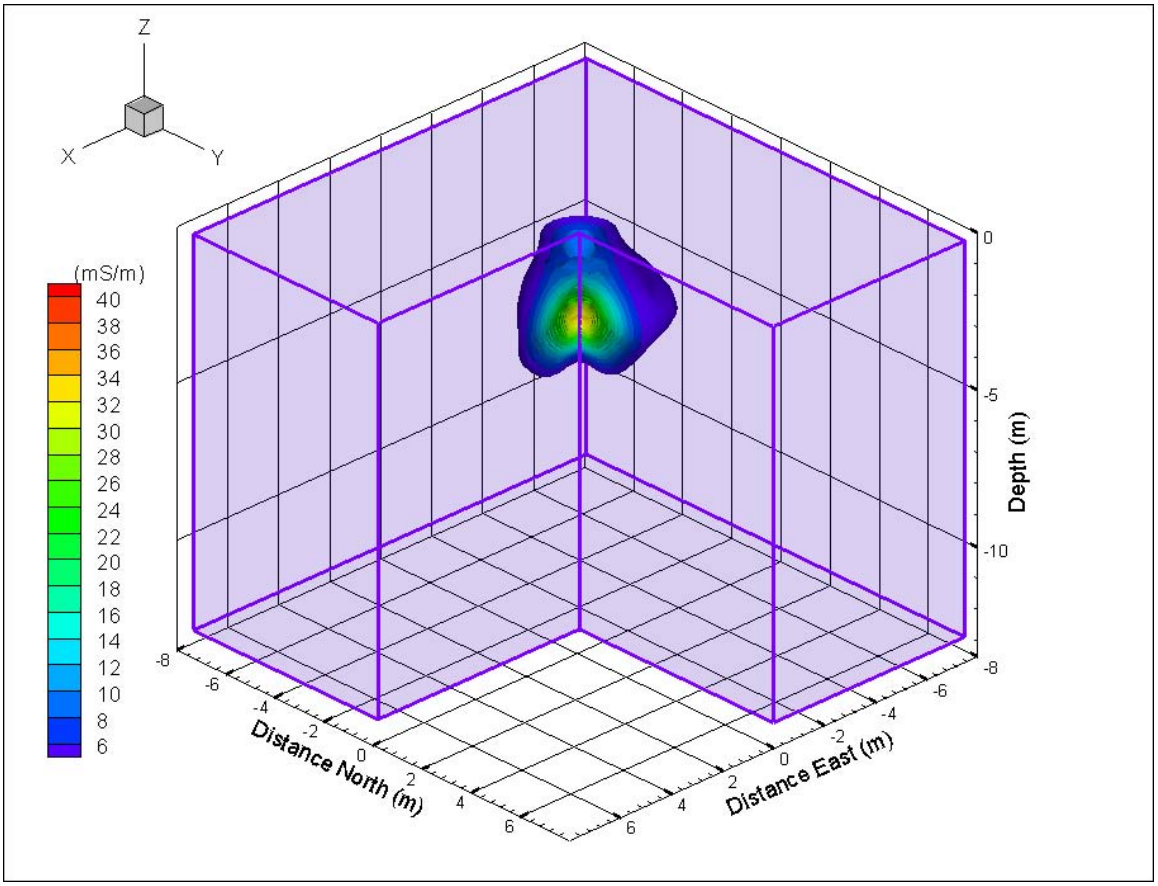


**Figure 39: Increase in conductivity (mS $m^{-1}$) from 3 days before the pulse began, measured 25 days after the salt pulse started.**

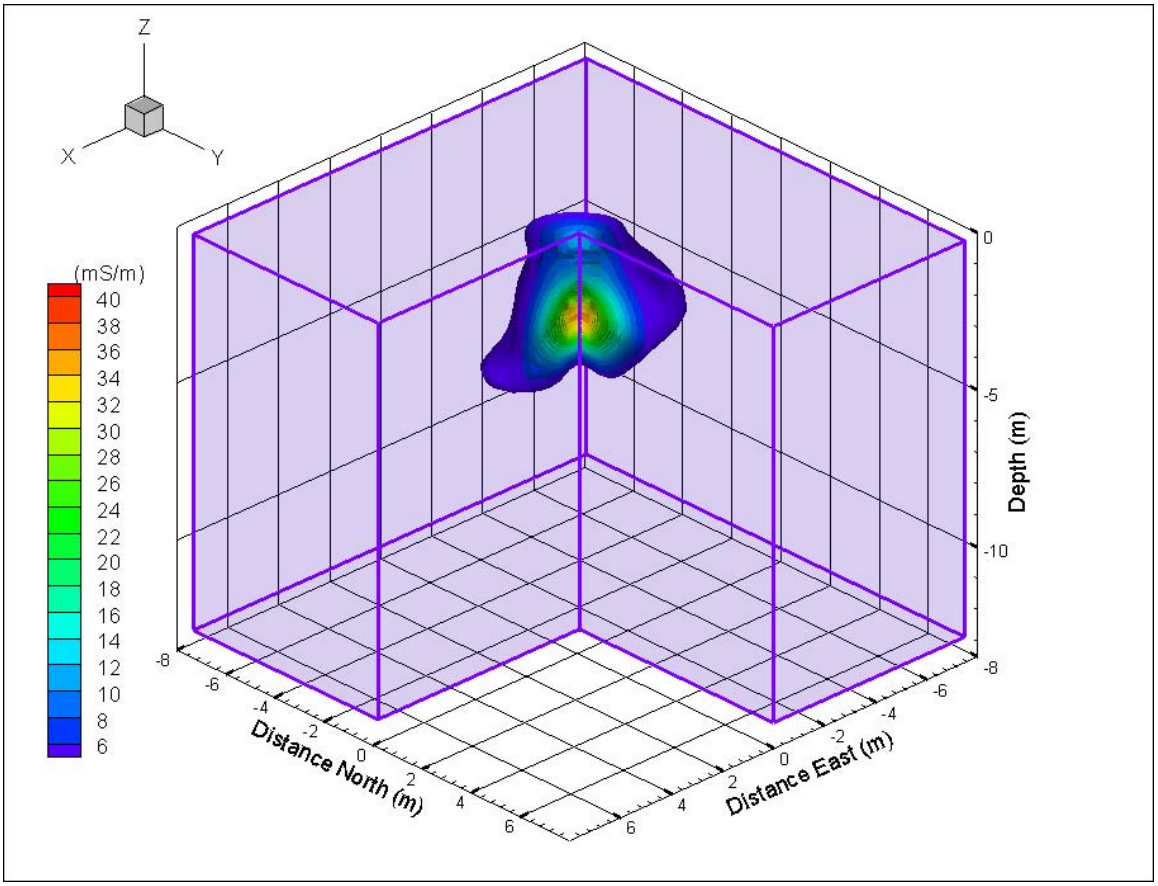


**Figure 40: Increase in conductivity (mS $m^{-1}$) from 3 days before the pulse began, measured 32 days after the salt pulse started.**

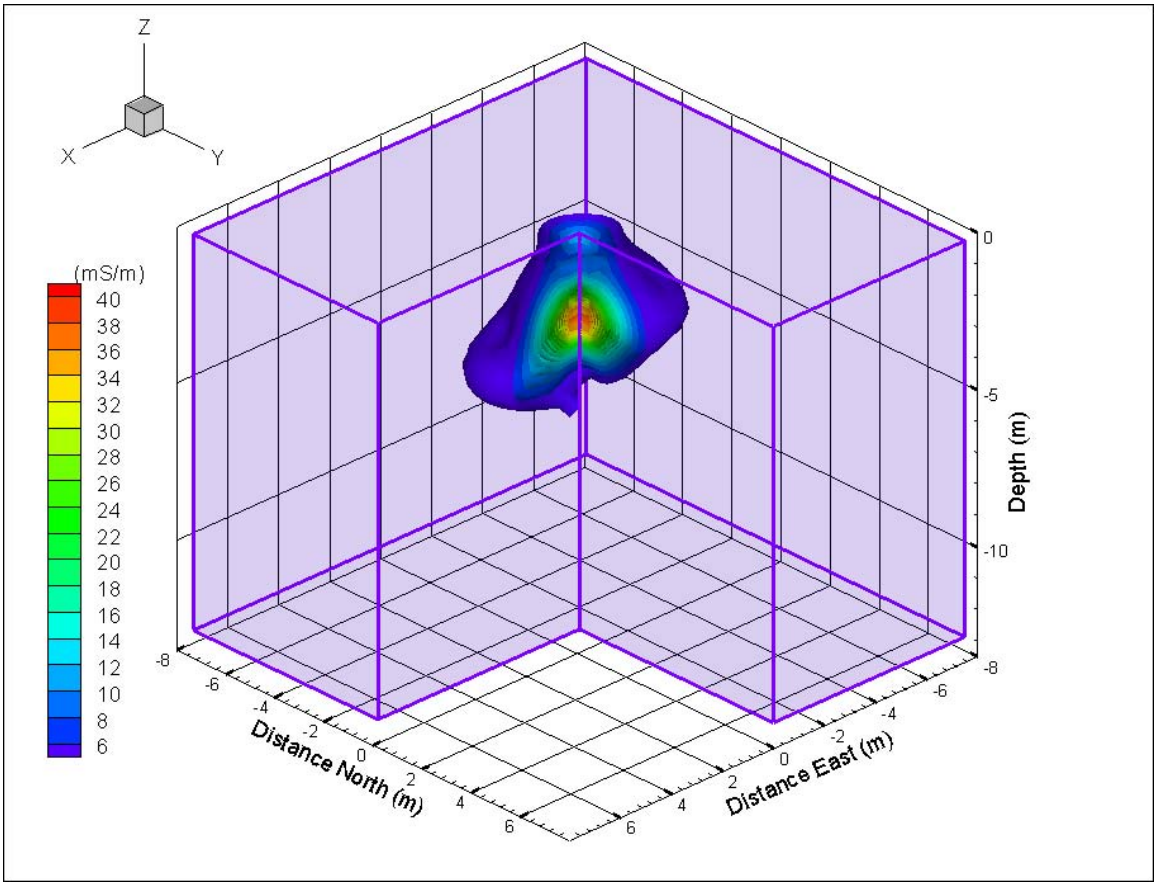


**Figure 41: Increase in conductivity (mS $m^{-1}$) from 3 days before the pulse began, measured 39 days after the salt pulse started.**

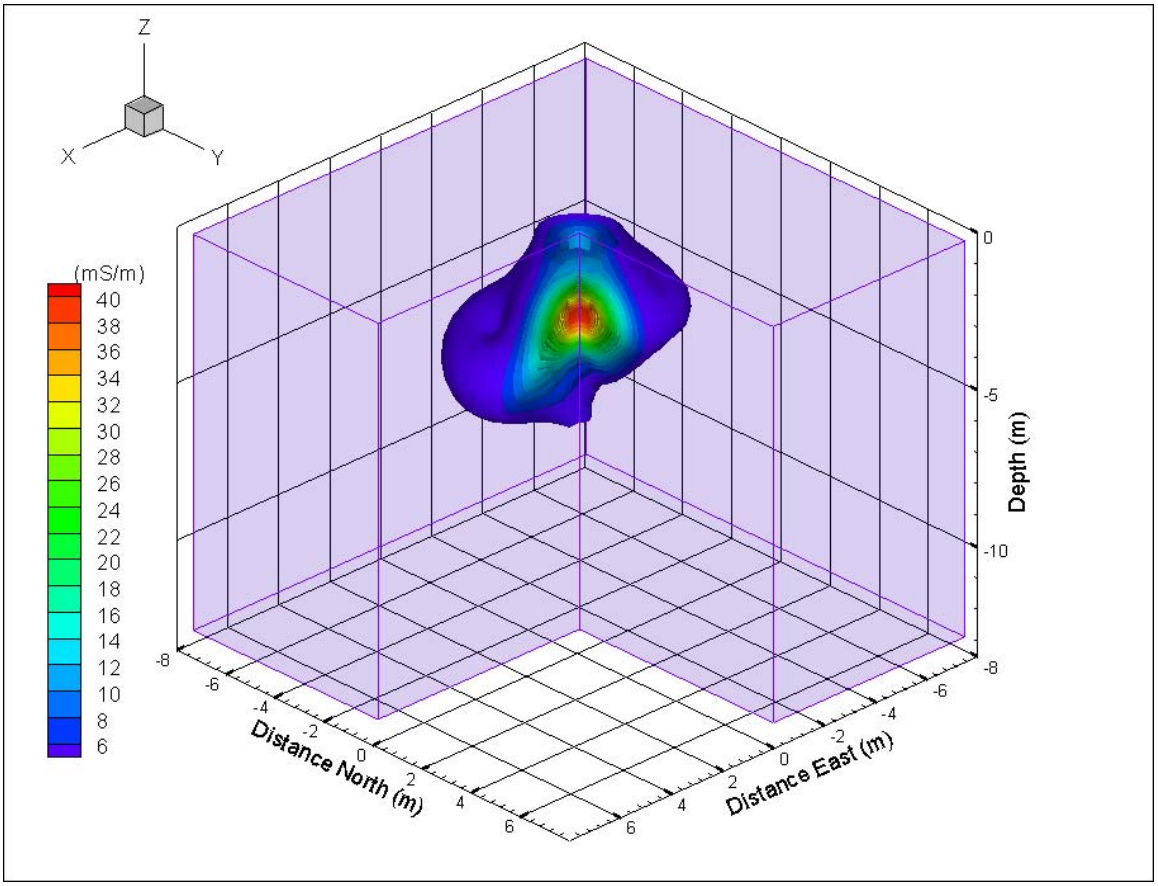


**Figure 42: Increase in conductivity (mS $m^{-1}$) from 3 days before the pulse began, measured 46 days after the salt pulse started.**

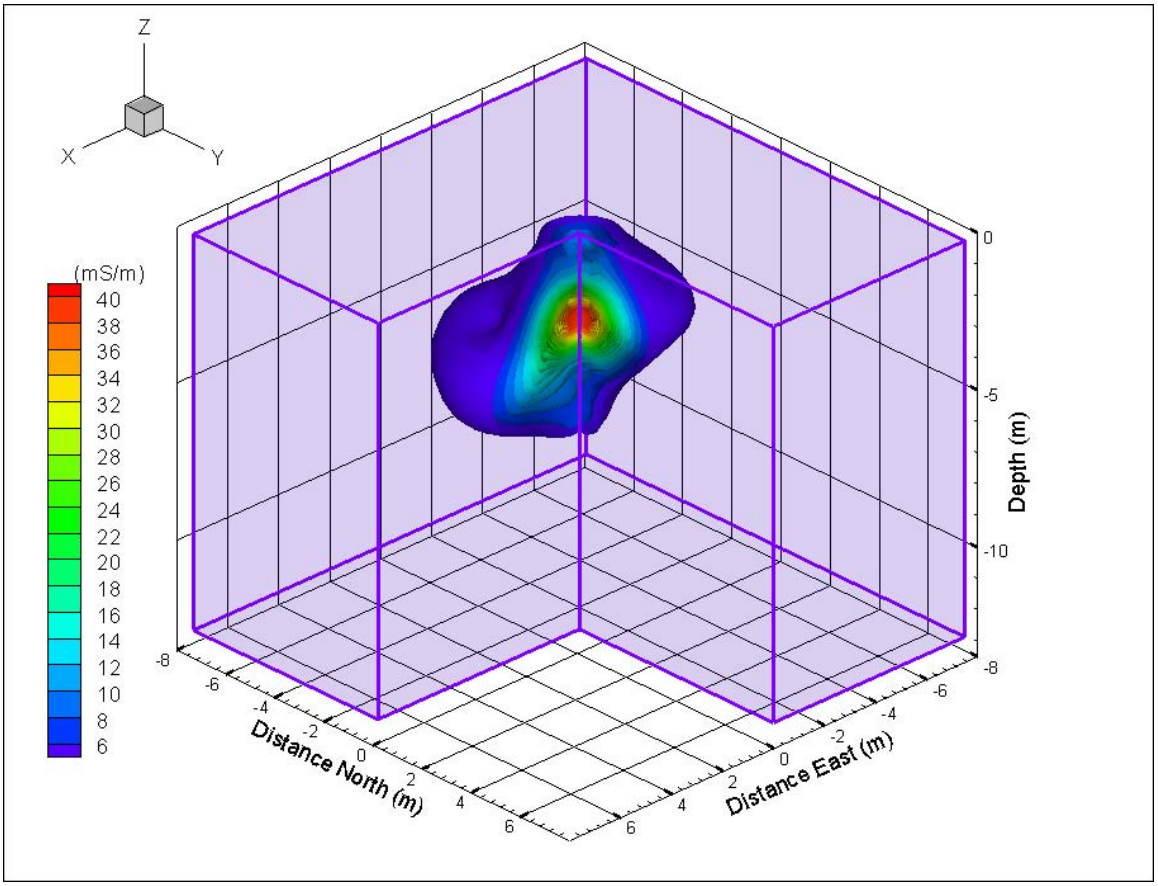


**Figure 43: Increase in conductivity (mS $m^{-1}$) from 3 days before the pulse began, measured 53 days after the salt pulse started.**

The increased conductivity seen Figure 44 is most likely due to the choice of iso-surfaces displayed and other interpolation options discussed in Appendix 1. Plotting all of the data with a minimum of 8 mS $m^{-1}$ instead of 6 mS $m^{-1}$ would have removed this anomaly. As will be seen in the sensitivity analysis, this slight increase in measured/interpolated low level conductivity will play a role in the mass calculated at a 4% threshold water content level.

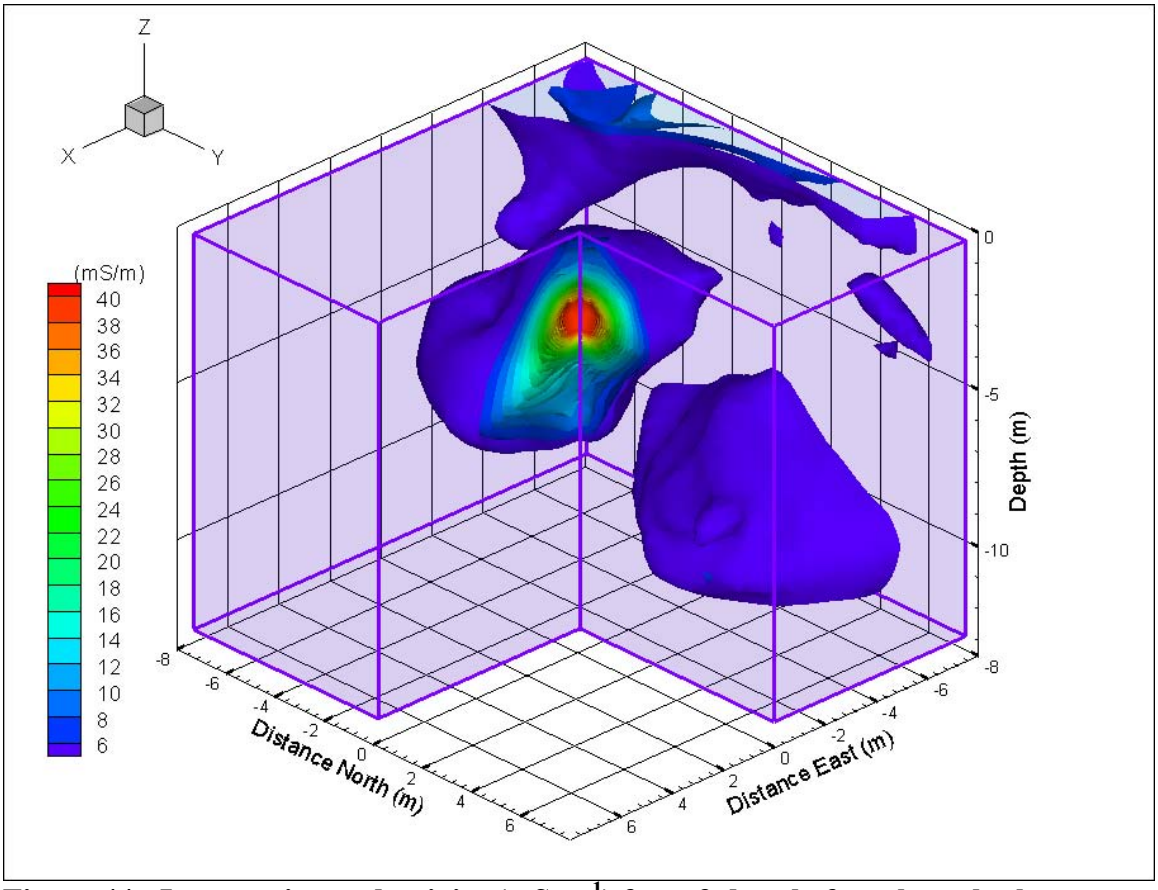


**Figure 44: Increase in conductivity (mS $m^{-1}$) from 3 days before the pulse began, measured 60 days after the salt pulse started.**

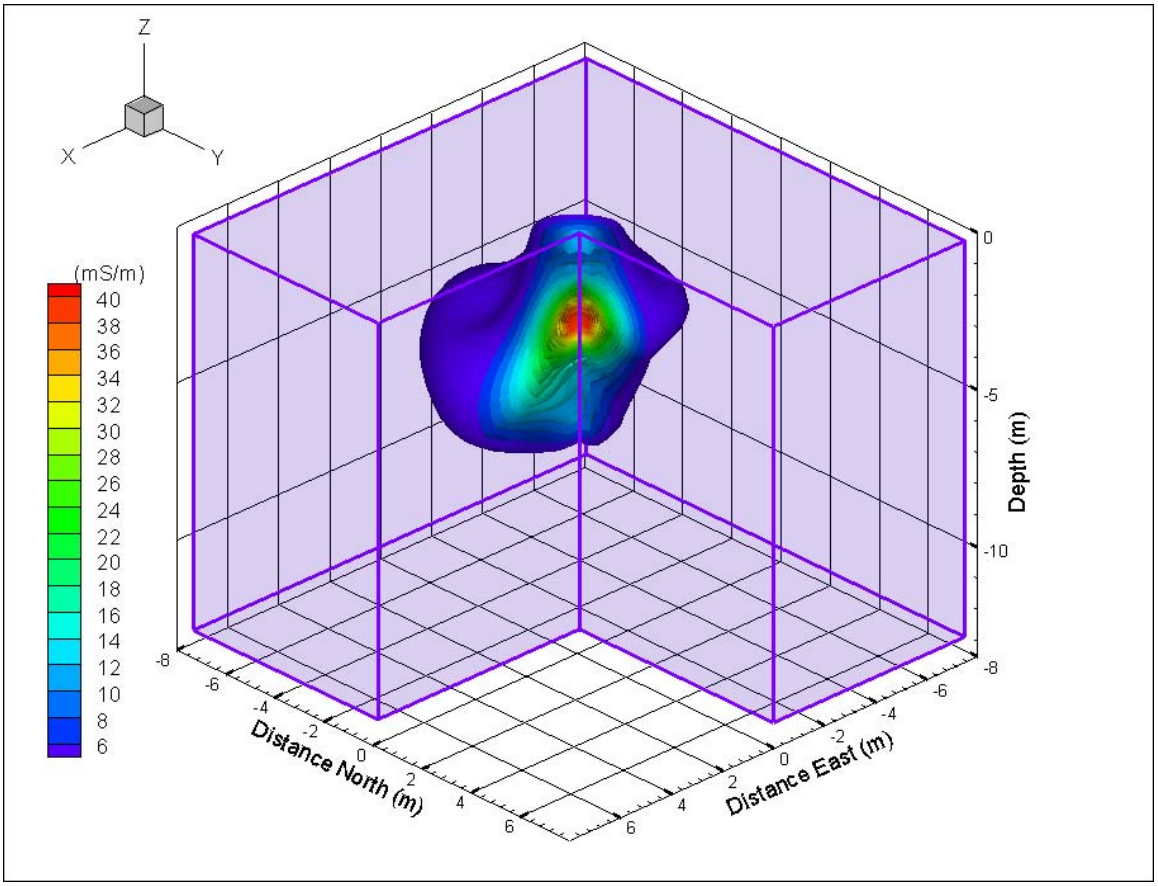


**Figure 45: Increase in conductivity (mS $m^{-1}$) from 3 days before the pulse began, measured 67 days after the salt pulse started.**

Figure 46 below is the last data set collected before the salt pulse ended, Figures 47-50 are images of data collected during the following 57-d tap water flush. During the flush, the zone of increased conductivity quickly disappears from directly under the infiltrometer near the surface. The zone of increased conductivity at 4-6m depth disappears much more slowly.

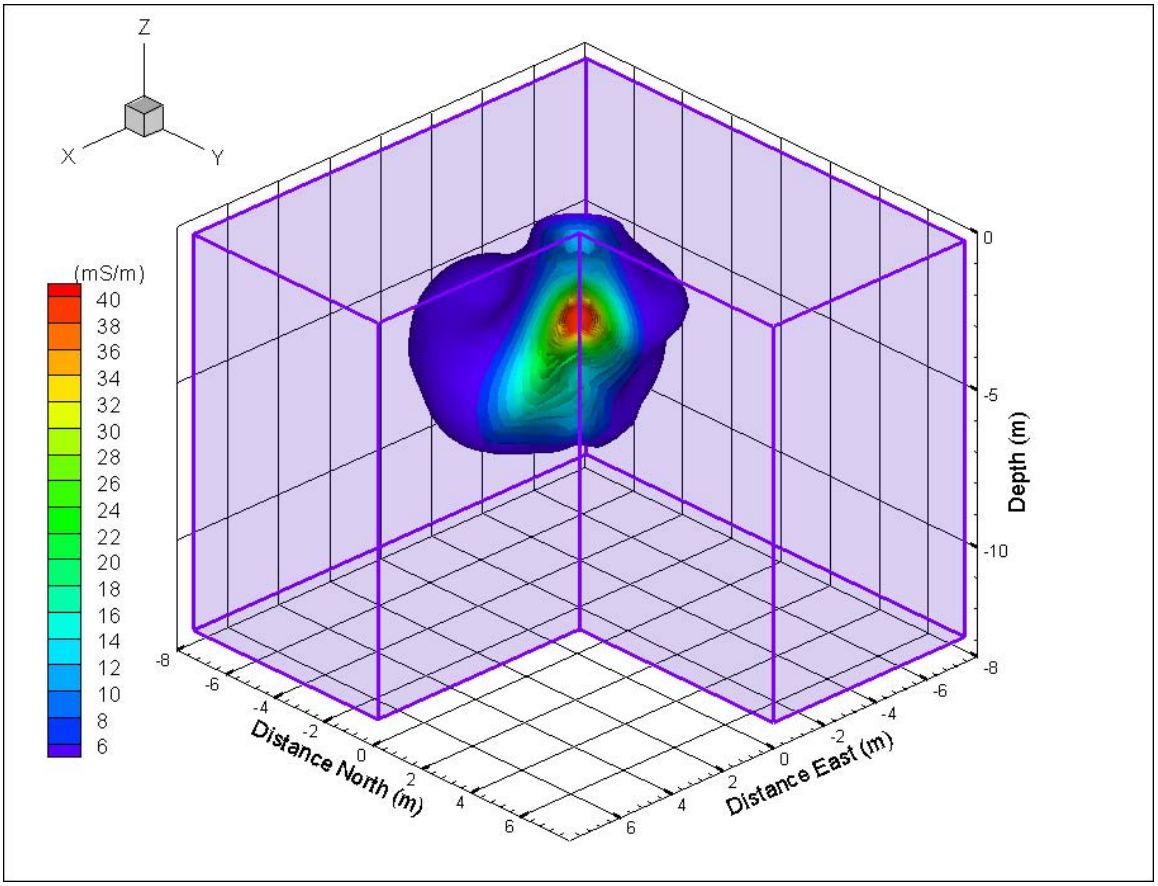


**Figure 46: Increase in conductivity (mS $m^{-1}$) from 3 days before the pulse began, measured 81 days after the salt pulse started.**

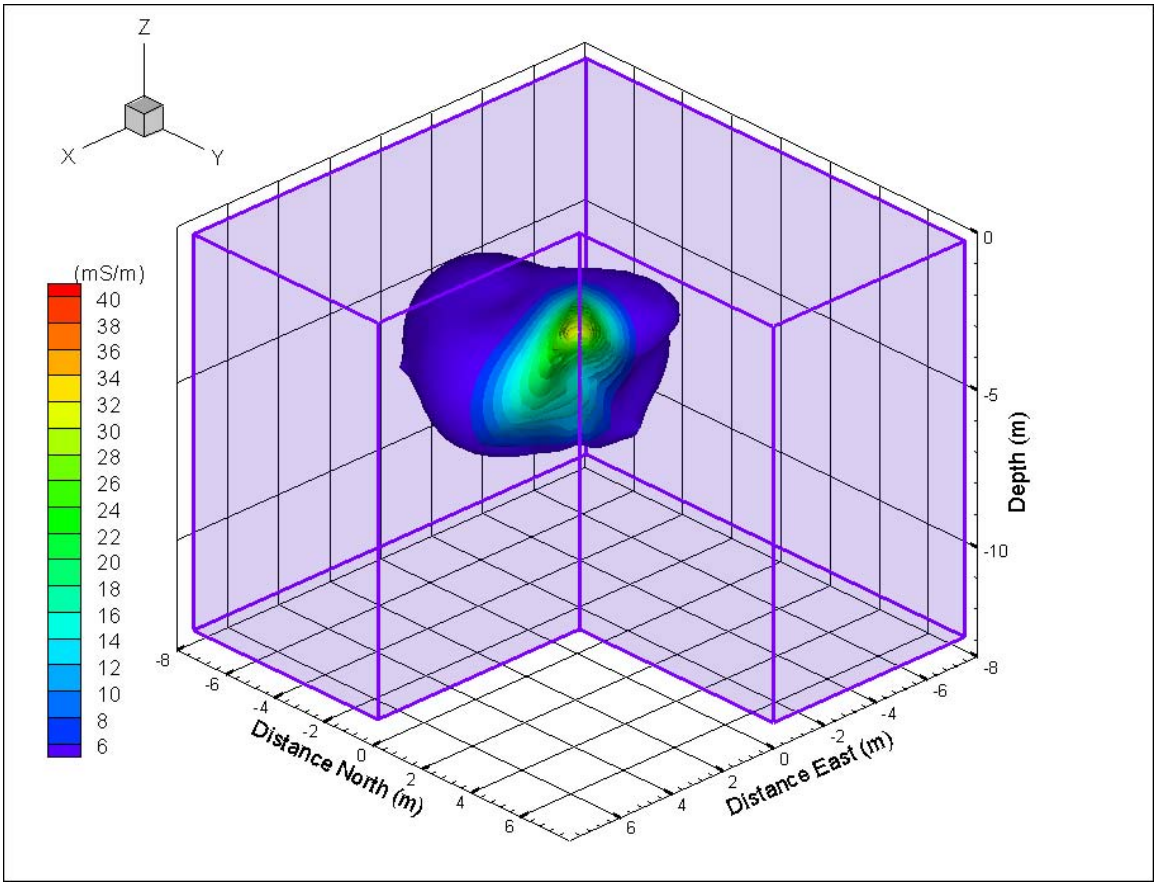


**Figure 47: Increase in conductivity (mS $m^{-1}$) from 3 days before the pulse began, measured 10 days after the salt pulse ended.**

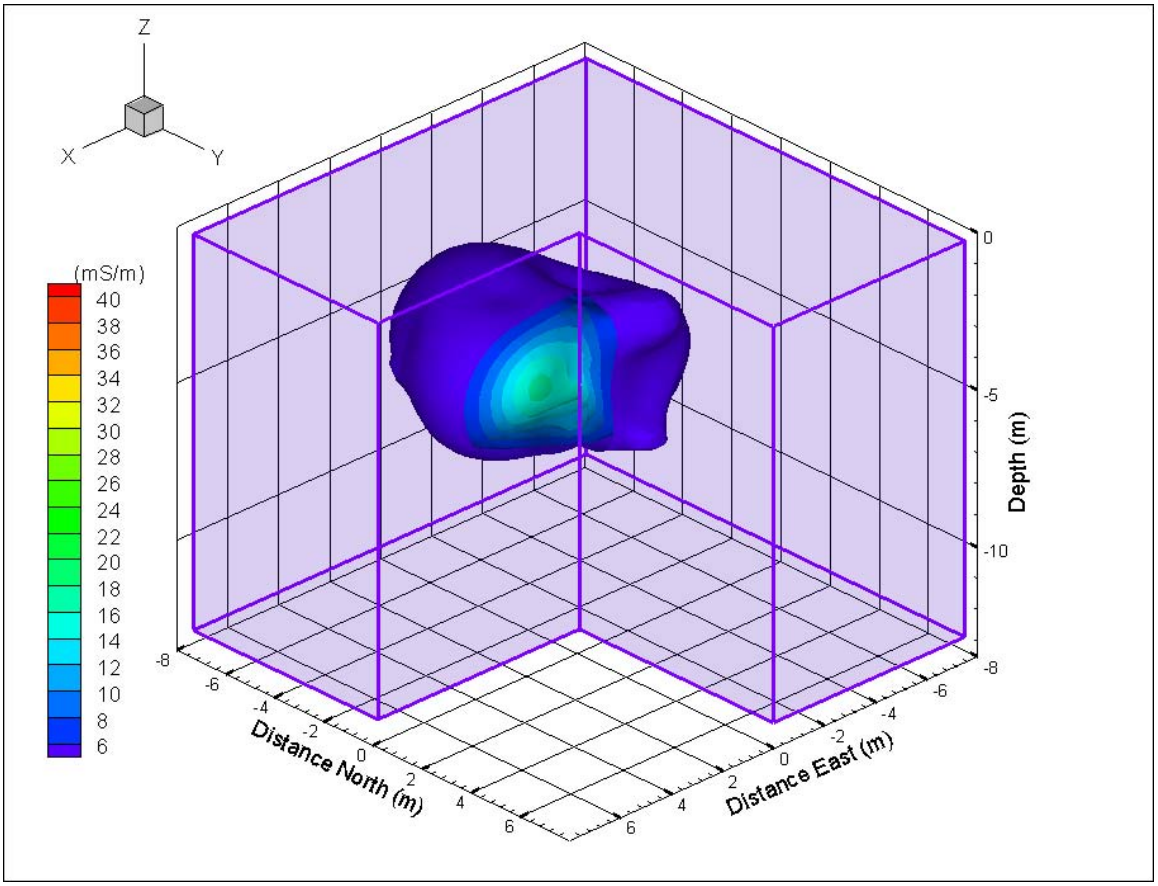


**Figure 48: Increase in conductivity (mS $m^{-1}$) from 3 days before the pulse began, measured 24 days after the salt pulse ended.**

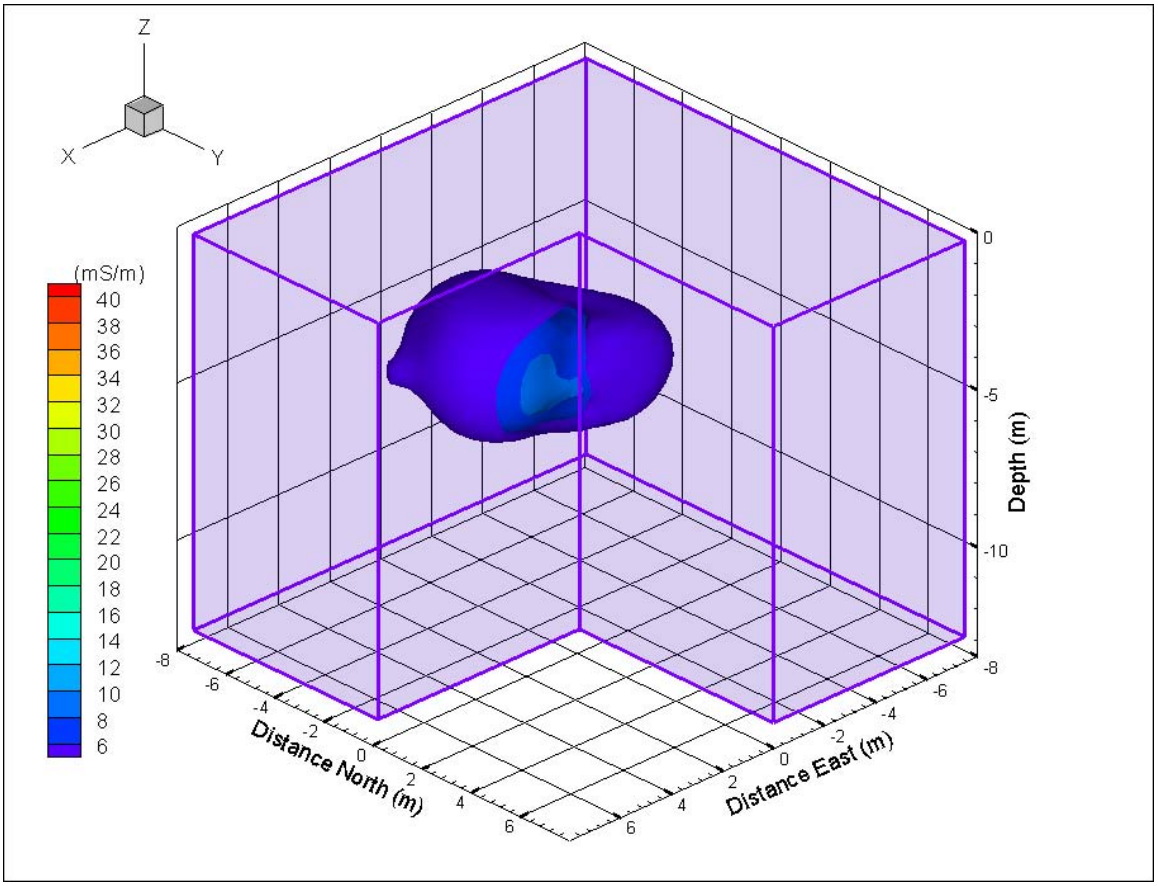


**Figure 49: Increase in conductivity (mS $m^{-1}$) from 3 days before the pulse began, measured 45 days after the salt pulse ended.**

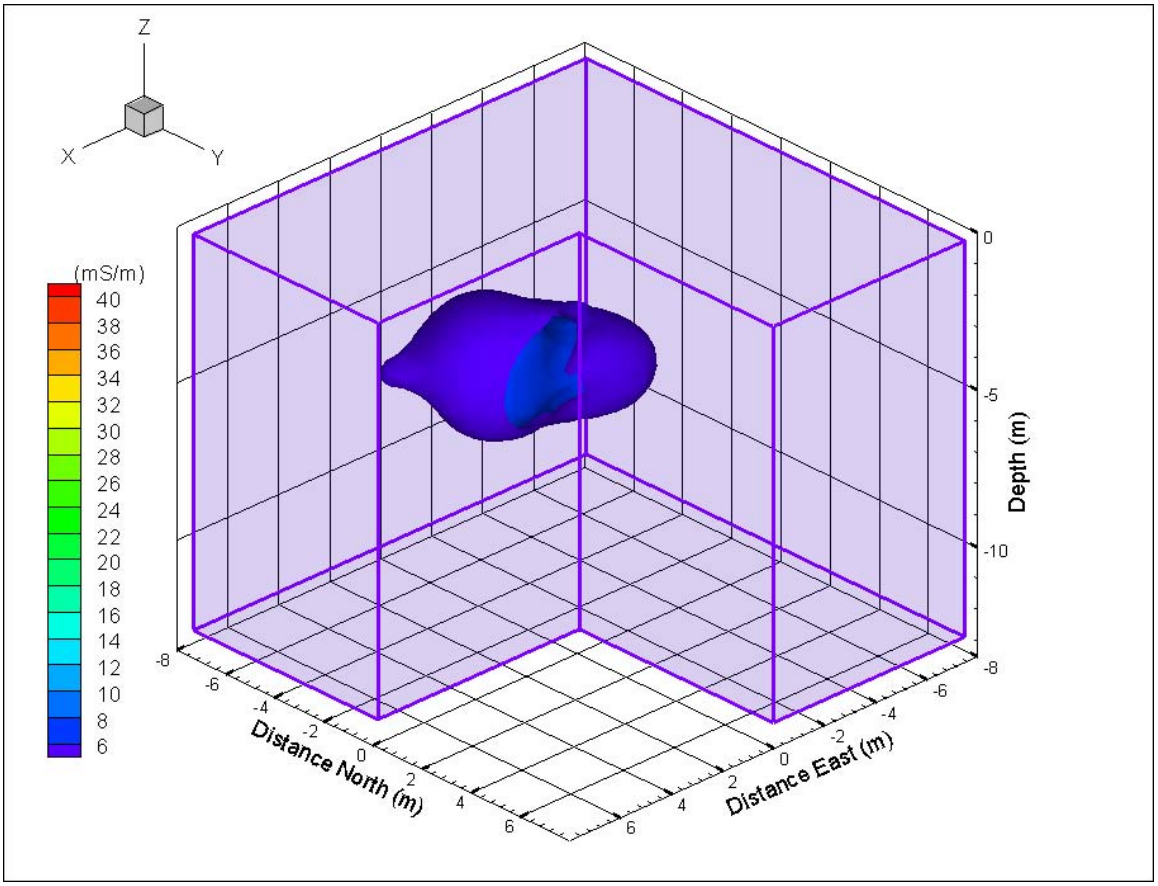


**Figure 50: Increase in conductivity (mS $m^{-1}$) from 3 days before the pulse began, measured 57 days after the salt pulse ended.**

Figures 51 and 52 were created from data set collected after infiltration had ended. The is a very sharp decrease in conductivity 7 days after infiltration ended (Figure 51), and slight increase in conductivity from that day is measured 21 days after infiltration ended (Figure 52). The readings taken 7 days after the pulse ended may not have been calibrated correctly, as discussed earlier, so this sharp decrease in conductivity is most likely false.

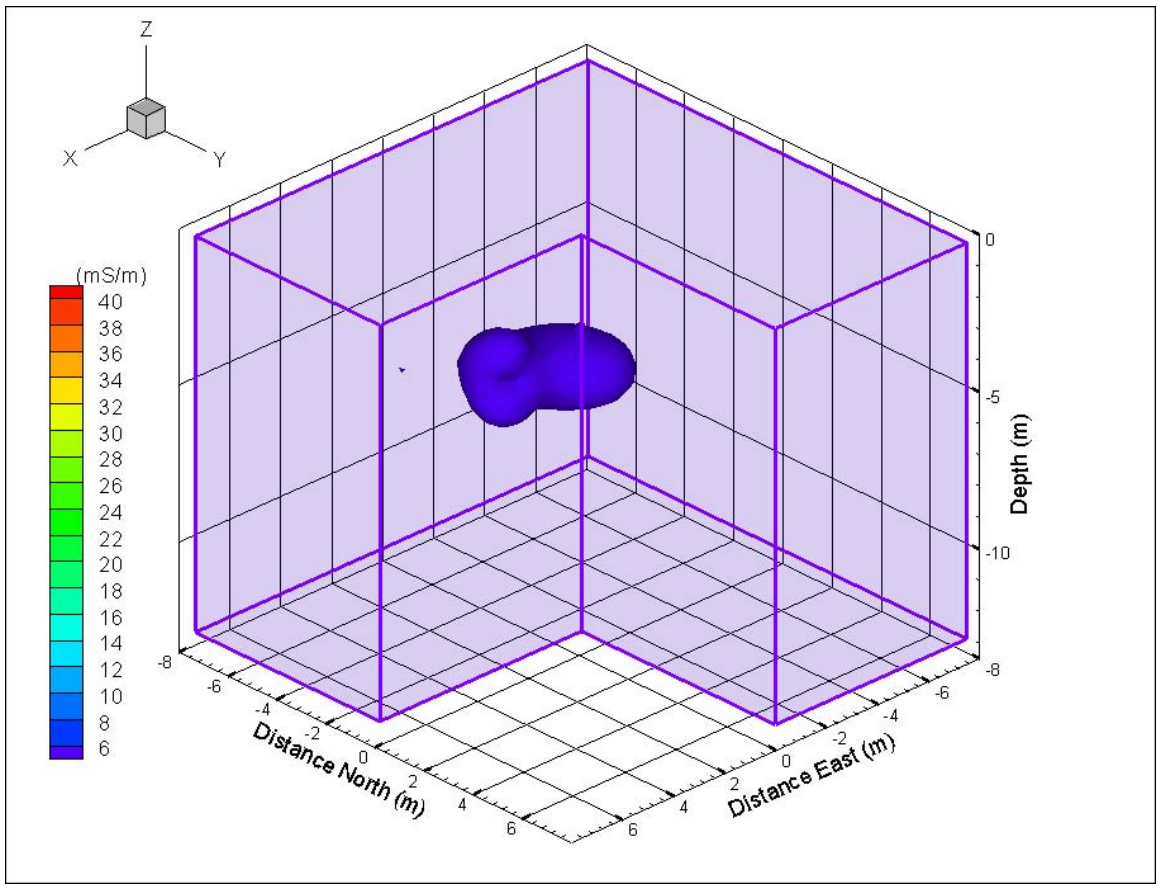


**Figure 51: Increase in conductivity (mS $m^{-1}$) from 3 days before the pulse began, measured 7 days after infiltration ended.**

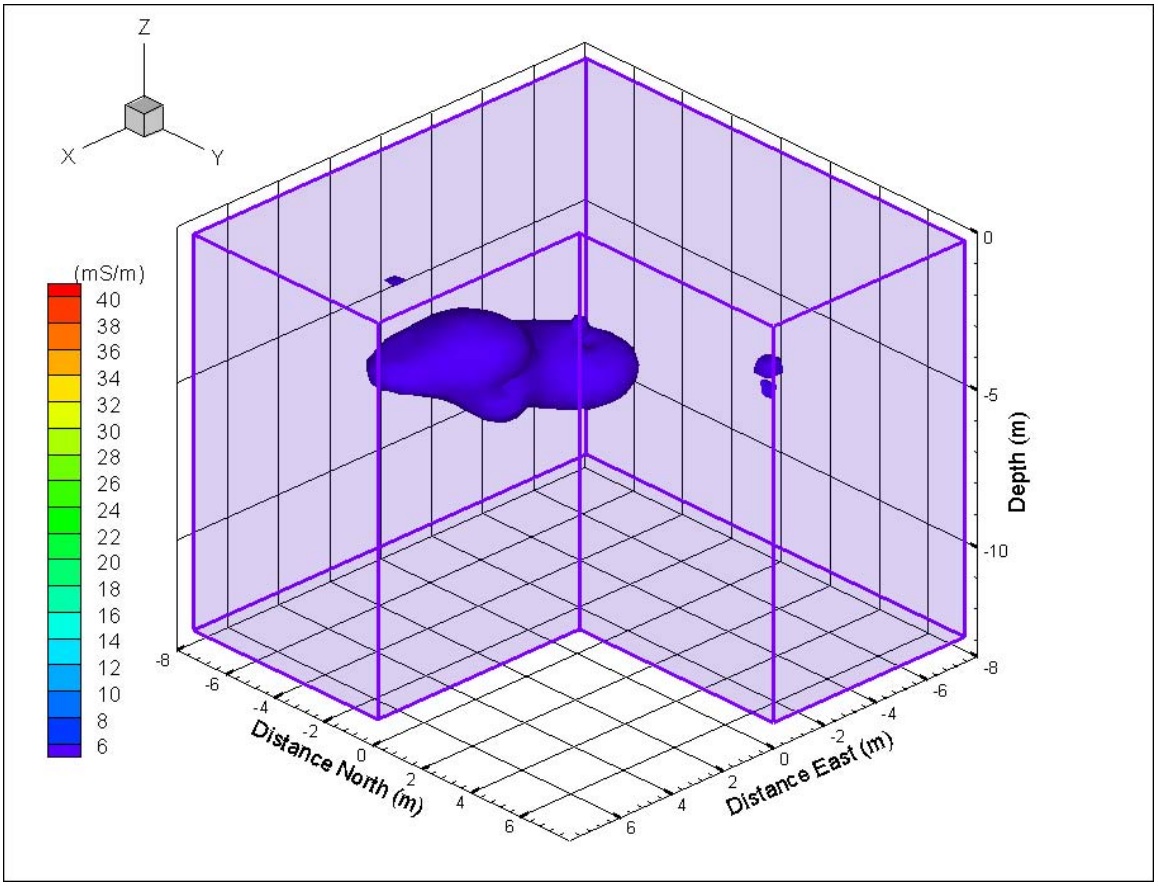


**Figure 52: Increase in conductivity (mS $m^{-1}$) from 3 days before the pulse began, measured 21 days after infiltration ended.**

**Mass Balance Calculations**

To verify that the EM39 measurements were accurately capturing the extent of the salt plume a mass balance approach was used to compare the mass of salt infiltrated at the surface with the mass of salt calculated in the soil water. To calculate the mass of salt in the soil water, the measured bulk soil conductivity was converted first to soil water conductivity and then to a concentration of NaCl. Using the volumetric water content measurement, the calculated concentration was converted to a total mass of NaCl, which was then compared to the actual mass infiltrated at the surface. As discussed earlier, these series of equations require estimates of soil conductivity (EM), soil water content (neutron probe data), clay content (continuous core sample based estimates), and temperature (thermocouples) for a temperature correction. Since most of this data was collected at different locations at the site, and have different measurement volumes, the data sets were first interpolated into the same 3D volume before performing any of the calculations. The volume used in the following calculations was described earlier, Figure 25-26. Other plotting volumes and interpolation options are discussed in Appendix 1, but had minimal effect on the overall mass balance.

A total mass of salt is calculated for each of the days that data was collected by summing the mass of salt in the soil water for each of the 59,976 cells in the 3D volume. A sensitivity analysis was conducted to determine the affect of threshold water content (immobile/mobile water content limit), percent clay estimate, and water content estimate on the calculated total mass. A summary of the different analysis is shown in Table 3, the labeling system is used in the legends of the following figures.

**Table 3: Summary of sensitivity analysis. The labels are referenced in the figure legends. Threshold water content values were 4%, 6.5%, 8%, 10% volumetrically. Water content estimates were: the actual neutron probe measurements measured for each month, an average of the 6 measured water contents for each cell, and two times the average water content for each cell. The soil percent clay estimates were based on sieve analysis results (max measured %clay was 25%), ½ of the estimated %clay for each cell (12.5% max), and twice the %clay for each cell (50% max).**

| Label | Immobile/Mobile limit vol. % | Water Content estimate | Max % Clay estimate | Temperature corrected |
|---|---|---|---|---|
| 4a | 4.0% | Measured | 25% | No |
| 4b | 4.0% | Measured | 25% | Yes |
| 4c | 4.0% | Measured | 12.5% | Yes |
| 4d | 4.0% | Measured | 50% | Yes |
| 4e | 4.0% | Avg | 25% | Yes |
| 4f | 4.0% | 2x Avg | 25% | Yes |
| 6a | 6.5% | Measured | 25% | No |
| 6b | 6.5% | Measured | 25% | Yes |
| 6c | 6.5% | Measured | 12.5% | Yes |
| 6d | 6.5% | Measured | 50% | Yes |
| 6e | 6.5% | Avg | 25% | Yes |
| 6f | 6.5% | 2x Avg | 25% | Yes |
| 8a | 8.0% | Measured | 25% | No |
| 8b | 8.0% | Measured | 25% | Yes |
| 8c | 8.0% | Measured | 12.5% | Yes |
| 8d | 8.0% | Measured | 50% | Yes |
| 8e | 8.0% | Avg | 25% | Yes |
| 8f | 8.0% | 2x Avg | 25% | Yes |
| 10a | 10.0% | Measured | 25% | No |
| 10b | 10.0% | Measured | 25% | Yes |
| 10c | 10.0% | Measured | 12.5% | Yes |
| 10d | 10.0% | Measured | 50% | Yes |
| 10e | 10.0% | Avg | 25% | Yes |
| 10f | 10.0% | 2x Avg | 25% | Yes |

Rhoades et al. (1989,1990) suggests a threshold water content of 10% to perform the calculation of soil salinity, but the calculable limit of immobile/mobile water content, as found by solving Eq [7], is 3.5% volumetrically. Rhoades et al (1976) also found however, that the value of threshold water content could be as low as 5% for sandy soils and as high as 14% in clay-rich soils. Lab analysis by Baker (2001) found that residual

moisture contents of soils from the site varied between 5.7% and 12.4%, with most of the samples falling between 6% and 8%. The sensitivity analysis by Rhoades et al. (1988) was focused on agricultural soils and the relationship between a saturated pasted extract and bulk soil conductivity measurement. In that sensitivity analysis the tested range of water content was 10-60% volumetrically. Additionally, the minimum bulk soil conductivity tested by Rhoades (1988,1990) was 200 mS $m^{-1}$, which is more the double the maximum bulk soil conductivity measured at our site. Since the soil water content was so low at our site, mass balance calculations were conducted at 4, 6.5, 8 and 10% threshold water contents. The result of changing this parameter, as well as temperature correcting the data is shown in Figure 53. The data is presented at the mass of salt calculated to be with in the volume for each data set. The cumulative amount of salt added at the surface is shown as a red line labeled "Infiltrated" in this and subsequent figures.

From Figure 53 it is clear that as the threshold water content value is decreased, the total mass of salt increases dramatically. The mass calculated with a 4% threshold water content is two orders of magnitude larger than the mass calculated with a 10% threshold water content. The cause for this increase in mass is understood by reexamining Eqs. [9-12]. If the interpolated soil water content for any given cell is below the threshold water content (ie, all of the water is considered immobile) Eq [10] becomes zero. If Eq. [10] is zero, Eq. [9] can not be solved, and soil water conductivity can not be calculated. Since almost all of the soil water contents measured are below 10%, varying the threshold water content limit significantly alters the number of cells considered to contain "mobile" salt, and therefore included in the calculation of total mass.

Presumably, if the soils at the site had higher water contents, as with the soils tested by Rhoades, the value of threshold water content would have less impact on the calculation of mobile water conductivity. The variation in calculated mass from one day to the next increases as the threshold water content limit is decreased for this same reason.

Figure 53 also shows that temperature correction of the data plays a strong part in the calculation of total mass. The overall effect of the temperature correction is an increase the mass calculated, with a smaller increase occurring as the summer progress and the average soil temperature warms to near the 25ºC correction temperature.

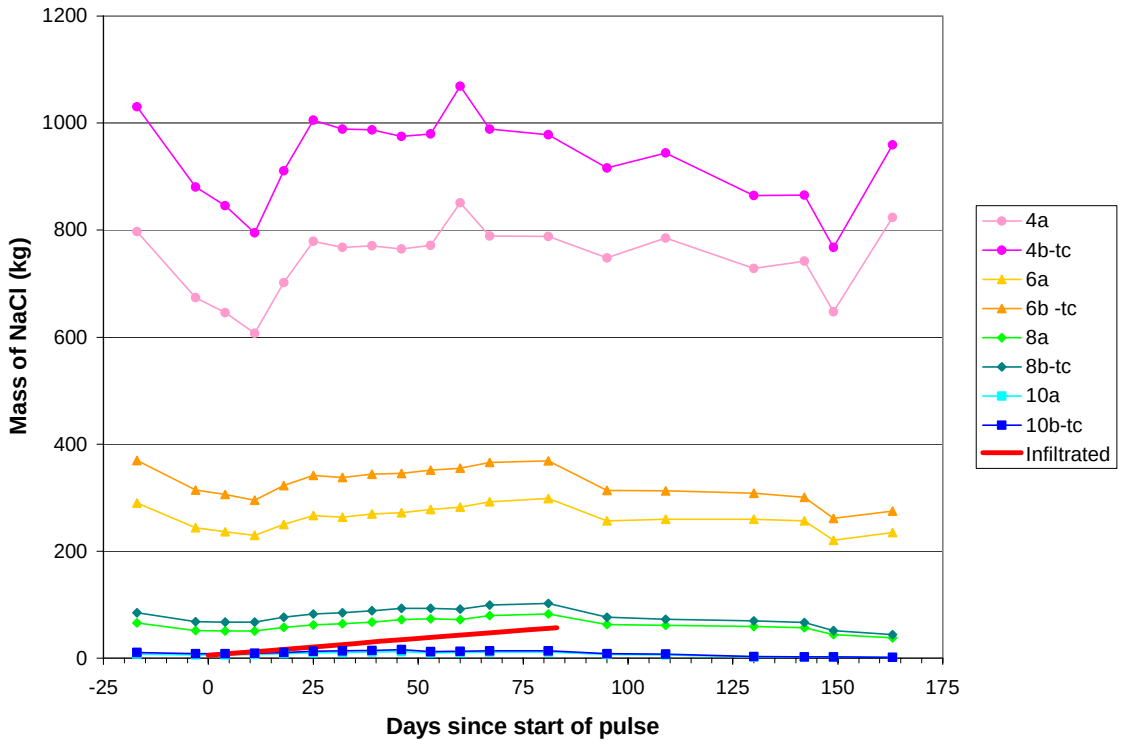


**Figure 53: Total mass in 3D volume for each scenario in sensitivity analysis, a denotes calculations from interpolations of raw EM39 data, b-tc denotes temperature corrected data.**

Because preexisting soil salts or other dissolved solids may be increasing the mobile water conductivity, the data was also calculated as a change in mass from pre-salt

pulse conditions. Figure 54 is the same data as presented in Figure 50, but now is plotted as the change in mass from 3 days prior to the salt pulse start. Mass calculations from 17 days prior to the salt pulse were not used to constrain pre-salt pulse conductivity due to poor temperature equilibration of the probe on this day. The mass results for this were day are included in the graphs of total mass to show the sensitivity of the probe to temperature equilibration.

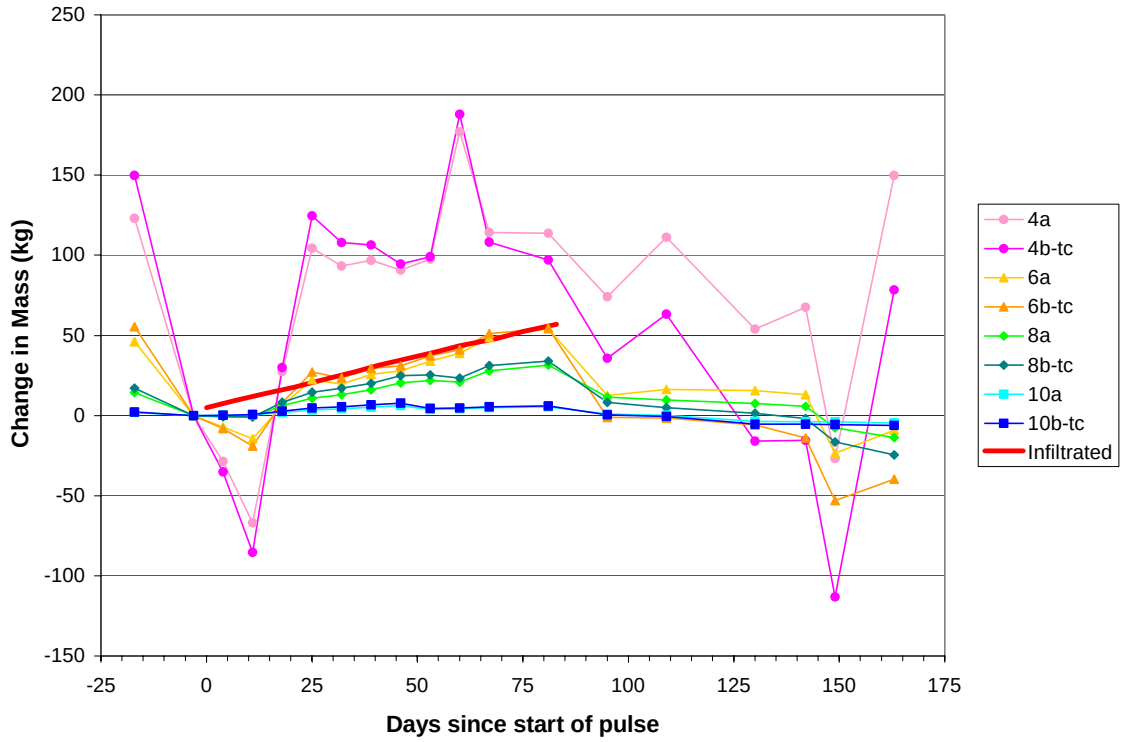


**Figure 54: Total mass calculated using 8% and 10% θt values, a denotes calculations from interpolations of raw EM39 data, b-tc denotes temperature corrected data.**

The calculations at 4% threshold water content show poor fit to the mass infiltrated in both Figures 53 and 54. Figure 55 shows the change in mass calculated for just the 6.5%, 8% and 10% threshold water contents. The over-calculation of mass at

6.5% threshold water content, Figure 53, has been eliminated by plotting the mass a change from background. The estimate at 8% threshold water content changes from an over estimate to an under estimate of the mass when compared to background. The calculated mass at 10% threshold water content is very small in both Figures 54 and 55. The data calculated using the 6.5% and 8% threshold water contents show a clear correlation to the timing of the end of the salt pulse and the end of infiltration, with a sharp decrease in mass seen after each event.

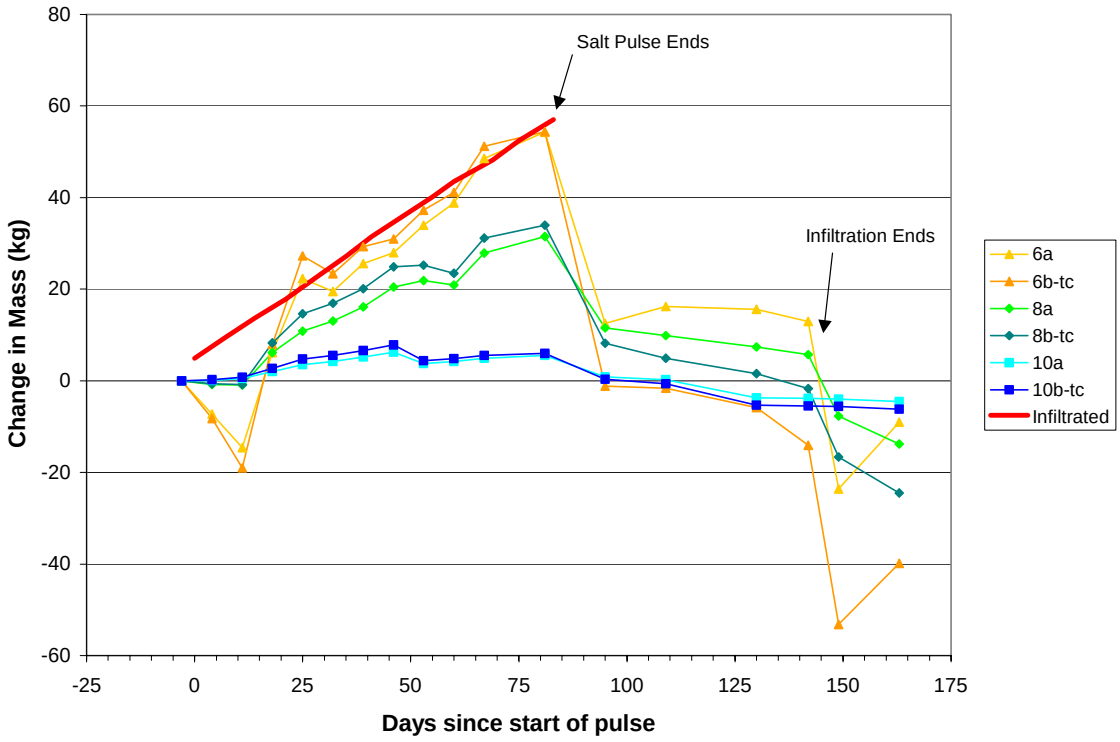


**Figure 55: Change in mass for 6.5, 8 and 10% threshold water contents, a denotes calculations from interpolations of raw EM39 data, b-tc denotes temperature corrected data.**

The affect of varying the percent clay estimate was also studied and shown in Figure 53. Calculations were made for each of the four threshold water content values

using the original percent clay estimate, half of the percent clay estimate, and twice the percent clay estimate. As with the temperature correction, the affect of changing the percent clay estimate was strongest at 4% threshold water content. The percent clay estimate had almost no affect on the calculated mass when the threshold water content was 10%, which agrees with the sensitivity analysis by Rhoades et al (1988). An increase in the percent clay estimate leads to a decrease in the calculated mass of salt. The decrease in salt mass is explained by examining Eq. [3], where it is seen that an increase in soil particle conductivity (due to percent clay increase) increases the first term in Eq. [3]. As the first term gets larger, the second term of the equation (soil water conductibility) decreases. All of the data for the percent clay analysis was temperature corrected.

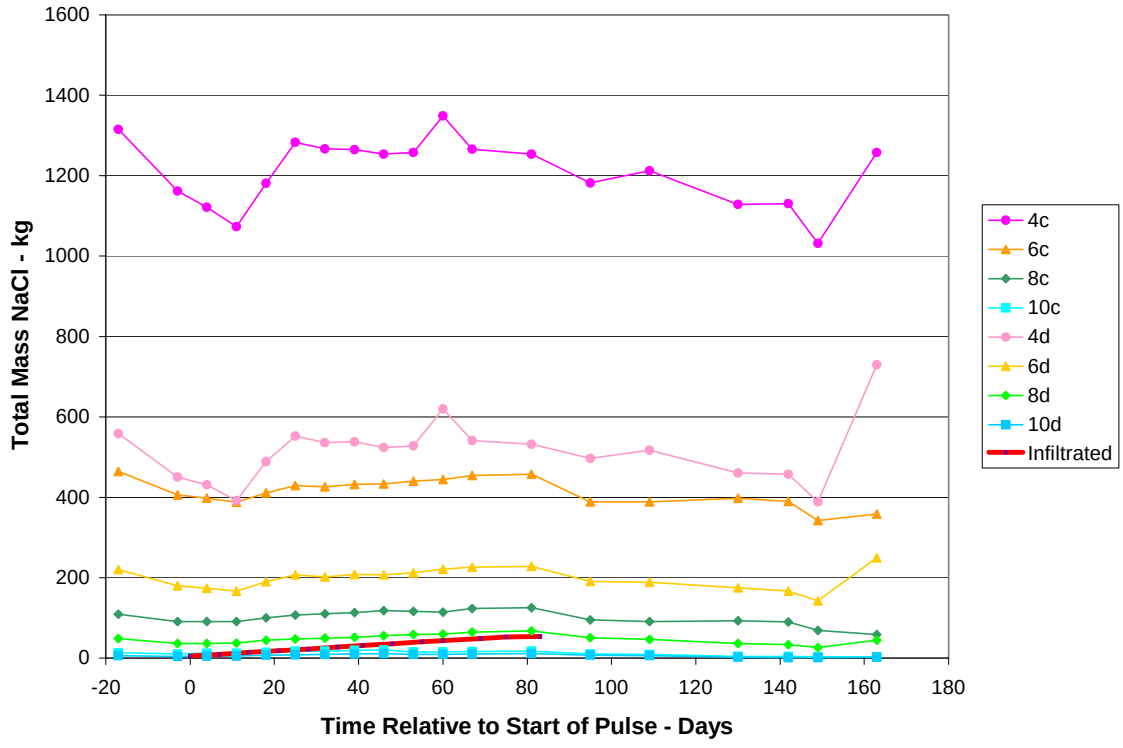


**Figure 56: Total mass for 6.5%, 8% and 10% threshold water contents, c denotes ½ the original clay estimate for each cell, d denotes twice the original clay estimate for each cell.**

In Figures 57 and 58 it is clear that the estimates with a 6.5% threshold water content give the closest fit with the infiltrated mass of salt. Estimates at 8% and 10% threshold water content consistently underestimate the actual mass infiltrated. The variation in mass from one day and the next decreases with increasing threshold water content. Doubling the percent clay caused a large increase in mass for the last data set collected, which is probably due to the low water content measured on that day.

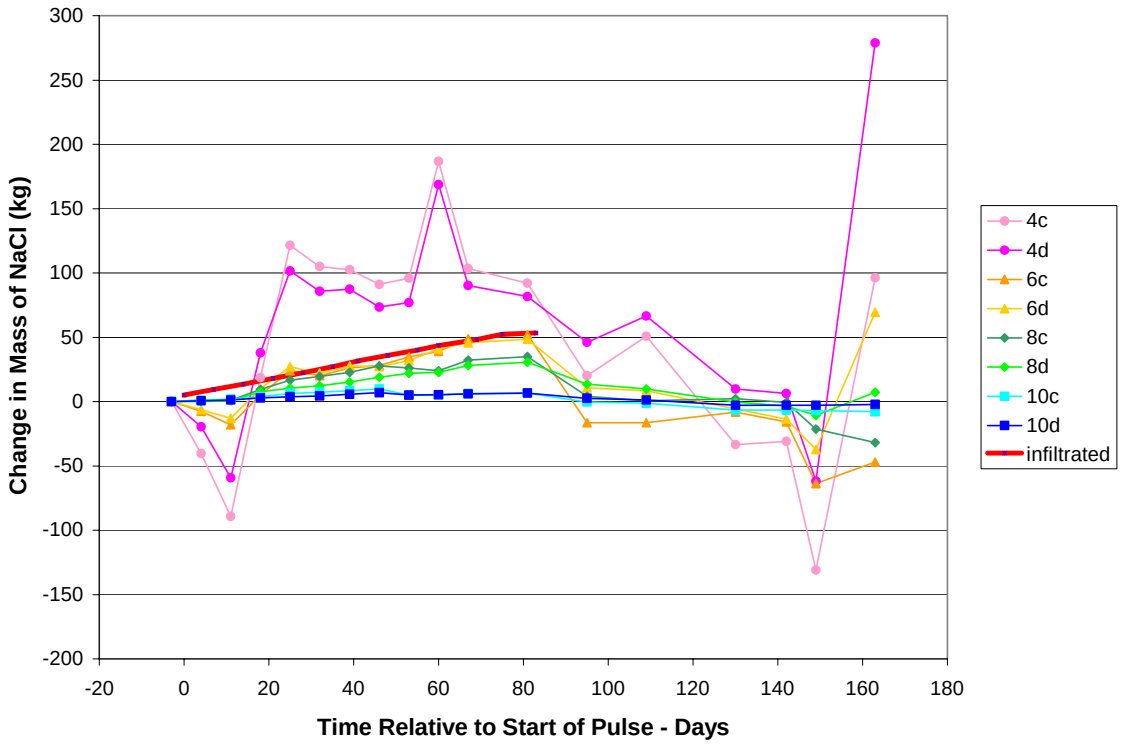


**Figure 57: Change in mass from 3 days before pulse started, c denotes ½ the original clay estimate for each cell, d denotes twice the original clay estimate for each cell.**

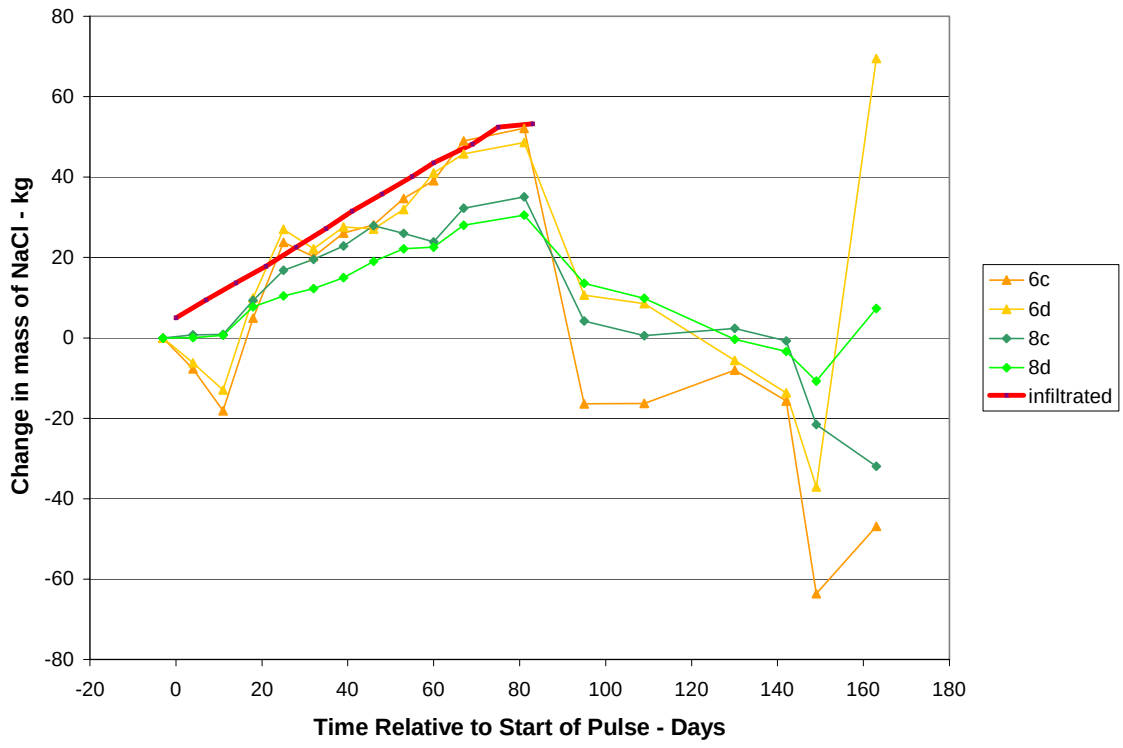


**Figure 58: Change in mass from 3 days before salt pulse starts at ½ and 2 times the original percent clay estimate for 6.5% and 8% threshold water content.**

Figure 59 shows the affect on of changing the actual water content measurement values (neutron probe readings) as well as the threshold water content values. In the previous mass balance results the mass was calculated using the actual water content measured each month. The same neutron probe measurement was used for the three or four EM measurements taken in that same month. However, if the neutron probe data was taken at the beginning of the month, for example, it might not be representative of the conditions measured with the EM at the end of the month. The repeatability of the neutron probe results show that this is probably not a significant change, however the mass calculation is sensitive to small changes in water content as already shown. To test this sensitivity the "measured" monthly water contents values were replaced with 1) an

average of the 6 monthly neutron probe readings collected during the salt pulse, and 2) twice the average water content.

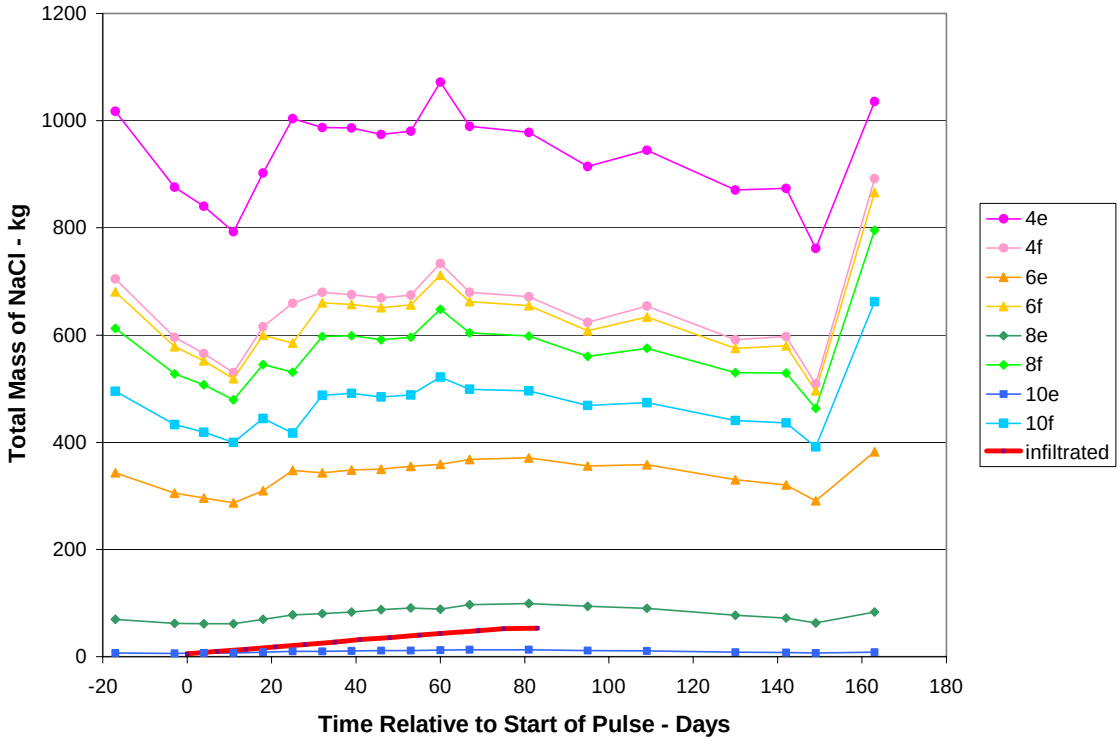


**Figure 59: Results showing the effect of changing the soil water content estimate, e denotes an average of the 6 monthly neutron readings, f denotes twice the average water content in each cell.**

Neutron probe and EM data were collected on the same two days after infiltration ended (last two data points in series). These final two neutron measurements were not used in the calculation of the average water content used in the sensitivity analysis, and it really is not appropriate to apply the average or twice average estimates to these days. The use of an average water content for the mass calculations of these days results in an increase in mass (the same effect as lowering the threshold water content).

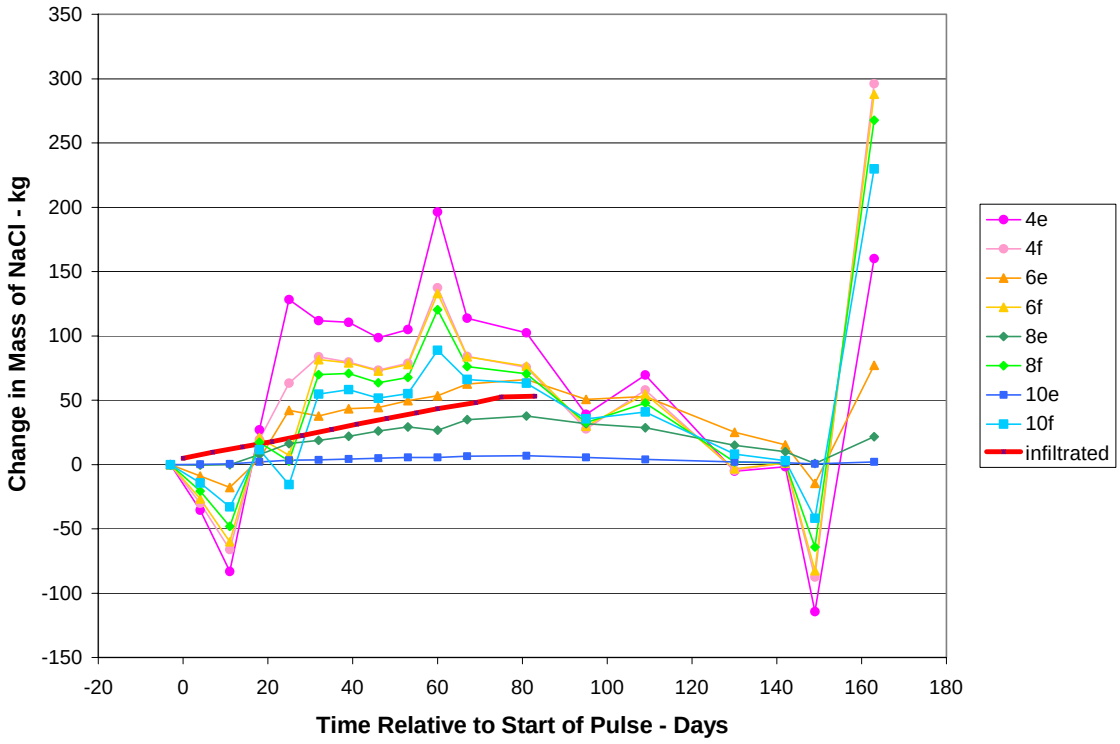


**Figure 60: Change in mass from 3 days before pulse started, e denotes an average of the 6 monthly neutron readings, f denotes twice the average water content in each cell.**

In both Figures 60 and 61, it is clear that doubling the estimate of soil water content both increases the total mass calculated, and increases the variation between one day and the next. It is very unlikely that the actual neutron probe measurements could have been off by this much however, and most conventional methods of determining soil water content should give accurate enough results to use in this calculation.

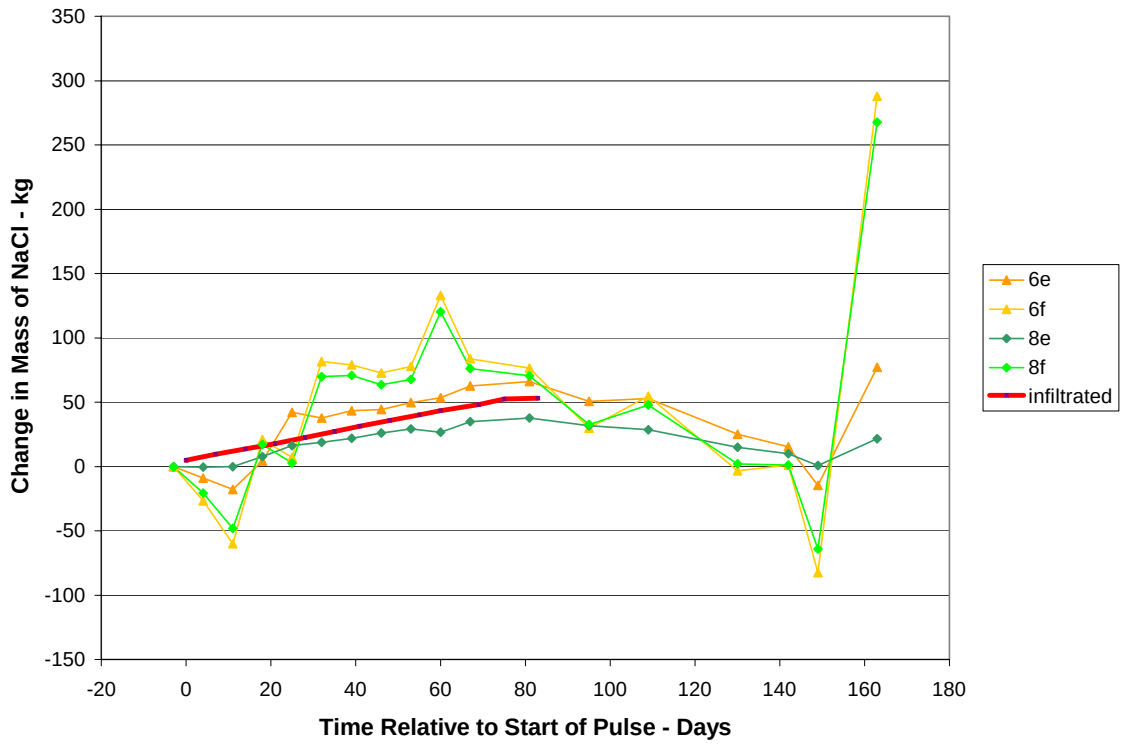


**Figure 61: Doubling the "measured" water content can cause the data to go from a good fit to a poor fit. Data for 6.5% and 8% threshold water content.**

Figure 62 shows just the results for all the 6.5% threshold water content analysis. All the trends are very similar, except for the calculations using variations of the estimated soil water content (e and f analysis). The decrease in mass during the initial days of the pulse and the sharp decrease in mass directly after infiltration ends are most likely due to nonlinearity of the model at $EC_w$ levels below 400 mS $m^{-1}$. The low conductivity of the tap water, which fills most of the pores during these days of very low calculated mass, is causing scatter in the results.

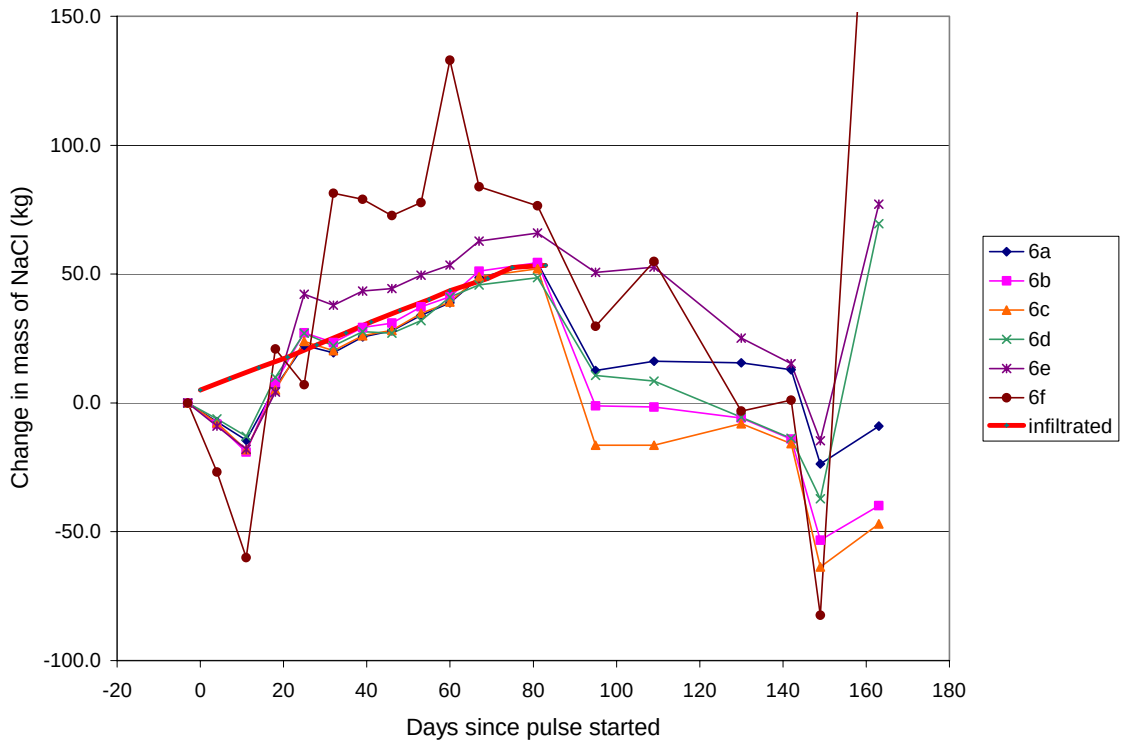


**Figure 62: The change in mass from 3 days before the salt pulse for all scenarios at 6.5% threshold water content.**

Figure 63 shows the estimated soil water mass of NaCl compared to the know mass of salt infiltrated at the surface. The fit is very good, $r^2 = 0.92$, for the original non-temperature corrected data. An ideal fit would be an $r^2 = 1$, slope= 1, and an intercept of 0. The fit of all the analysis is shown in Table 3. Estimates with 8% threshold water content actually have a higher $r^2$ than the 6.5% due to the less significant decrease in mass calculated at 8% during the first 3 data sets.

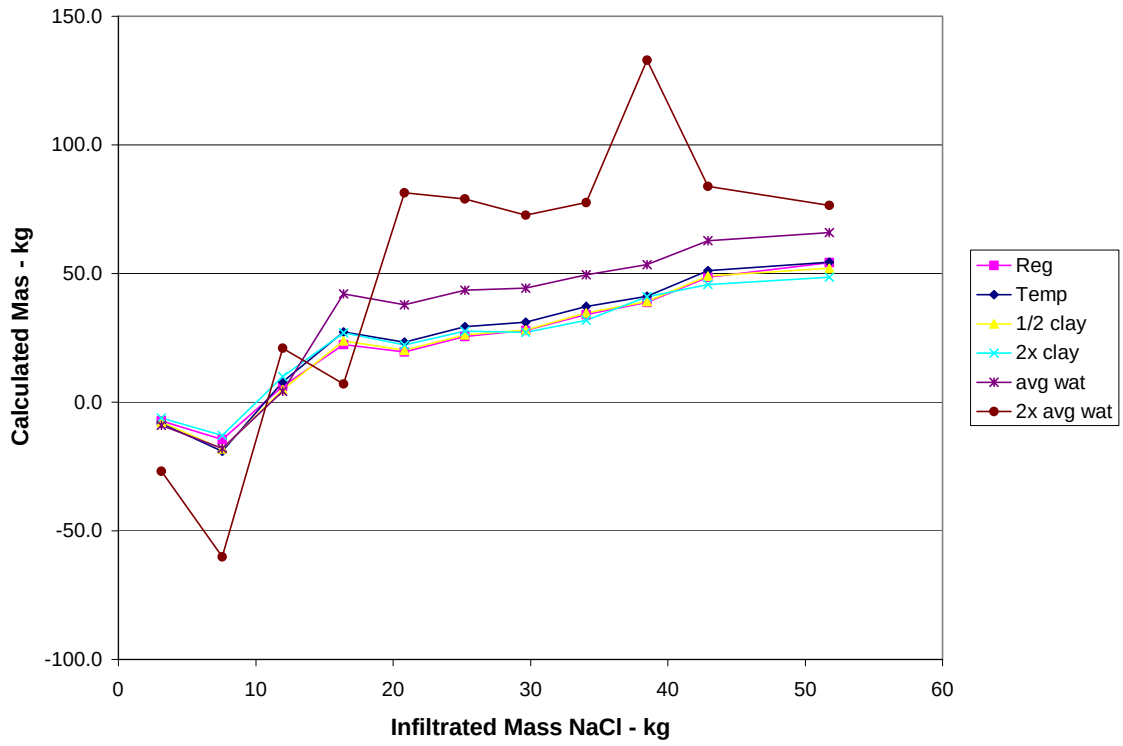


**Figure 63: Known infiltrated mass of NaCl vs the calculated mass of NaCl (kg). A perfect fit would have slope of 1 and an intercept of 0. The estimates with twice and half the average soil water content have the worst fit. Residuals, slopes and intercepts for these calculations are show in Table 4.**

**Table 4: Results of fitting a linear curve to calculated mass of salt to the known mass of infiltrated salt. A perfect fit would have a $r^2$ =1, a slope of 1, and an intercept of 0.**

| Label | threshold vol. water content | soil vol. water content estimate | Max % Clay estimate | Temperature corrected | r^2 | slope | intercept |
|---|---|---|---|---|---|---|---|
| 4a | 4.0% | Measured | 25% | No | 0.61 | 3.6 | -17 |
| 4b | 4.0% | Measured | 25% | Yes | 0.48 | 3.5 | -13.6 |
| 4c | 4.0% | Measured | 12.5% | Yes | 0.48 | 3.5 | -19.3 |
| 4d | 4.0% | Measured | 50% | Yes | 0.47 | 2.7 | -3.8 |
| 4e | 4.0% | Avg | 25% | Yes | 0.57 | 2.9 | -18.6 |
| 4f | 4.0% | 2x Avg | 25% | Yes | 0.5 | 3.6 | -13.9 |
| 6a | 6.5% | Measured | 25% | No | 0.92 | 1.3 | -11.3 |
| 6b | 6.5% | Measured | 25% | Yes | 0.87 | 1.4 | -10.9 |
| 6c | 6.5% | Measured | 12.5% | Yes | 0.89 | 1.4 | -12 |
| 6d | 6.5% | Measured | 50% | Yes | 0.86 | 1.2 | -7 |
| 6e | 6.5% | Avg | 25% | Yes | 0.82 | 1.7 | -8.9 |
| 6f | 6.5% | 2x Avg | 25% | Yes | 0.64 | 3 | -26.6 |
| 8a | 8.0% | Measured | 25% | No | 0.93 | 0.7 | -0.9 |
| 8b | 8.0% | Measured | 25% | Yes | 0.96 | 0.7 | -2.4 |
| 8c | 8.0% | Measured | 12.5% | Yes | 0.89 | 0.7 | 1.2 |
| 8d | 8.0% | Measured | 50% | Yes | 0.98 | 0.7 | -1.6 |
| 8e | 8.0% | Avg | 25% | Yes | 0.94 | 0.8 | -1.2 |
| 8f | 8.0% | 2x Avg | 25% | Yes | 0.66 | 2.4 | -23.2 |
| 10a | 10.0% | Measured | 25% | No | 0.64 | 0.1 | 0.9 |
| 10b | 10.0% | Measured | 25% | Yes | 0.49 | 0.1 | 1.7 |
| 10c | 10.0% | Measured | 12.5% | Yes | 0.29 | 0.1 | 3.3 |
| 10d | 10.0% | Measured | 50% | Yes | 0.78 | 0.1 | 1.3 |
| 10e | 10.0% | Avg | 25% | Yes | 0.94 | 0.1 | 0.4 |
| 10f | 10.0% | 2x Avg | 25% | Yes | 0.71 | 2.2 | -21.5 |

Lowering the threshold water content and lowering the percent clay estimate lead to an increase in mass of salt calculated in the mobile water. The cause of the increase in mass calculated when the percent clay estimate is lowered can be explained by examining Eq. [3]. The first term in this equation decreases as the percent clay estimate decreases, which effectively increases the second term (mobile water conductivity). Decreasing the percent clay decreases the relative amount of bulk conductivity attributed to soil particle conductivity and increases the relative amount of the soil water conductivity (effectively increasing the mobile salt content). The increase in mass calculated by reducing the threshold water content can be explained by examining Eqs. [9] and [10]. If a soil is determined to have no mobile water (below the threshold water content) a calculation of

$EC_w$ can not be performed. If all of the soil water is considered immobile, Eq [10] becomes zero, and Eq. [9] becomes invalid.

The reason the threshold water content has such a strong effect on the calculated mass is due to the low water contents measured at this site. Since most of the water contents are calculated to be between 4% and 10% the threshold water content has a very strong effect on the number of cells involved in the $EC_w$ calculation. Lab analysis by Baker (2001) support the findings of the sensitivity analysis of 6.5% threshold water content. If the water content of the soils at the site were generally higher, decreasing the threshold water content would have less of an impact. Rhoades et al (1988) model assumes that one of the main pathways for current is a continuous phase of soil water, which may not exist in sand soils until 20% water content.

# VI. Conclusions

The EM39 proved to be a fast and reliable method for measuring soil salinity and water content changes in the vadose zone. After modifying the data collection procedures to minimize the probe temperature fluctuations, the repeatability of the measurements was close to the reported 0.5 mS $m^{-1}$ noise level of the instrument. The stability of the shape of the wetted area (as measured with the neutron probe) increased our confidence that the changes in conductivity measured with the EM probe were due to the movement of the salt pulse. Images with both the neutron probe and EM39 data show that the infiltrated water moves directly down from the infiltrometer until spreading laterally at 5 m depth. Pathways reaching below the clay layer at 6 m depth were not detected with either technique, suggesting that water was moving out of the study area laterally along the clay layer instead moving downward through the study volume. The 3D imaging and mass balance results suggest that all of the infiltrated salt remains within the measured volume until the tap water flush began. This further suggests that flow rates along the clay layer were very slow and that fast flow-paths weren't quickly carrying the salt out of the measured volume.

Due to the very low water contents measured at the test site, the mass calculation was strongly dependent on the chosen threshold water content, or immobile/mobile water content limit. A calculation of $EC_w$ was not possible if all of the soil water for that particular cell was assumed immobile. This sensitivity to threshold water content means that small variations in the estimated total soil water content can have large effects on the calculated soil water concentration. Sensitivity analysis showed that the mass calculation was also affected to a lesser extent by the estimate of soil temperature and clay content.

Poor fit between calculated and known mass at the beginning of the salt pulse and the quick drop in mass during the tap water flush are most likely due to nonlinearity of the model at low levels of $EC_w$. The decrease in mass calculated as infiltration ended is due to the decrease in soil water content, resulting in fewer cells being included above the threshold water content.

The correlation of the calculated to known infiltrated mass, with $r^2$ values ranging between 0.98 and 0.50, was very good considering the very low conductivity at the site, presenting conditions at the lower ends of both the probe measurement capability and the limit of $EC_w$ model. Sensitivity analysis results show that the most important factor in the mass calculation at low levels of water content is the designation of threshold water content. A value of 6.5%, or even 8%, is more appropriate for this site than the 10% suggested for agricultural soils by Rhoades. The 6.5% threshold water content closely matches the average residual water contents measured in lab experiments by Baker (2001).

**Recommendations**

The EM39 probe proved to be a fast and accurate method to map salinity changes in the vadose zone. Data collection for each borehole was on the order of minutes, with an entire data set taking less than 2 hours to collect. GPR is a more common method of borehole surveying, but data collection is so tedious that it could frequently take more than one day to collect data from just 5 of the 13 boreholes. The EM39 device should be considered more often for use in salinity mapping.

Application of this technique to measure soil water conductivity in very arid soils is most accurate when accompanied with site specific soil analysis. Determination of the threshold water content for the soils at the site would be necessary through lab analysis, as well as accurate estimates of soil particle conductivity, or percent clay. The Rhoades et al (1990) model is nonlinear at $EC_w$ levels below 400 mS $m^{-1}$ and the model should not be applied below this level.

Data collection with the EM39 probe would be greatly improved if more information could be included in the output file. During data collection the speed of the winch is measured in real time, but is not included in the output file. Recording the speed of the probe is important to ensure repeatability between data sets, and is necessary to correct for vertical displacement if the probe was lowered too quickly down the borehole. Since the speed of the probe is not recorded with the rest of the raw data, accurate field notes must accompany each data set.

The EM39 probe would also be greatly improved if it could measure, and simultaneously record, temperature information. Although the probe is designed to compensate for temperature changes, it is apparent from data collected during the first

salt pulse that the probe needs to be temperature equilibrated with the soil to provide repeatable calibrations. If the EM39 probe could measure temperature, a temperature correction equation could be applied after the data was collected, and a temperature equilibration period might not be necessary. Temperature equilibration could be verified by checking for significantly small variations in temperature with time before calibration. The temperature data would be useful for comparing temperature differences from one data set to another, or how the average temperature changes with time and season. Temperature data taken in this manner may be misleading however, since the measurement will only be the probe temperature and not the soil. Since the goal is to keep the probe at a constant temperature, it would not give information about temperature variation with depth in the soil. A more robust temperature equilibration device within the probe could eliminate the need to temperature equilibrate the probe, or include temperature information in the output file.

# Appendices

## Notation in Appendices

| | |
|---|---|
| $\eta$ | fluid viscosity in poise [$gcm^{-1}s^{-1}$] |
| $\rho_s$ | soil particle density [2.65 g/cm^3] |
| $\rho_l$ | solution density [g/cm^3] |
| g | gravitational constant [981 cm/s^2] |
| t | time of measurement in seconds |
| h’ | hydrometer settling depth (cm) |
| R | uncorrected hydrometer reading (g L-1) |
| RL | reading on blank solution |
| $C_o$ | oven dry weight of sample |
| $\varepsilon$ | dielectric constant |
| L | Length of probe tines (150 mm in this study) |
| c | speed of light in free space ($3 \times 10^8$ m/s) |
| $L_a$ | apparent length of the probe tines from the trace |
| $V_0$ | Voltage entering the TDR probe |
| $V_1$ | voltage of the signal after reflection from the start of the probe |
| $V_f$ | voltage of the final reflected signal at $t \to \infty$. |

# Introduction

The information contained in the first three appendices was used in the mass balance calculations presented in the main body of this thesis. Appendices 1 contains the iso-surface maps of conductivity, temperature, and water content generated in Tecplot v.9 for each of the data sets. Appendices 2 contains the continuous core sample descriptions and particle size analysis data from Baker (2001), as well as unpublished results of hydrometer analysis preformed on four clay rich samples from those cores. Appendices 3 contains the raw EM39 data collected in each borehole during the application of the second salt pulse, as well as the standard deviation of the measurements at each depth.

The wide array of instrumentation that was installed at the test site offers many opportunities to compare the results of different techniques measuring similar properties. A comparison between the suction lysimeter and time domain reflectomety (TDR) probes (installed together at 24 locations at 3.5, 6 and 8 m depth) is also included in this thesis, but proved less useful than originally hoped, due to most of the probes being installed outside the wetted area. Appendices 4 is the suction lysimeter data, Appendices 5 is the TDR data, and Appendices 6 is the specific operating procedures used in each of the data techniques.

## Comparison of TDR and Suction Lysimeter Results

The EM39 proved to be fast and reliable method for monitoring water content and salinity changes in the vadose zone. A more complete story of the site is gained however, when the data from different techniques is combined. At first glance, the data from most of the nested TDR and suction lysimeters appears to tell us very little about the tracer

experiment, with possible tracer detection occurring at only six locations. While the suction lysimeter and TDR data sets are limited alone, their response (or lack of one) fits well when compared with the complicated flow pattern mapped out with the other techniques (EM39, GPR and neutron probe). The neutron probe data shows that the areas with the highest water content (<18% volumetrically) are directly below the infiltrometer and across the site between 5 and 6 meters depth (the same depth as the thick clay layer). The TDR and suction lysimeters are installed at 3.5 and 8 depth, just above and below the zone of high water content. Four probes were installed at 6 meters depth and showed good response to the salt pulses, as would be expected. The distribution of probes at this site exemplifies the drawbacks of data techniques that provide only point measurements.

Although some of the probes detect the salt pulse, there was a very significant time delay (60-200 days) between the beginning of the salt pulses and detection at the suction lysimeters; with two of the probes seeming to respond just as the sampling period ended. The suction lysimeter samples are also much more dilute than the original salt tracer, but this is expected since only a third of the infiltrometer was supplied with the saline solution, while the remaining two thirds of the infiltrometer . The slow response time and dilute concentrations lead to the conclusion that the infiltrated solutions become well mixed as they move laterally above the clay layer. The fact that the conductivity of the infiltrating water varies with location only further complicates interpretation of the suction lysimeter results Electromagnetic induction surveys have a distinct advantage over other electrical methods, such as electrical resistivity tomography (ERT) or time domain reflectometry (TDR), because there is no physical contact between the probe and the material being measured.

Below is a table showing the combined results from the TDR and suction lysimeter nested probes. The first salt pulse took approximately 200 days to reach ND, WD, NWIB and SWIA and the second salt pulse was not detected at any of these locations (lack of detection is likely due to the fact that infiltration ended 140 days after the second pulse started). Nine of the TDR and suction lysimeters were installed in soils that were so dry that data could not be collected at that location, interestingly though, at least one of the two probes worked at each location.

| Name | Depth (m) | TDR volumetric water content | Detect 1st Pulse? | First detection (days) | Detect 2nd Pulse? | First detection (days) | Notes |
|---|---|---|---|---|---|---|---|
| NS | 3.5 | 0.125 | no | | no | | |
| ES | 3.5 | 0.098 | no | | no | | |
| SS | 3.5 | 0.052 | no | | no | | |
| WS | 3.5 | 0.137 | no | | TDR? | 60 | suc lys only decreases |
| ND | 6.0 | 0.151 | Both | 200 | no | | |
| ED | 6.0 | 0.193 | TDR | 110 | no | | suc lys shows no change |
| SD | 6.0 | 0.184 | Both | 70 | Both | 60 | |
| WD | 6.0 | NA | Suc. Lys. | 200 | no | | TDR dry |
| NEIA | 8.0 | 0.109 | no | | no | | suc lys dry |
| NEIB | 8.0 | NA | no | | no | | TDR dry |
| NEOA | 8.0 | 0.089 | no | | no | | suc lys dry |
| NEOB | 8.0 | 0.112 | no | | no | | suc lys dry |
| NWIA | 8.0 | 0.136 | Both | 85 | Both | 75 | |
| NWIB | 8.0 | 0.104 | Suc. Lys. | 200 | no | | TDR no change |
| NWOA | 8.0 | NA | no | | no | | suc lys dry after 7 samples |
| NWOB | 8.0 | NA | no | | no | | TDR dry |
| SEIA | 8.0 | 0.094 | no | | no | | suc lys dry |
| SEIB | 8.0 | NA | no | | no | | TDR dry |
| SEOA | 8.0 | 0.088 | no | | no | | |
| SEOB | 8.0 | 0.090 | no | | no | | |
| SWIA | 8.0 | 0.159 | Suc. Lys. | 190 | no | | TDR no change |
| SWIB | 8.0 | 0.014 | no | | no | | both show only decrease |
| SWOA | 8.0 | no signal | no | | no | | suc lys shows only decrease |
| SWOB | 8.0 | 0.068 | TDR? | | Both | 30 | |

**Table: Summary of the TDR and suction lysimeter data.**

The infiltration of both pulses was only detected at two locations, SD and NWIA. Each of the pulses was detected with both the TDR and suction lysimeter probes at both of the locations agree well on arrival time. At both locations the first, low conductivity pulse, took approximately 10 days longer to arrive at the probes than the high

conductivity pulse. Both pulse arrived approximately 15 days quicker at the SD location (6 m depth) than at the NWIA location (8 m depth).

Unfortunately, data was not collected from either of these instruments until just prior to the start of the first salt pulse. The missing information about the arrival time of the initial wetting front and original pore water conductivity would have made the interpretation of this data more complete.

# Appendix 1 – Conductivity (EM39) Data

## 1.1 Temperature Sensitivity

Data collection with the EM39 began just prior to the start of the first salt pulse. Unfortunately, most of the data collected during this first salt pulse is very noisy and was not used in the interpretations made in this report. The cause of the unreliability of the data was difficult to determine, and the probe was even sent to Geonics to confirm the probe was working properly. Testing at Geonics showed the probe was working normally. Through a series of simple experiments, the largest cause of the data variability was discovered to be the temperature sensitivity of the probe, which is a surprising result because the probe is designed to compensate for temperature changes. Data collection procedures initially followed the Geonics EM39 manuals and are outlined later, but proved inadequate to deal with the large temperature difference between the probe, which warmed up rapidly in the sun, and the cool borehole at depth. Differences in probe temperature from one day to the next and from one borehole to the next caused variations in the calibration of the probe. The shape of the conductivity versus depth trends showed good repeatability, which ensures that the probe was correctly measuring the variations in conductivity, but the magnitude of the conductivity varied in different data sets due to variations in the calibrated zero value.

Another complication with the early EM data was a loss of resolution because the probe was lowered down the borehole too quickly. When the probe was lowered too fast, the whole trend becomes smoothed as seen in Figures 1.1.1 and 1.1.2 below. The data collected at the slower speed shows much more detail in the variation of conductivity due to better imaging of the thin layers in the stratigraphy. The depth measurement also becomes offset if the probe is lowered too quickly. Geonics provides an equation to

correct for this offset, if the speed of the probe is known, which is one of the parameters not recorded automatically with the data acquisition system. See the end of this appendix section for the correction equation.

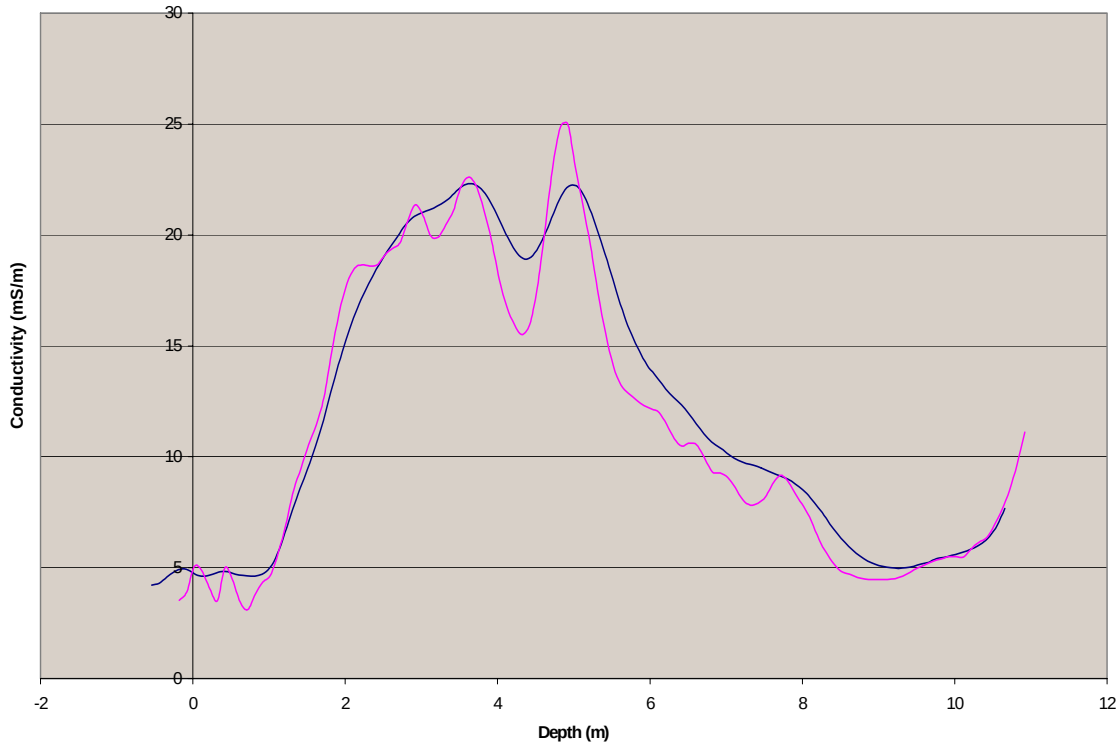


**Figure 1.1.1: Loss of resolution in measured conductivity (mS $m^{-1}$) with the probe lowered quickly (smooth line) and slowly (wavy line).**

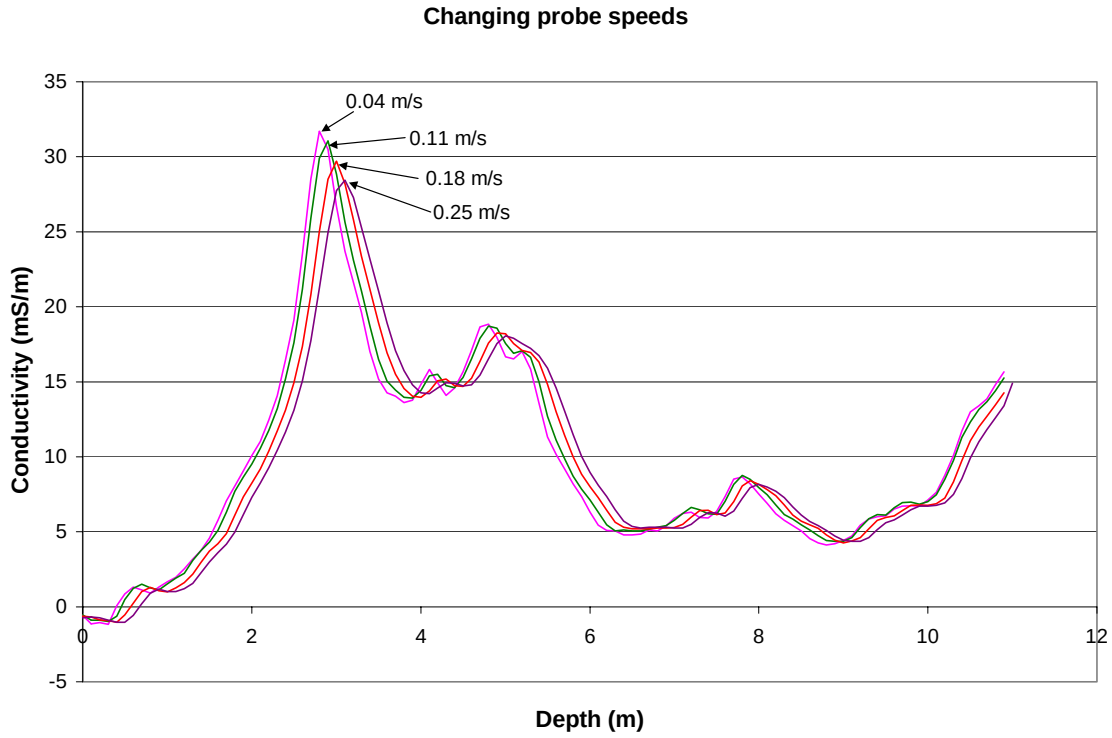


**Figure 1.1.2: Decrease in resolution and maximum conductivity measured due to increasing probe speed.**

Due primarily to time constraints, the data collected during the first salt pulse was not corrected for temperature drift or depth offset. Even if these corrections were performed, the data still has very low resolution, which makes it very difficult to detect the movement of the low conductivity first pulse. It is important to keep in mind that the salt pulse is only ever supplied to a third of the infiltrometer. The conductivity of the first salt was 275 mS m-1 and the other two thirds of the infiltrated water remained at about 80 mS m-1. Suction lysimeter data suggests the 275 mS m-1 is close to the pore water conductivity prior to the injection of the first pulse, making detection of the pulse even more difficult.

Due to the problems encountered with the data taken during the first salt pulse, the operating procedures were slightly modified before the second salt pulse. To ensure

that the probe underwent as little temperature change as possible, it was lowered and left at the bottom of a borehole for at least 45 min before it was calibrated. During data collection the probe was left at the bottom of a borehole while the winch and computer were moved on the surface. During the two hours necessary to collect data from all thirteen boreholes, the probe would only be on the surface for a total of 10 minutes. The probe was calibrated only once before each data session, and not before logging each borehole, as was previously done. The probe was also placed in the same location for every calibration to ensure that differences in the ambient magnetic field did not influence calibration.

These modifications to the original data collection procedures, as well as decreasing the speed of the probe, had a dramatic difference in the quality of the data. The repeatability of data from the second salt pulse is close to, or less, than the reported noise level of the instrument, which is 0.5 mS $m^{-1}$.

## 1.2 Raw Conductivity Data

Figures 1.2.1 through 1.2.19 are the raw EM39 data collected at the site.

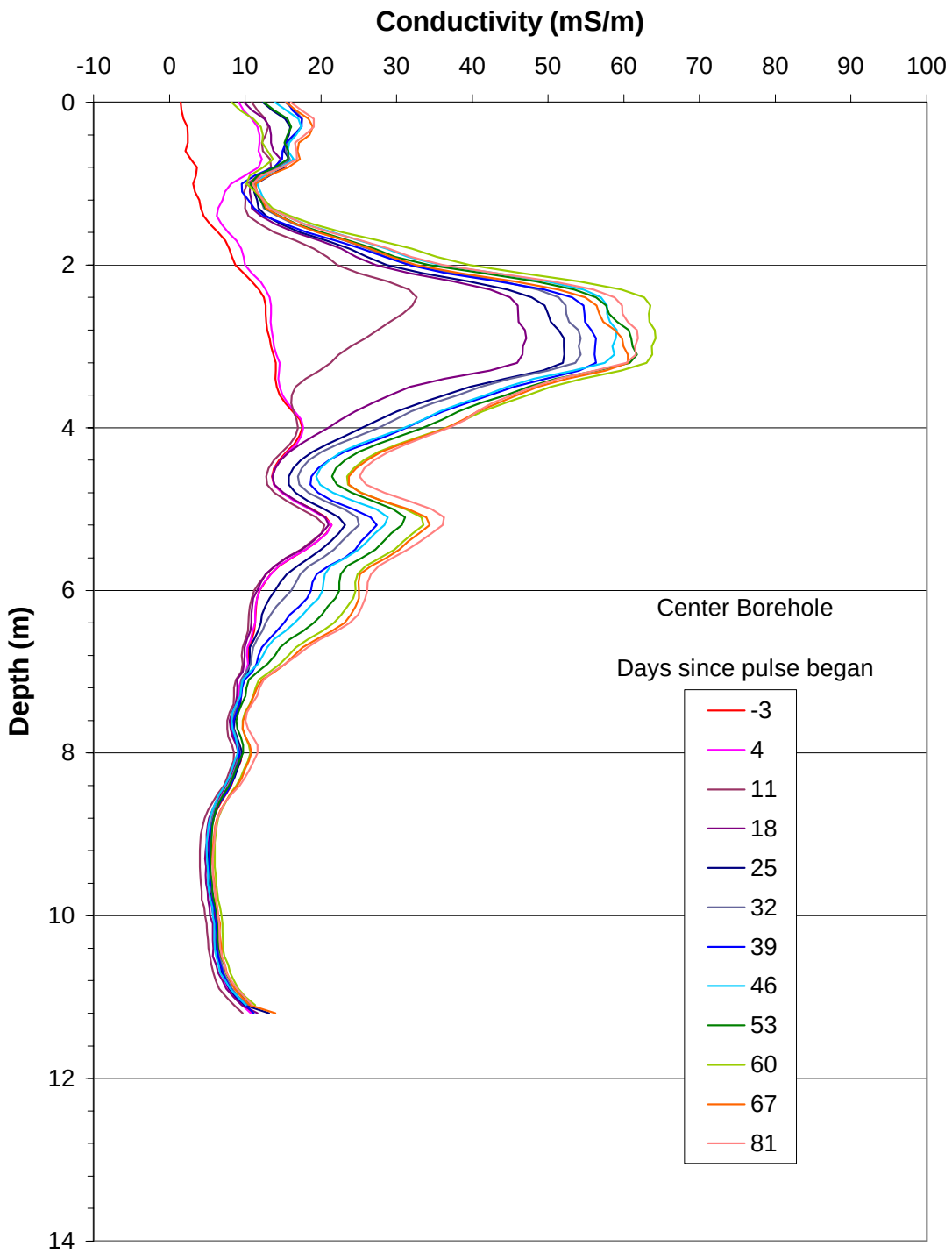


**Figure 1.2.1: Raw EM39 data collected from the center borehole during infiltration of the salt pulse.**

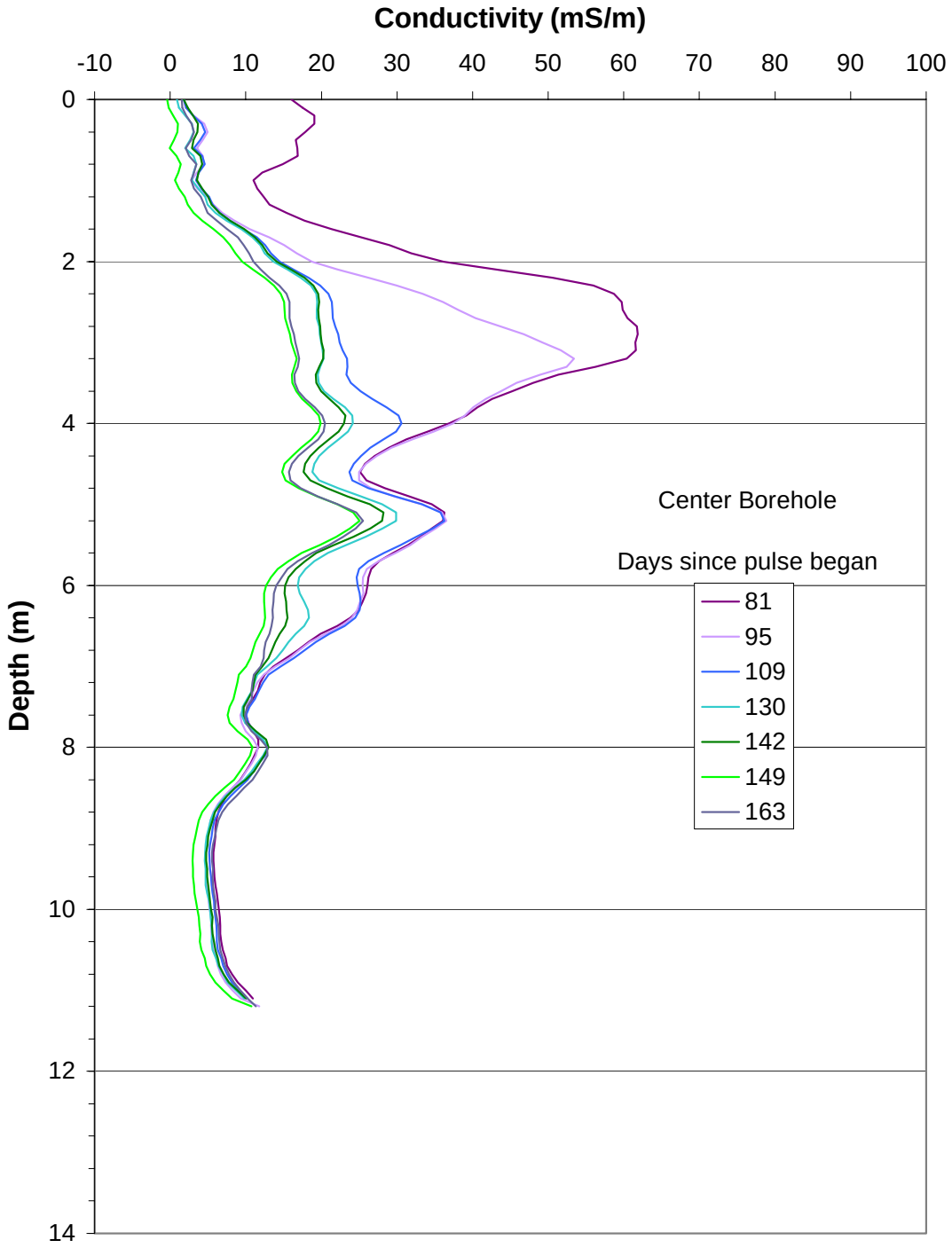


**Figure 1.2.2: Raw EM39 data collected from the center borehole during the tap water flush and after the end of infiltration (Day 142).**

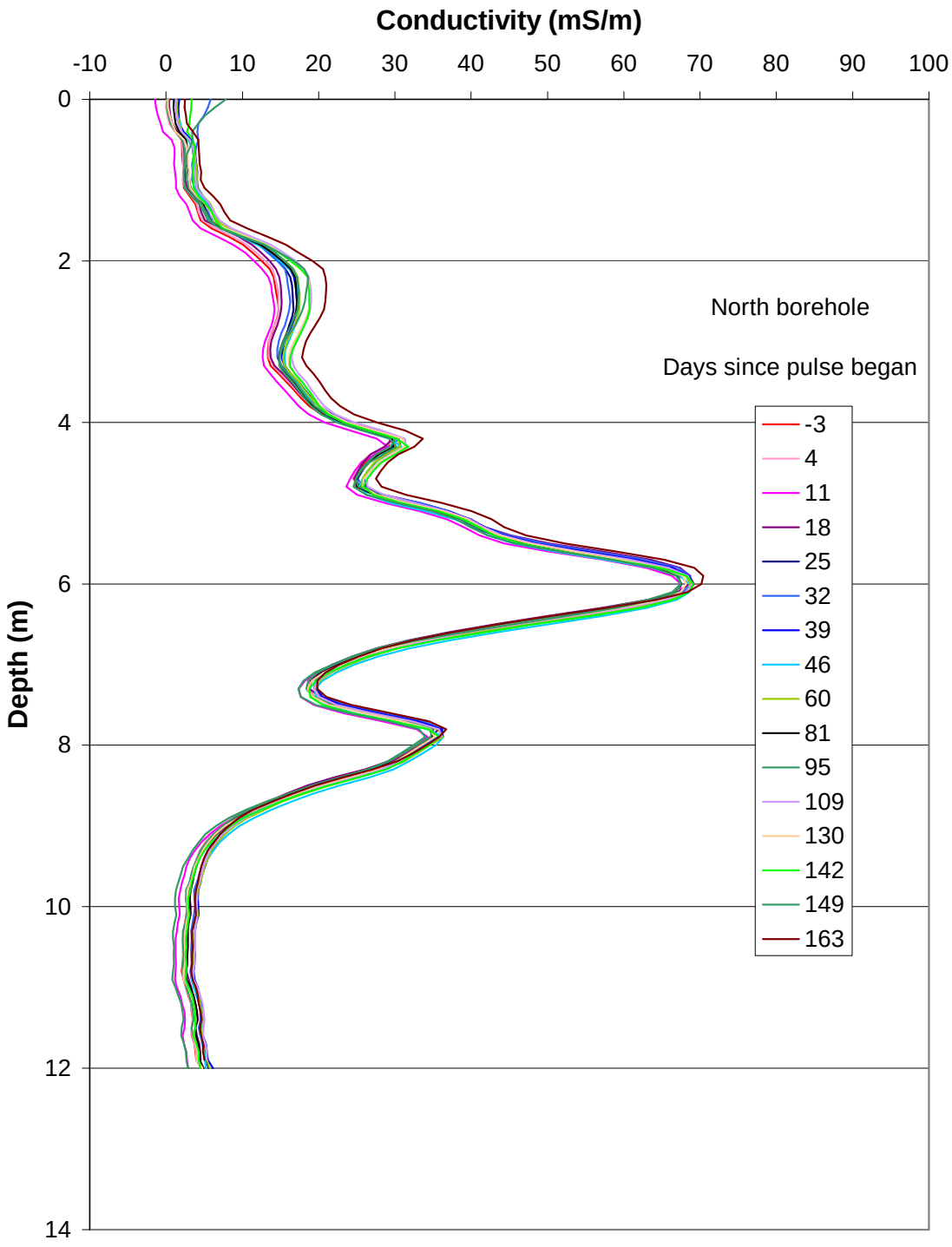


**Figure 1.2.3: Raw data collected in the North borehole from before the salt pulse began to 21 days after infiltration ended.**

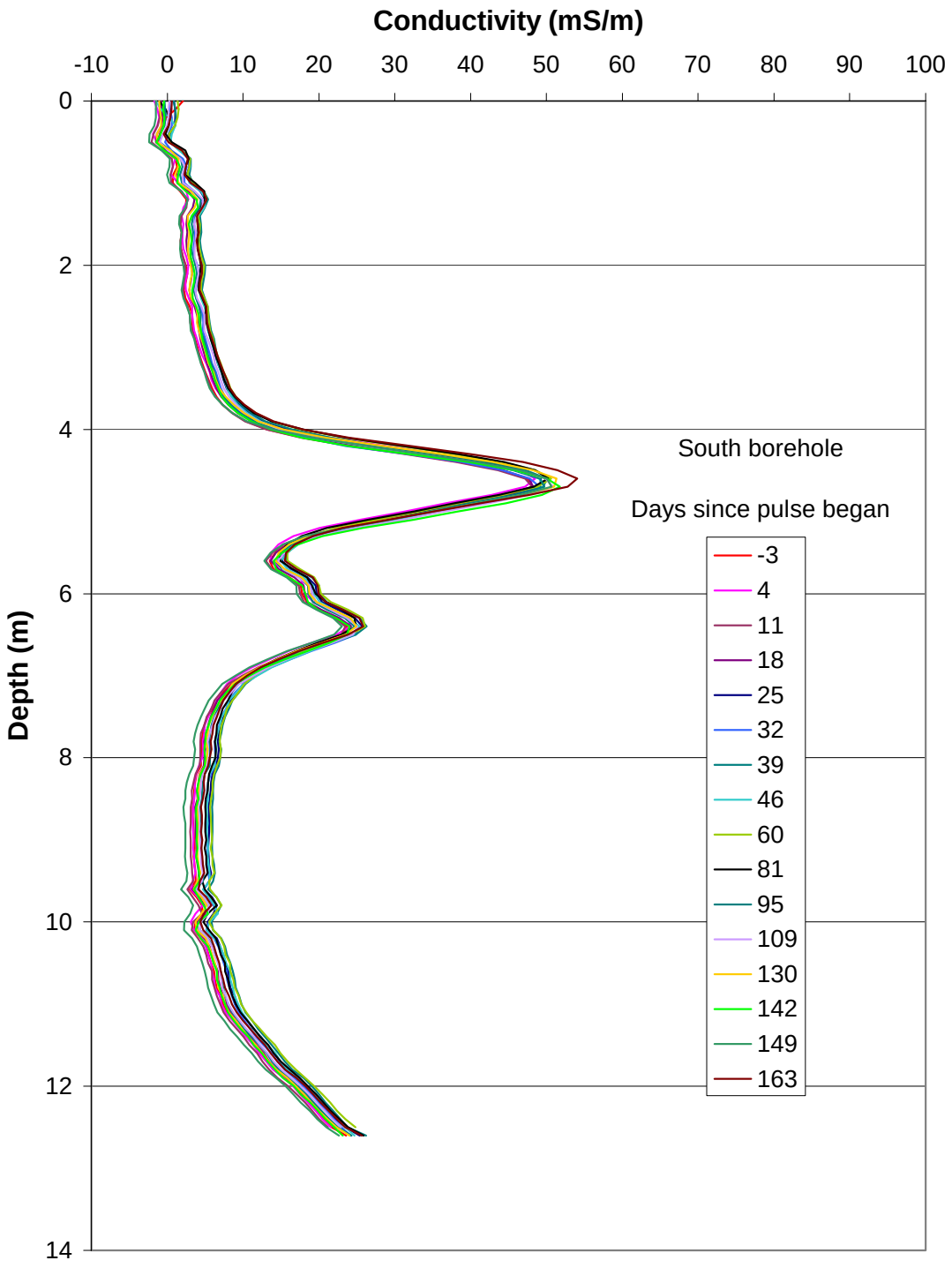


**Figure 1.2.4: Raw EM39 data collected in the South borehole from before the salt pulse began to 21 days after infiltration ended.**

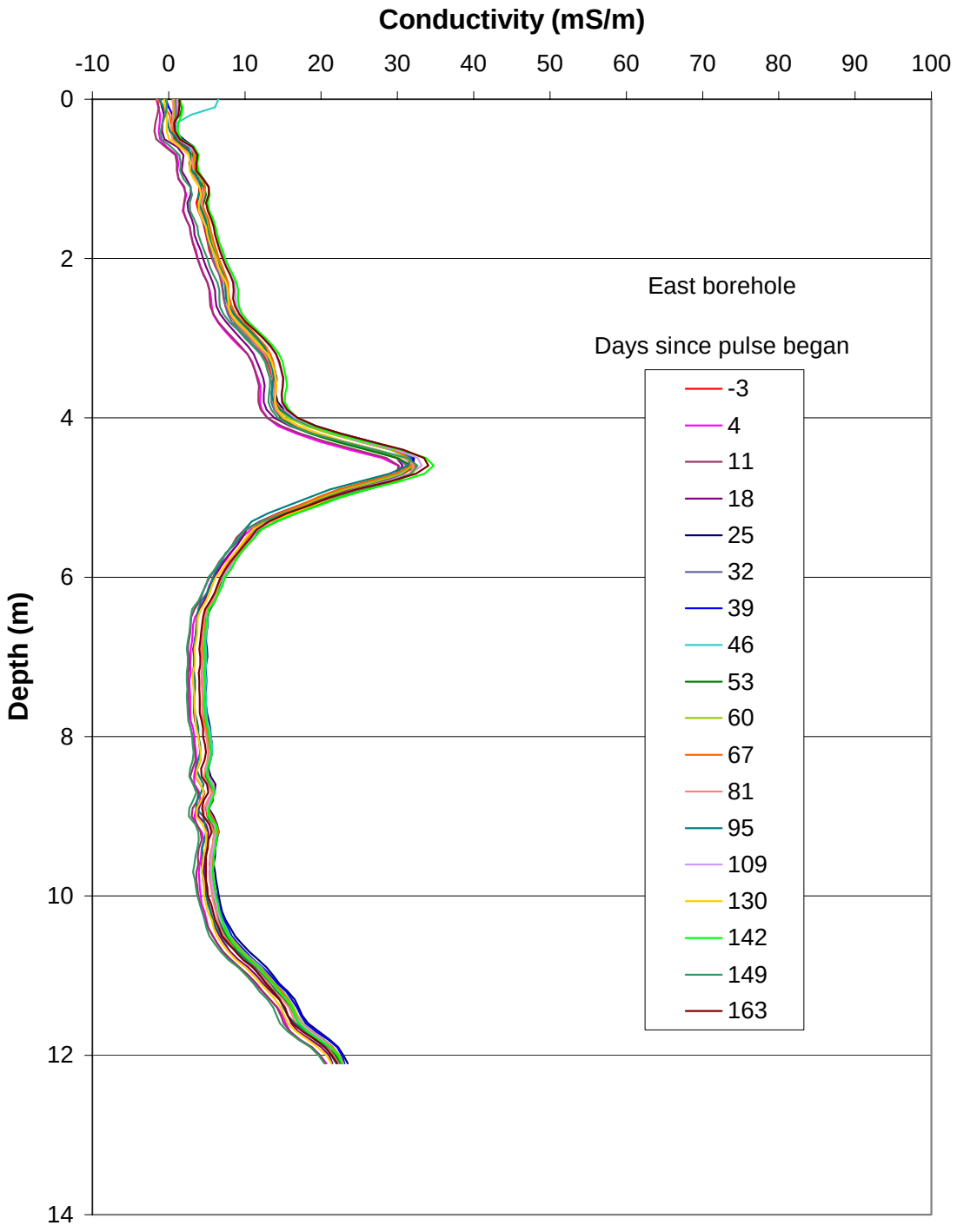


**Figure 1.2.5: Raw EM39 data collected in the East borehole from before the pulse began until 21 days after infiltration ended.**

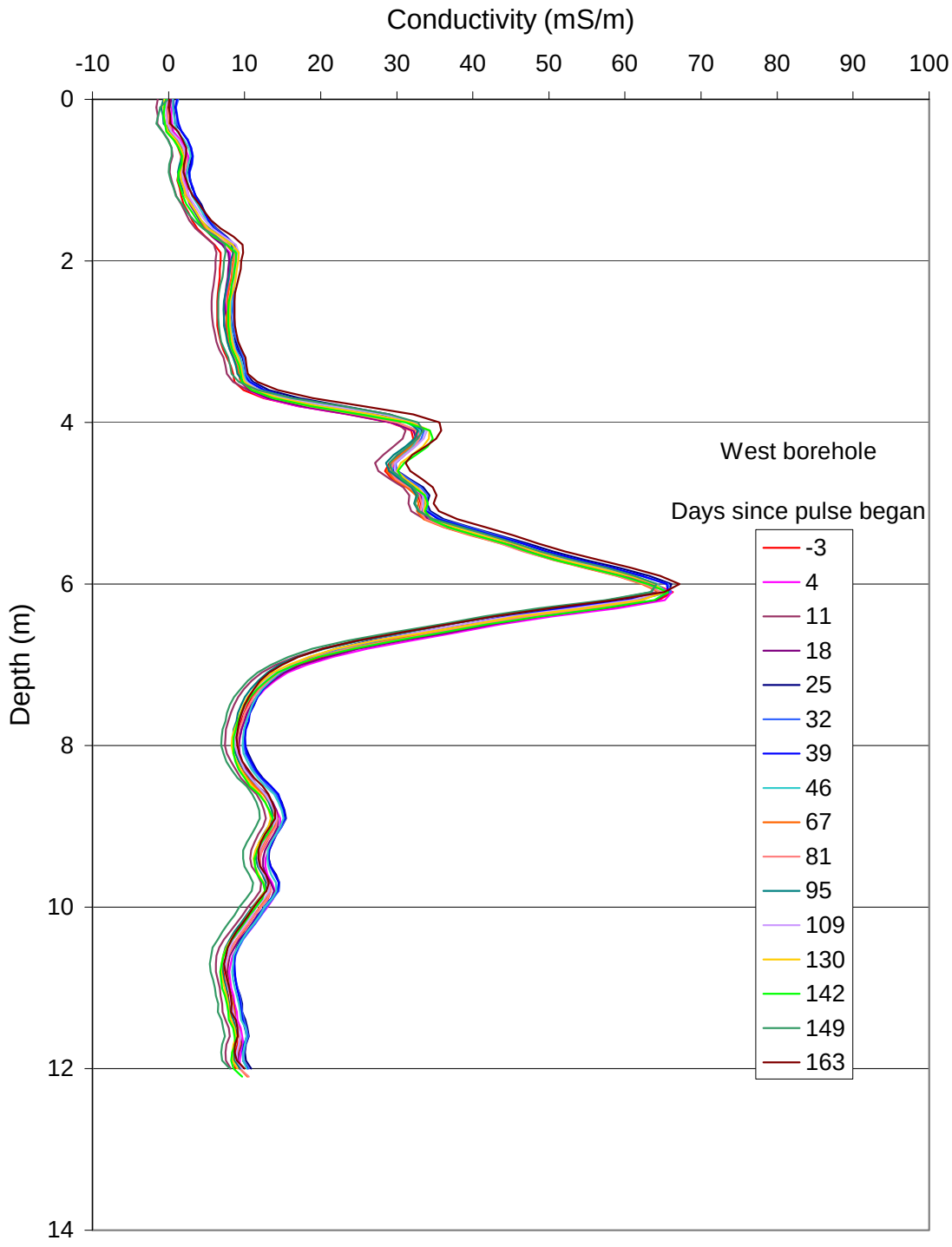


**Figure 1.2.6: Raw EM39 data collected in the West borehole from before the pulse began until 21 days after infiltration ended.**

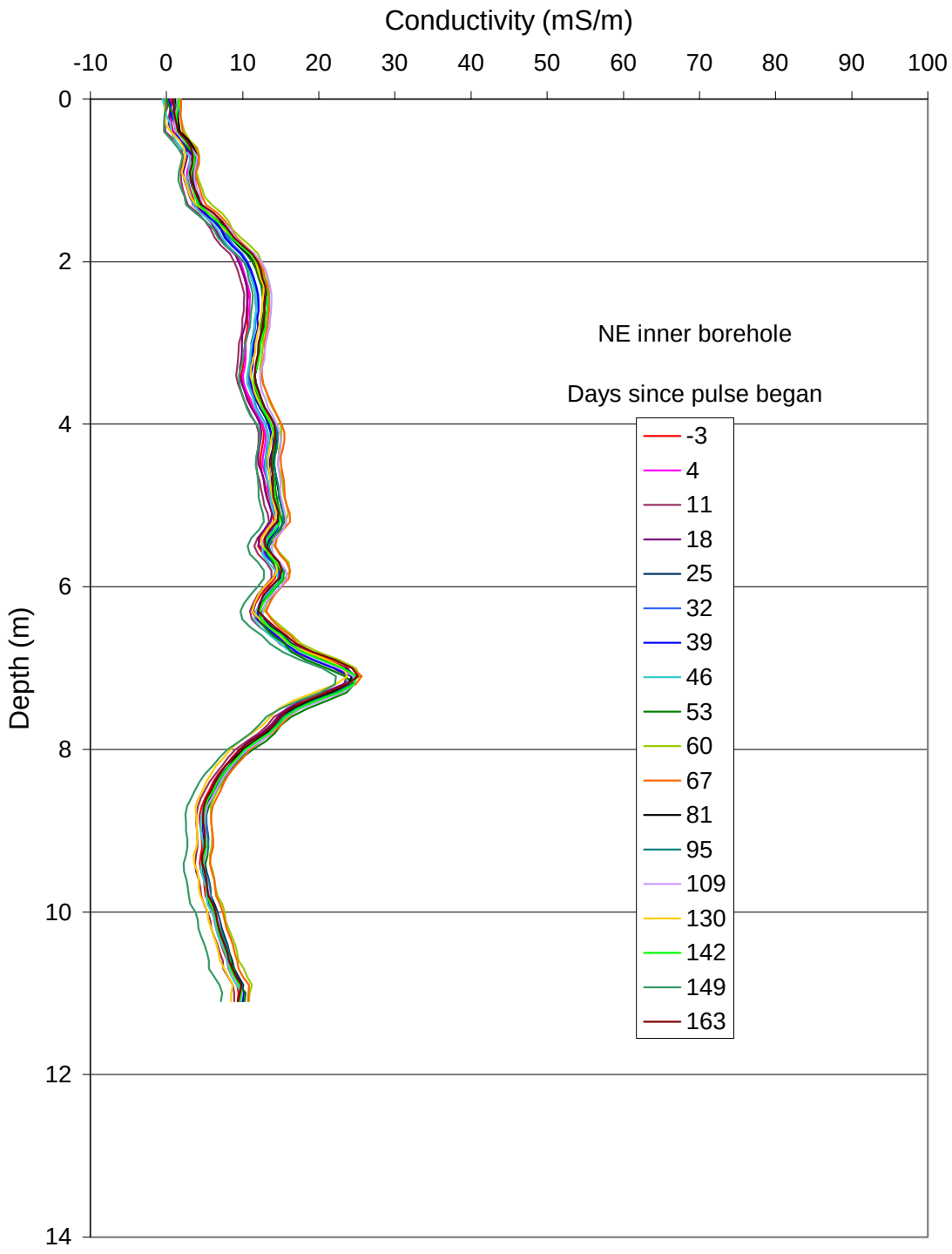


**Figure 1.2.7: Raw EM39 data collected in the North East Inner borehole from before the pulse began until 21 days after infiltration ended.**

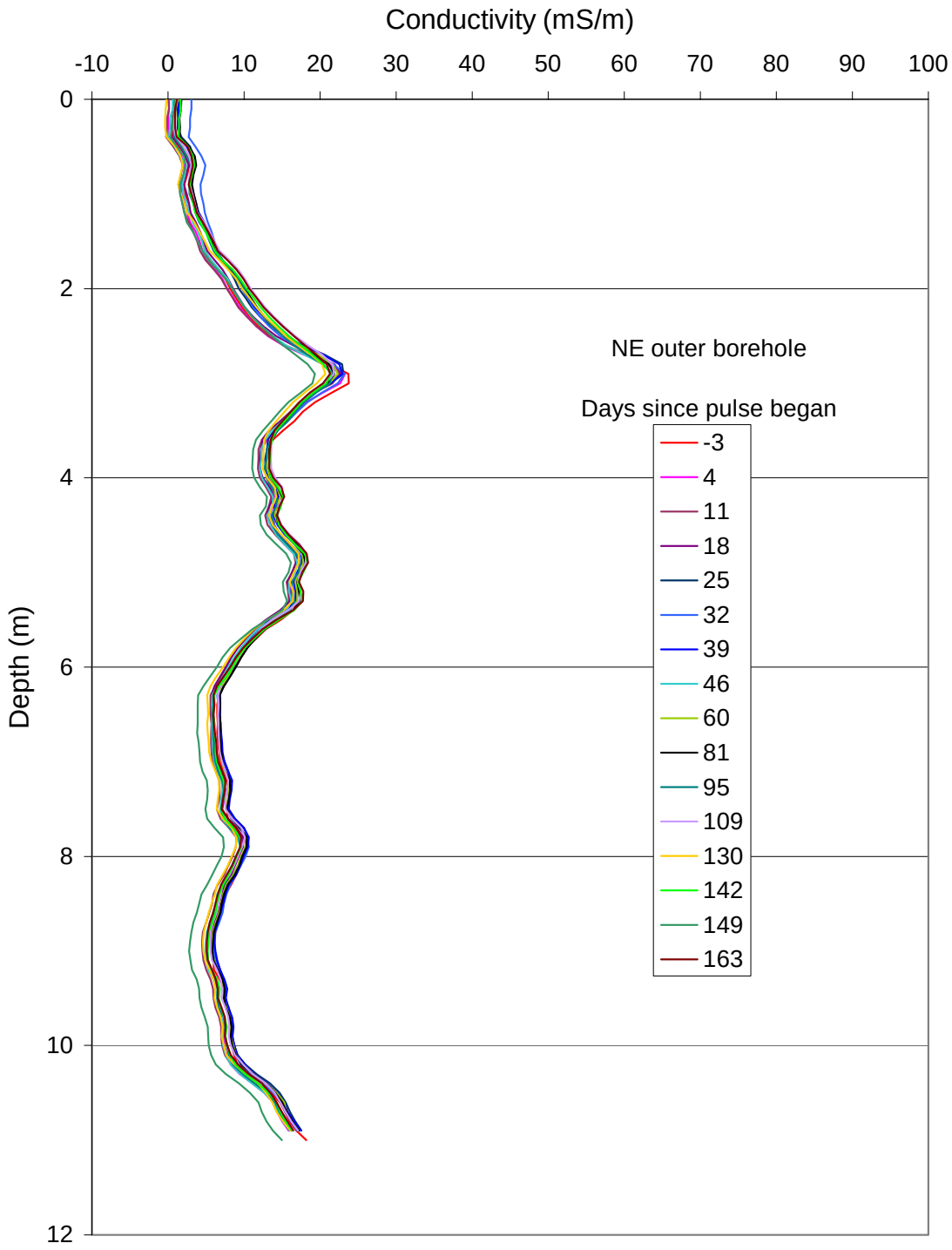


**Figure 1.2.8: Raw EM39 data collected in the North East outer borehole from before the pulse began until 21 days after infiltration ended.**

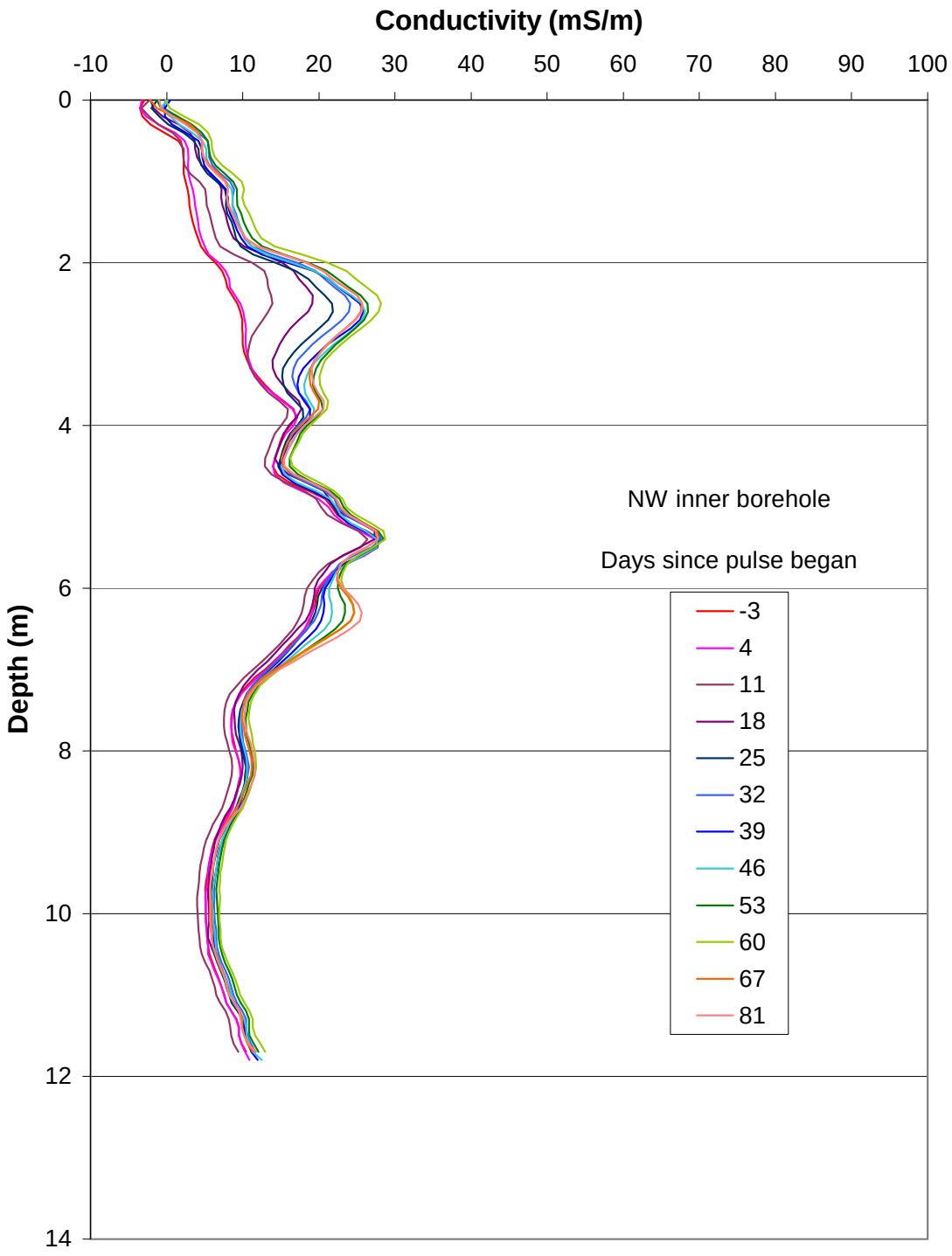


**Figure 1.2.9: Raw EM39 data collected in the North West inner borehole during the infiltration of the salt pulse.**

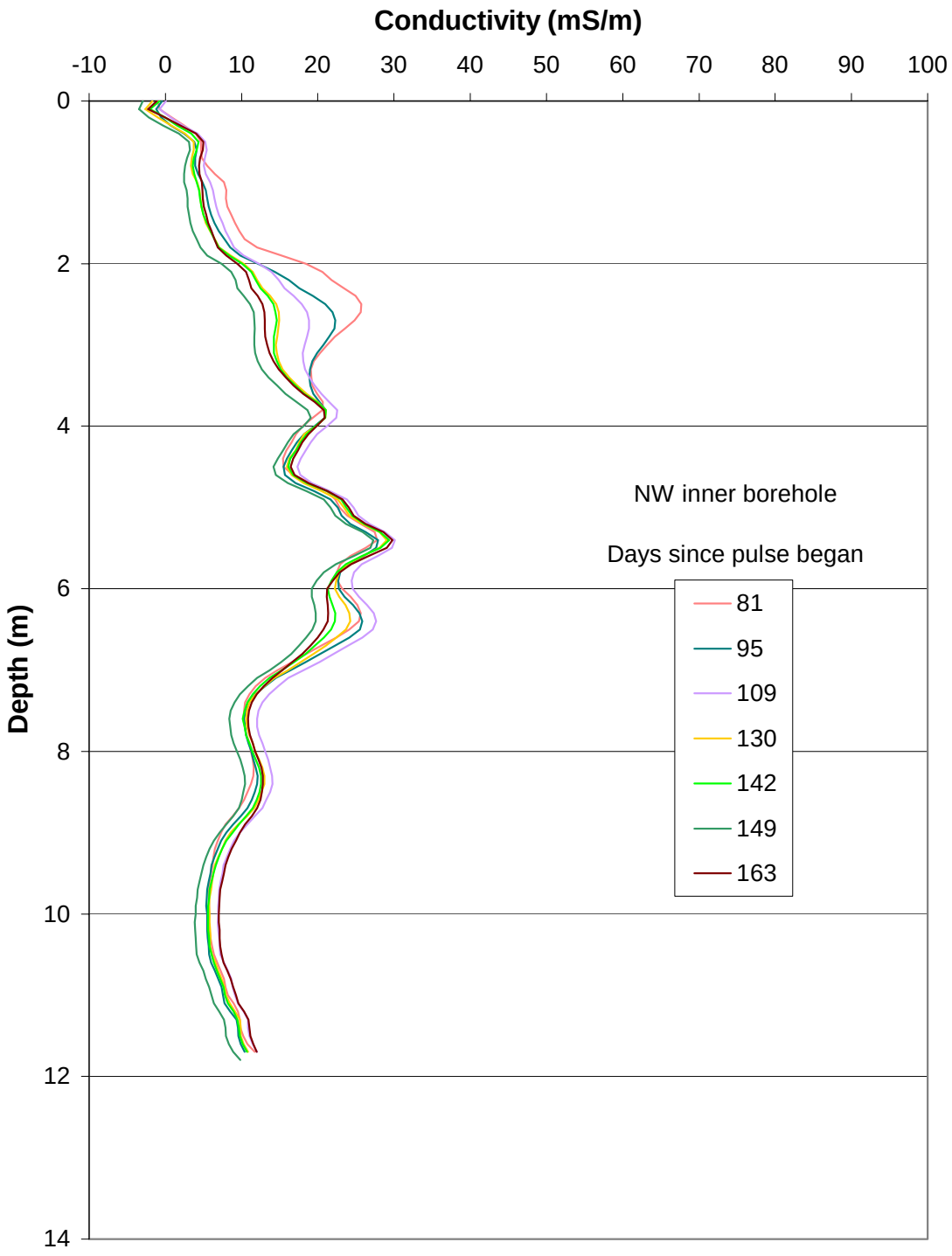


**Figure 1.2.10: Raw EM39 data collected in the North West inner borehole during the tap water flush and after the end of infiltration on Day 142.**

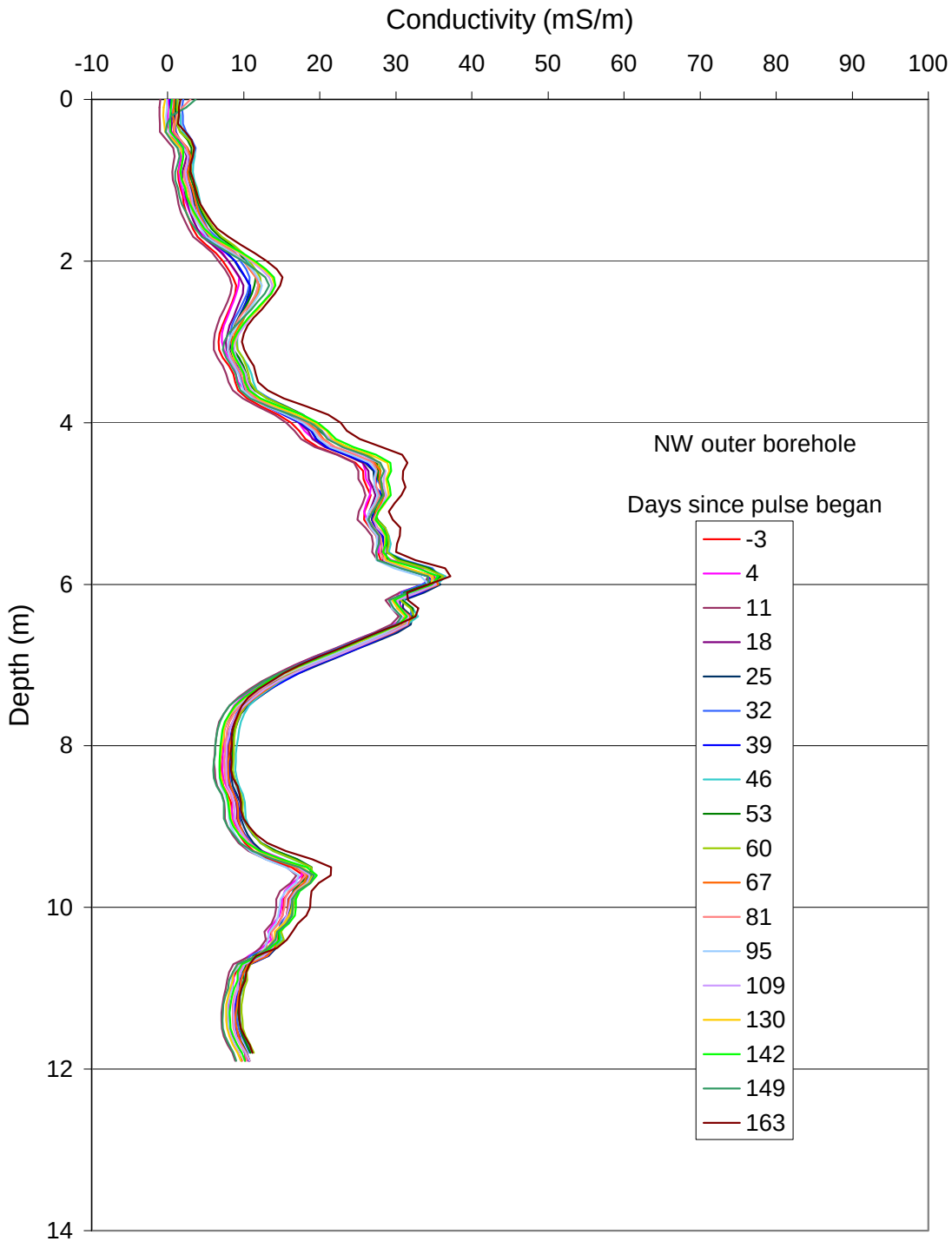


**Figure 1.2.11: Raw EM39 data collected in the North West outer borehole from before the pulse began until 21 days after infiltration ended.**

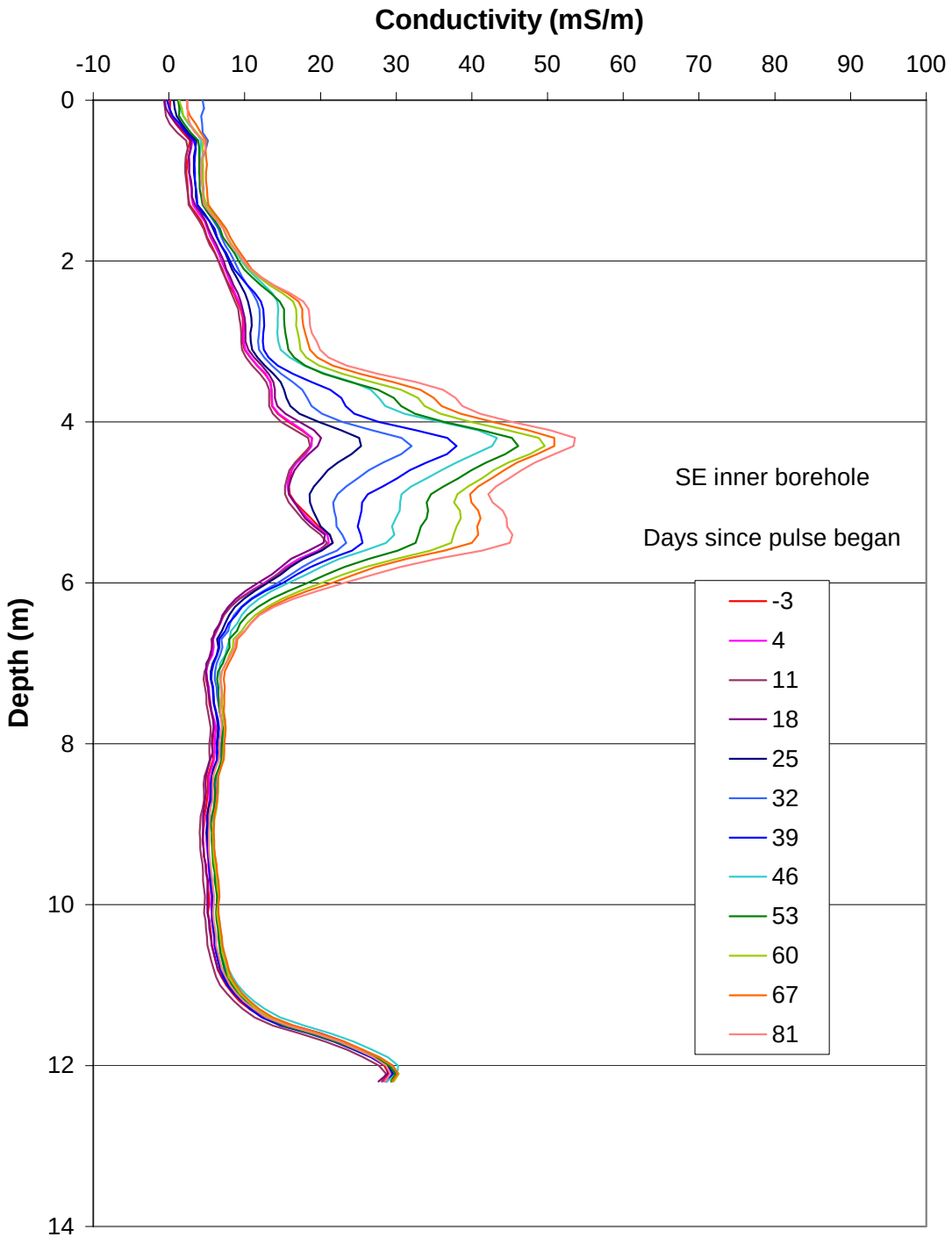


**Figure 1.2.12: Raw EM39 data collected in the South East Inner borehole during the infiltration of the salt pulse.**

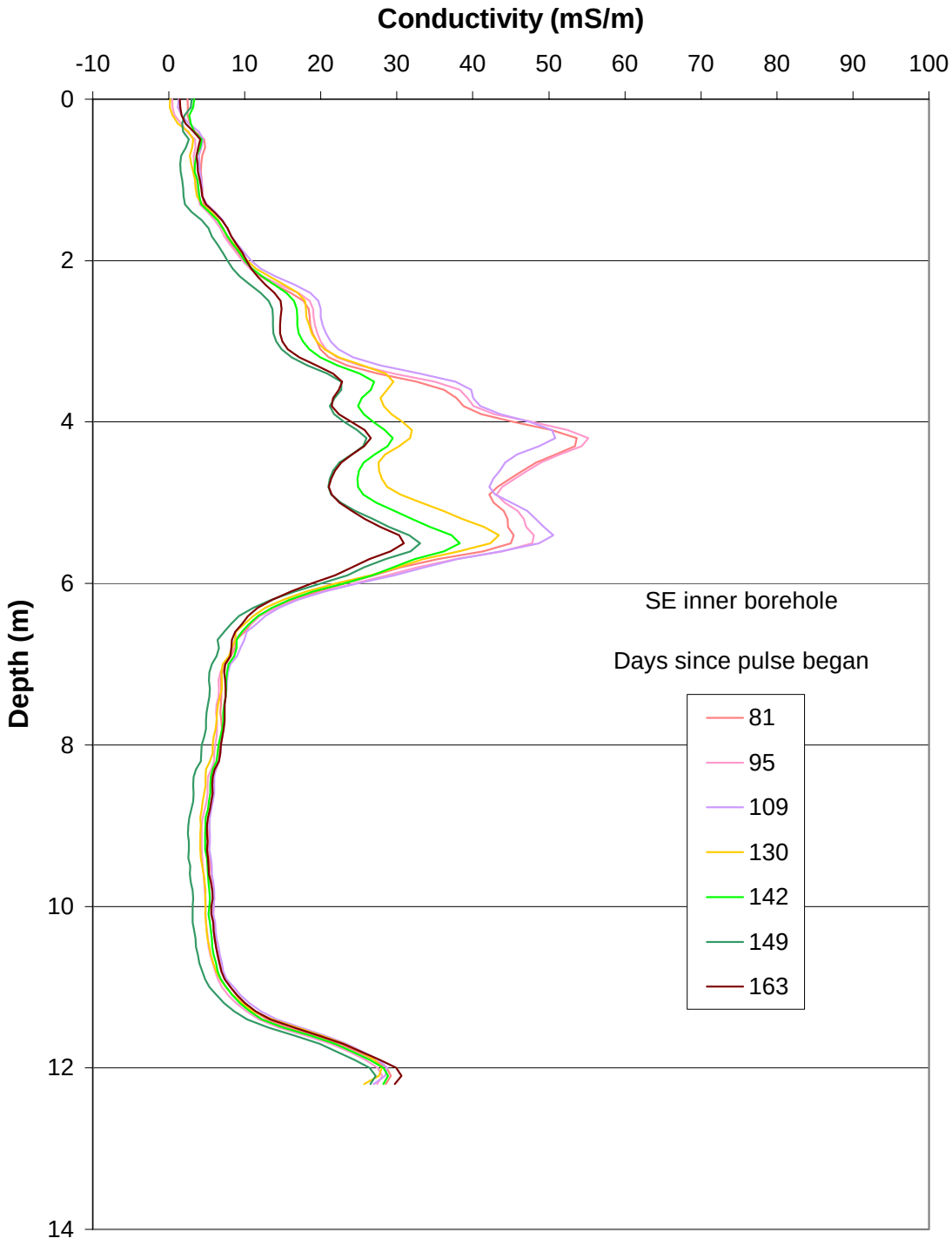


**Figure 1.2.13: Raw EM39 data collected in the South East Inner borehole during the tap water flush and after infiltration ended on Day 142.**

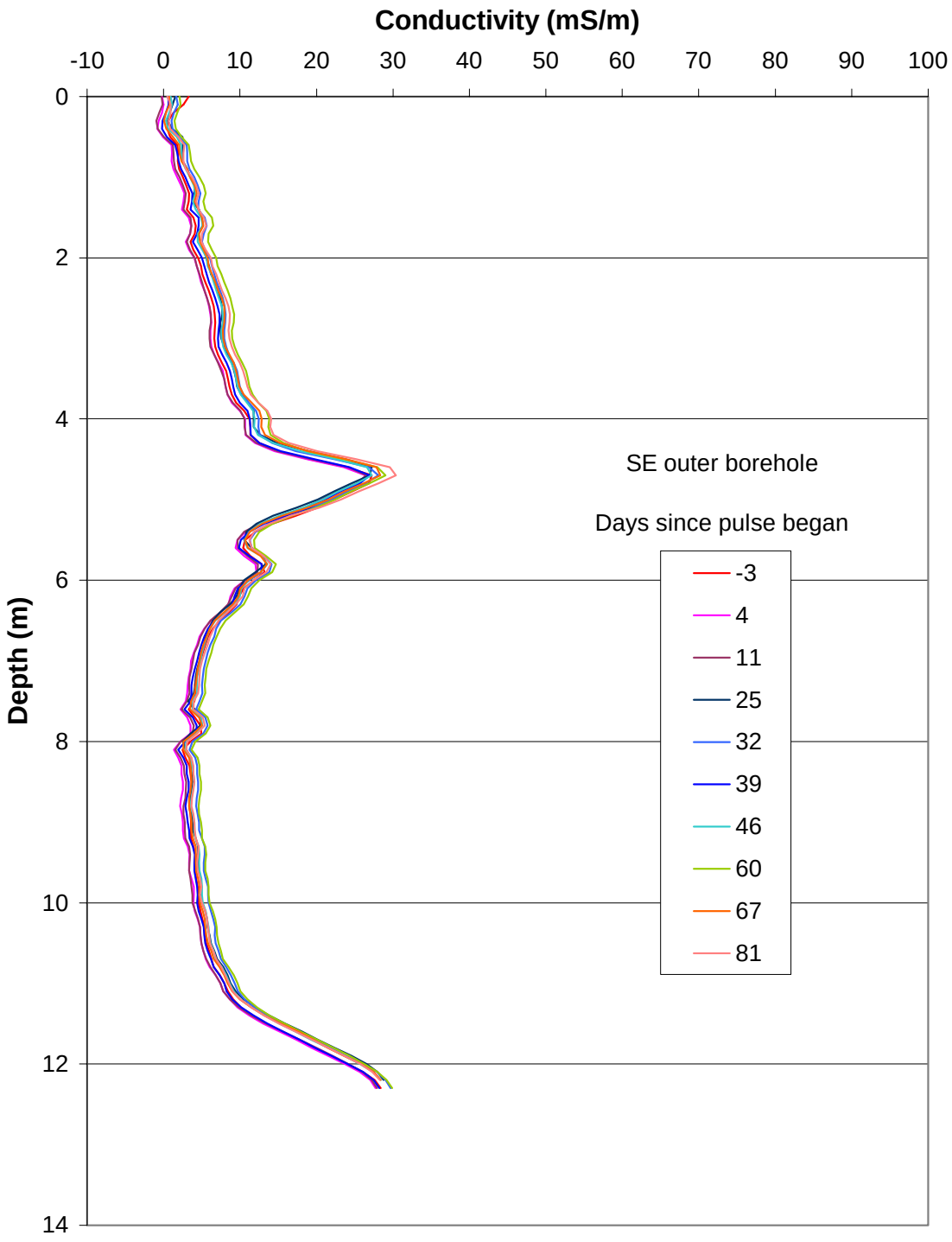


**Figure 1.2.14: Raw EM39 data collected in the South East outer borehole during the infiltration of the salt pulse.**

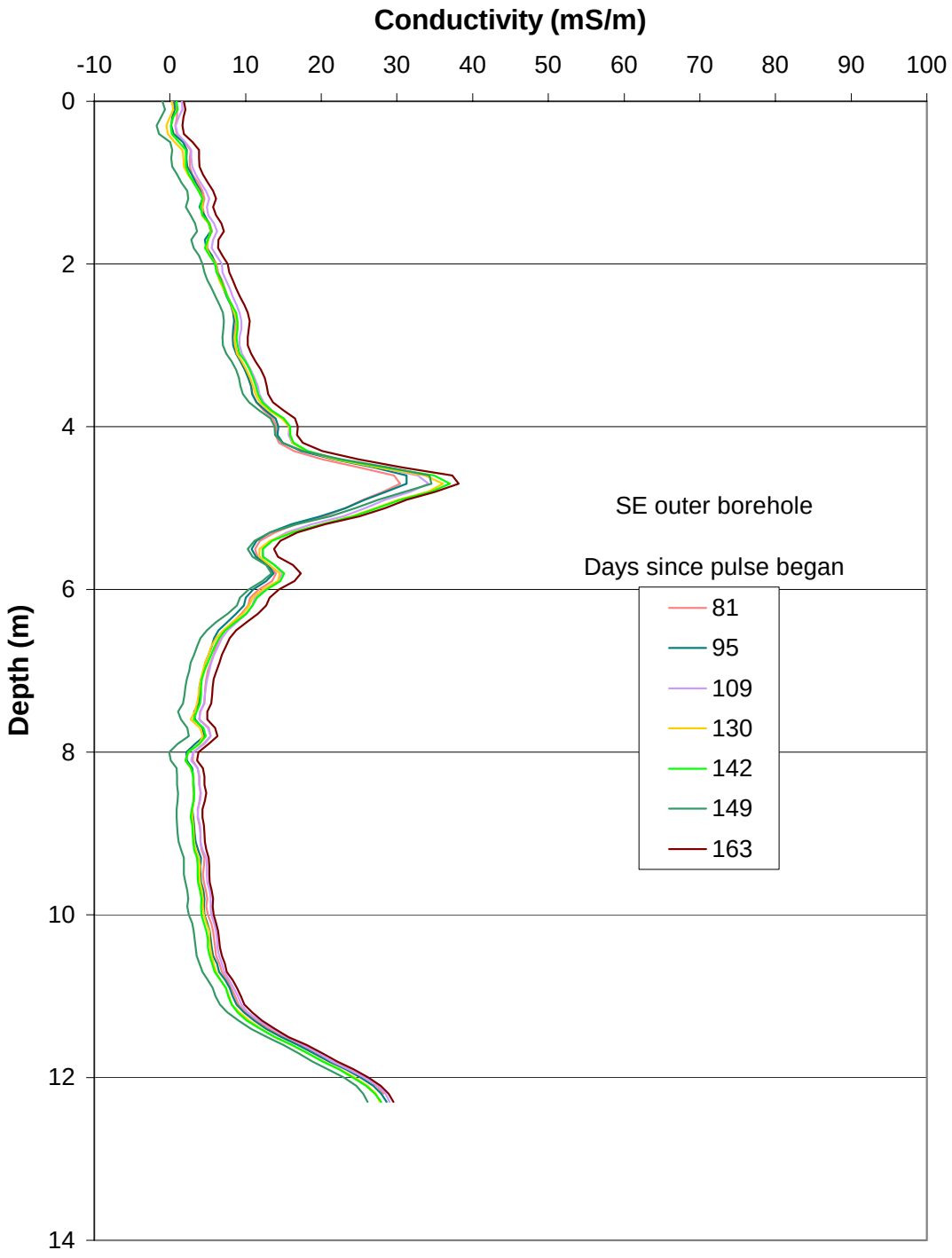


**Figure 1.2.15: Raw EM39 data collected in the South East outer borehole during the tap water flush and after infiltration ended on Day 142.**

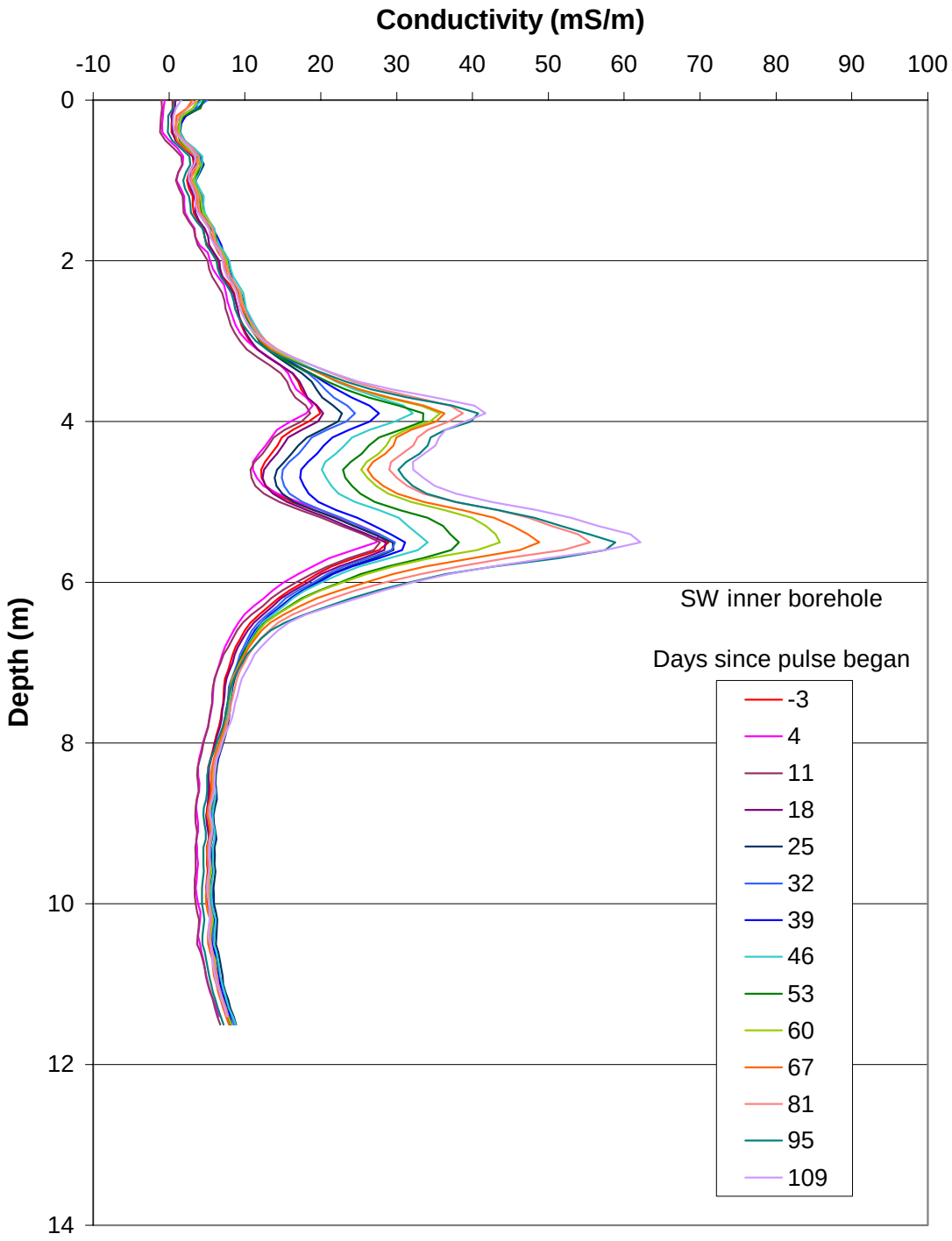


**Figure 1.2.16: Raw EM39 data collected in the South West Inner borehole showing an increase in conductivity until 24 days after the pulse ended.**

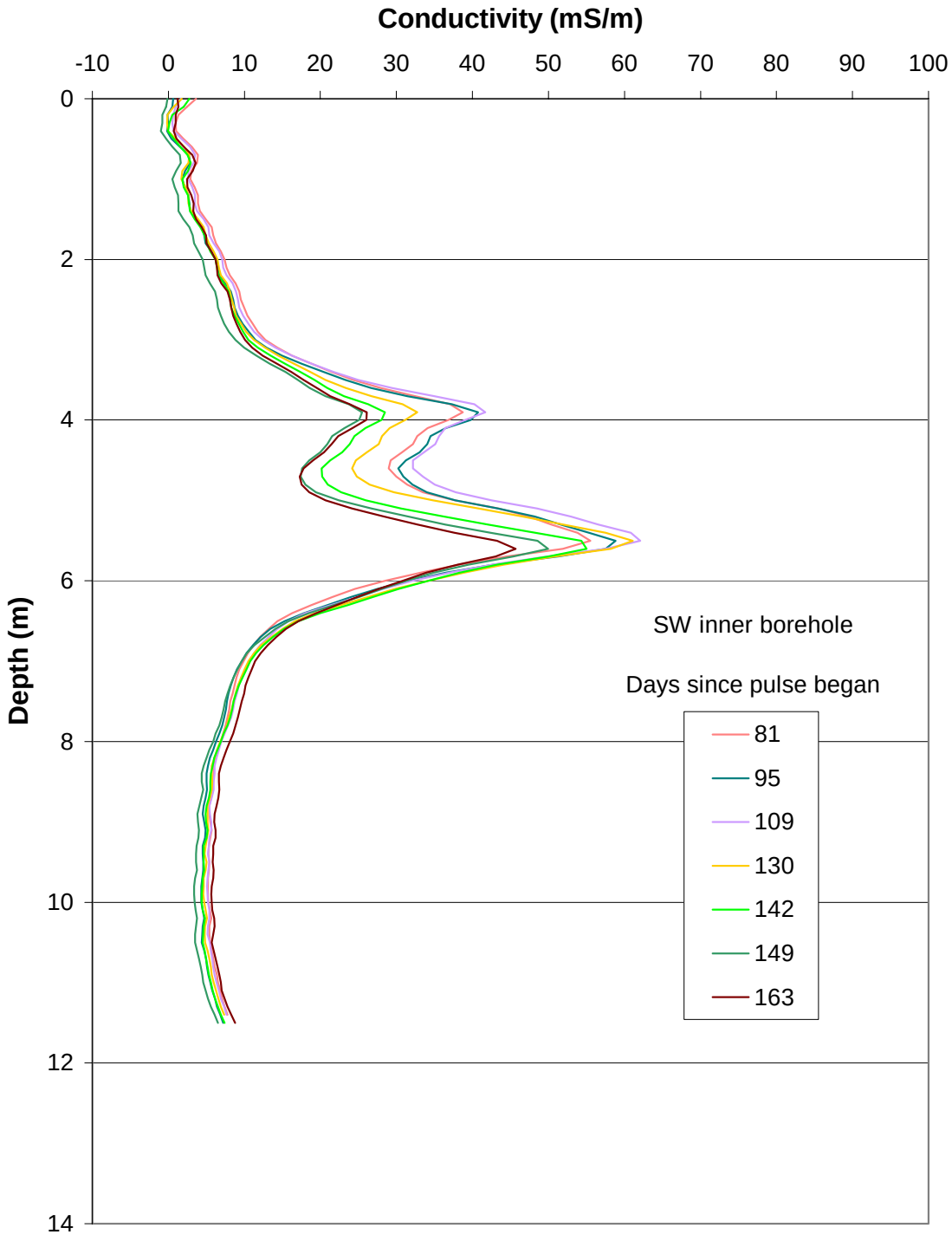


**Figure 1.2.17: Raw EM39 data collected in the South West Inner borehole during the tap water flush and after infiltration ended on Day 142.**

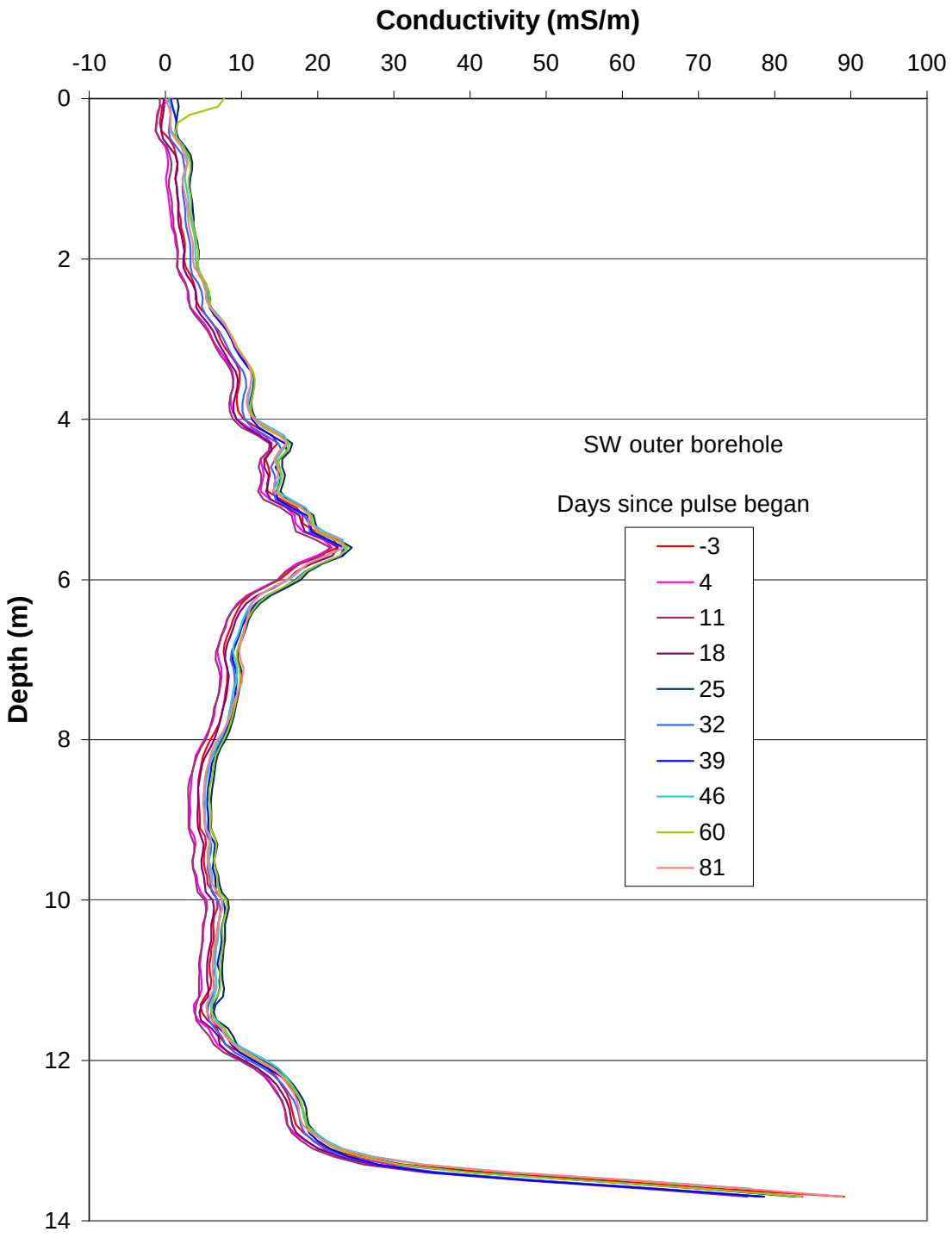


**Figure 1.2.18: Raw EM39 data collected in the South West outer borehole during the infiltration of the salt pulse.**

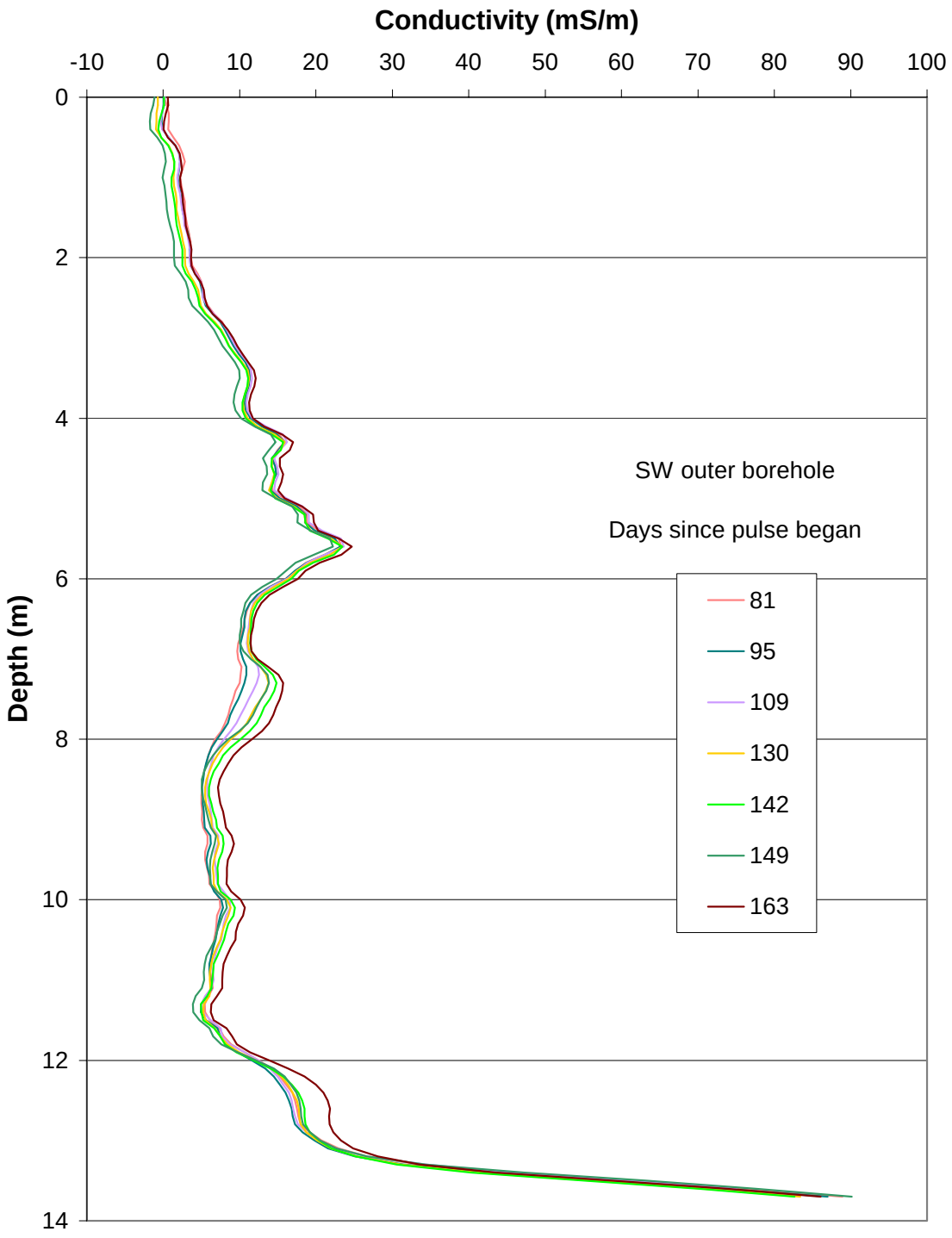


**Figure 1.2.19: Raw EM39 data collected in the South West outer borehole during the tap water flush and after infiltration ended on Day 142.**

## 1.3 Three Dimensional Images

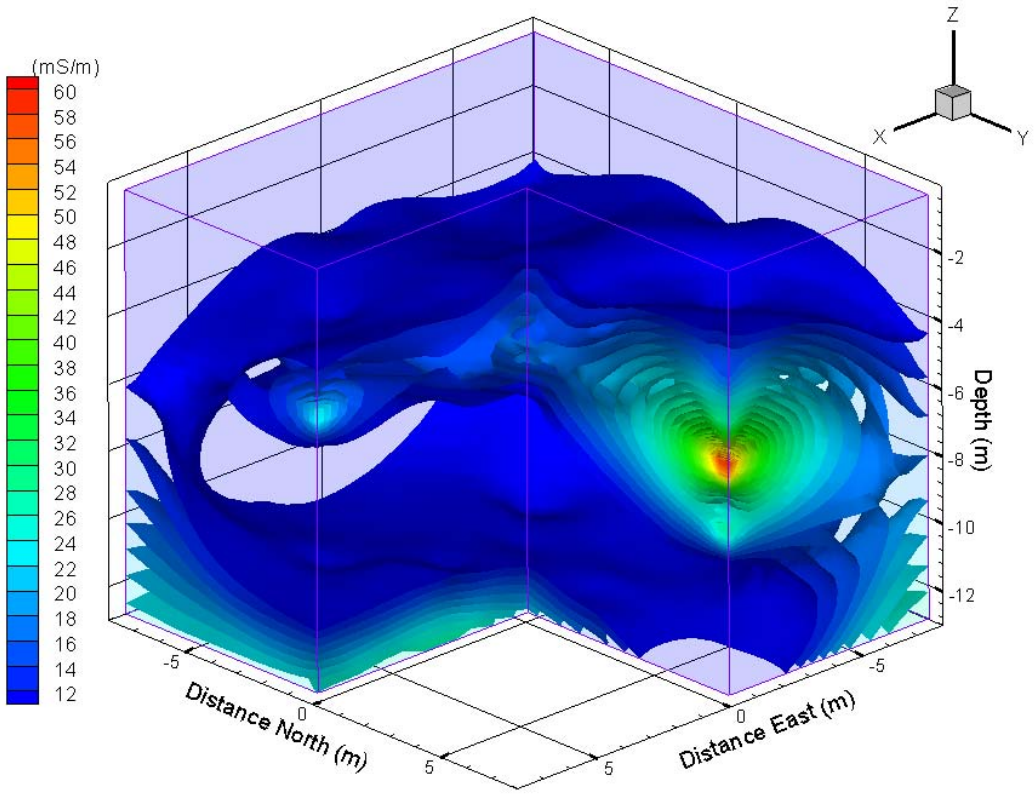


**Figure 1.3.1: Bulk soil conductivity (mS m-$^{1}$) measured 3 days before the salt pulse began**.

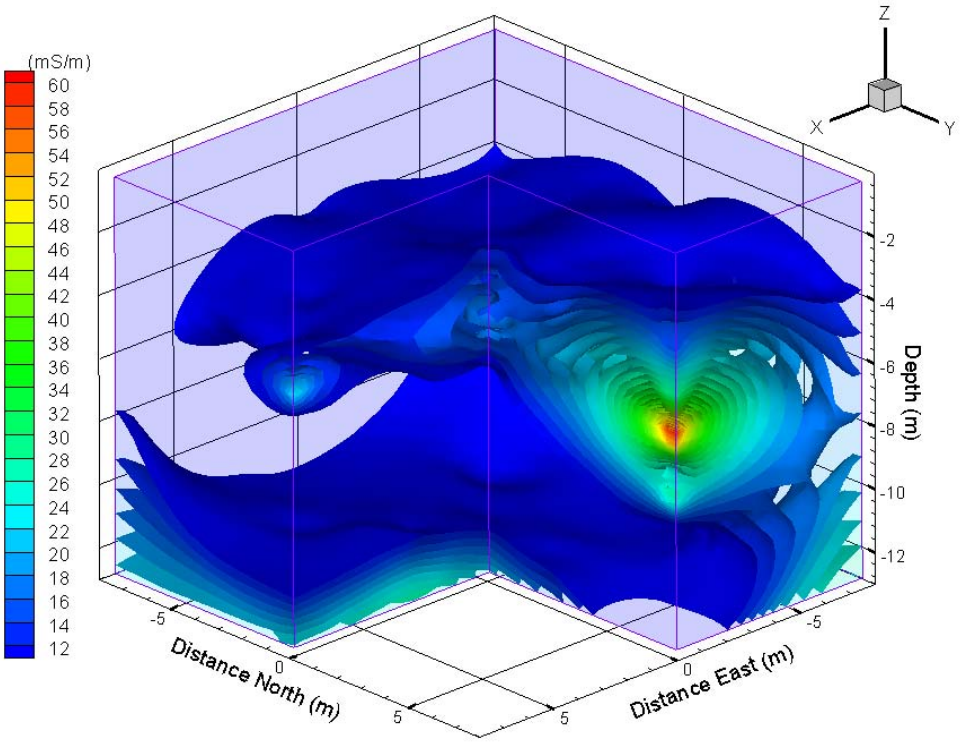


**Figure 1.3.2: Bulk soil conductivity (mS $m^{-1}$), 4 days after the salt pulse had begun**.

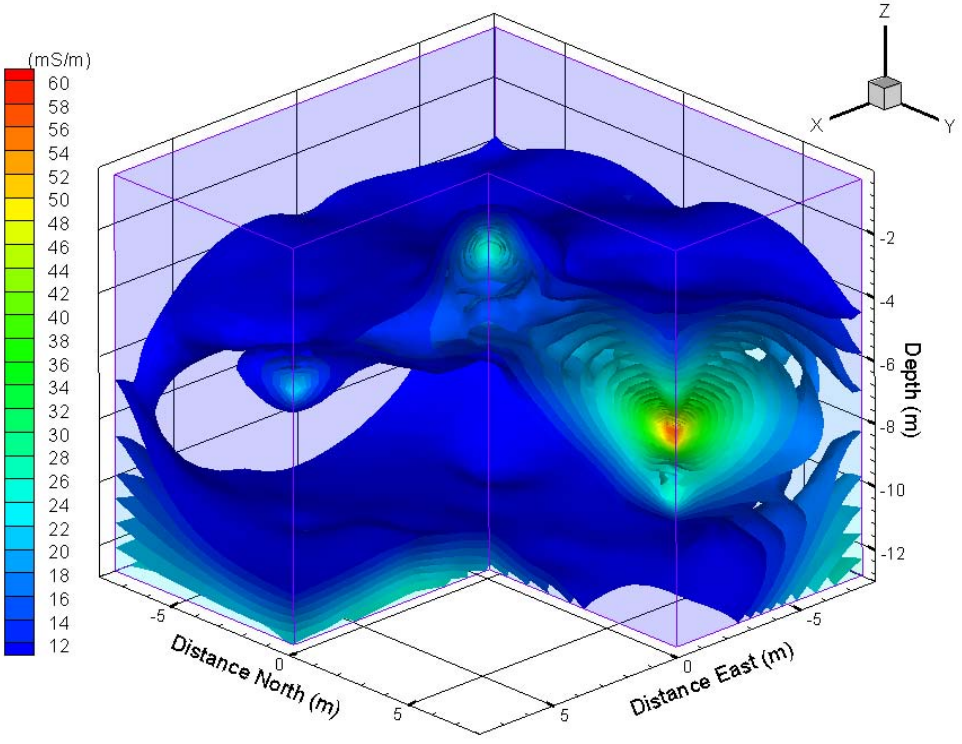


**Figure 1.3.3: Bulk soil conductivity (mS $m^{-1}$), 11 days after the salt pulse had begun.**

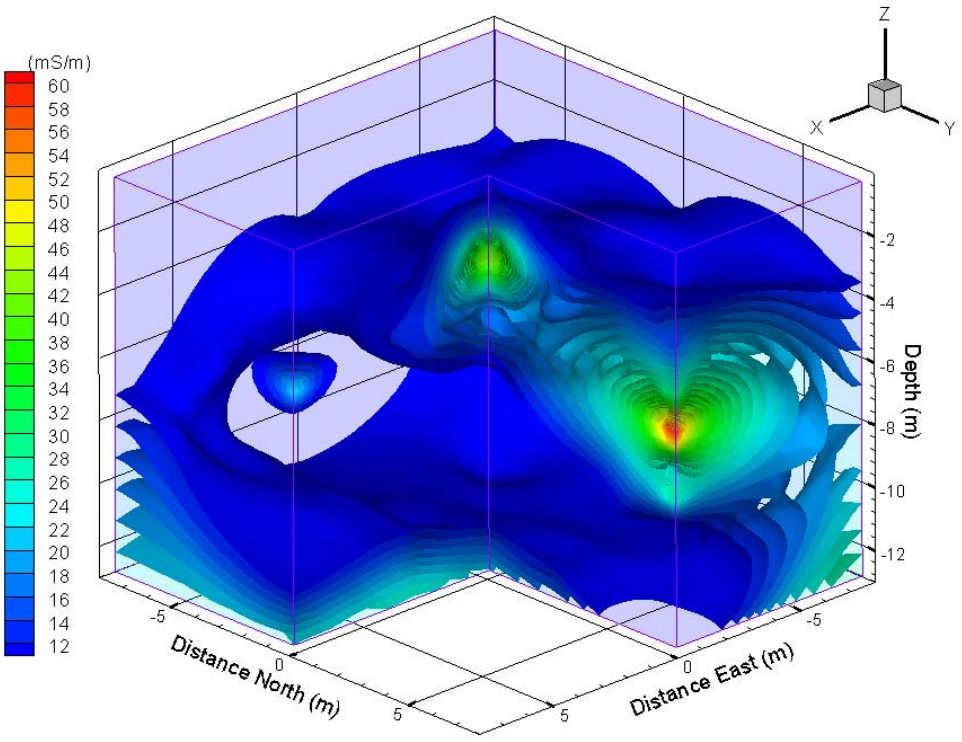


**Figure 1.3.4: Bulk soil conductivity (mS $m^{-1}$), 18 days after the salt pulse had begun.**

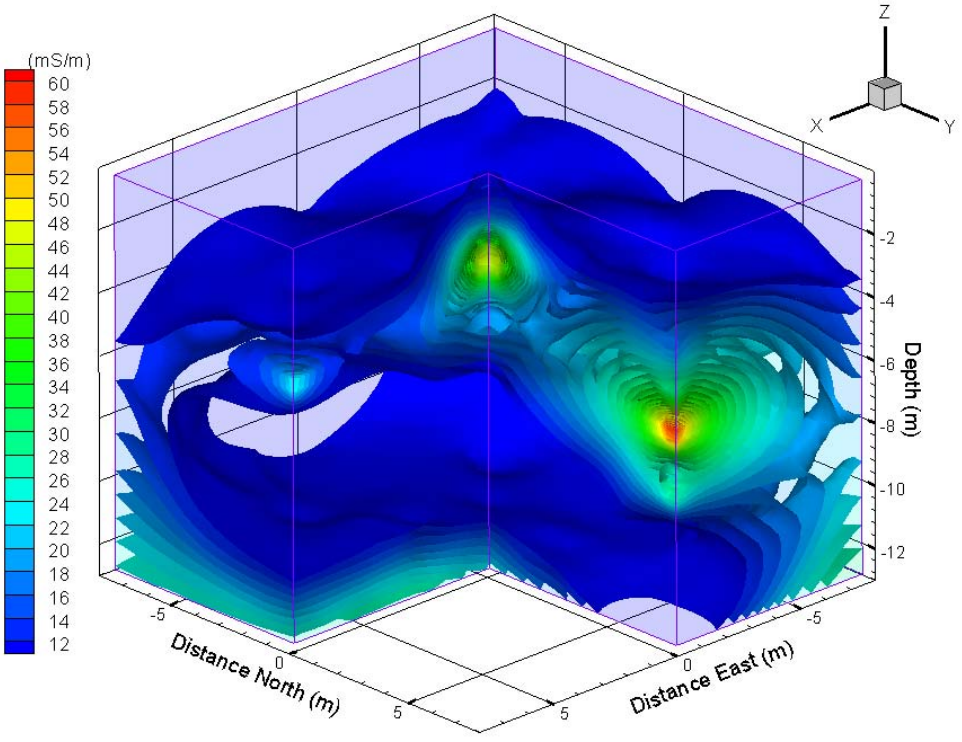


**Figure 1.3.5: Bulk soil conductivity (mS $m^{-1}$), 25 days after the salt pulse had begun.**

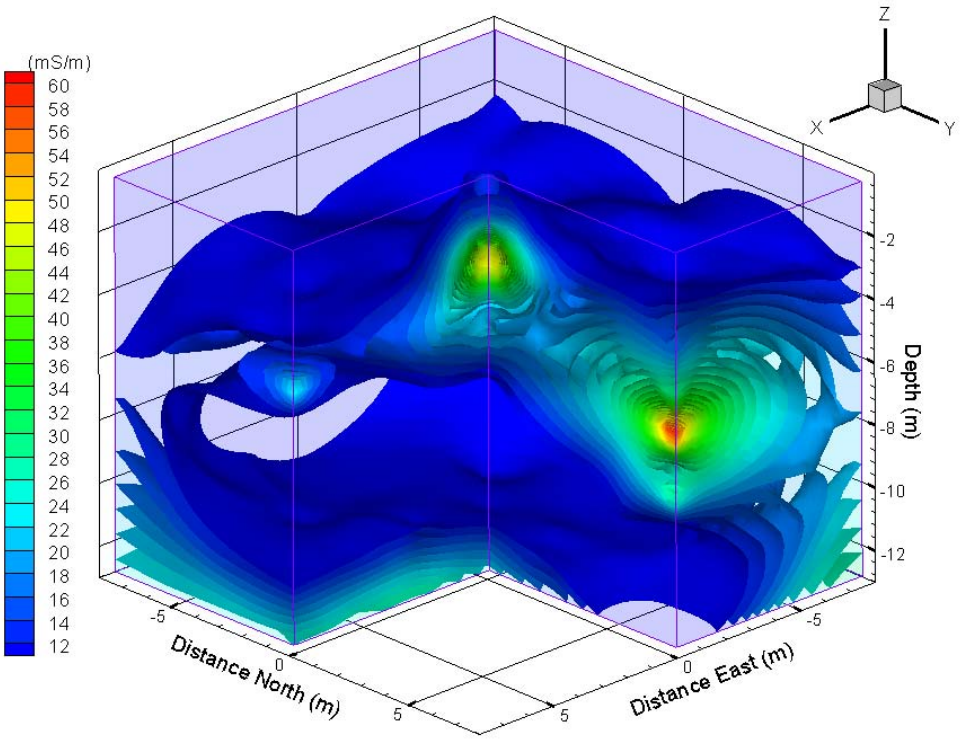


**Figure 1.3.6: Bulk soil conductivity (mS $m^{-1}$), 32 days after the salt pulse had begun.**

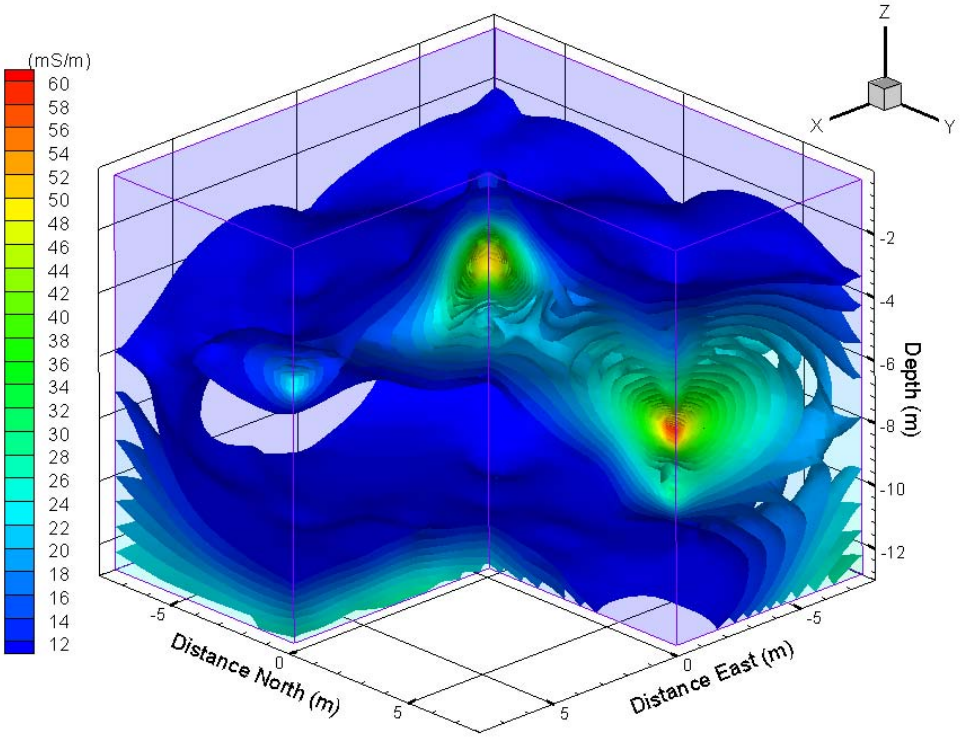


**Figure 1.3.7: Bulk soil conductivity (mS $m^{-1}$), 39 days after the salt pulse had begun.**

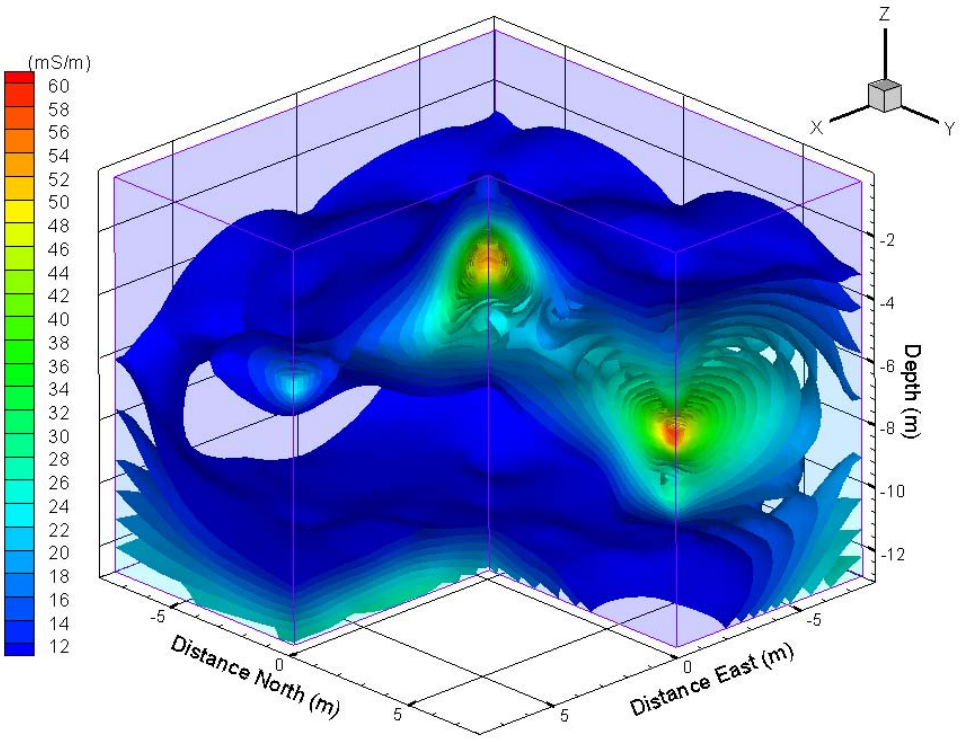


**Figure 1.3.8: Bulk soil conductivity (mS $m^{-1}$), 46 days after the salt pulse had begun.**

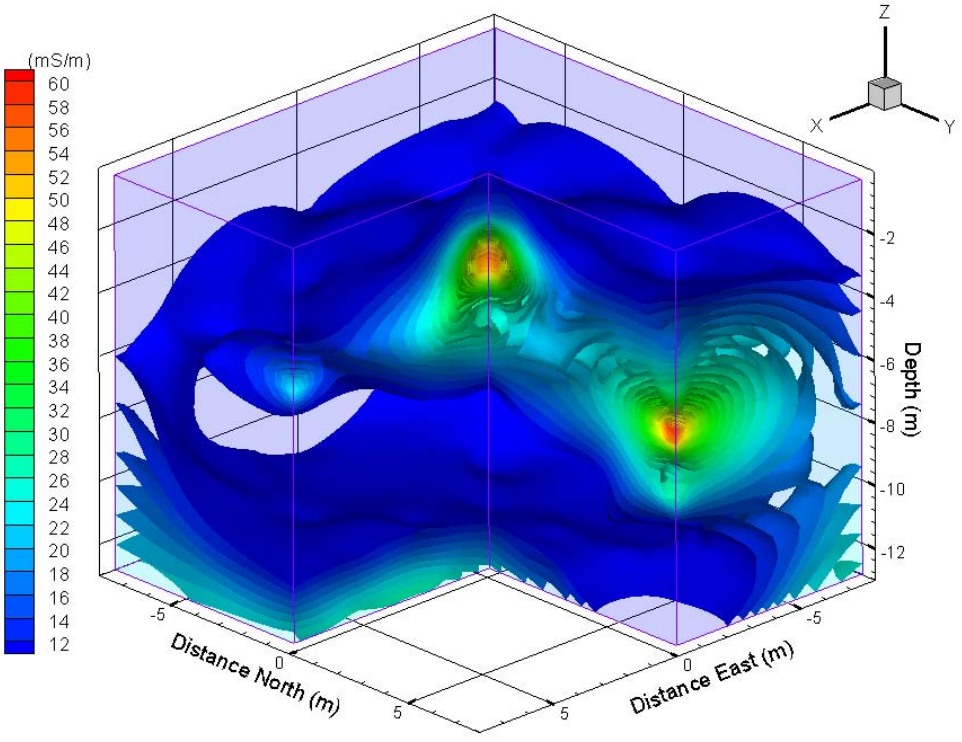


**Figure 1.3.9: Bulk soil conductivity (mS $m^{-1}$), 53 days after the salt pulse had begun.**

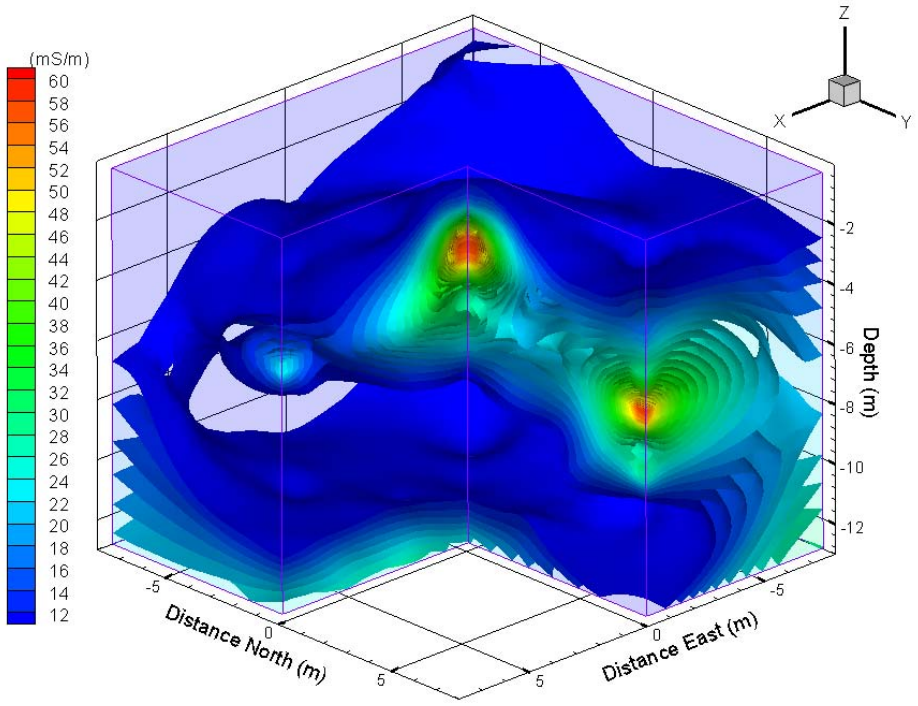


**Figure 1.3.10: Bulk soil conductivity (mS $m^{-1}$), 60 days after the salt pulse had begun.**

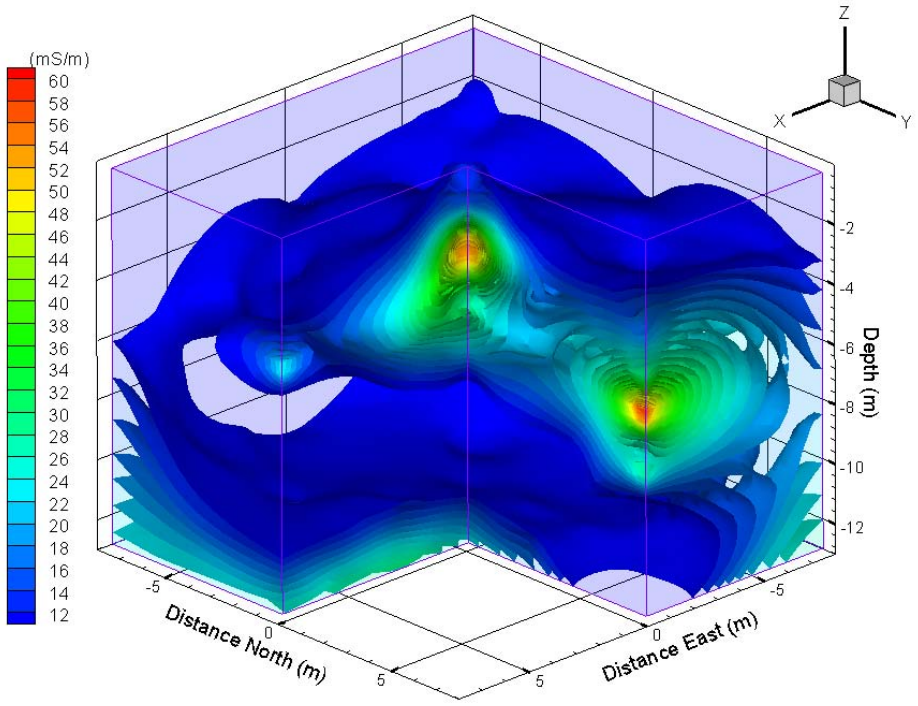


**Figure 1.3.11: Bulk soil conductivity (mS $m^{-1}$), 67 days after the salt pulse had begun.**

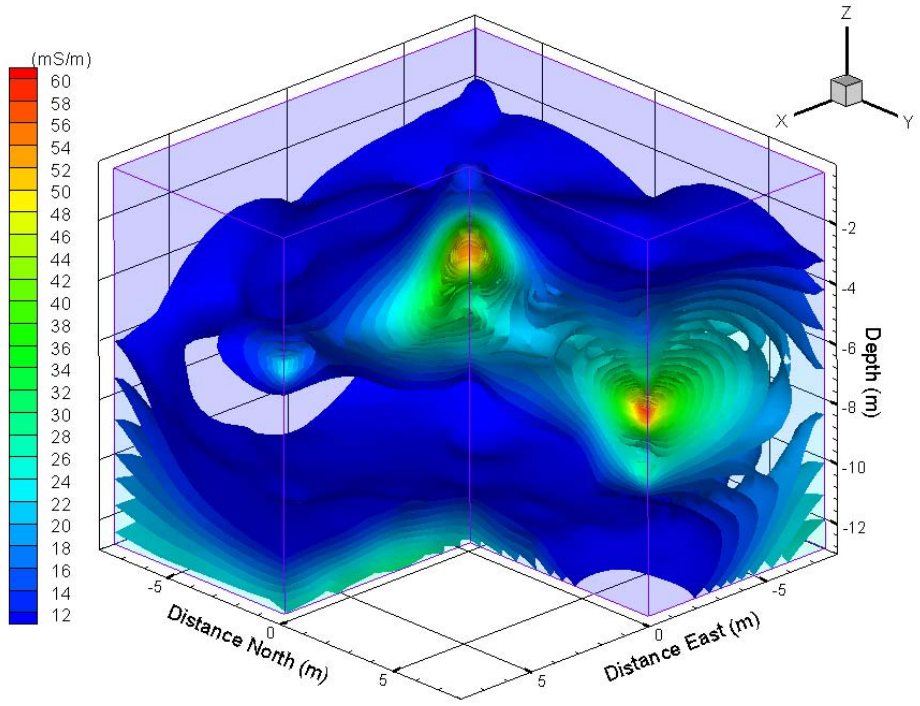


**Figure 1.3.12: Bulk soil conductivity (mS $m^{-1}$), 81 days after the salt pulse had begun.**

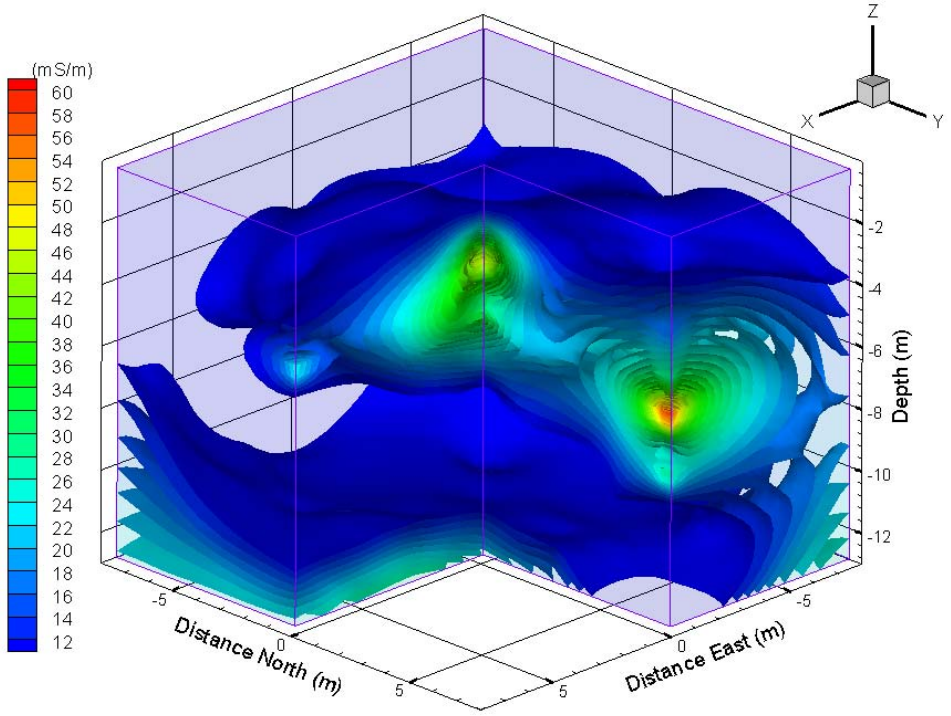


**Figure 1.3.13: ECa (mS $m^{-1}$), 10 days after the salt pulse ended (TRSP 95 days).**

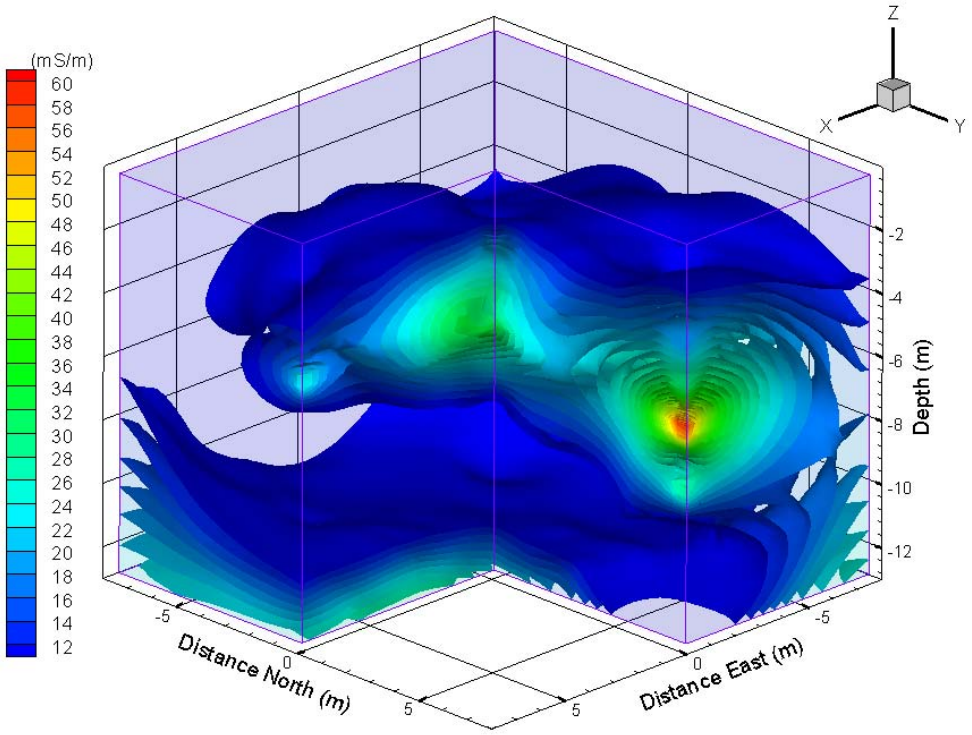


**Figure 1.3.14: ECa (mS m$^{-1}$), 24 days after the salt pulse ended (TRSP 109 days).**

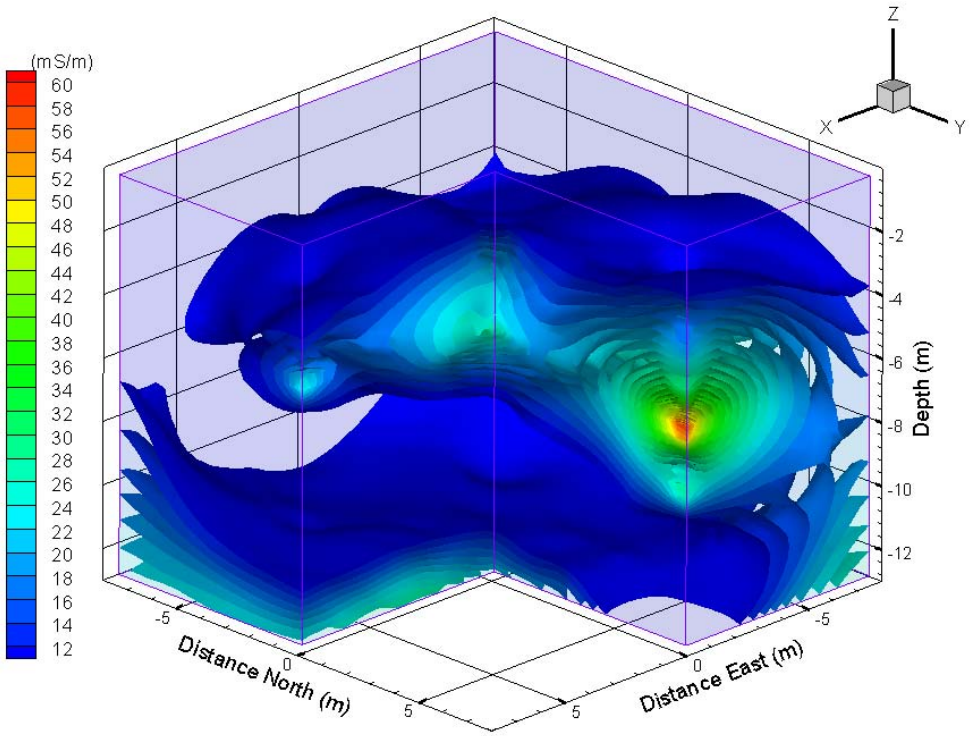


**Figure 1.3.15: ECa (mS m$^{-1}$), 45 days after the salt pulse ended (TRSP 130 days).**

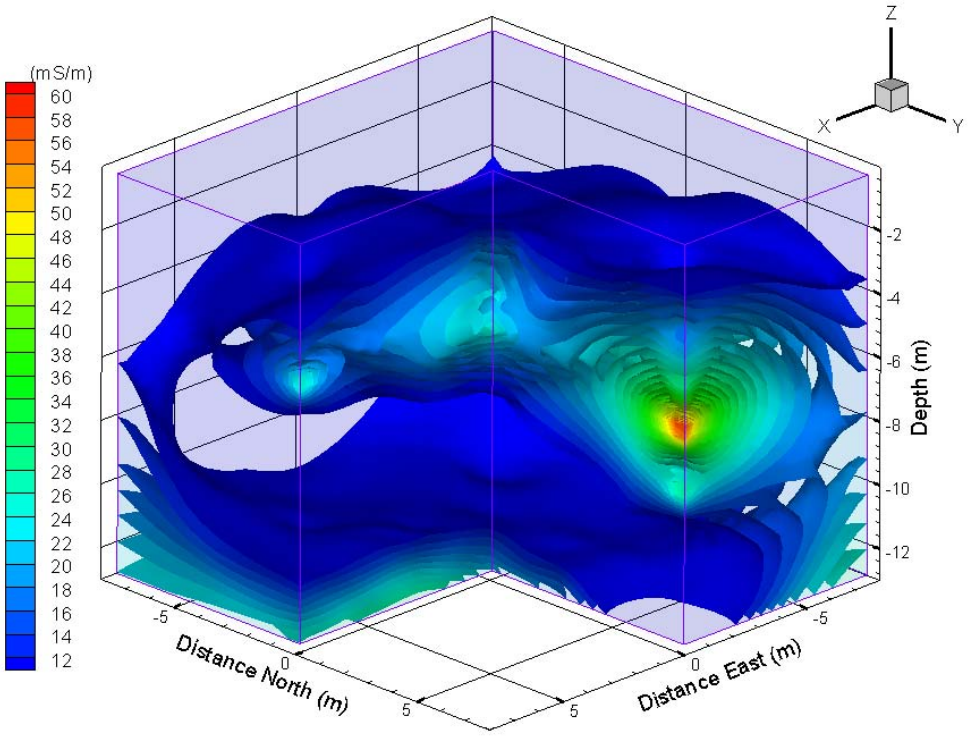


**Figure 1.3.16: ECa (mS m$^{-1}$), 57 days after the salt pulse ended (TRSP 142 days).**

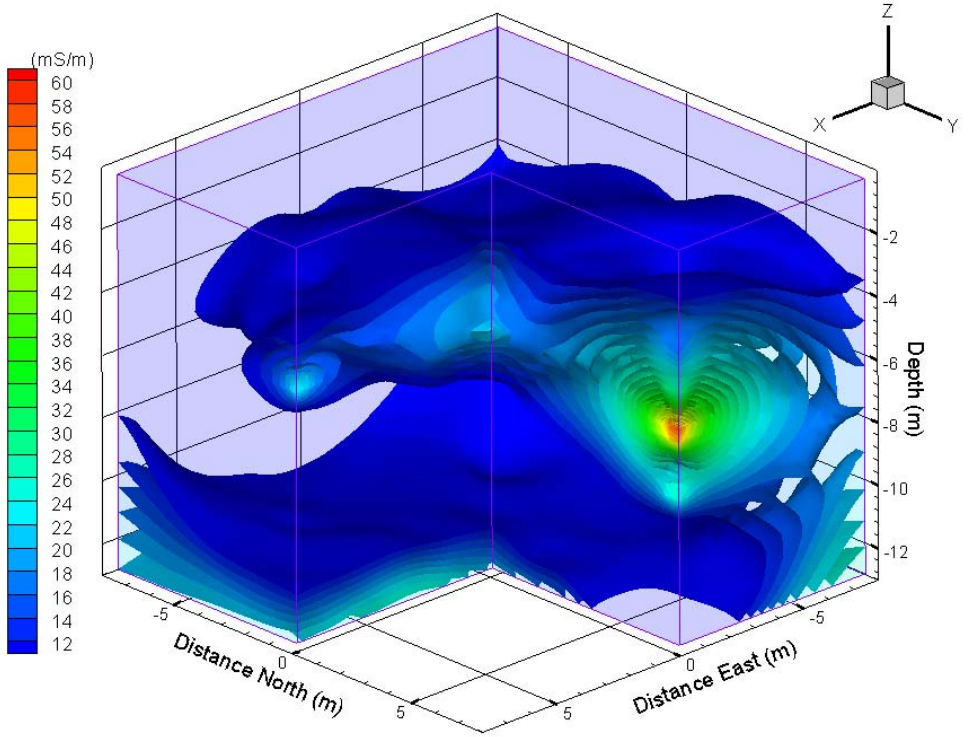


**Figure 1.3.17: ECa (mS m$^{-1}$), 7 days after infiltration ended (TRSP 149 days).**

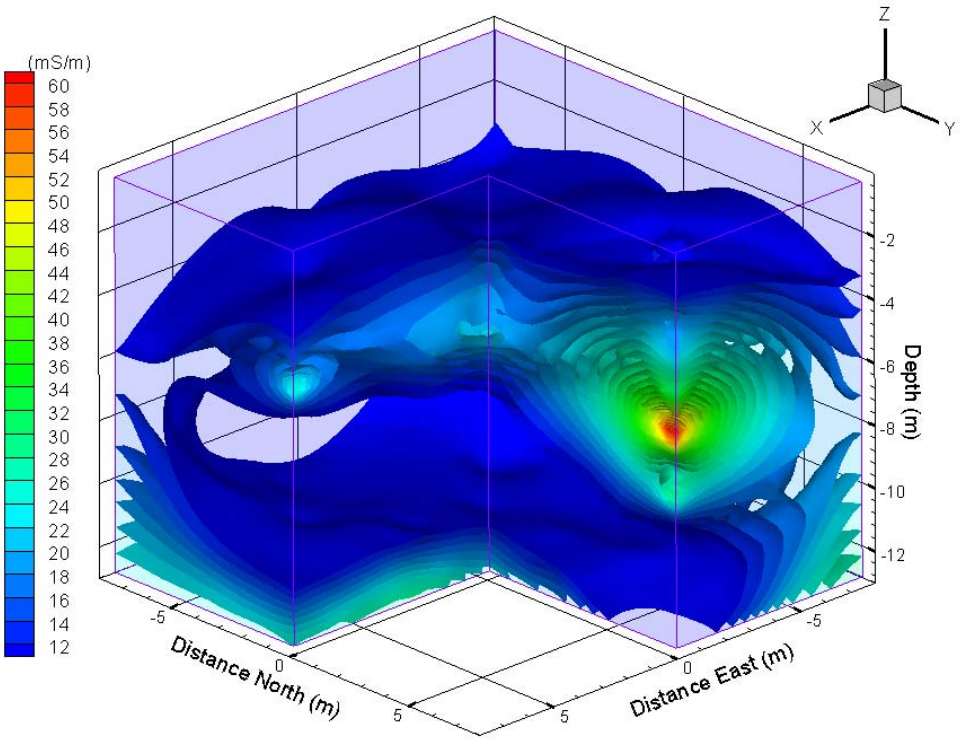


**Figure 1.3.18: ECa (mS $m^{-1}$), 21 days after infiltration ended (TRSP 163 days)**

## 1.4 Operating Procedures

The following operating instructions area condensed version of those provided with the Geonics Limited EM39 probe (1990) documentation. Modifications to this procedure were necessary to achieve a consistent calibration and were noted where appropriate.

### 1.4.1 Initial Set-Up

#### 1.4.1.1 System Set-Up

Position the tripod above the borehole so that the top of the tripod is at least 1m from the ground or 30cm from the top of the casing. Position the winch and console one

to two meters away from the borehole. Connect all of the cables between the tripod, winch, console and laptop. Before connecting the probe to the cable head, ensure that the fitting is well greased and free from sand and other particles. Also, ensure that the equipment is turned off ("BATT" switch in the "OFF" position) whenever connecting or disconnecting the probe from the cable head to avoid an electrical shock.

#### 1.4.1.2 Battery Condition

Check the condition of the battery pack located in the back of the console before taking any data. Set the sensitivity range switch "millisiemens/meter" to "BATT" "+" and "-" position. Set the battery mode switch to the "INT" position. The meter will now indicate the condition of the batteries. If the meter needle is below the "BATT" position for either positive or negative set, replace the batteries or check that the battery contacts are clean.

#### 1.4.1.3 Temperature Equilibration

Not mentioned in the instruction manual that accompanies the EM39 equipment, is the need to temperature equilibrate the probe before use. After setting the equipment up, use the winch to lower the probe to the bottom of the borehole. Leave the probe at the bottom of the borehole for a minimum of 45 minutes to an hour to ensure complete temperature equilibration. The temperature equilibration should be done before the instrument zero is checked.

#### 1.4.1.4 Instrument Zero

It is recommended in the EM39 operating manual that the nulling procedures are preformed before the logging of each borehole. To set the NULL of the instrument, pull the cable with the cable head from the winch so that you are at least 2 to 3 meters away from any metal objects (including any rings, watches or keys on your body). Attach the probe to the cable head and then lift the probe vertically in the air (at least 2 meters above the ground), holding it at the end opposite the connector.

To check the instrument zero, set the range switch to 1000 millisiemens/meter and the "BATT" switch to the "INT" position. Set the "GAMMA-COND." switch to the "COND." position. Now set the meter needle to the zero position using the "Q/P" control. Set the sensitivity switch to a higher sensitivity range (smaller millisiemens/meter setting) and further null the quadrature (conductivity) component.

When the quadrature component zero is obtained on the most sensitive range (30 millisiemens/meter), push the inphase switch (push button above the "I/P" control) and use the "I/P" control to the null the instrument inphase component. Release the "I/P" button and check that the quadrature component is still zero. Readjust "Q/P" if necessary.

After using this technique several times, it became apparent that calibrating before logging each borehole decreased the repeatability of the measurements from one day to the next. This error is most likely caused by the difficulty in finding an area of "zero" conductivity in which to calibrate the probe as we move from one borehole to the next. To minimize this error, we decided to calibrate the probe only once for each data set (one data set covers all 13 boreholes at the site). We also calibrated in the exact same location for each data set to ensure that the background conductivity was the same. Our

calibration site was a wooden fence post with a small section of PVC pipe on top to hold the probe in place. We would place the probe in the PVC pipe and make sure all metal objects (and humans) were far away before calibrating.

### 1.4.2 Collecting Data

#### 1.4.2.1 Probe Measurement Point

The measurement point of the EM39 probe is the center point between the probe receiver and transmitter coils and is located 68 cm from the bottom of the probe (opposite from the probe connector). This point has to be used as a reference for correlation with the log. We marked our probe at 118 cm from the bottom to account for the 50 cm of borehole casing that is above ground.

Before lowering the probe into the hole, make sure that the cable head connector is properly locked to the probe and the hole is free from obstacles. Lower the probe into the hole and line up the marking on the probe with the top of the borehole casing (the measurement point of the probe should then be approximately level with the ground surface).

#### 1.4.2.2 Recording Interval

Depending on the desired recording interval (resolution) the opto-encoder rate switch (on the tripod) could be set to send pulses at the following rates: 2.5, 5, 10, 20 and 40 cm per pulse. Ensure that the recording interval entered on the laptop matches the recording interval set on the tripod. All of the data sets for this site were taken at a recording interval of 10 cm per pulse.

#### 1.4.2.3 Speed of Logging

In order to not miss measuring any data points, it is necessary to observe that the combination of the cable speed and the recording rate interval do not exceed the maximum sampling interval of 2 samples per second. The following expression can be used to calculate the maximum speed of the cable during the recording:

$V_p = 120R$ where $V_p$ is the speed of the probe in meters/minute and R is the opto-encoder rate setting in meters per pulse. For example, the maximum velocity recording interval of 0.1 m/pulse would be 0.2 m/sec.

During data collection it is usually necessary to monitor the velocity to ensure that the speed of the winch remains constant during logging. The data collection program on the laptop will report the velocity in real-time, but does not save that information with the data file. To ensure repeatability, all data sets were collected at a speed of 0.100 meters/second, with $\pm 0.010$ m/s error due to inconsistencies with the winch motor.

### 1.4.3 Equipment Specifications

#### 1.4.3.1 Output Time Constant

Due to the instrument output time constant (rise time of 0.7 seconds), the log will be shifted from actual vertical position of formation by an amount proportional to the speed of logging. To determine the vertical displacement of the log the following approximate expression can be used:

$X = 0.02V_p$

where X is vertical displacement of the log in meters and $V_p$ is the speed of the probe in meters/minute.

For our data sets the velocity was always 0.100 m $s^{-1}$ or 6 m $min^{-1}$. That velocity leads to a displacement of 0.12 m.

#### 1.4.3.2 Range of Sensitivity and Accuracy

The range of conductivity measured is controlled by the sensitivity switch, which has five settings: 0-30, 100, 300, 1000, 3000 millisiemens per meter. When the range switch has to be changed during logging, allow a few seconds for stabilization before continuing with the measurement. The conductivity at the test site was found to never reach above 90 mS $m^{-1}$, so the 0-100 mS $m^{-1}$ setting was used for all data sets.

The measurement accuracy is reported in the manual as ±5% at 30 mS $m^{-1}$. The reported repeatability of the equipment is ±2% for conductivities ranging from 100 to 3000 mS $m^{-1}$ and ±2 mS $m^{-1}$ for 0-100 mS $m^{-1}$. The repeatability values are valid only when the probe temperature change is less than 10°C. The reported noise level of the probe is <0.5 mS m-1.

#### 1.4.3.3 EM39 Calibration Curve

A secondary calibration is necessary when the measured apparent conductivity is above approximately 800 mS $m^{-1}$. This correction is described in Technical Note – 20 (TN-20) included in the EM39 instruction manual. This correction is caused by departure from the “low induction number” approximation at high values of terrain conductivity.

Since the conductivity in this experiment never ranged above 100 mS $m^{-1}$, this correction was not used in any data sets.

# Appendix 2 – Neutron Probe Data

## 2.1 Introduction

Neutron probe data was collected monthly in each of the 13 access boreholes to measure soil volumetric water content. Measurements were made at 0.25 m intervals up to a total depth of 12 m. Specific operating procedures are outlined in section 3.3 of this Appendix. Three-dimensional images created with the moisture content data are presented in the following section. Although neutron probe data was collected during the entire infiltration experiment, only the data collected between the start of the high conductivity pulse and the end of infiltration is analyzed here. Two measurements were also taken in the month following the end of infiltration (149 and 163 days relative to the start of the pulse).

The images of water content distribution vary only slightly from one month to the next, but this is expected, since constant flux irrigation events had been occurring for approximately 1000 days prior to the data presented here. The zones of highest water content are directly below the infiltrometer and across the site at 4-6 m depth (the thick clay layer). There is also a zone of high water content at approximately 12 m depth, but this is poorly constrained, due to the few number of data points at this depth (some boreholes only reach 11 m depth).

The measurements taken after infiltration ended show only a small decrease in the wetted area, with the most noticeable decrease seen between 1-4 m below the infiltrometer. Water content is mostly unchanged at the surface directly below the infiltrometer and within the clay layer, even 21 days after infiltration had ended. The persistence of the high water content zone near the surface is most likely due to very low evaporation rates directly below the infiltrometer cover.

## 2.2 Three Dimensional Images

The following series of images were created in Tecplot v 9.0. The North East corner of the plotted area has been removed to better visualize the shape of the wetted area. All images are presented looking South West.

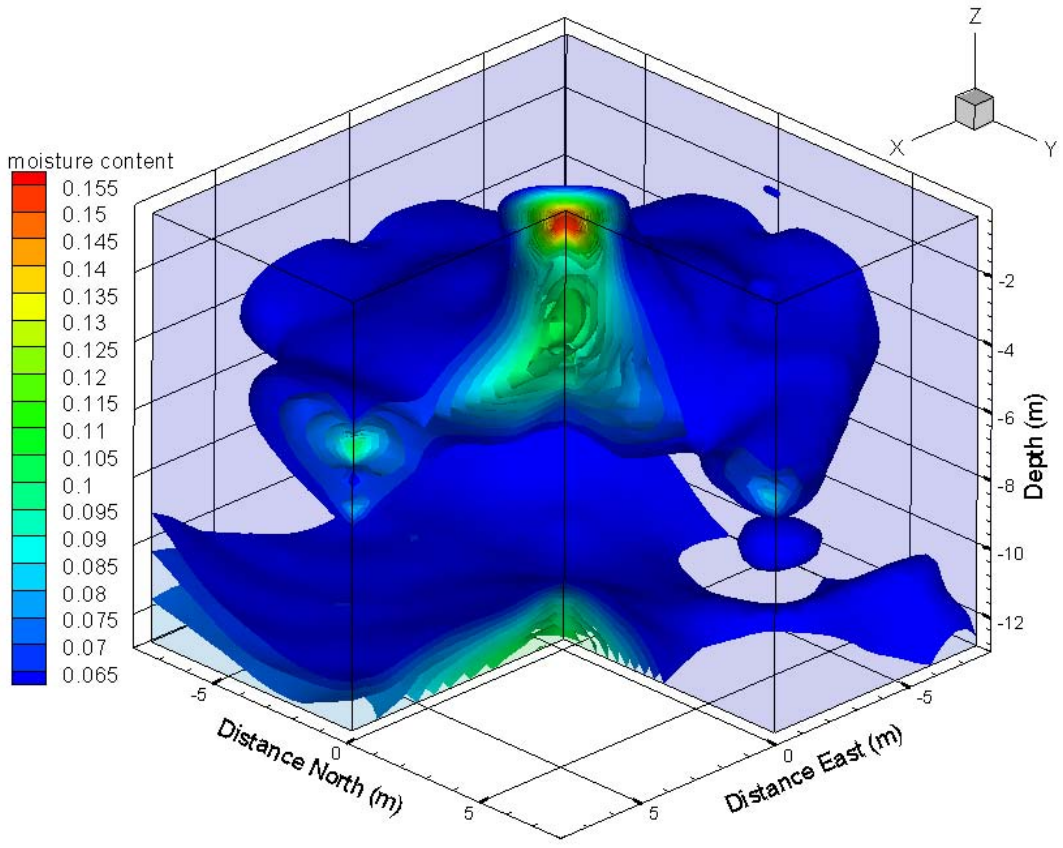


**Figure 2.2.1: Neutron probe data collected 38 days before the salt pulse began.**

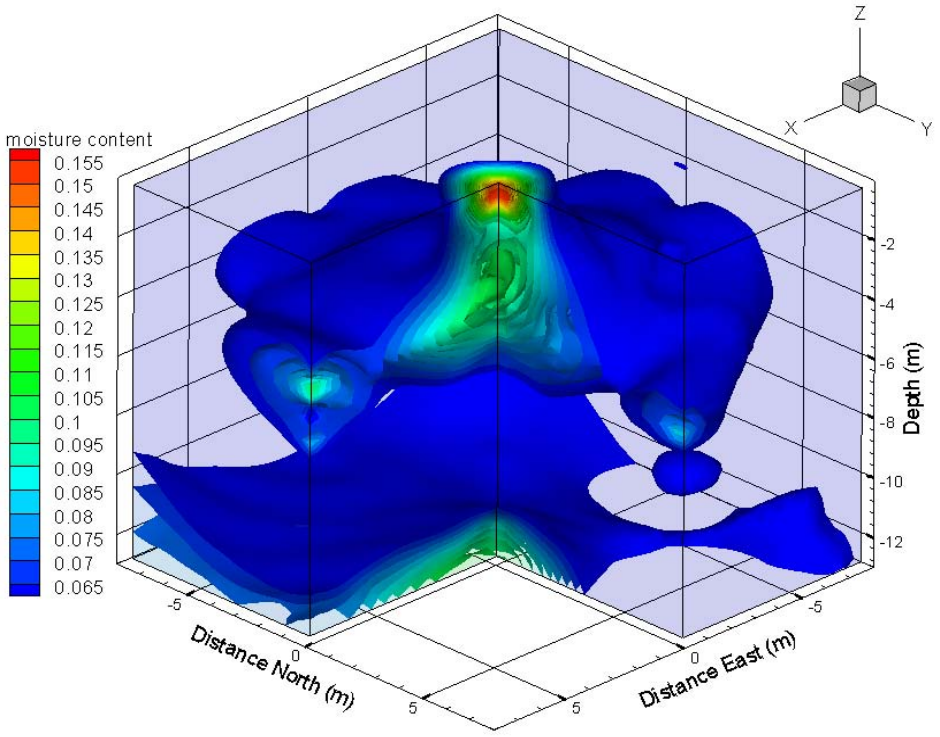


**Figure 2.2.2: Neutron probe data collected 10 days before the salt pulse began.**

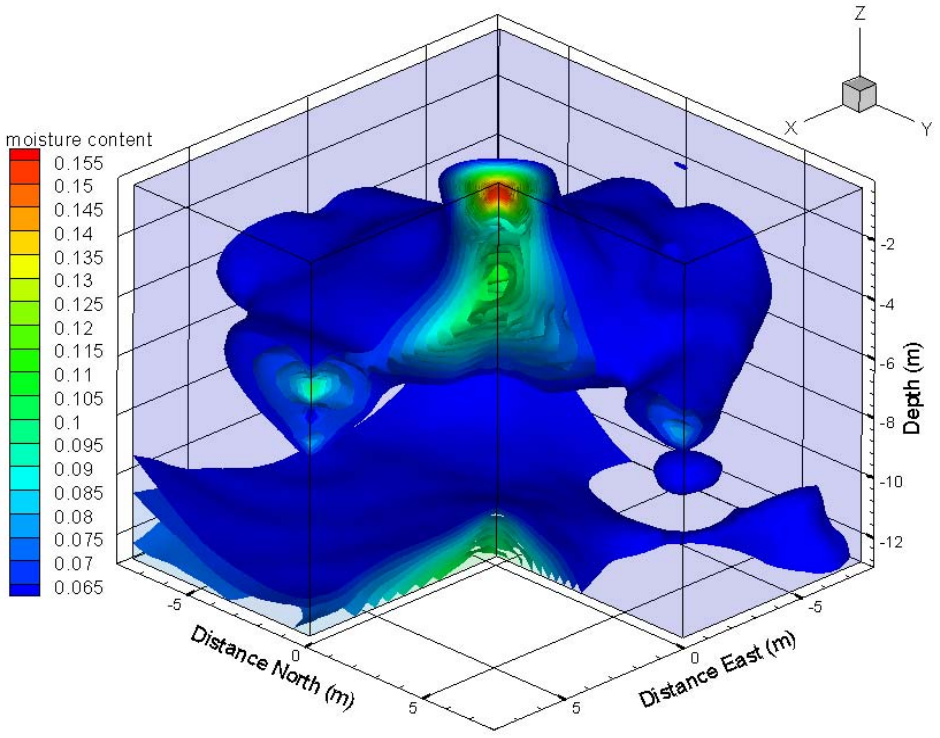


**Figure 2.2.3: Neutron probe data collected 35 after the salt pulse began.**

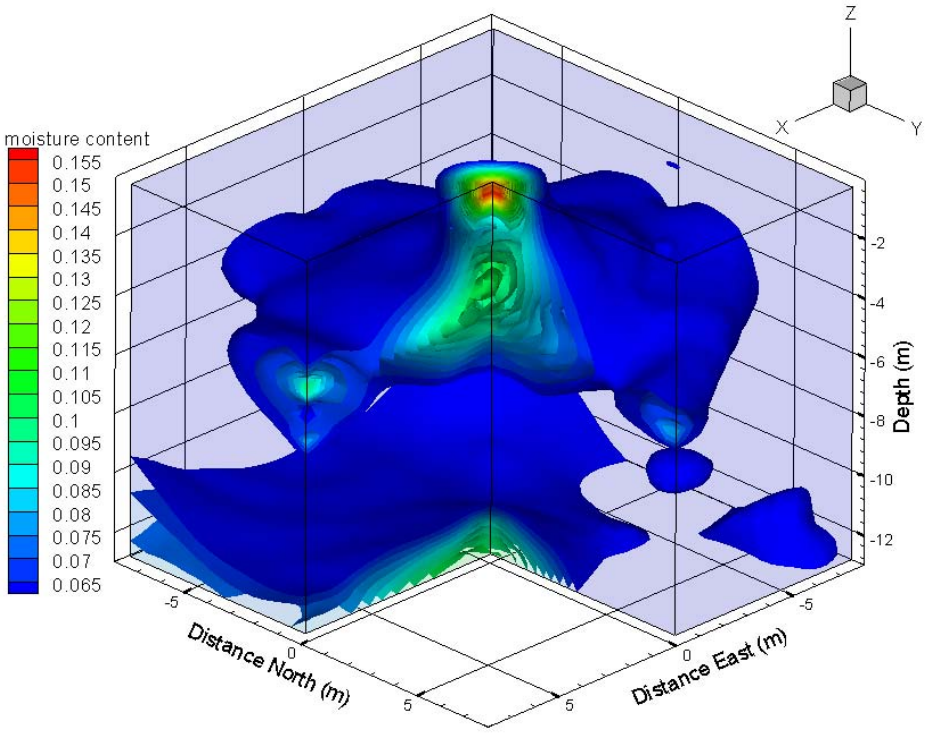


**Figure 2.2.4: Neutron probe data collected 62 days after the salt pulse began.**

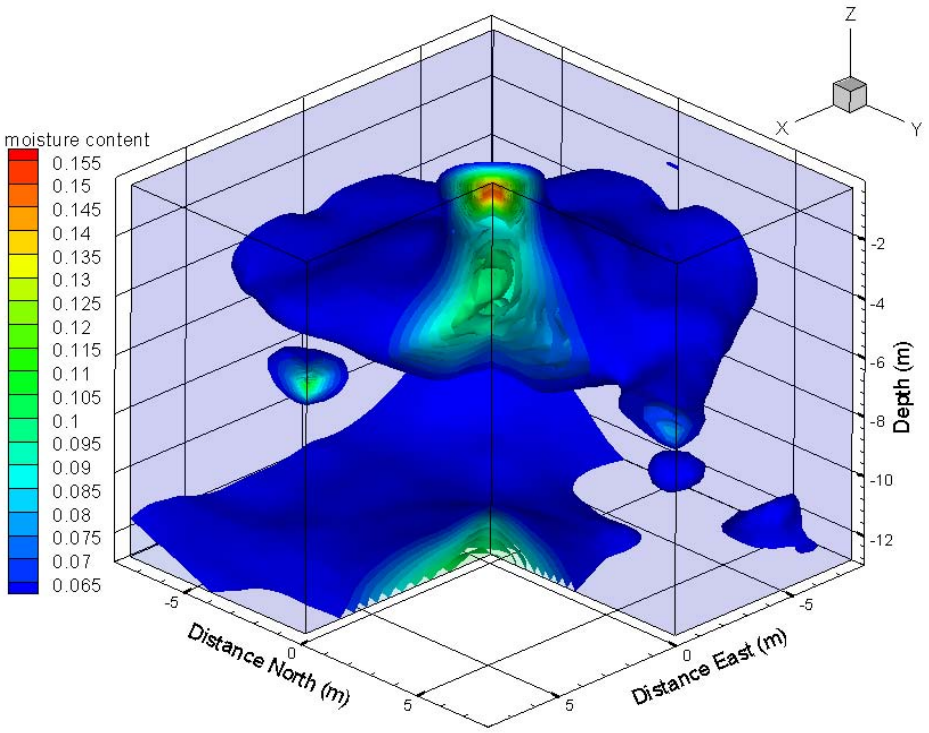


**Figure 2.2.5: Neutron probe data collected 101 days after the pulse began.**

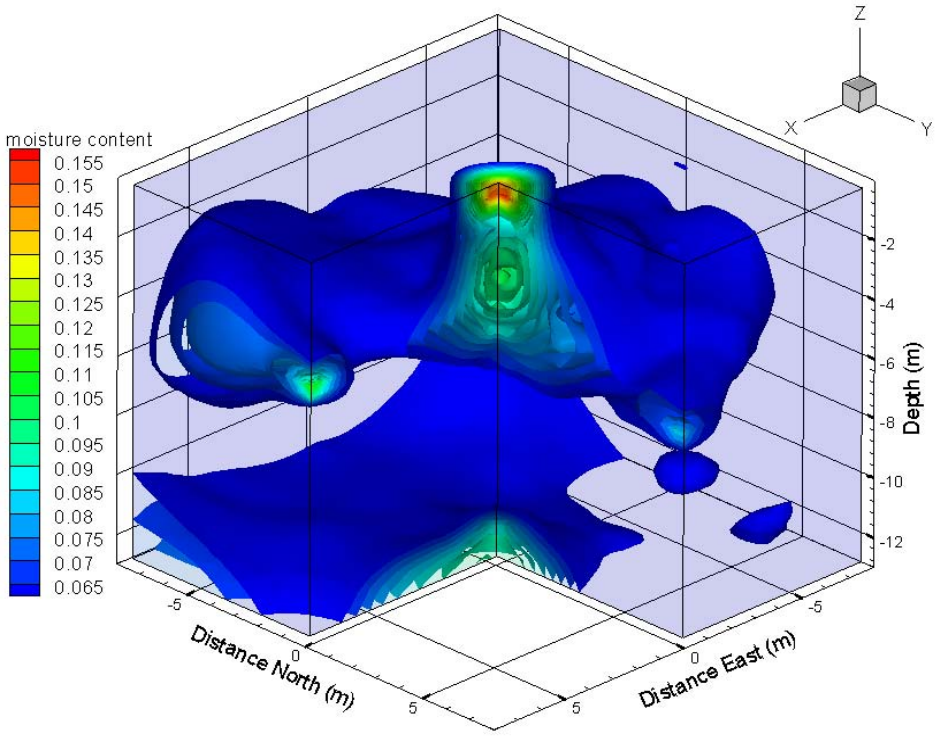


**Figure 2.2.6: Neutron probe data 135 days after the pulse began.**

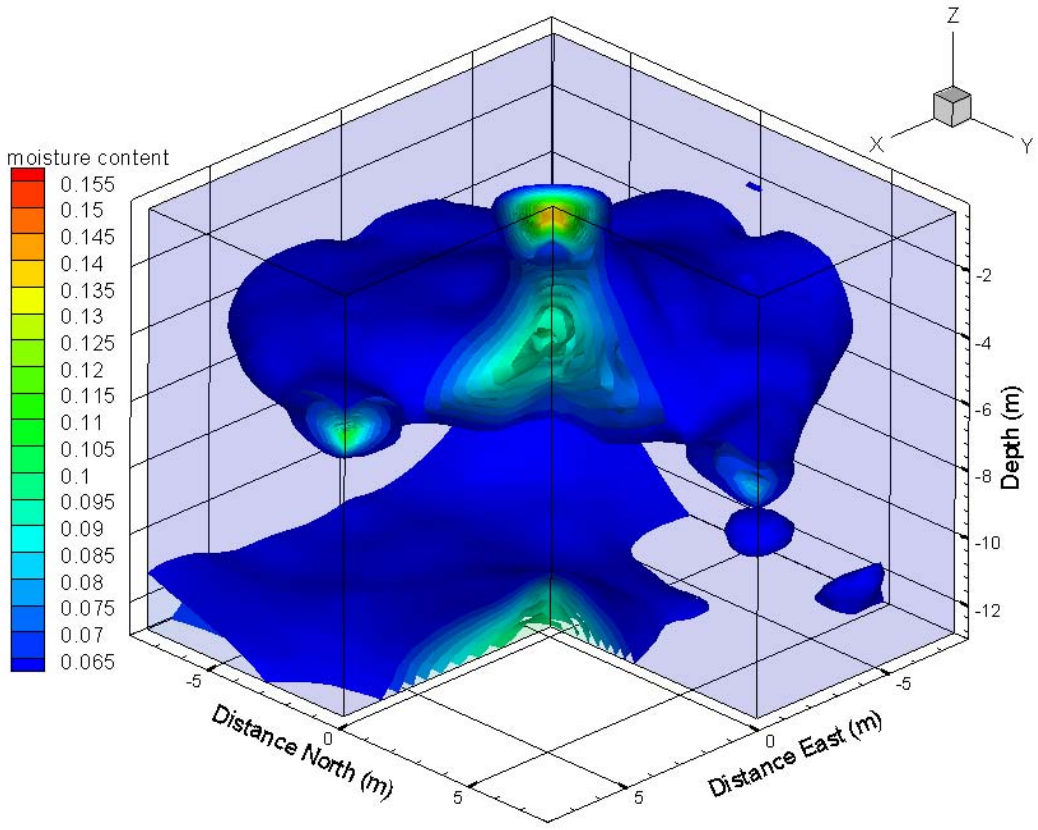


**Figure 2.2.7: Neutron probe data collected 149 days after the pulse began, and 7 days after infiltration ended.**

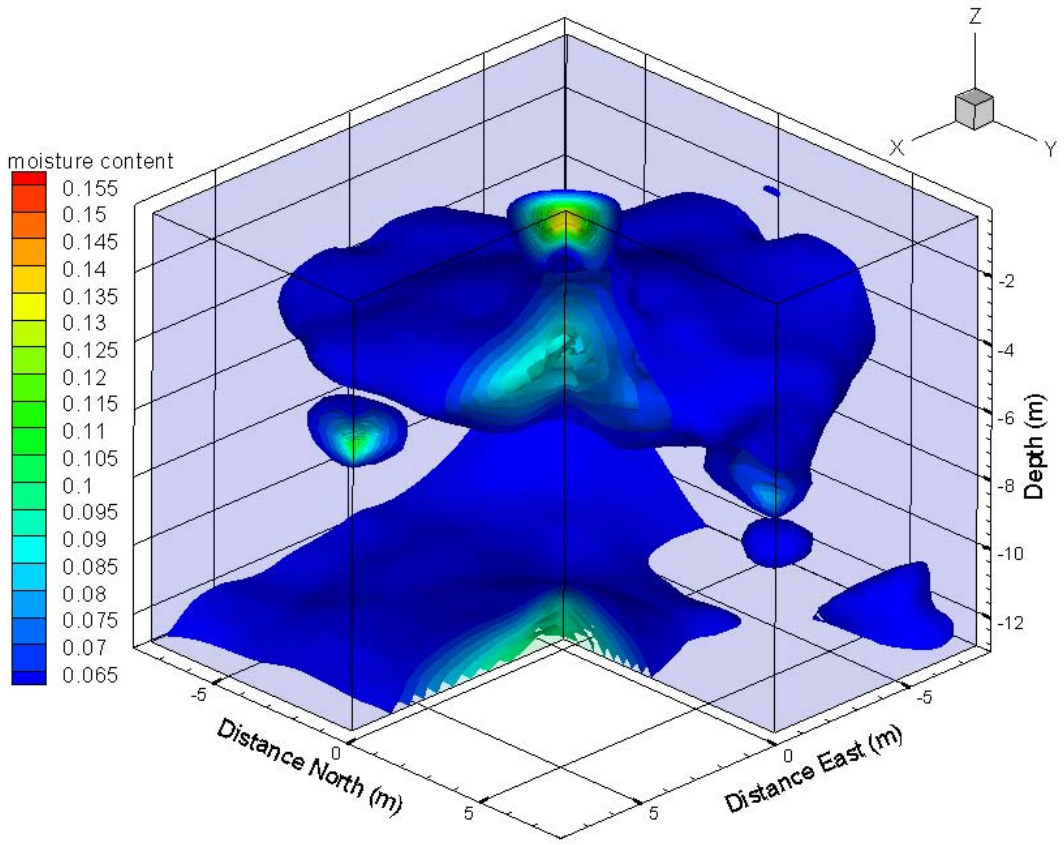


**Figure 2.2.8: Neutron probe data collected 163 days after the pulse began and 21 days after infiltration ended.**

## 2.3 Operating Procedures

### 2.3.1 System Setup

#### 2.3.1.1 Performing the Standard Count

Attach the cable to both ends of the probe. Place the probe on top of the tube of the standard count barrel. Lower the probe to the first silver stop. Press the STD key. Press step until the display asks "NEW STD?" Press the Enter key and step away from the probe. Wait for S#### (S followed by a four digit number) to appear and for the beeping to stop.

Once the beeping has stopped, press the step button to step through the screen display mode. The following will be displayed as you step through:

P ####- indicates the previous standard count

S ####- indicates the new standard count

Chi #.##- indicates the chi squared ratio of the new count

Write down all three of these numbers in the yellow field book. If the Chi number is out of the range 0.75 to 1.25, repeat the standard count. Press Enter to save the new standard count

#### 2.3.1.2 Selecting units

Select the units by pressing the Units key, step through the options by pressing the Step key. To collect the raw data, press enter when "MUNT CNT" appears on the display. Press the time key to select the sample time, step through the options by pressing the step key. When "Time32" appears on the display, press the Enter key.

#### 2.3.1.3 Setting the format

Every time we take data we want to clear the previous data that has already been downloaded. Clearing previous data is accomplished by setting the format. To set the format, press the FMT key. It will display a rec number, press step to continue to the next parameter. Then a key data number will appear (Key data is for other parameters to be entered), just hit step. Then depths will appear, we want 46 depths. To change depths just press the number of depths you want. Then press step. The display will read "SET FMT?," press Enter.

### 2.3.2 Taking Data

Press log and it will give an ID number, push the number you want for the designated hole. i.e. 1 for the ctr access tube. Look in the yellow number 1 book for the order and identification of access tubes. Press STEP and it will display K 1 0, press STEP. The next display will show TAKE 46. Lower the probe to the cable stop labeled 46 and press START. If you forget to lower the probe before taking your first measurement, press CLEAR and start again. The display will read COUNT 46. When the probe is taking a measurement at shallow depths you should keep a distance from the probe. Then it will beep and display M46.####. The number, #### is the raw count for that particular depth.

Press STEP to take a reading at the next depth. It will display TAKE 45. Lower the probe one stop and press START. Continue this process until you either reach the bottom of the hole or you take the last depth, TAKE 1. If you reach the bottom of the hole and there are several depths still to be taken, press STEP all the way through passed take one.

Now if you've taken the last depth or you've pressed step to get there, the display will say, "DATA OK?" Press ENTER to save the data. Then the display will read READY. It is ready to take measurements on another borehole. Pull up the cable until the probe latches with the top and move the probe to another borehole. Start the process over again by pressing log and repeat the procedure that was previously written. Once all the boreholes are logged, bring up the probe.

### 2.3.3 Downloading Data

Once data is taken hook up the probe to the computer in the data acquisition building by a cable. In the computer go the directory c:/aadir/hhgit/neutron/neuinf, type 123dump, enter 2 at the com port prompt, enter 2 for the 1200 baud rate. Enter the date using backslashes (i.e. 01/3/99), enter the path and file name based on the date i.e. c/aadir/hhgit/ neutron/neuinf/n052798.csv for neutron probe data on May 27, 1998. Enter N for hard copy (that wants to print the data), press enter and data should start downloading. Press Y for data okay then disconnect the cable. Then run neutron data reduction program for processing the data. Go to the shortcut on the desktop called Neutron.exe, double click. Under file enter data file to be processed and then press RUN. Next, go the shortcut entitled Moisture.exe, double click and enter file name and standard count and press run.

# Appendix 3 – Temperature Data

## 3.1 Introduction

One of the factors determining the ability of a material to conduct electrical current is temperature. Warmer materials tend to conduct electricity more than cooler ones. A temperature correction (Sheets and Hendrickx, 1995) was applied to the EM39 measurements of bulk soil conductivity to correct for temperature changes across the 6-month sampling period. Since temperature varies with depth and proximity to the infiltrometer, data from 39 thermocouples were interpolated into the same 3D volume as the EM data and neutron probe data. A temperature corrected conductivity calculation was then made for each cell in the volume. Thermocouple locations are indicated in Figure 8 in the main body of this thesis. Thermocouple depths were 0.1, 2, 4, 6, 8, and 13 m.

## 3.2 Three Dimensional Images

The following series of images were created in Tecplot v 9.0. The North East corner of the plotted area has been removed to better visualize the shape of the wetted area. All images are presented looking South West.

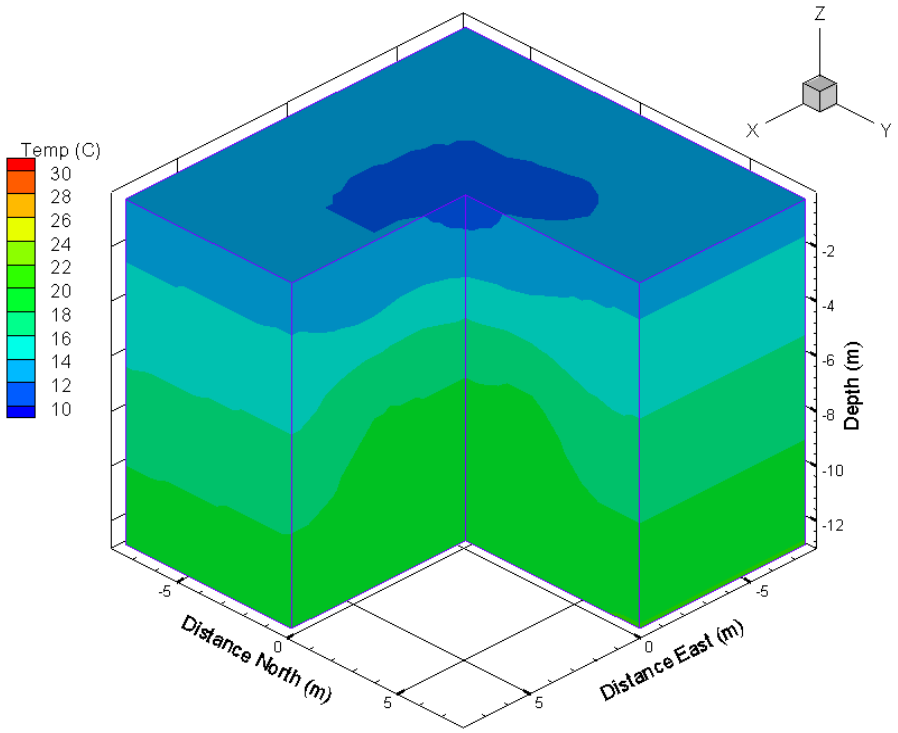


**Figure 3.2.1: Temperature data collected 3 days before the salt pulse began.**

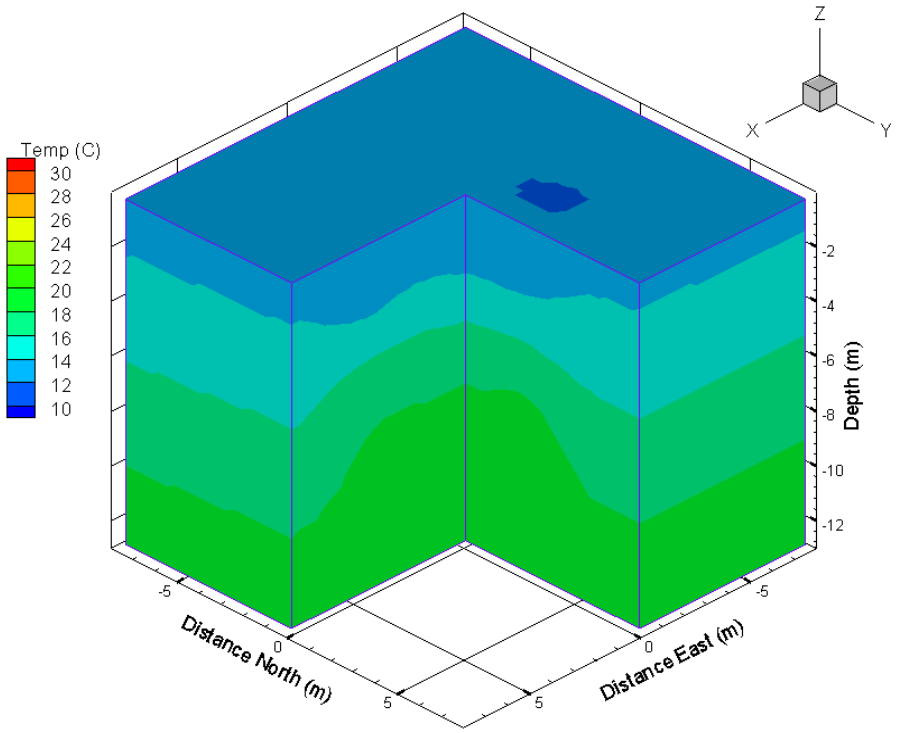


**Figure 3.2.2: Temperature data collected 4 days after the salt pulse began.**

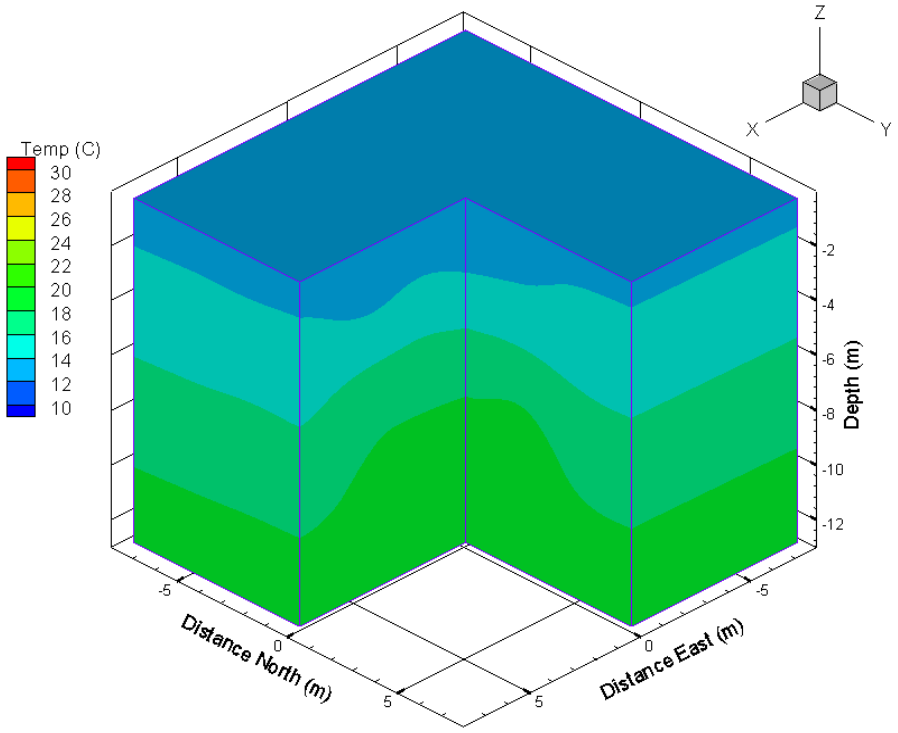


**Figure 3.2.3: Temperature data collected 11 days after the salt pulse began.**

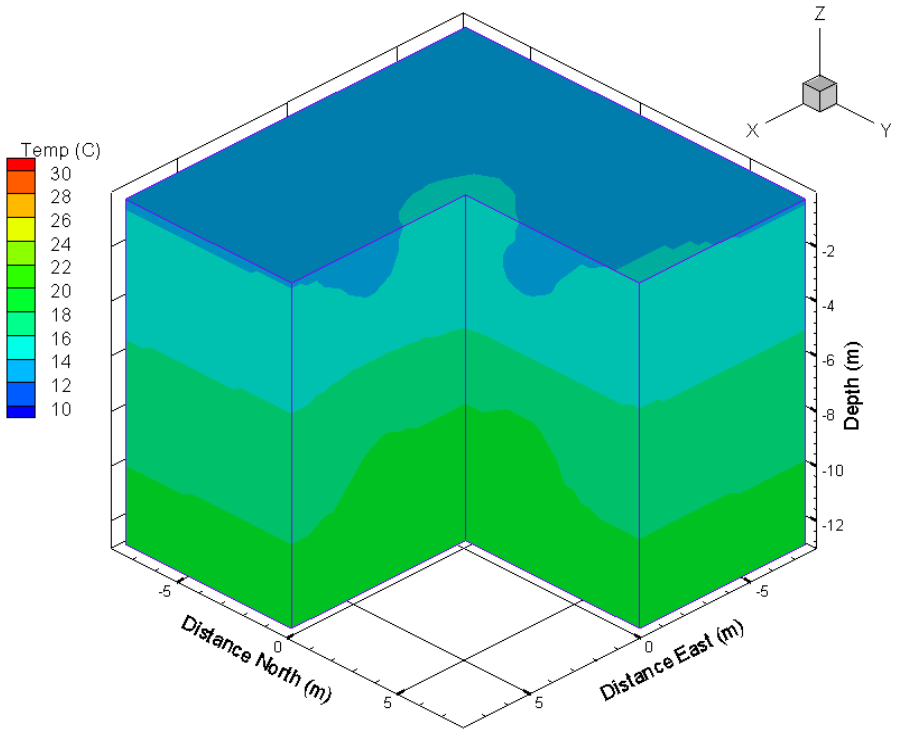


**Figure 3.2.4: Temperature data collected 18 days after the salt pulse began.**

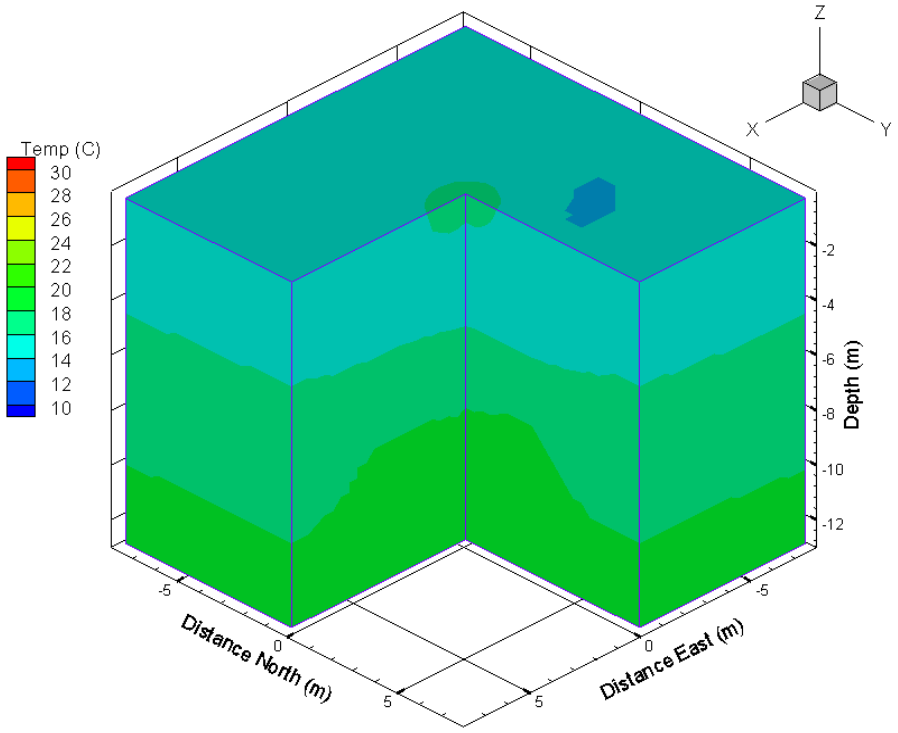


**Figure 3.2.5: Temperature data collected 25 days after the salt pulse began.**

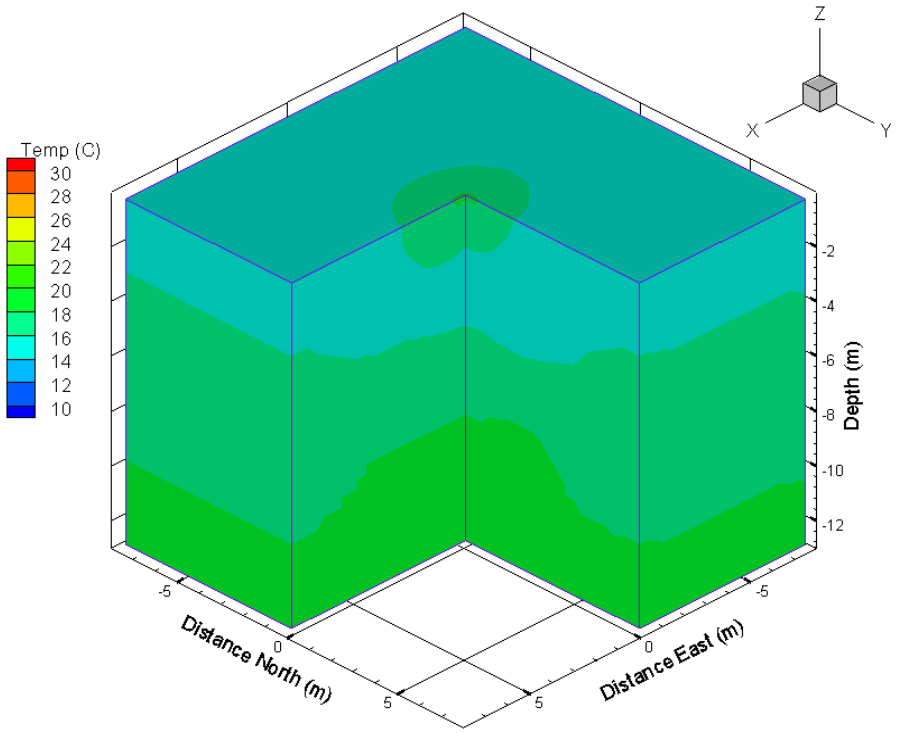


**Figure 3.2.6: Temperature data collected 32 days after the salt pulse began.**

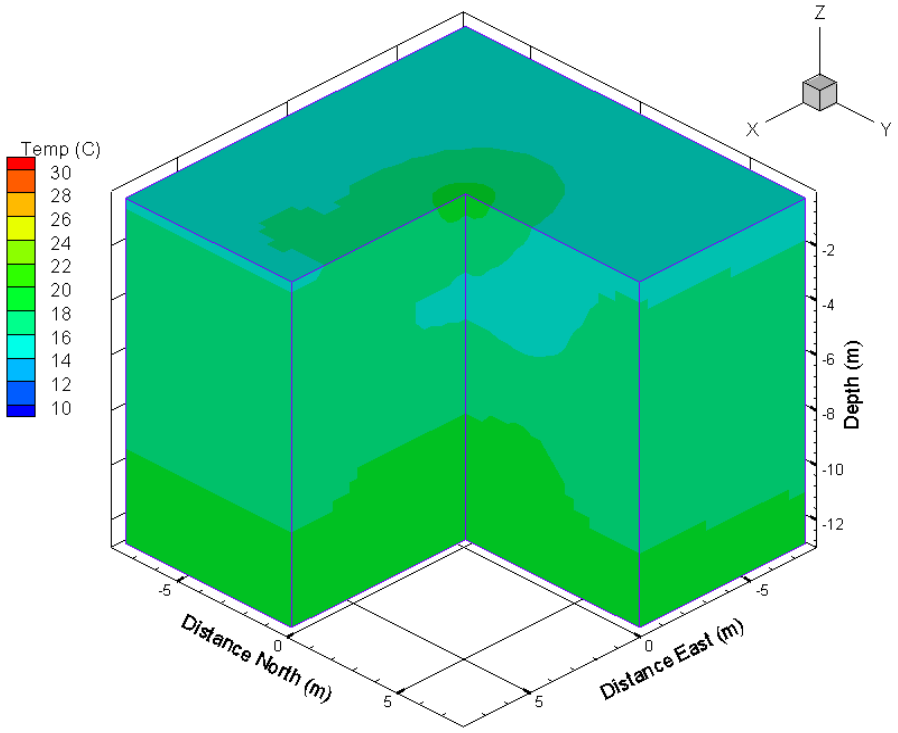


**Figure 3.2.7: Temperature data collected 39 days after the salt pulse began.**

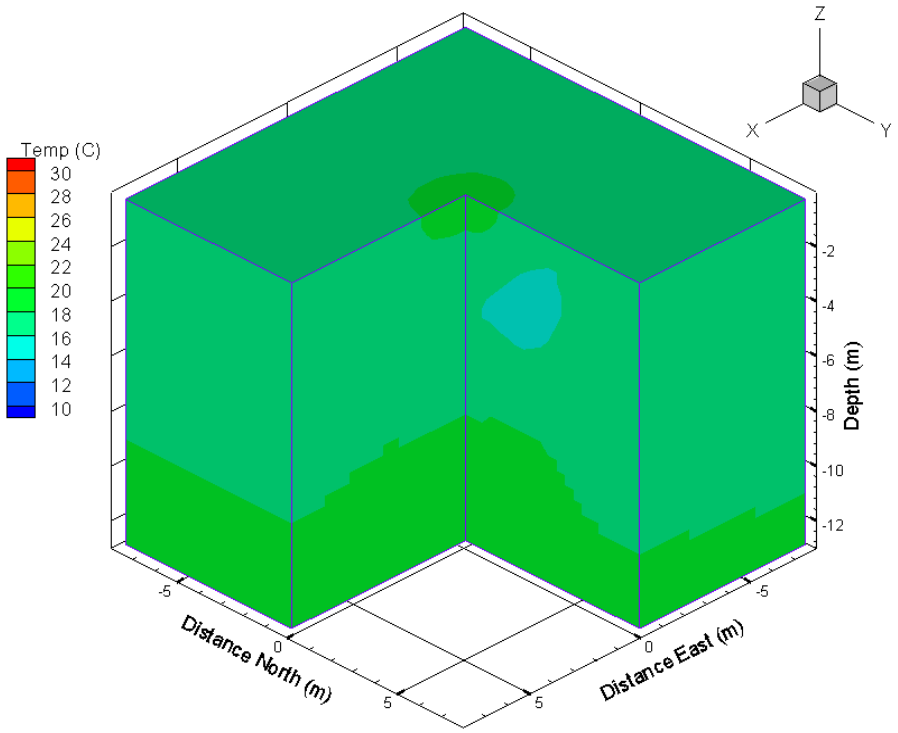


**Figure 3.2.8: Temperature data collected 46 days after the salt pulse began.**

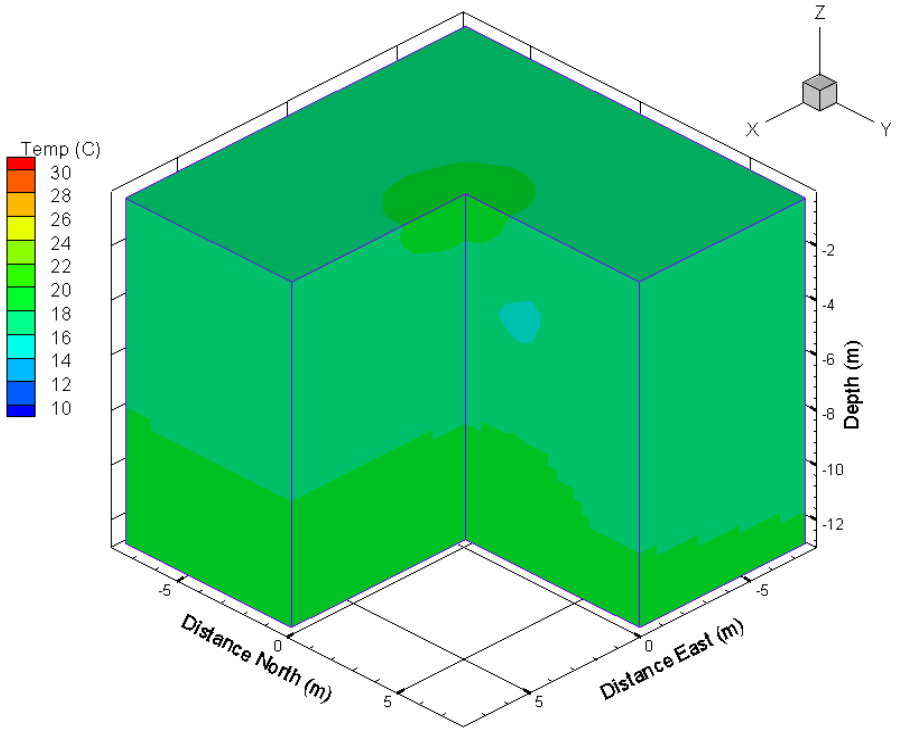


**Figure 3.2.9: Temperature data collected 53 days after the salt pulse began.**

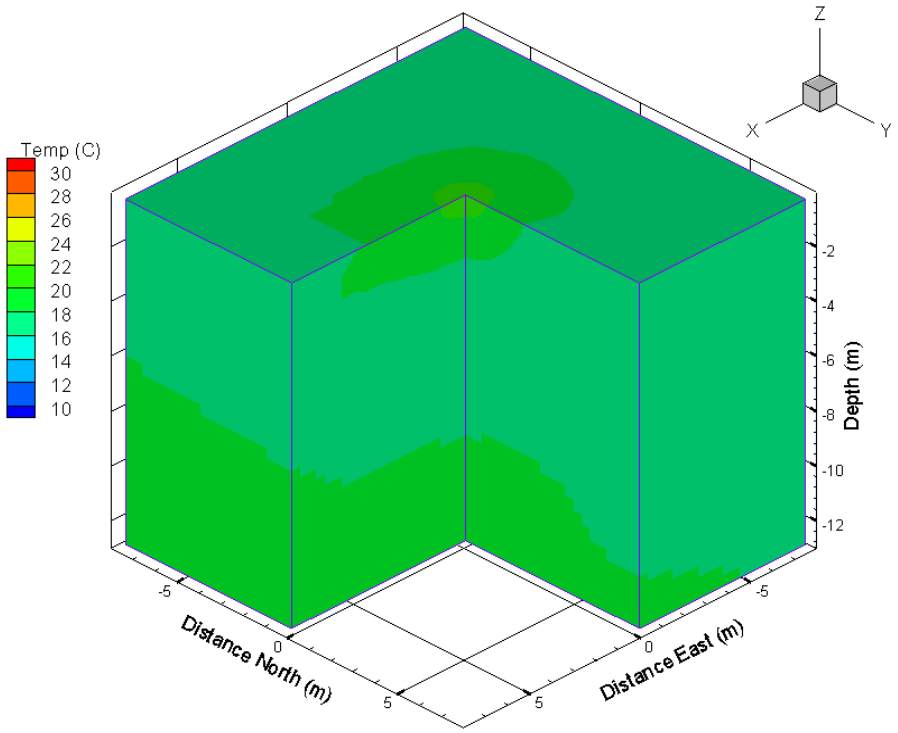


**Figure 3.2.10: Temperature data collected 60 days after the salt pulse began.**

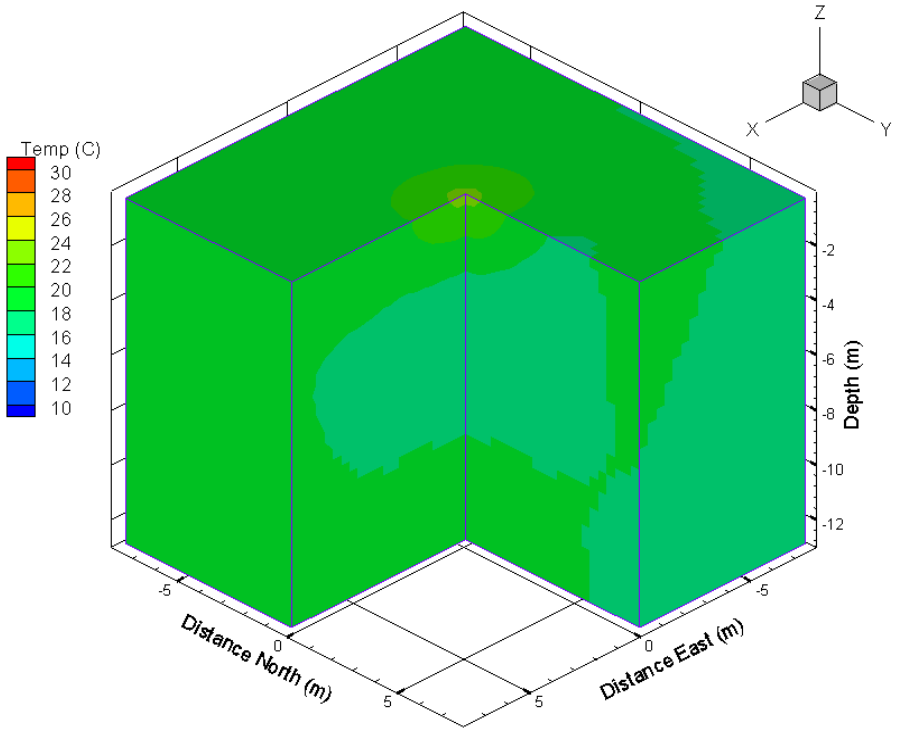


**Figure 3.2.11: Temperature data collected 67 days after the salt pulse began.**

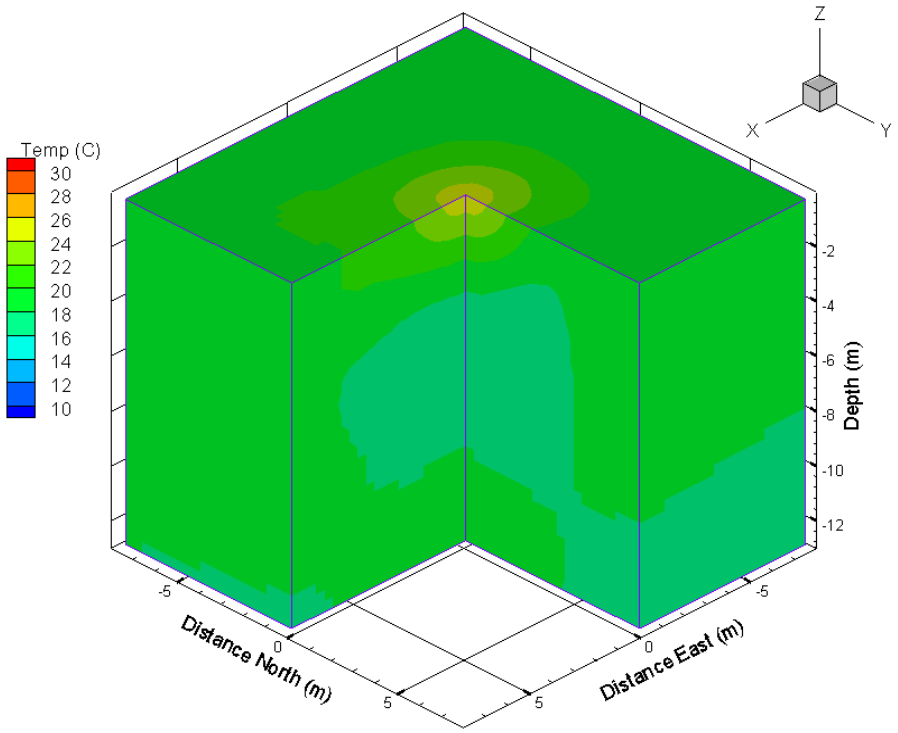


**Figure 3.2.12: Temperature data collected 81 days after the salt pulse began.**

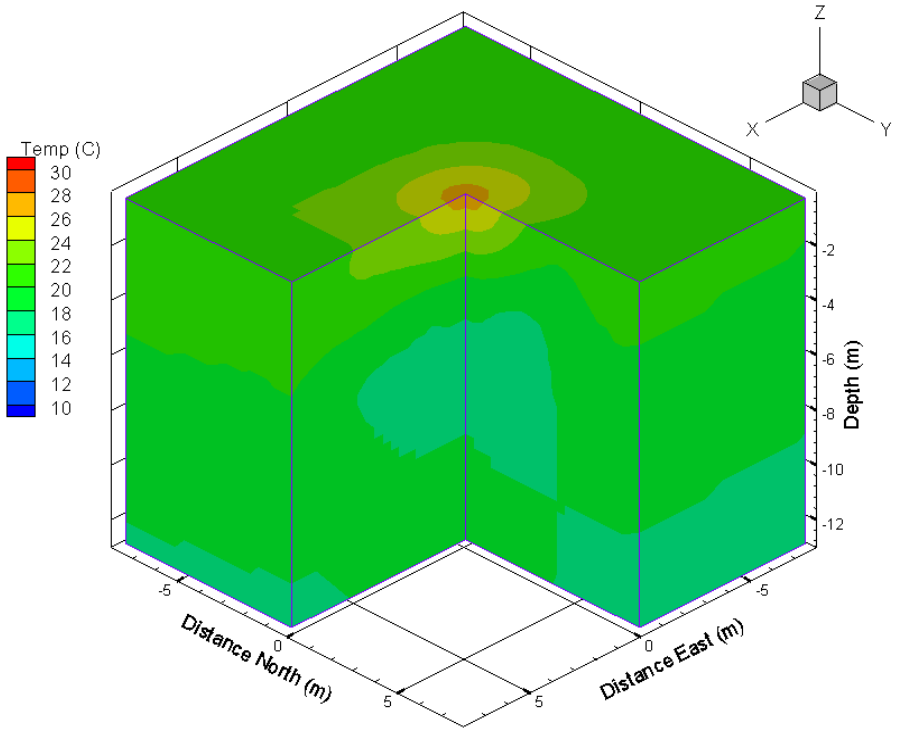


**Figure 3.2.13: Temperature data collected 95 days after the salt pulse began.**

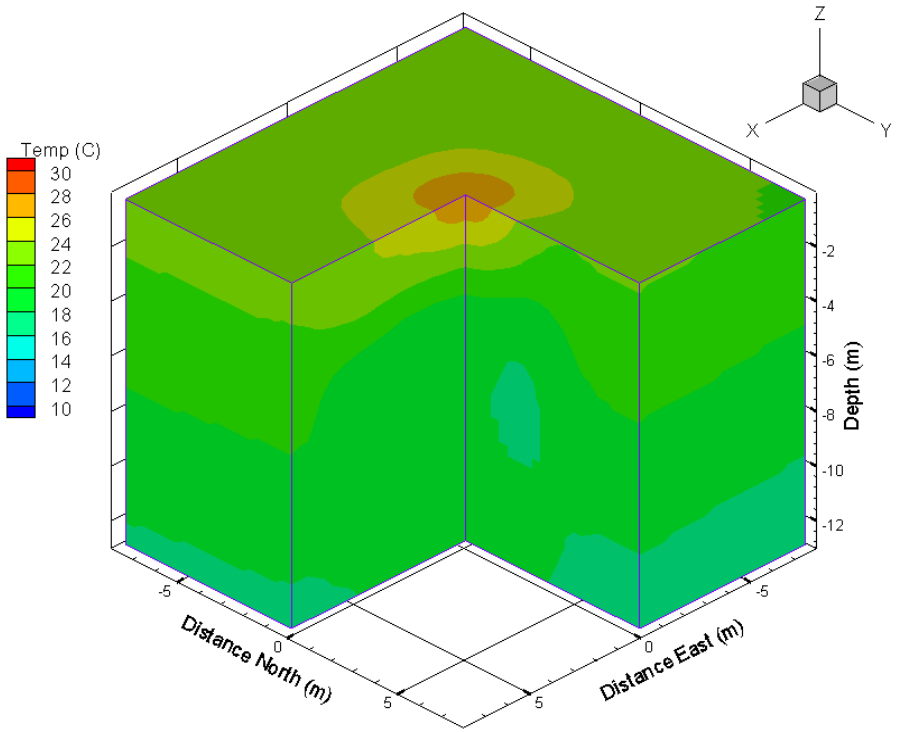


**Figure 3.2.14: Temperature data collected 109 days after the salt pulse began.**

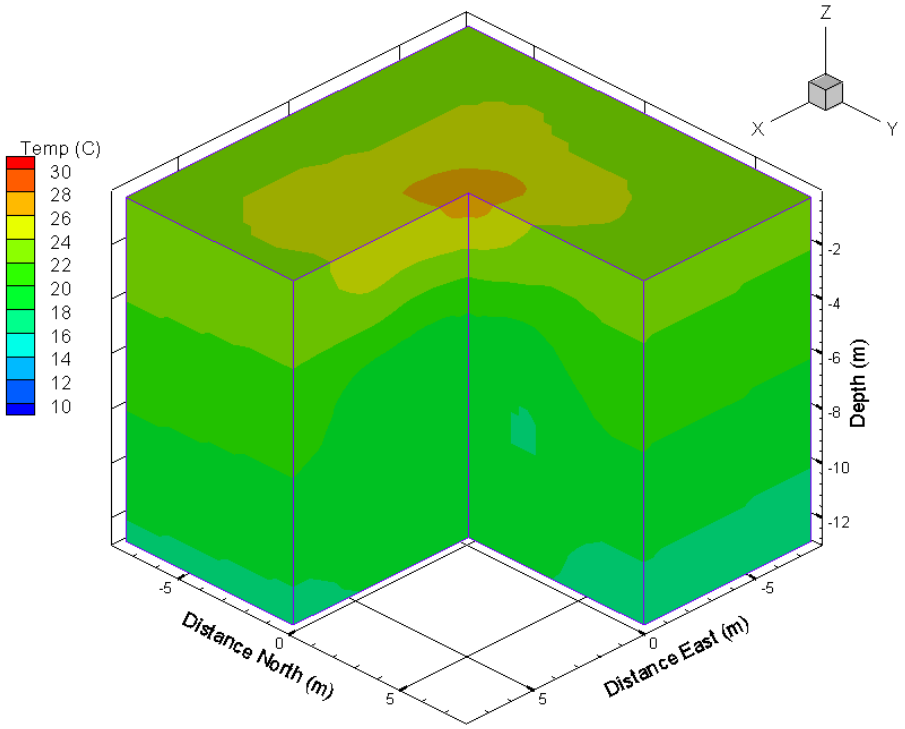


**Figure 3.2.15: Temperature data collected 130 days after the salt pulse began.**

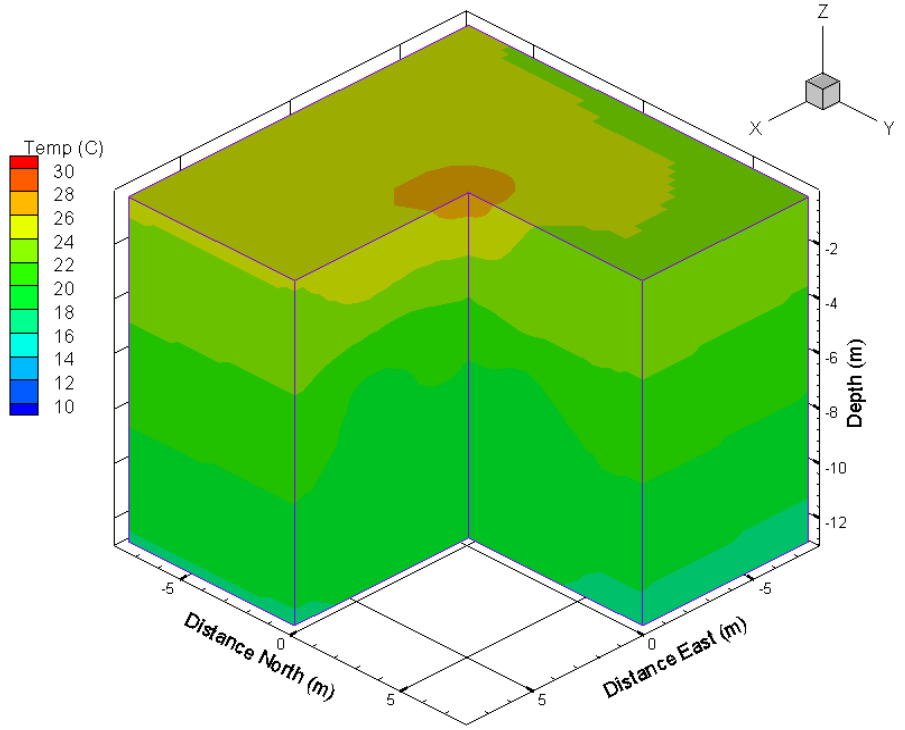


**Figure 3.2.16: Temperature data collected 142 days after the salt pulse began.**

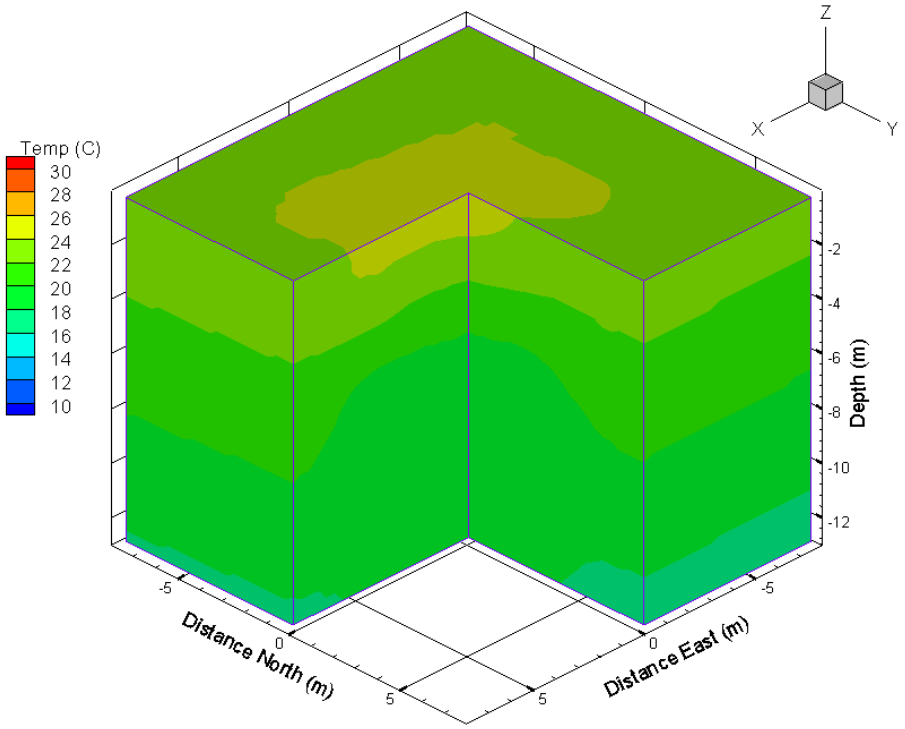


**Figure 3.2.17: Temperature data collected 149 days after the salt pulse began.**

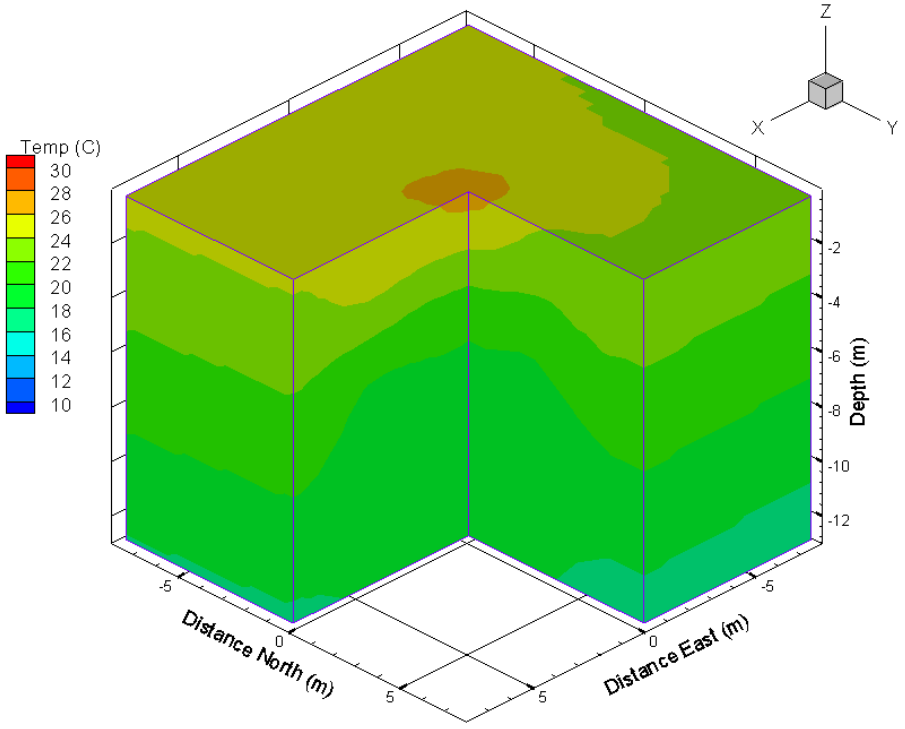


**Figure 3.2.18: Temperature data collected 163 days after the salt pulse began.**

# Appendix 4 – Particle Size Analysis

## 4.1 Introduction

Extensive analysis of the hydraulic properties of soils collected from the test site were performed by K. Baker in her 2001 New Mexico Tech thesis work, and most of the data presented in this section is based on her characterization of the site. Her work focused on the hydraulic properties of the soil, but included sieve method particle size analysis of 25 samples from the NorthWest continuous core sample. The sieve analysis is a simple procedure of passing a soil sample through a series of sieves with progressively finer mesh. The mass of soil left in each sieve tells the percent of the sample with a finer grainer size. For exact methods, refer to Baker (2001).

The sieve method worked well for most of the soil samples tested, however this method cannot distinguish between silt and clay sized particles, so a separate method, hydrometer testing, was performed on the four finest grained samples from the NW core. The mass percentage of silt and clay sized particles was so small in most samples that hydrometer testing was not deemed necessary for the twenty other samples. The results of the hydrometer testing were not published in by Baker however. The hydrometer calculations are preformed here to create a basis for the percent clay estimates needed to calculate soil particle conductivity in the Rhoades (1990) model. Since the soil analysis was only preformed on samples from the NW continuous core, a correlation between stratigraphic units was made based on the textural descriptions in Figures 4.1.1 through 4.1.4.

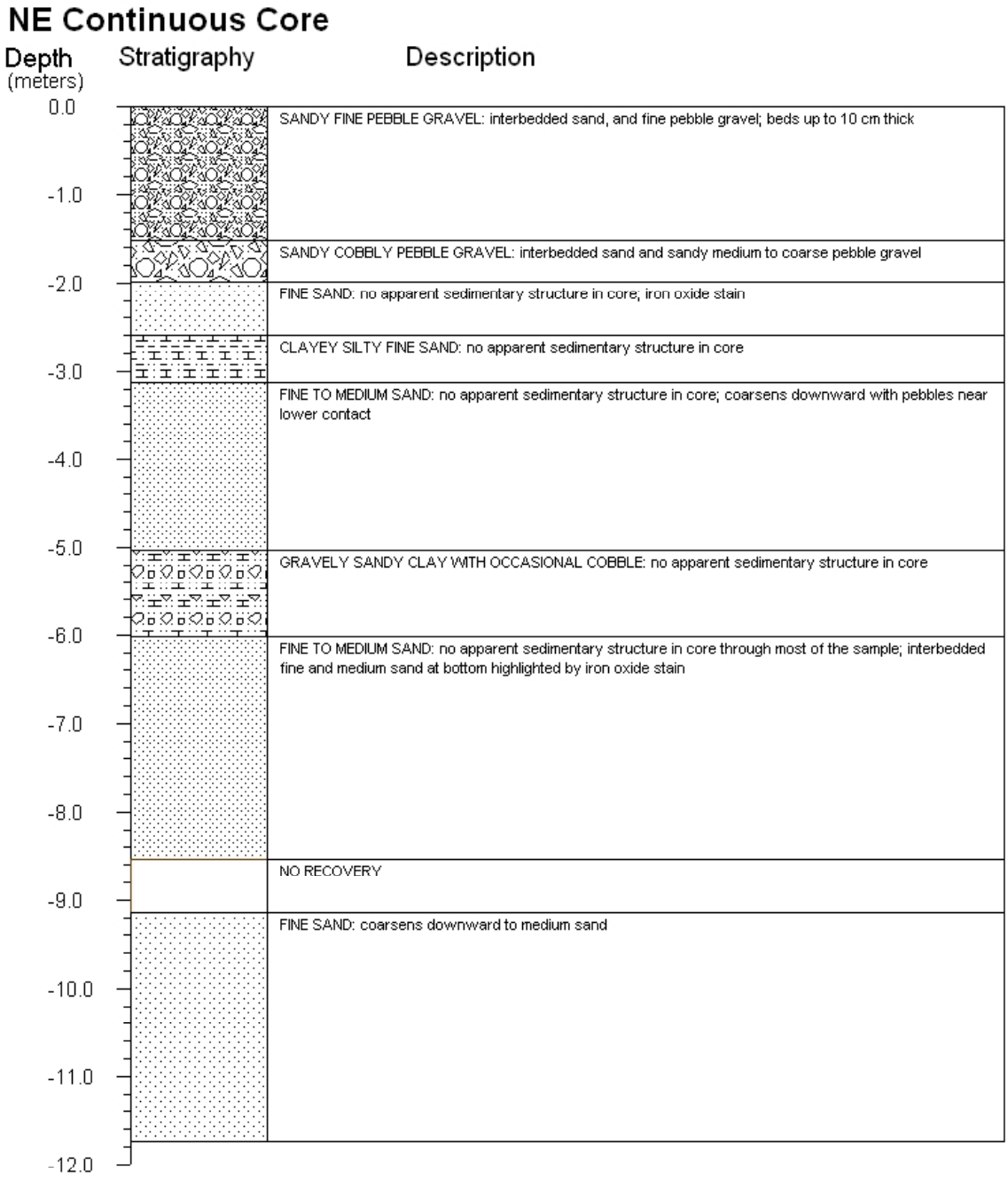


**Figure 4.1.1: Stratigraphic Column of NE Core. (Baker, 2001)**

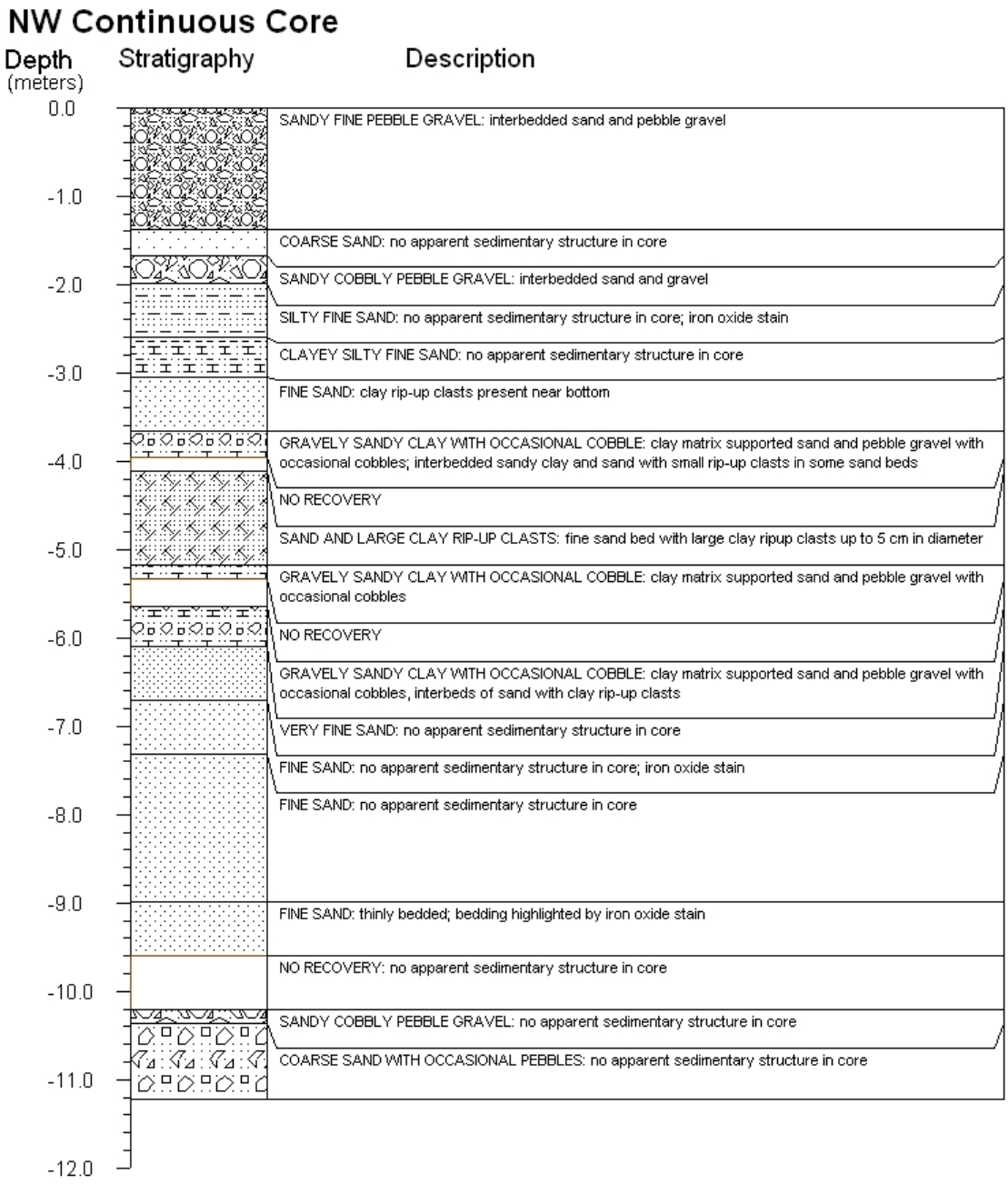


**Figure 4.1.2: Stratigraphic column of NW Core. (Baker, 2001)**

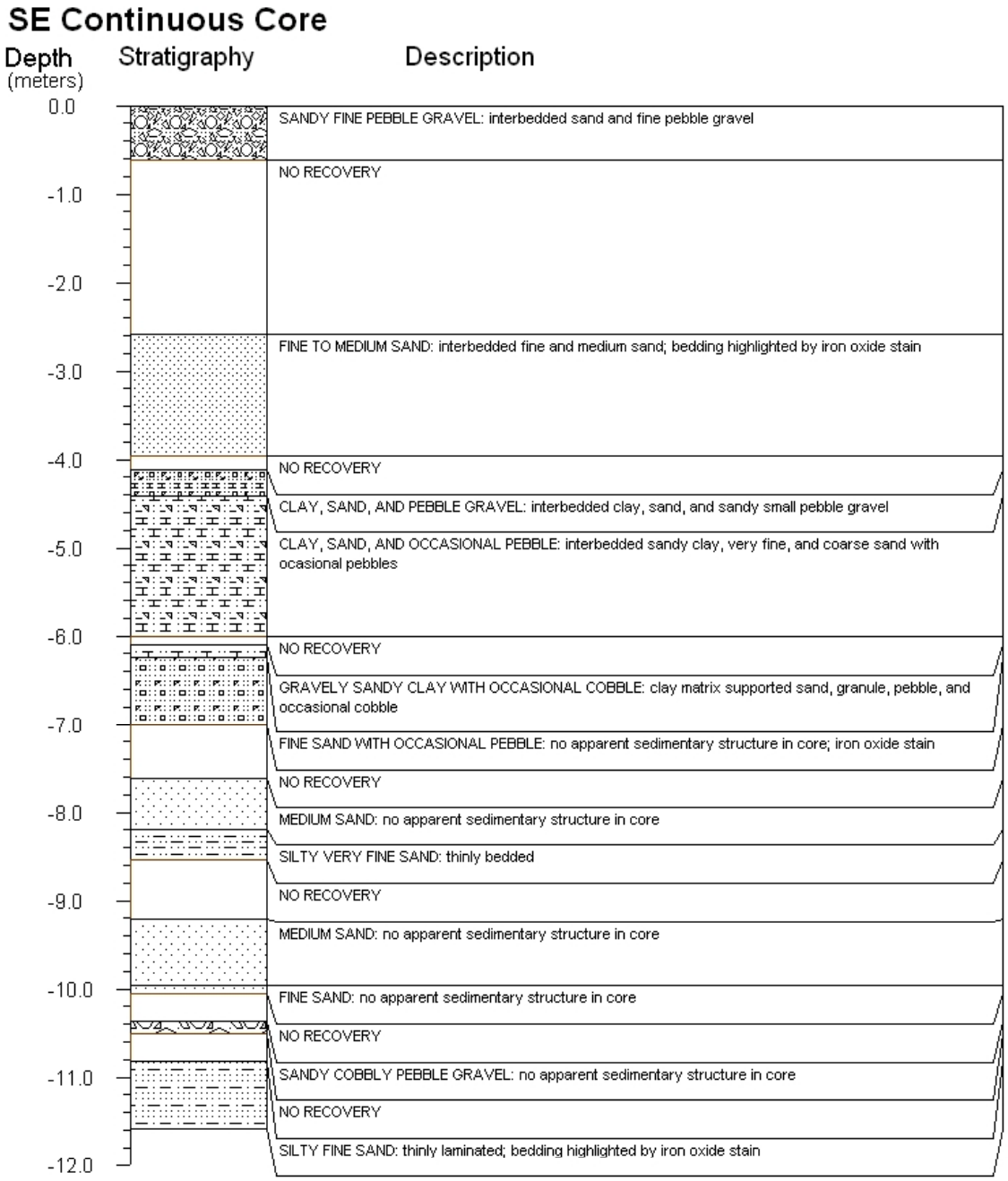


**Figure 4.1.3: Stratigraphic column of SE Core. (Baker, 2001)**

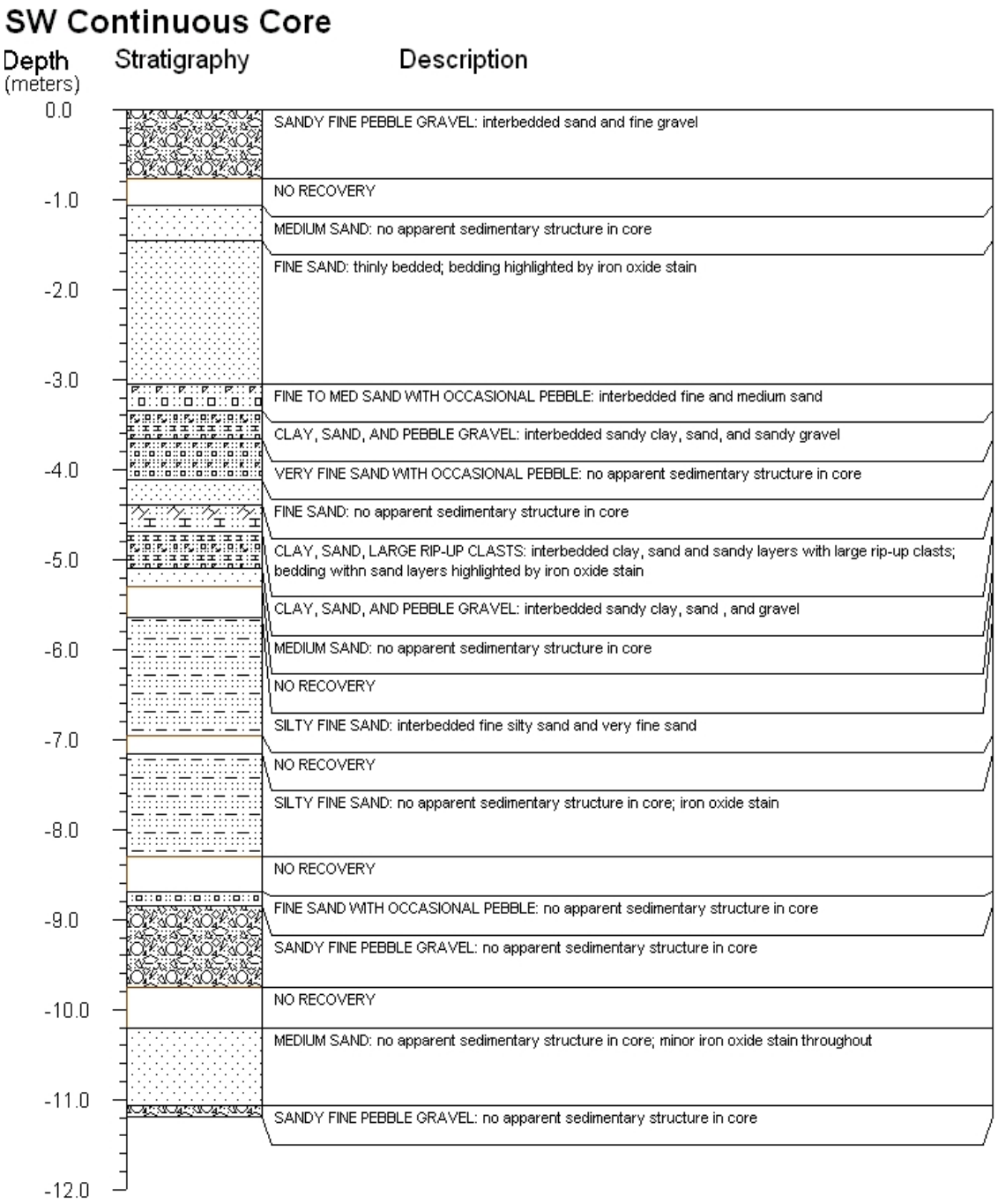


**Figure 4.1.4: Stratigraphic column of SW Core. (Baker, 2001)**

## 4.2 Sieve Method Analysis

For most samples (20 of the 24), the mass percentage of clay and silt sized particles was very small and a sieve method was sufficient to describe to particle size distribution. The sieve method analysis is simple procedures of passing a soil sample through a series of sieves with progressively finer mesh. The mass of sample left behind in each sieve tells what percentage of the sample had a finer grain size. Table 4.1.2 is a summary of the sieve analysis, for more detail on the exact methods and results see Baker 2001. An example from Baker 2001, is given to help understand how sieve method analysis results are interpreted. Table 4.1.1 shows the mesh sizes used in this analysis.

| | | | |
|---|---|---|---|
| Example: | 4mm particles | 10% (of total mass) | 90% finer than 4mm |
| | 2mm particles | 20% | 70% finer than 2mm |
| | 1mm particles | 50% | 20% finer than 1 mm |
| | .05 mm particles | 20% | 0% finer than .05 mm |

| Particle Description (sieve) | Particle Size | $\phi$ Values |
|---|---|---|
| very coarse sand (#20) | 1-2 mm | -1-0 |
| coarse sand (#40) | 0.5-1 mm | 0-1 |
| medium sand (#60) | 0.25-0.5 mm | 1-2 |
| fine sand (#150) | 0.16-0.25 mm | 2-3 |
| very fine sand (#270) | 0.053-0.16 mm | 3-4 |

**Table 4.2.1: Udden Wentworth particle size scale for sand size particles (Baker, 2001).**

| smallest grain size (mm) | sieve # | NW1 wt fraction | NW2 wt fraction | NW4 wt fraction | NW5 wt fraction | NW7 wt fraction | NW8 wt fraction | NW9 wt fraction | NW10 wt fraction |
|---|---|---|---|---|---|---|---|---|---|
| <.053 | bottom | 0.007 | 0.010 | 0.004 | 0.032 | 0.015 | 0.019 | 0.027 | 0.031 |
| 0.053 | 270 | 0.008 | 0.017 | 0.018 | 0.023 | 0.121 | 0.128 | 0.071 | 0.073 |
| 0.106 | 140 | 0.032 | 0.065 | 0.104 | 0.057 | 0.467 | 0.428 | 0.302 | 0.430 |
| 0.25 | 60 | 0.228 | 0.276 | 0.557 | 0.162 | 0.372 | 0.211 | 0.359 | 0.366 |
| 0.5 | 35 | 0.315 | 0.278 | 0.284 | 0.200 | 0.019 | 0.031 | 0.129 | 0.078 |
| 1 | 18 | 0.139 | 0.108 | 0.026 | 0.156 | 0.003 | 0.030 | 0.029 | 0.022 |
| 2 | 10 | 0.270 | 0.244 | 0.006 | 0.369 | 0.004 | 0.153 | 0.084 | 0.000 |

| grain size (mm) | sieve # | NW11 wt fraction | NW12 wt fraction | NW16 wt fraction | NW17 wt fraction | NW18 wt fraction | NW19 wt fraction | NW20 wt fraction | NW21 wt fraction |
|---|---|---|---|---|---|---|---|---|---|
| <.053 | bottom | 0.034 | 0.021 | 0.020 | 0.017 | 0.011 | 0.091 | 0.008 | 0.010 |
| 0.053 | 270 | 0.181 | 0.133 | 0.245 | 0.157 | 0.141 | 0.281 | 0.089 | 0.090 |
| 0.106 | 140 | 0.616 | 0.629 | 0.720 | 0.788 | 0.818 | 0.596 | 0.802 | 0.764 |
| 0.25 | 60 | 0.145 | 0.192 | 0.010 | 0.038 | 0.029 | 0.025 | 0.097 | 0.122 |
| 0.5 | 35 | 0.016 | 0.011 | 0.001 | 0.000 | 0.000 | 0.004 | 0.003 | 0.012 |
| 1 | 18 | 0.004 | 0.004 | 0.000 | 0.000 | 0.000 | 0.001 | 0.000 | 0.001 |
| 2 | 10 | 0.005 | 0.010 | 0.004 | 0.000 | 0.000 | 0.002 | 0.000 | 0.000 |

| grain size (mm) | sieve # | NW22 wt fraction | NW23 wt fraction | NW24 wt fraction | NW25 wt fraction | NW27 wt fraction |
|---|---|---|---|---|---|---|
| <.053 | bottom | 0.022 | 0.023 | 0.028 | 0.020 | 0.004 |
| 0.053 | 270 | 0.179 | 0.122 | 0.090 | 0.055 | 0.014 |
| 0.106 | 140 | 0.722 | 0.543 | 0.451 | 0.261 | 0.303 |
| 0.25 | 60 | 0.072 | 0.256 | 0.357 | 0.443 | 0.489 |
| 0.5 | 35 | 0.004 | 0.043 | 0.045 | 0.163 | 0.116 |
| 1 | 18 | 0.001 | 0.008 | 0.000 | 0.033 | 0.030 |
| 2 | 10 | 0.000 | 0.006 | 0.029 | 0.024 | 0.044 |

**Table 4.1.2: Particle size distribution data for the NW core sample with the sieve method of analysis. (Baker, 2001)**

## 4.3 Hydrometer Analysis

Hydrometer testing was conducted on the four samples from the NW core with the highest clay contents. The hydrometer testing requires mixing a soil sample into a solution and then measuring how the density of the solution changes as suspended particles settle out of the solution. Due to time constraints and other complications, the particle size analysis of the hydrometer testing was not completed by Baker, 2001. Baker 2001, did describe the following equations for the calculation of mean particle diameter (silts and clays):

$$X = \theta t^{-1/2} \ (\mu m)$$

$X$ = mean particle diameter

$\theta$ = sedimentation parameter defined as: $\theta = 1000\left(Bh'\right)^{1/2}$ [$\mu m \ min^{1/2}$]

where $B = (30\ \eta\ /[g\ (\rho_s - \rho_l)])$

$\eta$ = fluid viscosity in poise [$gcm^{-1}s^{-1}$]

$\rho_s$ = soil particle density [2.65 g/cm^3]

$\rho_l$ = solution density [g/cm^3]

g = gravitational constant [981 cm/s^2]

t = time of measurement in seconds

h' = hydrometer settling depth (cm)

where $h' = -0.164R + 16.3$ (for ASTM 152H soil hydrometer @ $30^o$ C)

R = uncorrected hydrometer reading (g L-1)

To determine sand, silt, and clay percentages, plot P vs. log X where $P = C/C_0 \times 100$

Where $C = R-R_L$

RL = reading on blank solution

$C_o$ = oven dry weight of sample

The following tables show the data collected during the hydrometer process and the necessary calculations to convert this information into a particle size distribution. The data is also presented as a series of figures showing the mean particle diameter in mm and the mass percent with a finer grain size. Samples were divided in half to test repeatability (designated a and b). A summary of the hydrometer testing is shown in Table 4.3.1. The geologic unit number refers to the correlated units described by Baker (2001), and shown in Figure 4 of the main body.

| Hydrometer Sample ID | Geologic Unit | Description | Approximate Depth (m) | % Silt and Clay | % Clay |
|---|---|---|---|---|---|
| 14a | 1 | sand | 1.0 | 7.0 | 3.5 |
| 14b | 1 | sand | 1.0 | 7.0 | 3.5 |
| 27a | 1 | sand | 1.0 | 6.3 | 3.1 |
| 27b | 1 | sand | 1.0 | 6.0 | 3.0 |
| 6-4.1 | 6 | clay | 4.0 | 59.9 | 32.3 |
| 6-4.1 | 6 | clay | 4.0 | 61.1 | 30.6 |
| 2-8.1 | 2 | clay | 8.0 | 40.7 | 7.4 |
| 2-8.2 | 2 | clay | 8.0 | 45.0 | 8.3 |
| 8-8.1a | 8 | clay | 8.0 | 29.9 | 10.0 |
| 8-8.1b | 8 | clay | 8.0 | 50.0 | 10.9 |
| 8-8.2a | 8 | clay | 8.0 | 30.5 | 10.2 |
| 8-8.2b | 8 | clay | 8.0 | 57.9 | 9.7 |

**Table 4.3.1: Summary of hydrometer testing showing %silt and clay as well as just %clay.**

| | | | | | | | | θ | X(mean part dia) | X(mean part dia) |
|---|---|---|---|---|---|---|---|---|---|---|
| sample | t(min) | h' (cm) | R | R(L) | C | Co | **P(=C/Co)** | [cm*s^(1/2)] | (mm) | (microns) |
| 6-4.1 | 0.5 | 13.676 | 16 | 3 | 13 | 21.7087 | 0.599 | 0.039 | 0.071 | 71.2 |
| temp=20 | 1 | 13.676 | 16 | 3 | 13 | | 0.599 | 0.039 | 0.050 | 50.4 |
| degrees C | 3 | 13.84 | 15 | 3 | 12 | | 0.553 | 0.039 | 0.029 | 29.3 |
| | 10 | 14.168 | 13 | 3 | 10 | | 0.461 | 0.040 | 0.016 | 16.2 |
| | 30 | 14.332 | 12 | 3 | 9 | | 0.415 | 0.040 | 0.009 | 9.4 |
| | 60 | 14.332 | 12 | 3 | 9 | | 0.415 | 0.040 | 0.007 | 6.7 |
| | 90 | 14.496 | 11 | 3 | 8 | | 0.369 | 0.040 | 0.005 | 5.5 |
| | 120 | 14.496 | 11 | 3 | 8 | | 0.369 | 0.040 | 0.005 | 4.7 |
| | 1440 | 14.66 | 10 | 3 | 7 | | 0.322 | 0.040 | 0.001 | 1.4 |
| | | | | | | % Clay | 32.245 | | | |

**Table 4.3.2: Sample 6-4.1, measured solution density with time and particle size calculation.**

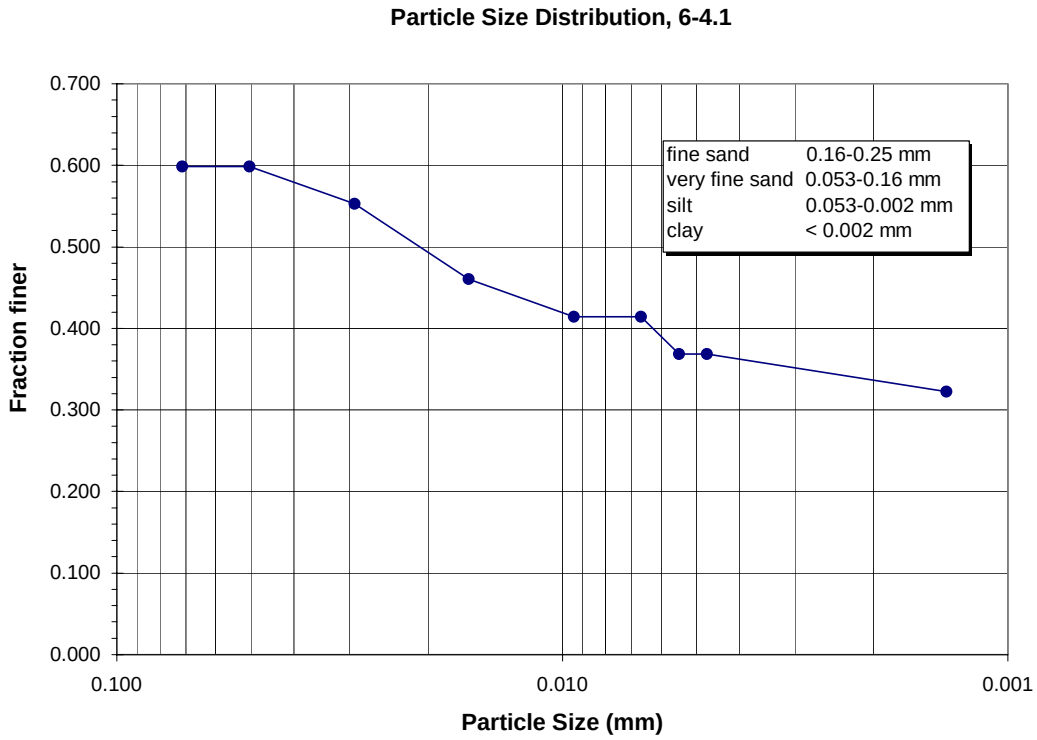


**Figure 4.3.1: Mass fraction of the original sample with a finer particle size.**

| | | | | | | | | θ | X(mean part dia) | X(mean part dia) |
|---|---|---|---|---|---|---|---|---|---|---|
| sample | t(min) | h' (cm) | R | R(L) | C | Co | **P(=C/Co)** | [cm*s^(1/2)] | (mm) | (microns) |
| 6-4.2 | 0.5 | 12.528 | 23 | 3 | 20 | 32.7327 | 0.611 | 0.037 | 0.068 | 68.2 |
| temp=20 | 1 | 12.528 | 23 | 3 | 20 | | 0.611 | 0.037 | 0.048 | 48.2 |
| degrees C | 3 | 12.856 | 21 | 3 | 18 | | 0.550 | 0.038 | 0.028 | 28.2 |
| | 10 | 13.184 | 19 | 3 | 16 | | 0.489 | 0.038 | 0.016 | 15.6 |
| | 30 | 13.512 | 17 | 3 | 14 | | 0.428 | 0.039 | 0.009 | 9.1 |
| | 60 | 13.676 | 16 | 3 | 13 | | 0.397 | 0.039 | 0.007 | 6.5 |
| | 90 | 13.676 | 16 | 3 | 13 | | 0.397 | 0.039 | 0.005 | 5.3 |
| | 120 | 13.84 | 15 | 3 | 12 | | 0.367 | 0.039 | 0.005 | 4.6 |
| | 1440 | 14.168 | 13 | 3 | 10 | | 0.306 | 0.040 | 0.001 | 1.4 |
| | | | | | | % Clay | 30.550 | | | |

**Table 4.3.3: Sample 6-4.2, measured solution density with time and particle size calculation.**

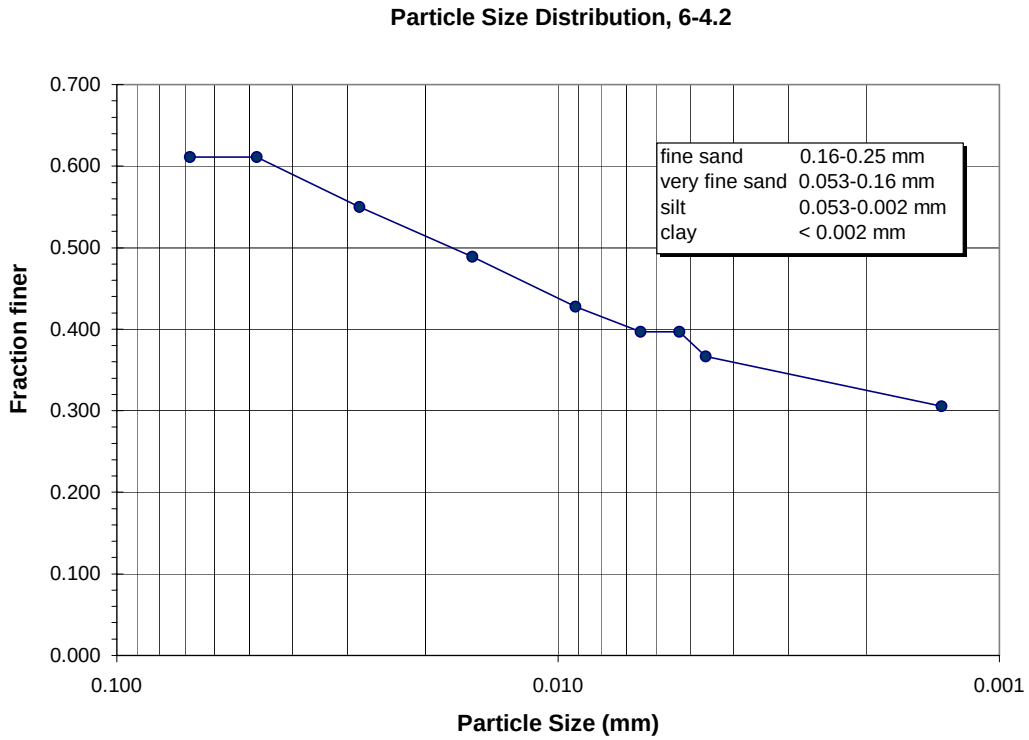


**Figure 4.3.2: Mass fraction of the original sample with a finer particle size.**

| | | | | | | | | θ | X(mean part dia) | X(mean part dia) |
|---|---|---|---|---|---|---|---|---|---|---|
| sample | t(min) | h' (cm) | R | R(L) | C | Co | **P(=C/Co)** | [cm*s^(1/2)] | (mm) | (microns) |
| 2-8.1 | 0.5 | 13.84 | 15 | 3 | 12 | 26.9996 | 0.444 | 0.039 | 0.072 | 71.7 |
| temp=20 | 1 | 14.004 | 14 | 3 | 11 | | 0.407 | 0.039 | 0.051 | 51.0 |
| degrees C | 3 | 14.66 | 10 | 3 | 7 | | 0.259 | 0.040 | 0.030 | 30.1 |
| | 10 | 14.988 | 8 | 3 | 5 | | 0.185 | 0.041 | 0.017 | 16.7 |
| | 30 | 15.152 | 7 | 3 | 4 | | 0.148 | 0.041 | 0.010 | 9.7 |
| | 60 | 15.316 | 6 | 3 | 3 | | 0.111 | 0.041 | 0.007 | 6.9 |
| | 90 | 15.316 | 6 | 3 | 3 | | 0.111 | 0.041 | 0.006 | 5.6 |
| | 120 | 15.316 | 6 | 3 | 3 | | 0.111 | 0.041 | 0.005 | 4.9 |
| | 1440 | 15.48 | 5 | 3 | 2 | | 0.074 | 0.042 | 0.001 | 1.4 |
| | | | | | | % Clay | 7.408 | | | |

**Table 4.3.4: Sample 2-8.1, measured solution density with time and particle size calculation.**

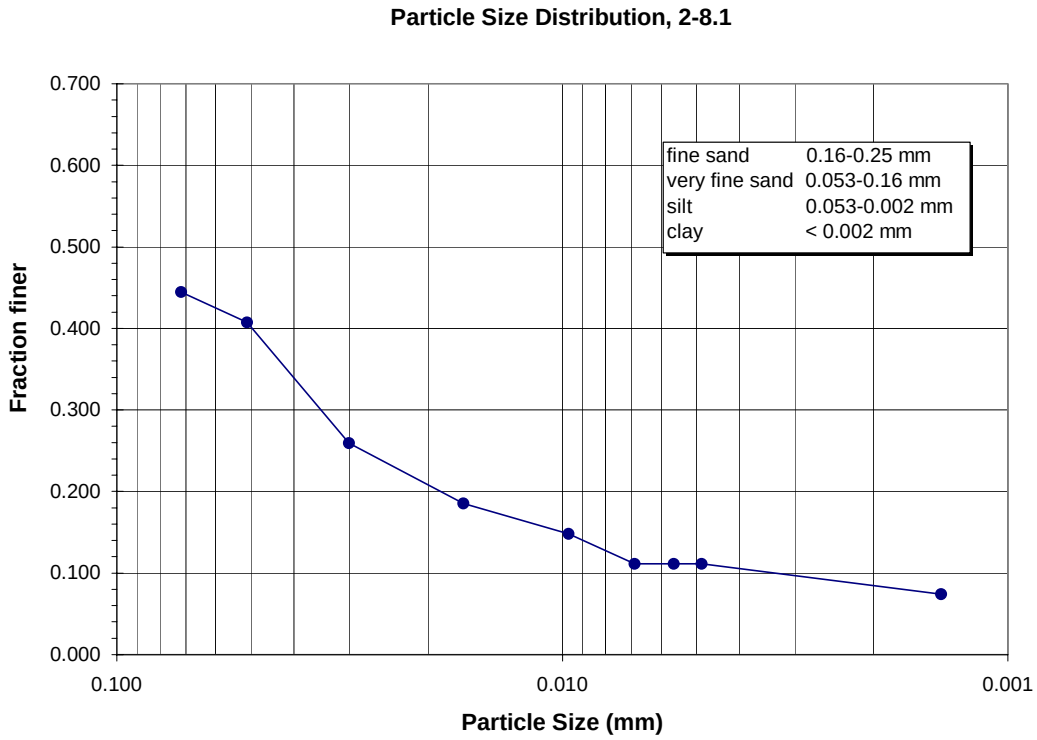


**Figure 4.3.3: Mass fraction of the original sample with a finer particle size.**

| | | | | | | | | θ | X(mean part dia) | X(mean part dia) |
|---|---|---|---|---|---|---|---|---|---|---|
| sample | t(min) | h' (cm) | R | R(L) | C | Co | **P(=C/Co)** | [cm*s^(1/2)] | (mm) | (microns) |
| 2-8.2 | 0.5 | 12.856 | 21 | 3 | 18 | 36.0149 | 0.500 | 0.038 | 0.069 | 69.1 |
| temp=20 | 1 | 13.512 | 17 | 3 | 14 | | 0.389 | 0.039 | 0.050 | 50.1 |
| degrees C | 3 | 14.332 | 12 | 3 | 9 | | 0.250 | 0.040 | 0.030 | 29.8 |
| | 10 | 14.824 | 9 | 3 | 6 | | 0.167 | 0.041 | 0.017 | 16.6 |
| | 30 | 14.988 | 8 | 3 | 5 | | 0.139 | 0.041 | 0.010 | 9.6 |
| | 60 | 15.152 | 7 | 3 | 4 | | 0.111 | 0.041 | 0.007 | 6.8 |
| | 90 | 15.152 | 7 | 3 | 4 | | 0.111 | 0.041 | 0.006 | 5.6 |
| | 120 | 15.152 | 7 | 3 | 4 | | 0.111 | 0.041 | 0.005 | 4.8 |
| | 1440 | 15.316 | 6 | 3 | 3 | | 0.083 | 0.041 | 0.001 | 1.4 |
| | | | | | | % Clay | 8.330 | | | |

**Table 4.3.5: Sample 2-8.2, measured solution density with time and particle size calculation.**

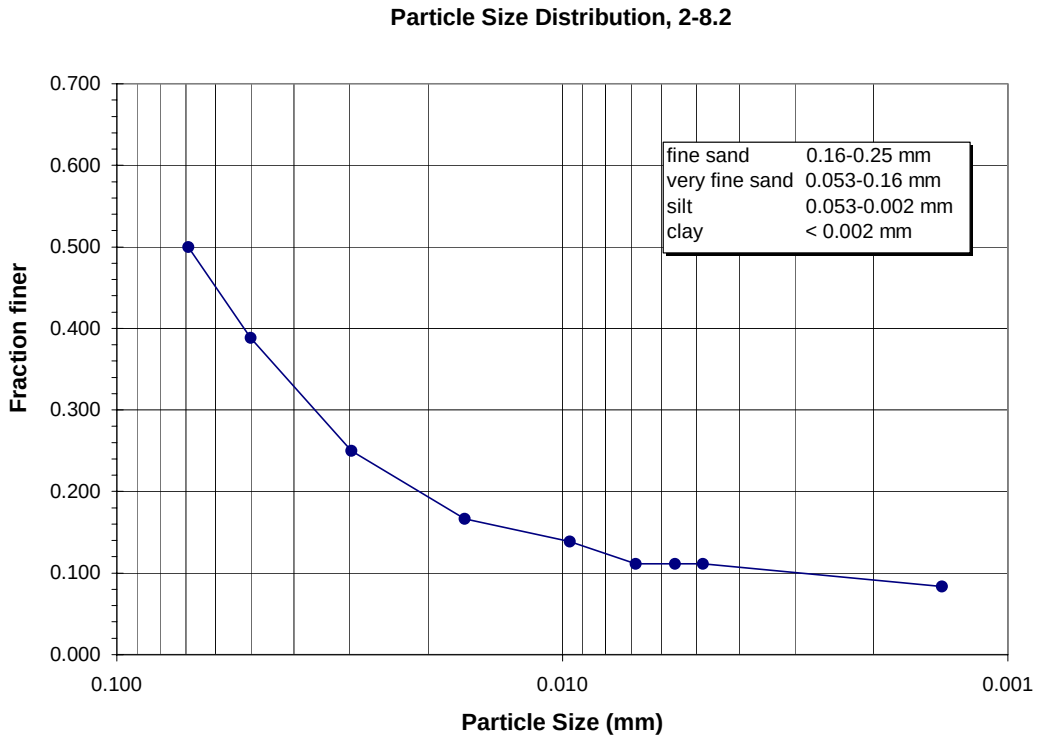


**Figure 4.3.4: Mass fraction of the original sample with a finer particle size.**

| | | | | | | | | θ | X(mean part dia) | X(mean part dia) |
|---|---|---|---|---|---|---|---|---|---|---|
| sample | t(min) | h' (cm) | R | R(L) | C | Co | **P(=C/Co)** | [cm*s^(1/2)] | (mm) | (microns) |
| 8-8.1a | 0.5 | 14.332 | 12 | 3 | 9 | 30.0738 | 0.299 | 0.0399 | 0.0729 | 72.9 |
| temp=20 | 1 | 14.332 | 12 | 3 | 9 | | 0.299 | 0.040 | 0.052 | 51.6 |
| degrees C | 3 | 14.66 | 10 | 3 | 7 | | 0.233 | 0.040 | 0.030 | 30.1 |
| | 10 | 14.824 | 9 | 3 | 6 | | 0.200 | 0.041 | 0.017 | 16.6 |
| | 30 | 14.988 | 8 | 3 | 5 | | 0.166 | 0.041 | 0.010 | 9.6 |
| | 60 | 15.152 | 7 | 3 | 4 | | 0.133 | 0.041 | 0.007 | 6.8 |
| | 90 | 15.152 | 7 | 3 | 4 | | 0.133 | 0.041 | 0.006 | 5.6 |
| | 120 | 15.152 | 7 | 3 | 4 | | 0.133 | 0.041 | 0.005 | 4.8 |
| | 1440 | 15.316 | 6 | 3 | 3 | | 0.100 | 0.041 | 0.001 | 1.4 |
| | | | | | | % Clay | 9.975 | | | |

**Table 4.3.6: Sample 8-8.1a, measured solution density with time and particle size calculation.**

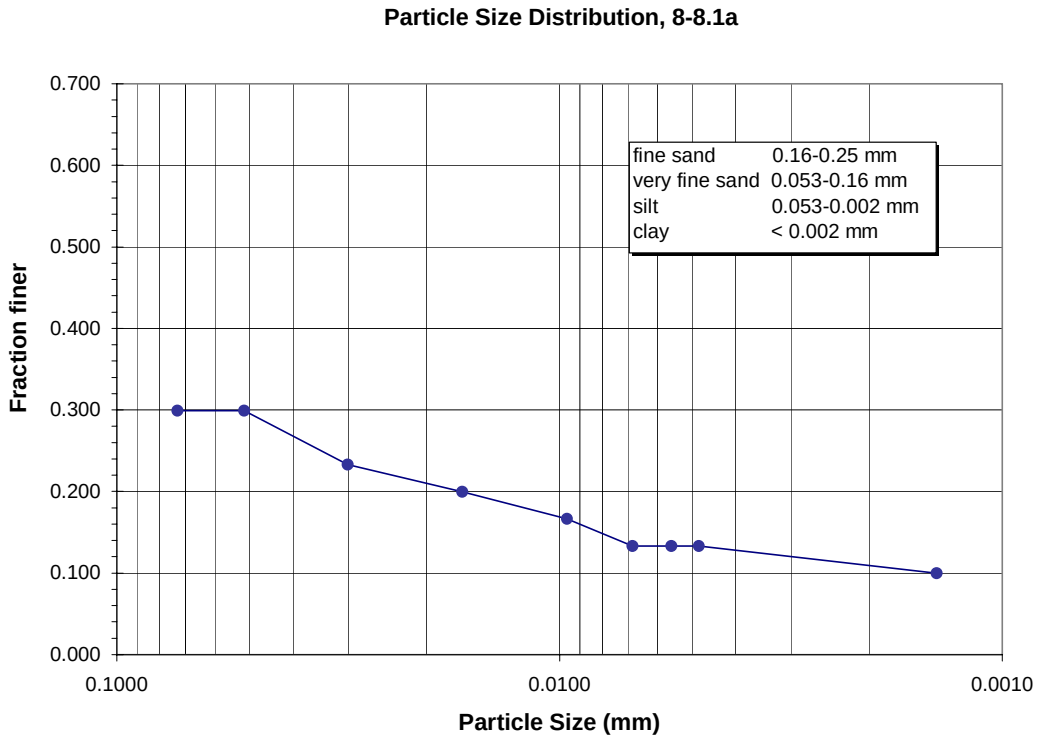


**Figure 4.3.5: Mass fraction of the original sample with a finer particle size.**

| | | | | | | | | θ | X(mean part dia) | X(mean part dia) |
|---|---|---|---|---|---|---|---|---|---|---|
| sample | t(min) | h' (cm) | R | R(L) | C | Co | **P(=C/Co)** | [cm*s^(1/2)] | (mm) | (microns) |
| 8-8.1b | 0.5 | 13.184 | 19 | 3 | 16 | 27.619 | 0.579 | 0.038 | 0.070 | 69.9 |
| temp=20 | 1 | 13.84 | 15 | 3 | 12 | | 0.434 | 0.039 | 0.051 | 50.7 |
| degrees C | 3 | 14.66 | 10 | 3 | 7 | | 0.253 | 0.040 | 0.030 | 30.1 |
| | 10 | 14.988 | 8 | 3 | 5 | | 0.181 | 0.041 | 0.017 | 16.7 |
| | 30 | 15.152 | 7 | 3 | 4 | | 0.145 | 0.041 | 0.010 | 9.7 |
| | 60 | 15.152 | 7 | 3 | 4 | | 0.145 | 0.041 | 0.007 | 6.8 |
| | 90 | 15.316 | 6 | 3 | 3 | | 0.109 | 0.041 | 0.006 | 5.6 |
| | 120 | 15.316 | 6 | 3 | 3 | | 0.109 | 0.041 | 0.005 | 4.9 |
| | 1440 | 15.316 | 6 | 3 | 3 | | 0.109 | 0.041 | 0.001 | 1.4 |
| | | | | | | % Clay | 10.862 | | | |

**Table 4.3.7: Sample 8-8.1b, measured solution density with time and particle size calculation.**

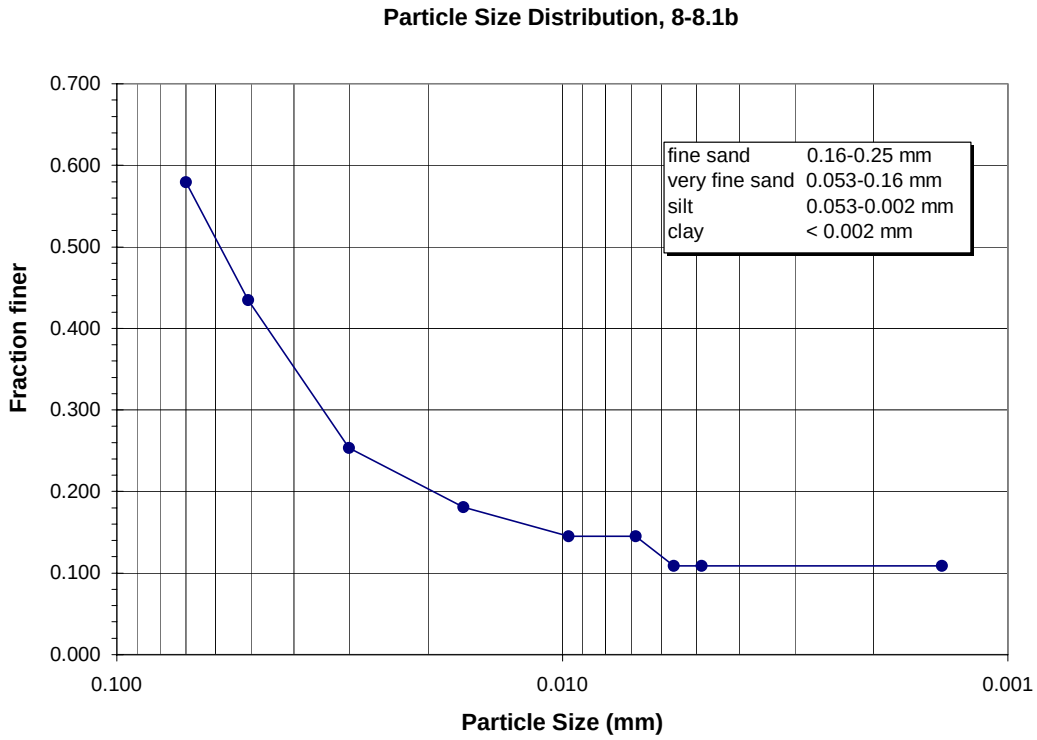


**Figure 4.3.6: Mass fraction of the original sample with a finer particle size.**

| | | | | | | | | θ | X(mean part dia) | X(mean part dia) |
|---|---|---|---|---|---|---|---|---|---|---|
| sample | t(min) | h' (cm) | R | R(L) | C | Co | **P(=C/Co)** | [cm*s^(1/2)] | (mm) | (microns) |
| 8-8.2a | 0.5 | 14.168 | 13 | 3 | 10 | 29.5273 | 0.339 | 0.040 | 0.073 | 72.5 |
| temp=20 | 1 | 14.332 | 12 | 3 | 9 | | 0.305 | 0.040 | 0.052 | 51.6 |
| degrees C | 3 | 14.824 | 9 | 3 | 6 | | 0.203 | 0.041 | 0.030 | 30.3 |
| | 10 | 14.988 | 8 | 3 | 5 | | 0.169 | 0.041 | 0.017 | 16.7 |
| | 30 | 15.152 | 7 | 3 | 4 | | 0.135 | 0.041 | 0.010 | 9.7 |
| | 60 | 15.152 | 7 | 3 | 4 | | 0.135 | 0.041 | 0.007 | 6.8 |
| | 90 | 15.152 | 7 | 3 | 4 | | 0.135 | 0.041 | 0.006 | 5.6 |
| | 120 | 15.152 | 7 | 3 | 4 | | 0.135 | 0.041 | 0.005 | 4.8 |
| | 1440 | 15.316 | 6 | 3 | 3 | | 0.102 | 0.041 | 0.001 | 1.4 |
| | | | | | | % Clay | 10.160 | | | |

**Table 4.3.8: Sample 8-8.2a, measured solution density with time and particle size calculation.**

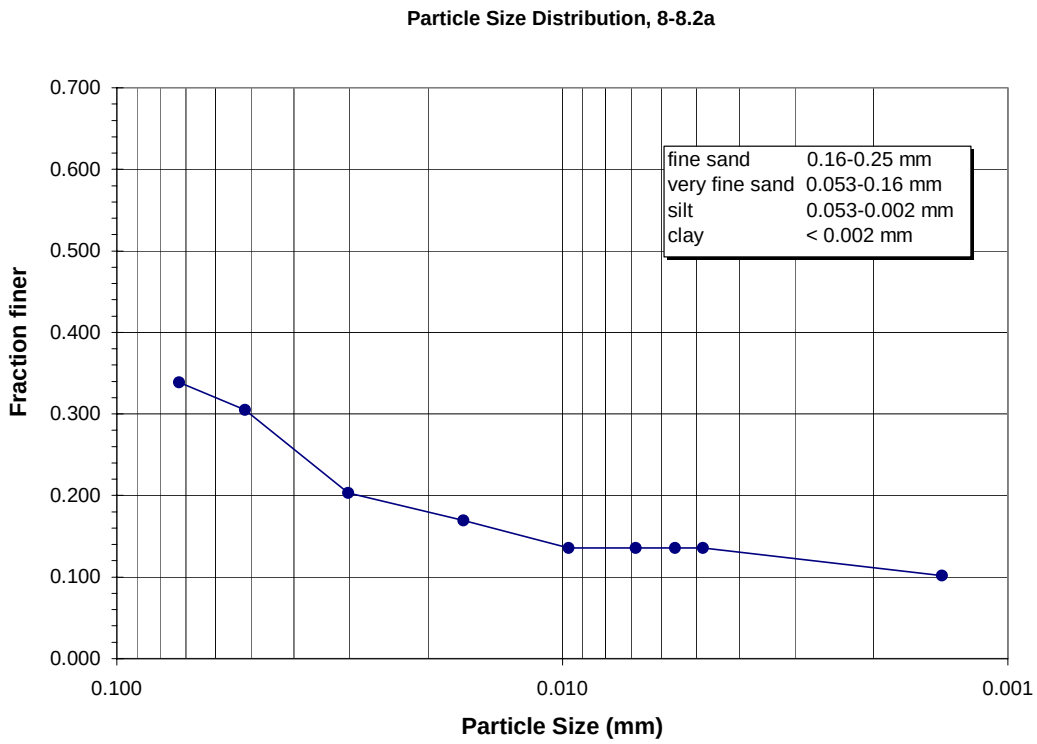


**Figure 4.3.7: Mass fraction of the original sample with a finer particle size.**

| | | | | | | | | θ | X(mean part dia) | X(mean part dia) |
|---|---|---|---|---|---|---|---|---|---|---|
| sample | t(min) | h' (cm) | R | R(L) | C | Co | **P(=C/Co)** | [cm*s^(1/2)] | (mm) | (microns) |
| 8-8.2b | 0.5 | 11.872 | 27 | 3 | 24 | 41.446 | 0.579 | 0.036 | 0.066 | 66.4 |
| temp=20 | 1 | 11.872 | 27 | 3 | 24 | | 0.579 | 0.036 | 0.047 | 46.9 |
| degrees C | 3 | 14.004 | 14 | 3 | 11 | | 0.265 | 0.039 | 0.029 | 29.4 |
| | 10 | 14.496 | 11 | 3 | 8 | | 0.193 | 0.040 | 0.016 | 16.4 |
| | 30 | 14.824 | 9 | 3 | 6 | | 0.145 | 0.041 | 0.010 | 9.6 |
| | 60 | 14.824 | 9 | 3 | 6 | | 0.145 | 0.041 | 0.007 | 6.8 |
| | 90 | 14.988 | 8 | 3 | 5 | | 0.121 | 0.041 | 0.006 | 5.6 |
| | 120 | 14.988 | 8 | 3 | 5 | | 0.121 | 0.041 | 0.005 | 4.8 |
| | 1440 | 15.152 | 7 | 3 | 4 | | 0.097 | 0.041 | 0.001 | 1.4 |
| | | | | | | % Clay | 9.651 | | | |

**Table 4.3.9: Sample 8-8.2b, measured solution density with time and particle size calculation.**

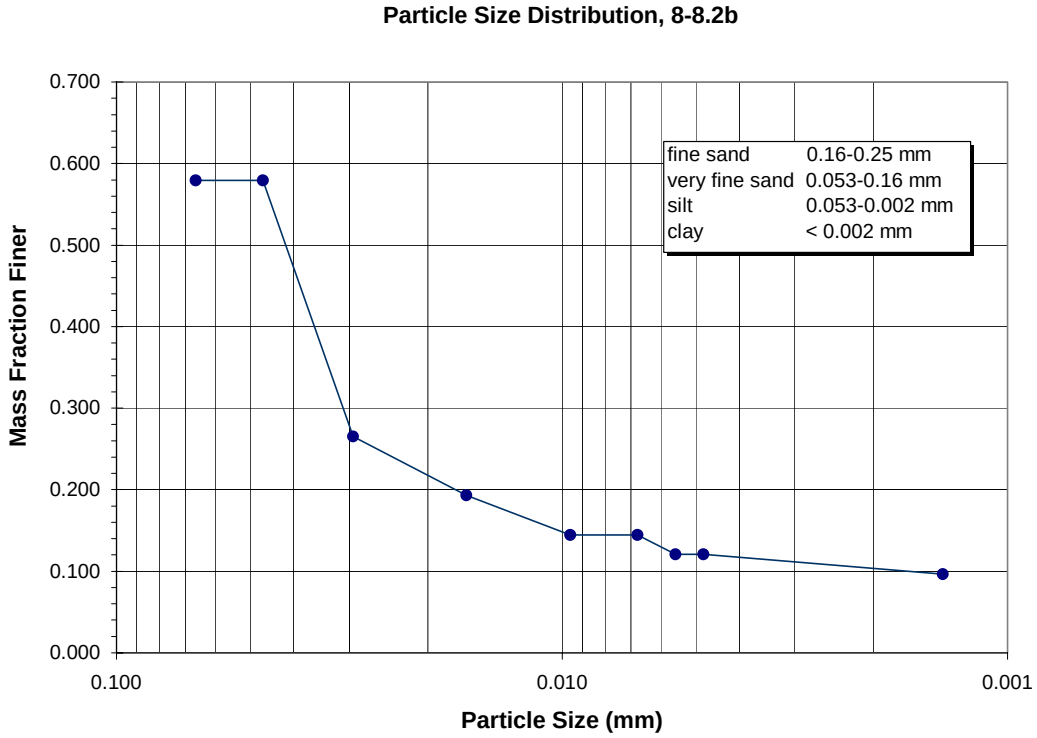


**Figure 4.3.8: Mass fraction of the original sample with a finer particle size.**

| | | | | | | | | θ | X(mean part dia) | X(mean part dia) |
|---|---|---|---|---|---|---|---|---|---|---|
| sample | t(min) | h' (cm) | R | R(L) | C | Co | **P(=C/Co)** | [cm*s^(1/2)] | (mm) | (microns) |
| 14a | 0.5 | 15.48 | 5 | 3 | 2 | 28.4487 | 0.070 | 0.042 | 0.076 | 75.8 |
| temp=20 | 1 | 15.48 | 5 | 3 | 2 | | 0.070 | 0.042 | 0.054 | 53.6 |
| degrees C | 3 | 15.48 | 5 | 3 | 2 | | 0.070 | 0.042 | 0.031 | 30.9 |
| | 10 | 15.48 | 5 | 3 | 2 | | 0.070 | 0.042 | 0.017 | 16.9 |
| | 30 | 15.48 | 5 | 3 | 2 | | 0.070 | 0.042 | 0.010 | 9.8 |
| | 60 | 15.48 | 5 | 3 | 2 | | 0.070 | 0.042 | 0.007 | 6.9 |
| | 90 | 15.48 | 5 | 3 | 2 | | 0.070 | 0.042 | 0.006 | 5.6 |
| | 120 | 15.644 | 4 | 3 | 1 | | 0.035 | 0.042 | 0.005 | 4.9 |
| | 1440 | 15.644 | 4 | 3 | 1 | | 0.035 | 0.042 | 0.001 | 1.4 |
| | | | | | | % Clay | 3.515 | | | |

**Table 4.3.10: Sample 14a, measured solution density with time and particle size calculation.**

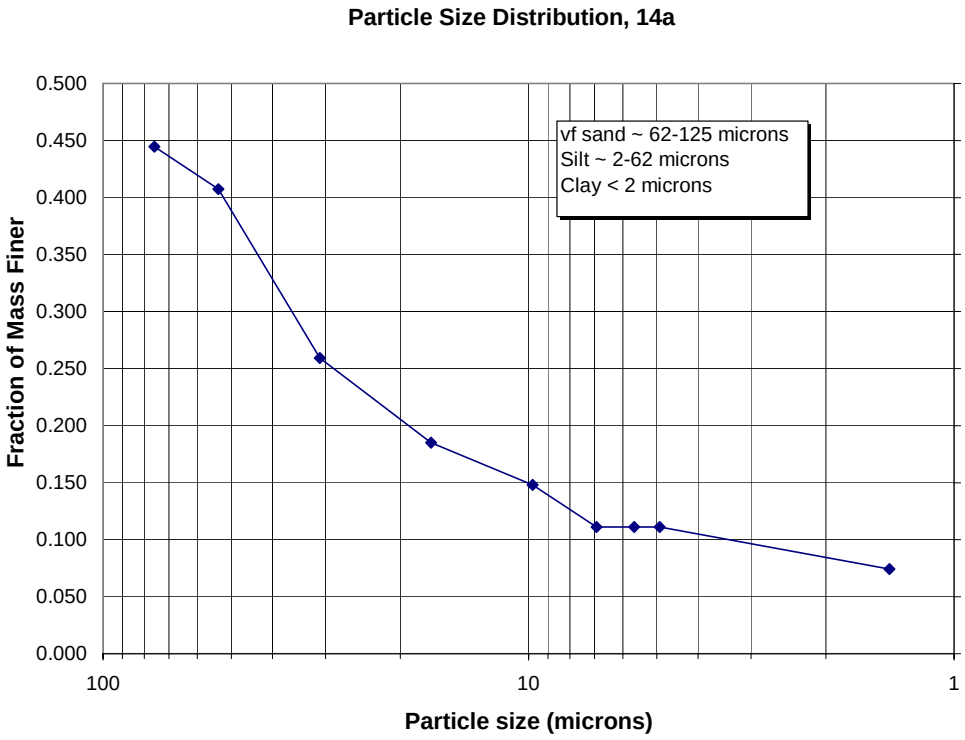


**Figure 4.3.9: Mass fraction of the original sample with a finer particle size.**

| | | | | | | | | θ | X(mean part dia) | X(mean part dia) |
|---|---|---|---|---|---|---|---|---|---|---|
| sample | t(min) | h' (cm) | R | R(L) | C | Co | **P(=C/Co)** | [cm*s^(1/2)] | (mm) | (microns) |
| 14b | 0.5 | 15.48 | 5 | 3 | 2 | 28.7256 | 0.070 | 0.042 | 0.076 | 75.8 |
| temp=20 | 1 | 15.48 | 5 | 3 | 2 | | 0.070 | 0.042 | 0.054 | 53.6 |
| degrees C | 3 | 15.48 | 5 | 3 | 2 | | 0.070 | 0.042 | 0.031 | 30.9 |
| | 10 | 15.48 | 5 | 3 | 2 | | 0.070 | 0.042 | 0.017 | 16.9 |
| | 30 | 15.48 | 5 | 3 | 2 | | 0.070 | 0.042 | 0.010 | 9.8 |
| | 60 | 15.48 | 5 | 3 | 2 | | 0.070 | 0.042 | 0.007 | 6.9 |
| | 90 | 15.48 | 5 | 3 | 2 | | 0.070 | 0.042 | 0.006 | 5.6 |
| | 120 | 15.644 | 4 | 3 | 1 | | 0.035 | 0.042 | 0.005 | 4.9 |
| | 1440 | 15.644 | 4 | 3 | 1 | | 0.035 | 0.042 | 0.001 | 1.4 |
| | | | | | | % Clay | 3.481 | | | |

**Table 4.3.11: Sample 14b, measured solution density with time and particle size calculation.**

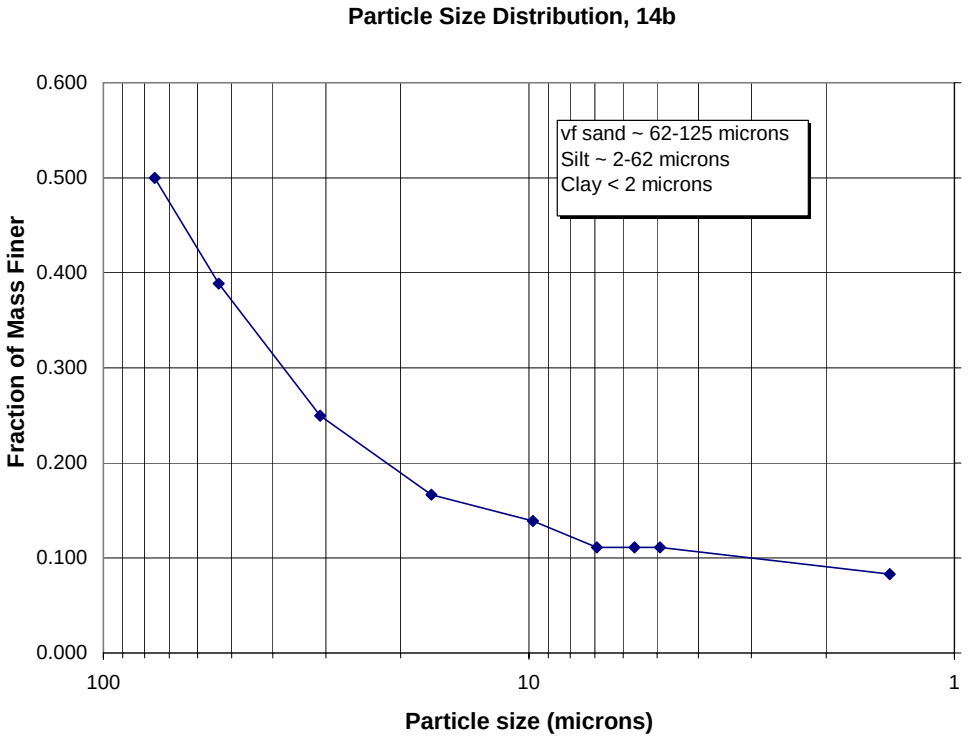


**Figure 4.3.10: Mass fraction of the original sample with a finer particle size.**

| | | | | | | | | θ | X(mean part dia) | X(mean part dia) |
|---|---|---|---|---|---|---|---|---|---|---|
| sample | t(min) | h' (cm) | R | R(L) | C | Co | **P(=C/Co)** | [cm*s^(1/2)] | (mm) | (microns) |
| 27a | 0.5 | 15.48 | 5 | 3 | 2 | 31.8428 | 0.063 | 0.042 | 0.076 | 75.8 |
| temp=20 | 1 | 15.48 | 5 | 3 | 2 | | 0.063 | 0.042 | 0.054 | 53.6 |
| degrees C | 3 | 15.48 | 5 | 3 | 2 | | 0.063 | 0.042 | 0.031 | 30.9 |
| | 10 | 15.48 | 5 | 3 | 2 | | 0.063 | 0.042 | 0.017 | 16.9 |
| | 30 | 15.48 | 5 | 3 | 2 | | 0.063 | 0.042 | 0.010 | 9.8 |
| | 60 | 15.48 | 5 | 3 | 2 | | 0.063 | 0.042 | 0.007 | 6.9 |
| | 90 | 15.48 | 5 | 3 | 2 | | 0.063 | 0.042 | 0.006 | 5.6 |
| | 120 | 15.644 | 4 | 3 | 1 | | 0.031 | 0.042 | 0.005 | 4.9 |
| | 1440 | 15.644 | 4 | 3 | 1 | | 0.031 | 0.042 | 0.001 | 1.4 |
| | | | | | | % Clay | 3.140 | | | |

**Table 4.3.12: Sample 27a, measured solution density with time and particle size calculation.**

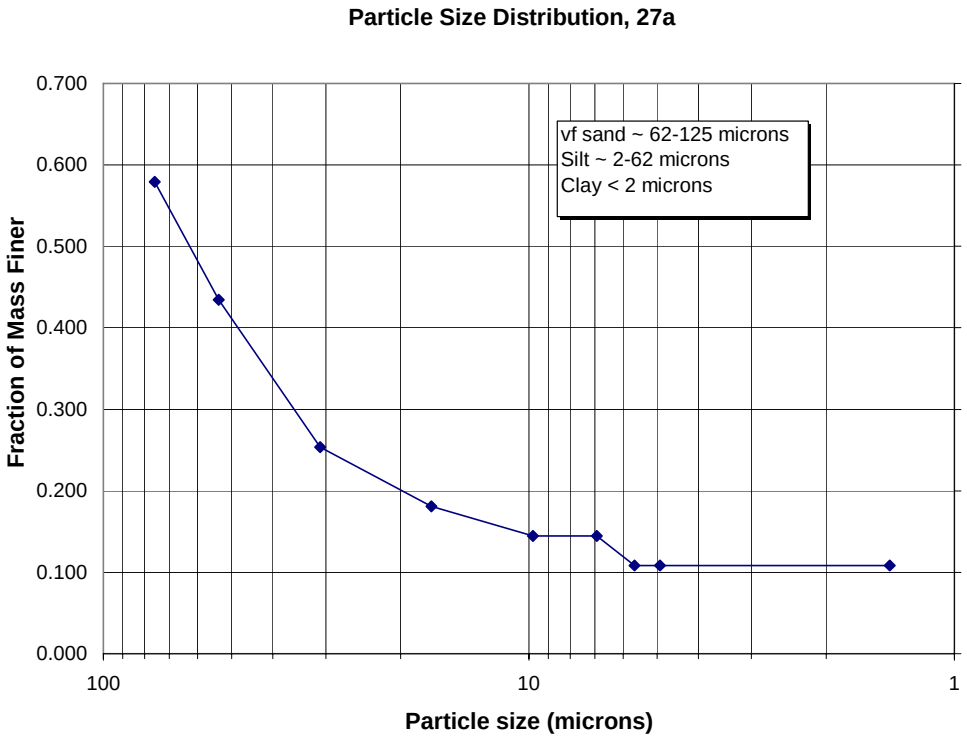


**Figure 4.3.11: Mass fraction of the original sample with a finer particle size.**

| | | | | | | | | θ | X(mean part dia) | X(mean part dia) |
|---|---|---|---|---|---|---|---|---|---|---|
| sample | t(min) | h' (cm) | R | R(L) | C | Co | **P(=C/Co)** | [cm*s^(1/2)] | (mm) | (microns) |
| 27b | 0.5 | 15.48 | 5 | 3 | 2 | 33.4002 | 0.060 | 0.042 | 0.076 | 75.8 |
| temp=20 | 1 | 15.48 | 5 | 3 | 2 | | 0.060 | 0.042 | 0.054 | 53.6 |
| degrees C | 3 | 15.48 | 5 | 3 | 2 | | 0.060 | 0.042 | 0.031 | 30.9 |
| | 10 | 15.48 | 5 | 3 | 2 | | 0.060 | 0.042 | 0.017 | 16.9 |
| | 30 | 15.48 | 5 | 3 | 2 | | 0.060 | 0.042 | 0.010 | 9.8 |
| | 60 | 15.48 | 5 | 3 | 2 | | 0.060 | 0.042 | 0.007 | 6.9 |
| | 90 | 15.48 | 5 | 3 | 2 | | 0.060 | 0.042 | 0.006 | 5.6 |
| | 120 | 15.644 | 4 | 3 | 1 | | 0.030 | 0.042 | 0.005 | 4.9 |
| | 1440 | 15.644 | 4 | 3 | 1 | | 0.030 | 0.042 | 0.001 | 1.4 |
| | | | | | | % Clay | 2.994 | | | |

**Table 4.3.13: Sample 27b, measured solution density with time and particle size calculation.**

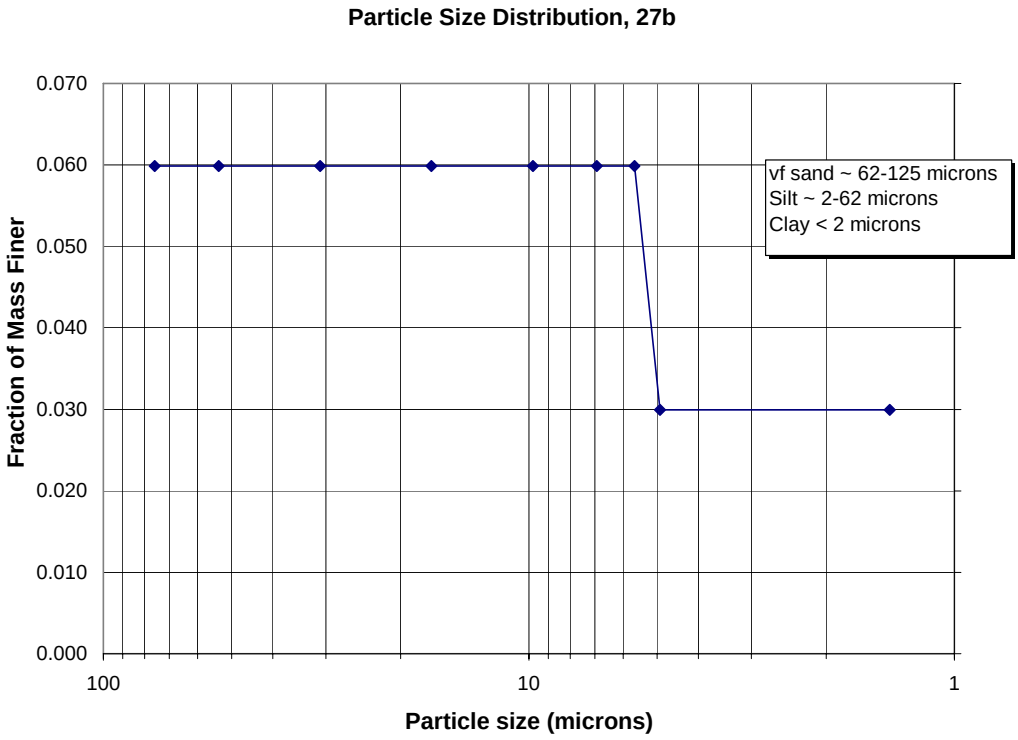


**Figure 4.3.12: Mass fraction of the original sample with a finer particle size.**

# Appendix 5 – Suction Lysimeter Data

## 5.1 Introduction

Suction lysimeters, or soil solution samplers, are simple devices that can be used to collect samples of the soil pore water. A suction lysimeter is a porous cup at the end of a length of PVC pipe. A vacuum is applied to the cup to draw in sample, then the vacuum is reversed to force the sample to the surface. The disadvantage of this technique is the limited sampling volume. Most of the suction lysimeters used in this project happened to be just outside of the wetted area and never detected the saline tracers. Several of the lysimeters were to dry to even produce samples.

Response of the suction lysimeters to the saline tracer varied. Some locations detected both pulses, while other locations only detected one. The time of the pulse arrival also varied between 30 days and 200 days at different locations. Response time does not seem correlated with depth, with the fastest response occurring at 8 m depth. A longer sampling time after the injection of the second salt pulse would have been beneficial at locations that showed a very delayed response to the first salt injection. A possible explanation for lysimeters that only detected the second salt pulse is the low conductivity of the first pulse. Pre-injection data suggests that the pore water conductivity is already very similar, if not greater, than the first salt tracer conductivity. The saline water was also only supplied to a third of the infiltrometer, which further weakens the tracer signal.

Overall, the data collected with the suction lysimeters agrees well with the TDR probes from the same locations, and with the neutron probe and EM39 data as well. The small sampling volume with this technique limits the information we can gain from this data set.

## 5.2 Suction Lysimeter Construction and Installation

The suction lysimeters used for this study were constructed at Sandia National Laboratories and consist of a sealed porous cup that is connected to the surface with a pair of flexible Nalgene tubes. To collect a solution sample, a vacuum is applied to one tube while the other one is clamped shut. After a period of time the vacuum is reversed and the sample is forced to the surface through the other tube, which is now unclamped. See Figure 5.2.1 below.

The suction lysimeters and TDR probes are nested together at 24 locations at the STVZ field site. Sixteen of the probes are installed around the infiltrometer at 8 meters depth, an additional eight are nested at 3.5 and 6 meters depth near the four corners of the infiltrometer. The labeling system used to identify the probes is based on distance from the infiltrometer for the probes at 8 m and based on depth for the eight probes nested at the infiltrometer corners. For example the lysimeter at 3.5 m at the south corner of the infiltrometer is SS (south shallow), or the two lysimeters closest to the infiltrometer in the northwest quadrant are labeled NWIA and NWIB (north-west Inner A and B). The exact labeling system and site layout is shown in Figure 8.

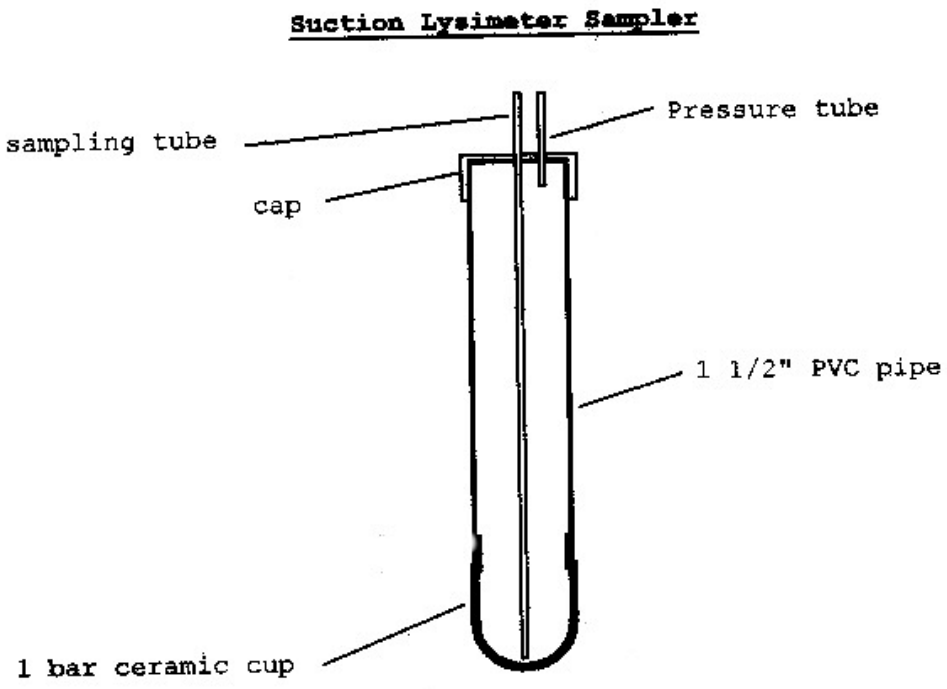


**Figure 5.2.1: Diagram of a Suction Lysimeter probe (Ropeke, 1995).**

## 5.3 Data Collection

The first soil solution samples were collected approximately 600 days after the start of infiltration, which is roughly 200 days before the start of the first salt pulse. Unfortunately, a replacement part was required for the Orion conductivity probe, which is used to measure the electrical conductivity of the soil solutions, approximately 30 days after the start of the first salt pulse. The solution samples from the eight lysimeters nested at the corners of the infiltrometer were retested and show that the probe had been behaving erratically prior to repair. The retested data shows the same overall trend as the readings taken with the faulty probe, but the deviation between readings is smaller.

The time interval between data collection varied, but samples were collected a minimum of once a month. The vacuum pressure and duration the pressure was applied were kept constant for all 24 lysimeters throughout the 2-year sampling period.

## 5.4 Results

The four shallowest suction lysimeters, at 3.5 meters depth, do not appear to have detected either of the two salt pulses as seen in Figure 5.3 below. The East and North solution samples remain at almost constant conductivity, while the solutions gathered from the West lysimeter steadily decline in conductivity during the sampling period. The South lysimeter may have begun to detect the saline injections just as the sampling period ended.

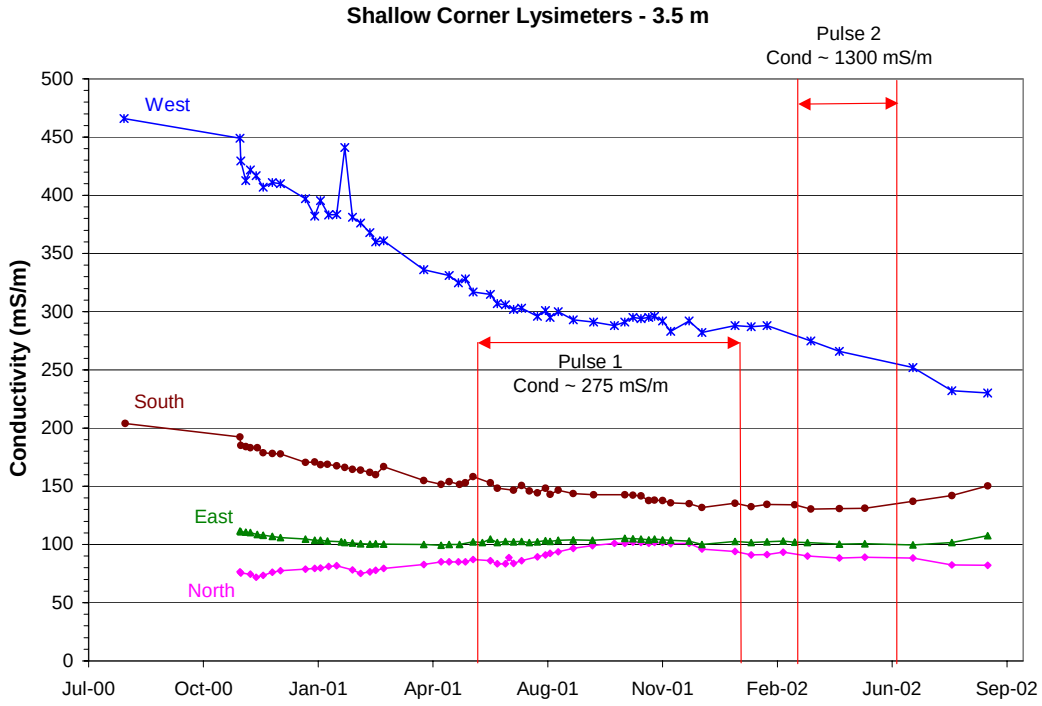


**Figure 5.4.1: EC of solution samples collected from lysimeters at 3.5 meters depth.**

Three of the four lysimeters at 6 meters depth appear to have detected the saline tracers that were added, as seen in Figure 5.4.1. It appears that the first salt pulse reached the North and West lysimeters at almost the same time, just as the pulse ended. The first

salt pulse is detected much quicker at the South lysimeter, but the detection to the higher concentration pulse is less clear. The East lysimeter did not appear to detect either of the salt pulses, and shows only a slow decrease in conductivity during the sampling period. All of the lysimeters show an initial decline in conductivity as sampling begins.

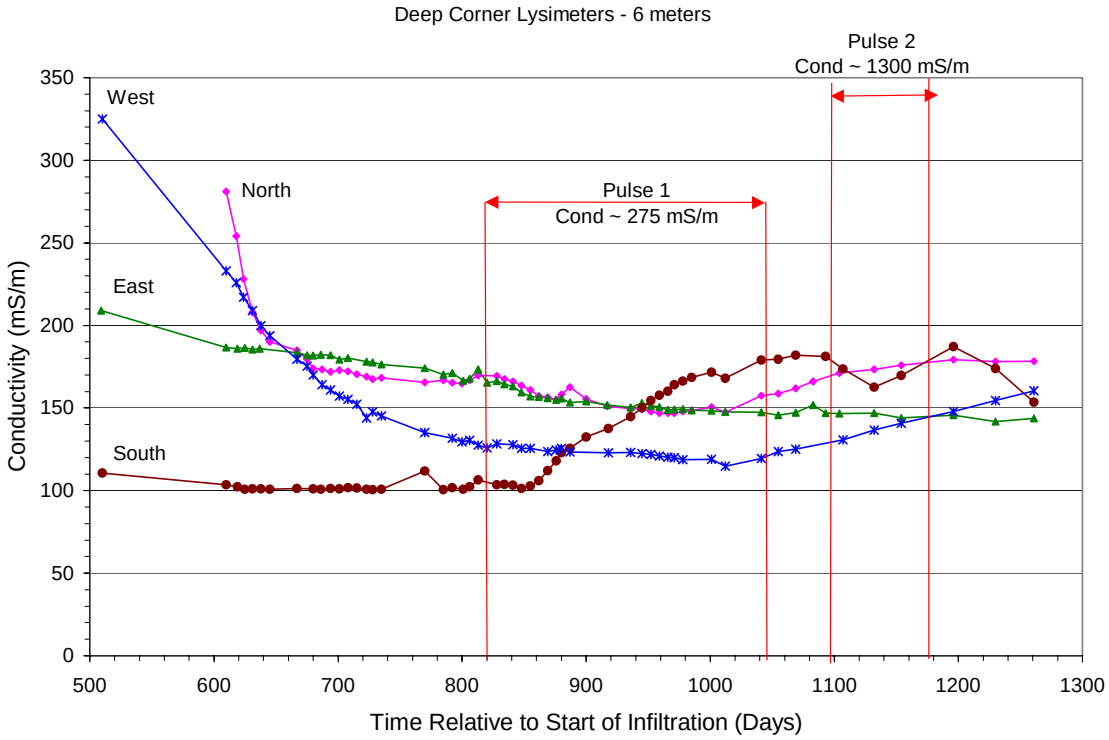


**Figure 5.4.2: The EC of solution samples collected from lysimeters at 6 meters depth.**

The data from the lysimeters at 8 meters depth has been presented in a series of graphs, see Figures 5.4 through 5.7. The lysimeters labeled as "Inner" are less than a meter from the edge of the infiltrometer, the lysimeters labeled "Outer" are less than 3 meters away, see Figure for site layout. Of the 16 lysimeters located at 8 meters depth, only three appear to have clearly detected the addition of either salt pulse. North West

Inner A and South West Outer B both seem to show a very strong response to the second salt pulse just at the sampling period ended. South West Inner A shows a clear increase in conductivity after the first salt pulse, but not for the second pulse. North East Inner B and North West Inner B also show slight increases in conductivity with time, but the trend is not clearly related to the salt pulses. The remaining suction lysimeters at 8 meters depth showed almost no change during the sampling period. Four of the suction lysimeters (North East Inner A, Outer A and Outer B and South East Inner A) did not produce solution samples.

Many of the suction lysimeters across the site show a curious trend of sharply decreasing conductivity as the first few (10 –15) samples were collected. Unfortunately, early solution testing may be unreliable because the conductivity probe being used to test the solution samples began to behave erratically and had to be repaired a few months after sampling had begun. All of the data at 3.5 and 6 m depth was retested after the probe was repaired. The retested data from the shallower depths was nearly identical to the original data, with less variation near the time that the probe failed. Data from 8 m depth was not retested and this data is indicated in the figures.

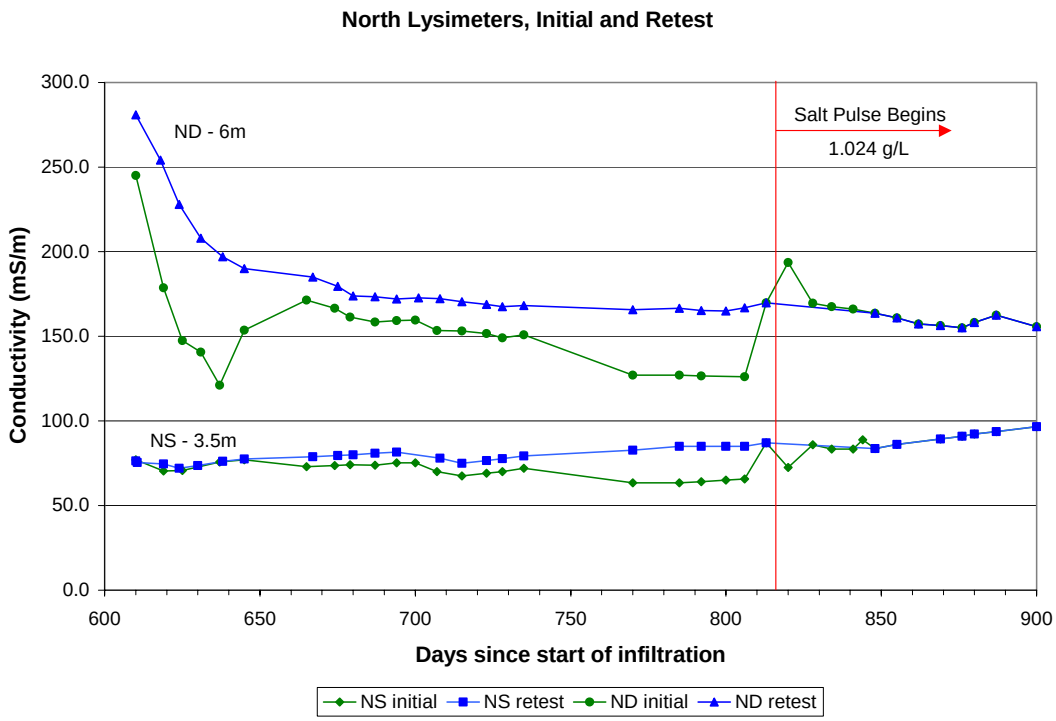


**Figure 5.4.3: Retested and original measurements of soil solution EC from NS and ND samples.**

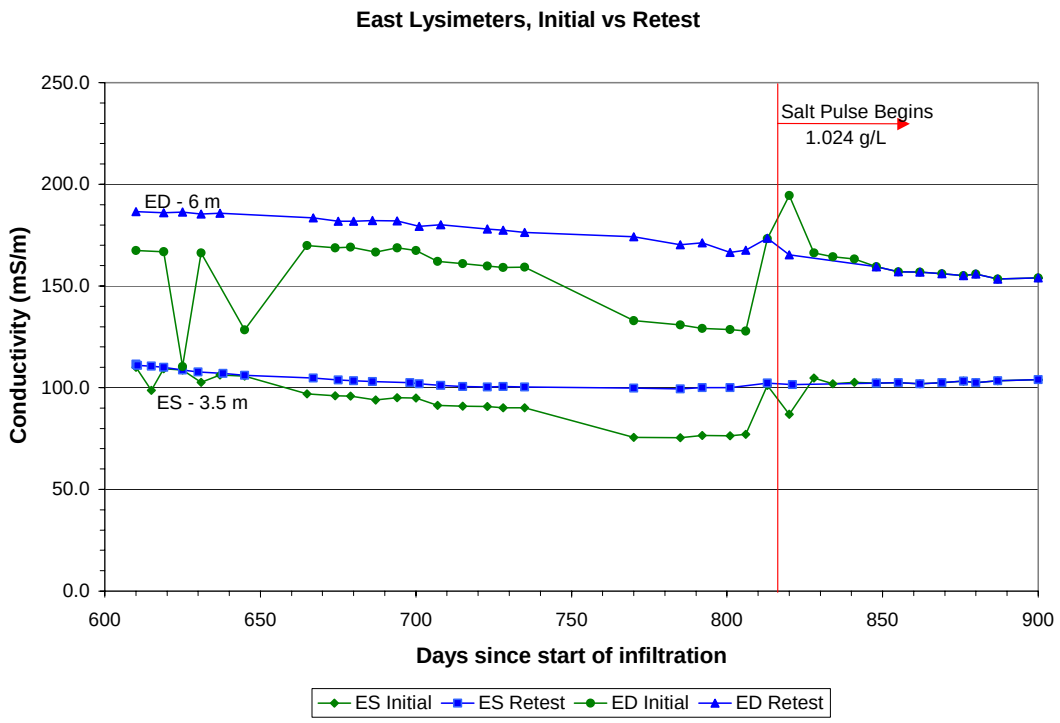


**Figure 5.4.4: Retested and original measurements of samples from ES and ED.**

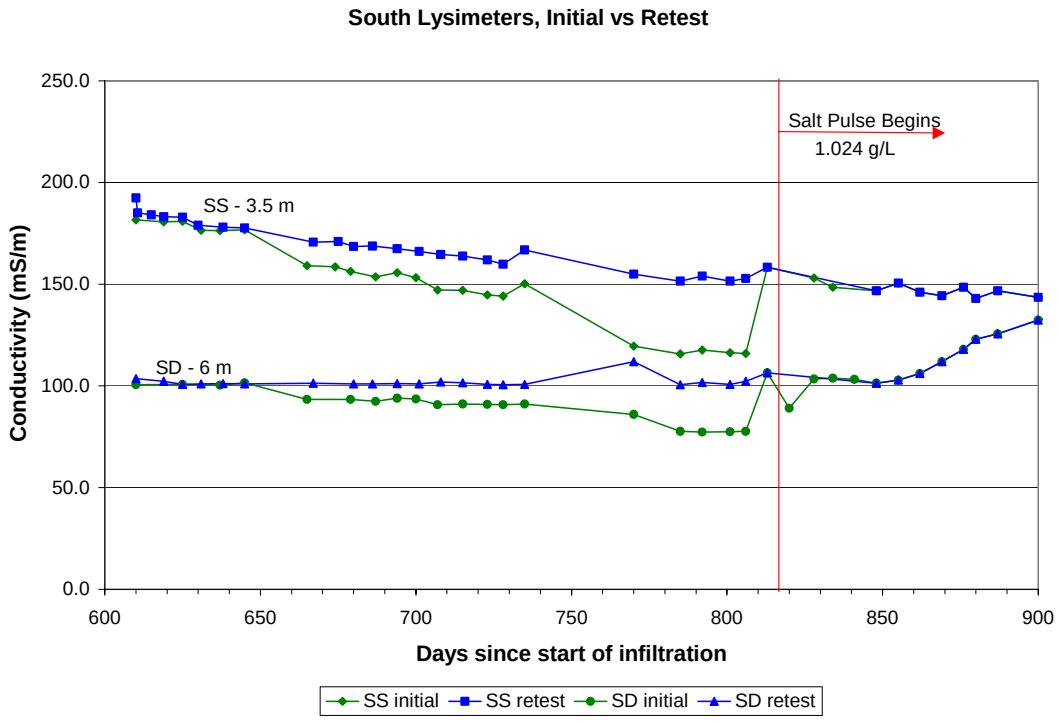


**Figure 5.4.6: Retested and original measurements of soil solution EC.**

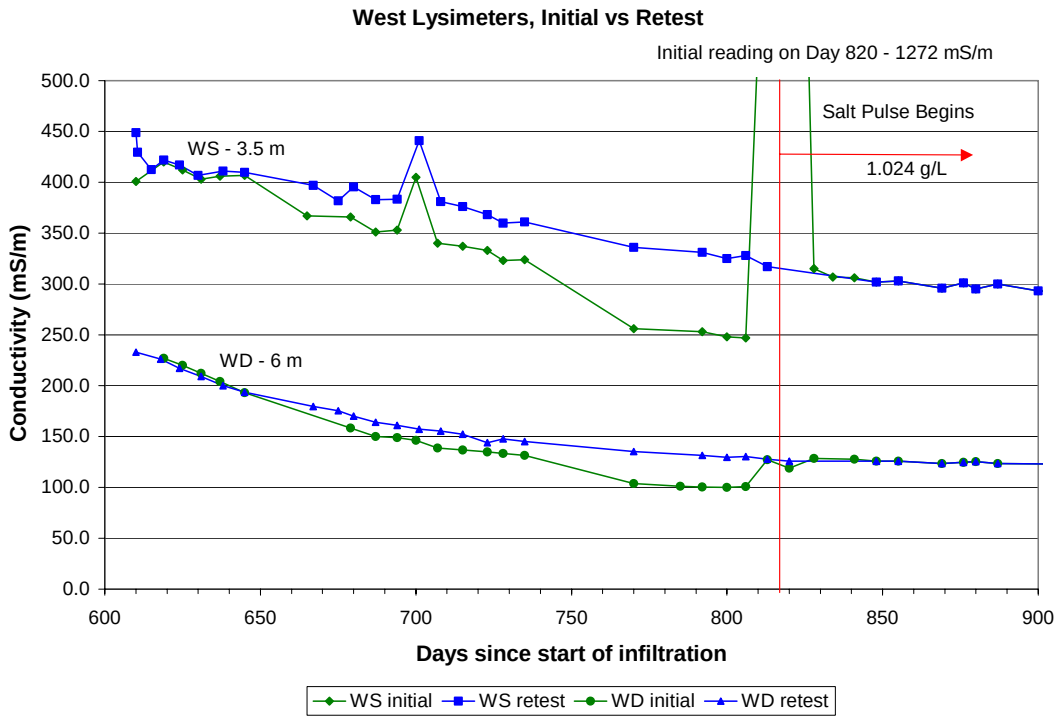


**Figure 5.4.7: Retested and original measurements of soil solution EC.**

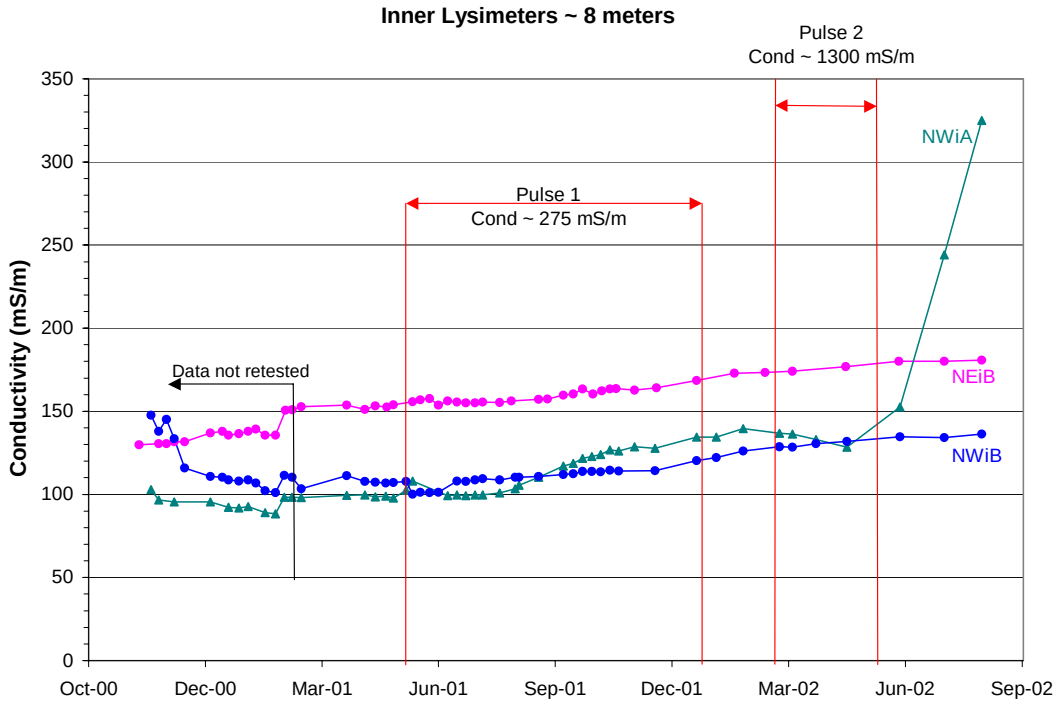


**Figure 5.4.8: Electrical conductivity of solution samples from the North Inner lysimeters.**

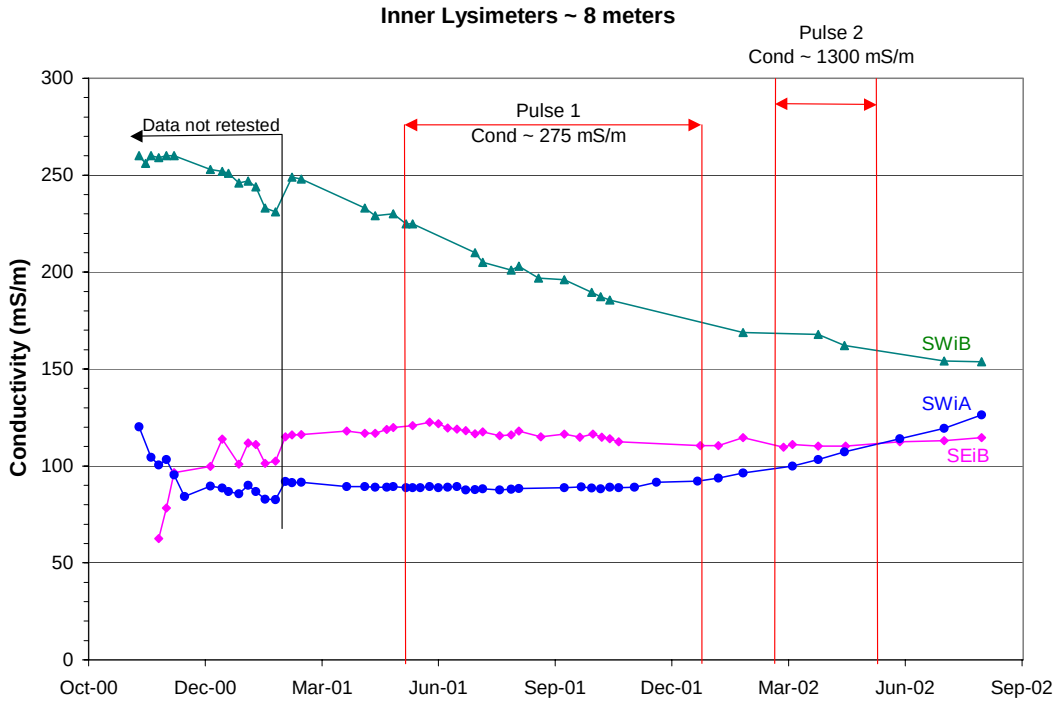


**Figure 6.4.8: Electrical conductivity of solution samples from the South Inner lysimeters.**

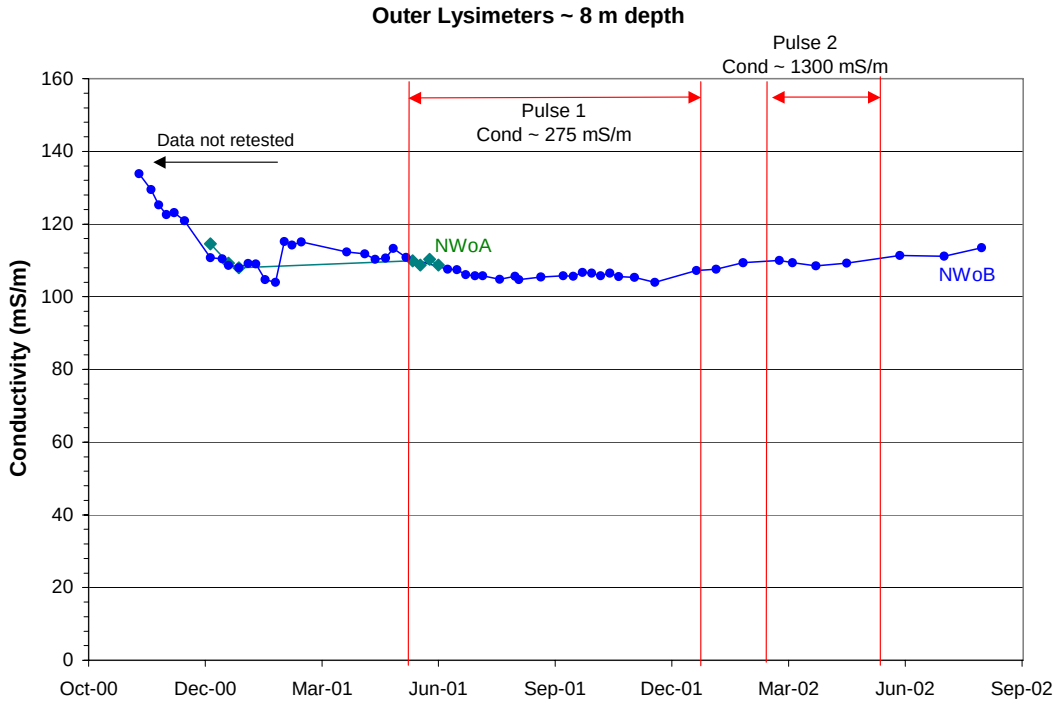


**Figure 6.4.9: Electrical conductivity of solution samples from the North Outer lysimeters.**

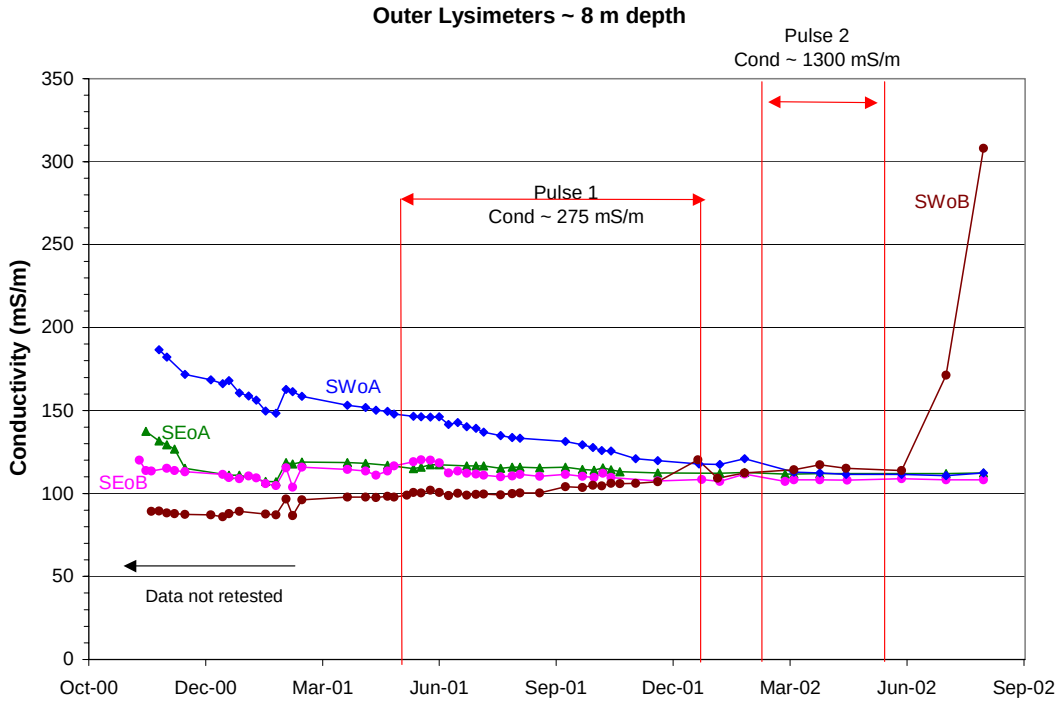


**Figure 5.4.9: Electrical conductivity of solution samples from the South Outer lysimeters.**

Samples were periodically collected from the saline solution tank and tested with the Orion conductivity probe. Samples were often collected while a submersible pump mixed the solution for 5 minutes just prior to infiltration. Routine samples were not collected of the regular water that was infiltrated to the rest of the infiltrometer. The first three data points on the graph where taken while mixing the first salt solution, and show the increase from background conductivity. The standard procedure for filling the salt tank (every 5 days), was to subtract the current water level from the full level (gradations marked on the tank) and calculate the mass of salt needed. The deviations in salt tank conductivity are due errors in the estimate of salt added to the tank and to sampling errors.

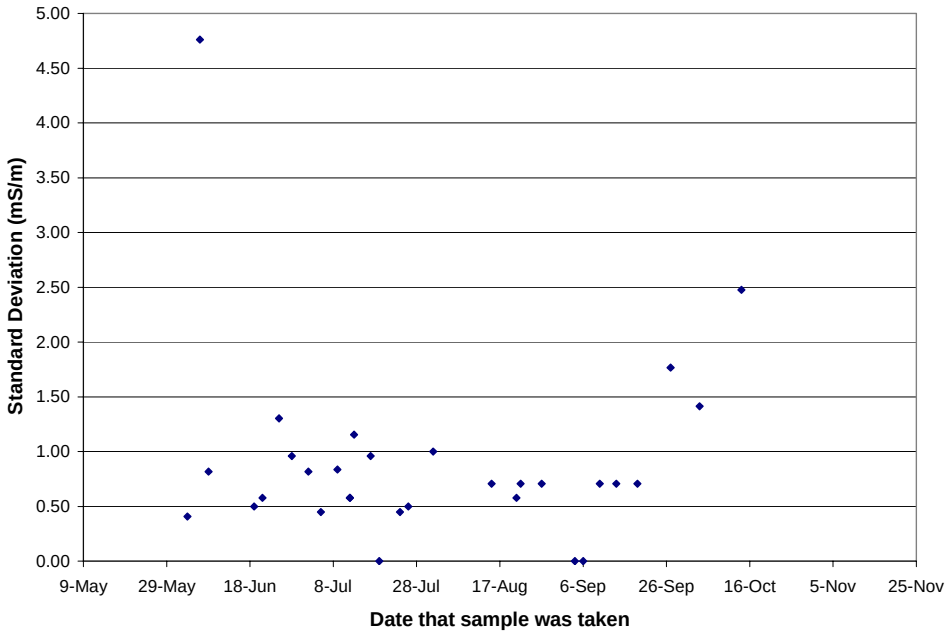


**Figure 5.4.11: Standard deviation of random samples that were retested (an average of 3 times) over a period of several months. The average deviation between all the retested samples is 1 mS $m^{-1}$.**

## 5.5 Conclusions

It is difficult to draw conclusions on the shape of the wetted area or movement of the salt tracers using only the suction lysimeter data. Unfortunately, most of the 24 probes appear to be installed either too deep or too far away from the infiltrometer to detect any significant conductivity changes from the salt pulses. A comparison with the neutron probe data verifies that most of the infiltrated water remains directly below the infiltrometer, until spreading out over the clay layer at approximately 6 m depth. These results could be misleading for a number of reasons however. Since the first samples were collected 600 days after the start of infiltration, we do not know which lysimeters were able to extract soil solution first.

An interesting decrease in soil solution conductivity is seen in the first 10 to 15 samples collected from many of the lysimeters, especially in samples from the North or West quadrants. A possible explanation is that the vacuum created while collecting the sample is slightly increasing flow around the lysimeter, which is flushing out the original higher conductivity pore water. Gathering pre-infiltration data would have given us better understanding of the in-situ soil water conductivity. This trend of decreasing conductivity could also be due to a flushing of contaminants introduced into the porous cups during lysimeter construction or installation. A third, and less likely, explanation for this trend is that the early readings are false due to an unreliable conductivity probe used to test the samples. After the probe was repaired (approximately 30 days after sampling began) all of the samples from 3.5 and 6 m depth were retested as seen in Figure, and show the same trends as the original data.

The two lysimeters showing the largest increase in conductivity after the addition of the second salt pulse (SWOB and NWIA) are at 8 m depth, As expected from the neutron probe data, the lysimeters at 6 m depth show the clearest response to the salt tracers.

## 5.6 Suction Lysimeter Operating Procedures

### 5.6.1 Sample Collection

Each of the 24 suction lysimeter probes has two polyurethane tubes (one blue and one clear) that reach the surface. The individual probes and their tubing are separated and labeled with both metal and plastic tags. The blue tube reaches the bottom of the porous cup and is used to remove the water sample. The clear tube reaches just below the top of the porous cup is used when applying pressure to the cup.

Four probes at a time can be connected to the vacuum pump using an adapted length of clear tubing. Connect the ends of the clear tubes from the probes to the tube attached to the vacuum pump. To create suction within the porous cup the ends of the blue tubing must be closed with either a stopper or clamp. Leave the probes under moderate pressure for approximately and hour and a half.

To collect the sample, first turn off the vacuum pump. Open or unclamp one of the blue tubes and place a collection bottle under it. Switch the tubing on the vacuum pump so that air is now being blown into the lysimeters and then turn the pump on. Opening one of the outlet tubes is necessary before turning the pump on to prevent any tubing from blowing off any fittings or from forcing the water sample back out through the porous cup.

### 5.6.2 Sample Analysis

The conductivity of the soil solutions is tested with an Orion Conductivity Probe. The probe can be calibrated automatically with AutoCal solution (a solution the probe is programmed to recognize automatically for a large range of temperatures) or by using the Direct Calibration option with a solution of know conductivity. The Direct Calibration method requires the input of the temperature corrected conductivity for the solution used in the calibration. Recalibrate the probe after testing roughly ten samples.

Often, due to small sample size, the solutions have to be transferred to a test tube to be analyzed. The solution must be large enough to cover the metal temperature sensor (approximately the bottom third of the probe should be submersed).

Rinse and pat dry the test tubes and conductivity probe between each sample to avoid contamination.

# Appendix 6 – TDR data

## 6.1 Introduction

Common methods for measuring soil salinity are often limited to taking soil samples and determining the electrical conductivity of a solution extracted from a saturated sample. Conventional nondestructive methods for measuring water content are usually limited to the use of neutron probes. Time Domain Reflectometry (TDR) probes can provide both measurements at the same location with little destruction to the surrounding material. TDR utilizes technology designed to find breaks in cables by generating a signal, sending it down a waveguide in the soil, and analyzing the reflected wave. The shape of the reflected wave is determined by the electrical properties, or dielectric constant, of the material around it. TDR is able to measure water content due to the vast contrast in the dielectric constant of water (~80) and that of soil particles (~3).

Topp et al. (1980) showed that a unique relationship existed between the relative dielectric constant ($\varepsilon$) and the volumetric water content ($\theta$) for a large range of soils and that this relationship is mostly insensitive to changes in the bulk density, temperature, salinity and mineral composition of the soil.

$$\theta = -5.3\times10^{-2} + 2.92\times10^{-2}\varepsilon - 5.5\times10^{-4}\varepsilon^2 + 4.3\times10^{-6}\varepsilon^3 \qquad [6.1]$$

Using time domain reflectometery, the dielectric constant of the medium is found by measuring the transit time (t) of an electromagnetic pulse launched along a pair of metallic, parallel rods of known length (L) embedded in a porous medium. The equation for this relationship as described by Persson et al (1998) and others is below. In these equations, c is the speed of light in free space (3 x$10^8$ m/s) and $L_a$ is the apparent length of the probe (calculated from the trace using the distance per division setting).

$$\varepsilon = \left(\frac{ct}{L}\right)^2 = \left(\frac{L_a}{L}\right)^2 \qquad [6.2]$$

In a saline soil, the electromagnetic pulse becomes attenuated and this attenuation can be used as a measure of bulk soil conductivity, $EC_a$ (Dalton, 1984).

$$EC_a = \left(\frac{\varepsilon^{1/2}}{120\pi L}\right)\left(\frac{V_1}{V_f}\right)\left[\frac{(2V_0 - V_f)}{(2V_0 - V_1)}\right] \qquad [6.3]$$

$V_0$ - the TDR pulse output

$V_1$ - the magnitude of the signal after reflection from the start of the probe

$V_f$ - the magnitude of the final reflected signal at $t \to \infty$.

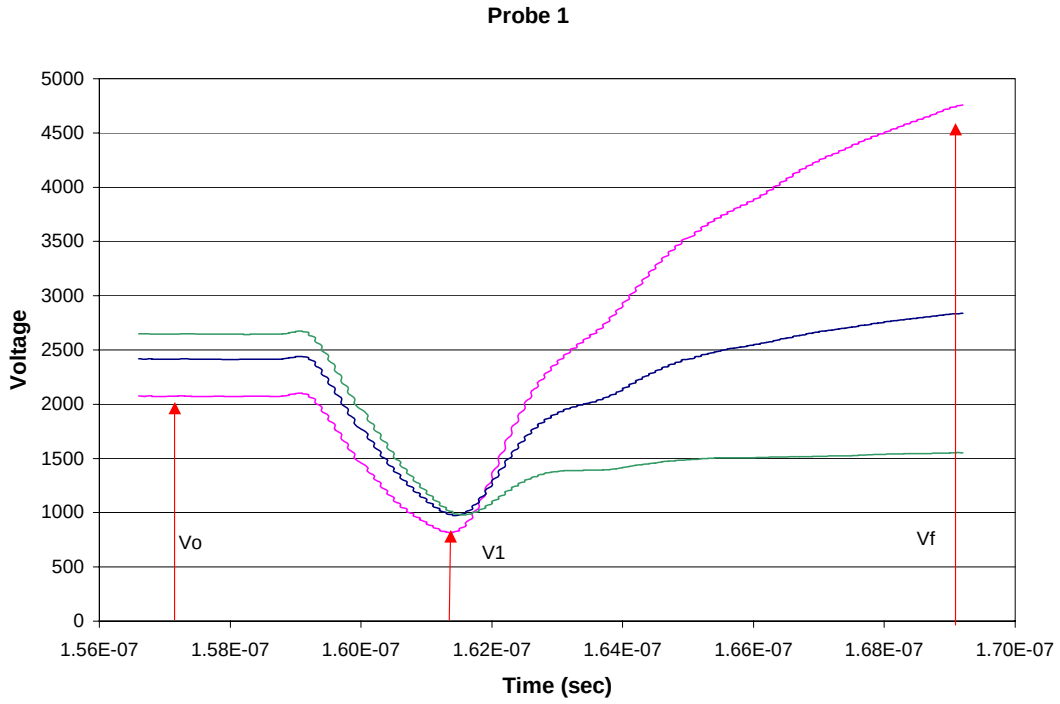


**Figure 6.1.1: TDR traces showing an increase in apparent soil conductivity and the relative position of $V_o$, $V_i$ and $V_f$.**

Figure 6.1.1 is a sample of one of the reflected waves recorded at the site, it is clear from this figure that Eq. [6.3] will result in a negative value for $EC_{a,}$ because the magnitude of is often $V_f$ is so much greater than the magnitude of $V_o$. Unfortunately, almost all of the data collected from the TDR probes installed at the site show this same trend. This peculiarity was not mentioned in the literature, but was also measured by Ropeke (1995) monitoring a $Cl^-$ tracer with both suction lysimeters and TDR probes. Ropeke's approach to this problem was to adopt an empirical relationship, since the change in soil water conductivity is indirectly proportional to the final reflected voltage:

$$\frac{C}{C_0} = \frac{1}{R}\frac{(V_{fo} - V_{io}) - (V_f - V_i)}{(V_{fo} - V_{io})} \qquad [6.4]$$

C = concentration of reading

Co = concentration before salt pulse

Vio, Vfo= Initial and final voltage before salt pulse

Vi, Vf = Initial and final voltage of reading

R = Empirical correction factor

This approach was used to analyze the TDR data is this study for changes in bulk soil conductivity.

The temperature dependence of the TDR water content measurement depends on soil texture and electrical conductivity. The results of Persson and Berndtsson (1998) suggest a temperature correction of $-0.00269\theta°C^{-1}$ for sandy soils. In clayey and organic soils the correction factor is smaller and can even be positive. The negative value of the correction factor indicates a decrease in water content measurement with increases in temperature. The temperature effect on bulk electrical conductivity was found to be independent of soil texture.

Although a temperature correction was only preformed on TDR data collected during a series of lab experiments, Persson (1998) also reported that differences in soil properties between probes at different locations probably cause larger errors in water content measurement than temperature effects. Temperature effects would be most important when comparing changes in water content at the same probe over time and not between probes at different locations. Water content measurements from the probes show little variation over time however, suggesting that the temperature effects were small.

## 6.2 Lab Experiments

Twenty-four TDR probes were buried at various locations and depths across the test site with the objective of monitoring the breakthrough curves of the two pulses of NaCl. Before data was collected with the field probes, a set of laboratory experiments were conducted with the goals of 1) developing calibration curves between TDR measured relative voltage and both bulk soil electrical conductivity and soil water conductivity; 2) investigating the measurement variability between different TDR probes; and 3) investigating the sensitivity of the TDR bulk conductivity measurement to changes in texture (grain size) and water content. Some of the problems facing these objectives include the fact that the probes were installed in sands with unknown grain size distribution and bulk density, and before any calibration was preformed. Data was also not collected from the probes until just prior to the first salt pulse and subsequently data does not exist of the dry soil conditions or of the advancement of the wetting front.

In these experiments, three identical columns were used along with three TDR probes identical to the probes installed at the field site. Solutions of various conductivities were pumped through the screened bottom of the columns and flowed out through an overflow ports near the top of the columns. The tops of the columns were open to the air.

The first experiment was performed to determine the maximum conductivity the TDR probe could measure before the reflected signal became entirely attenuated. This simple experiment consisted of placing a probe in a bucket of water and slowly adding salt to the water to increase the conductivity. Published values for the maximum measurable soil water conductivity vary with probe design and the input voltage used. Our probe shows a non-linear response to the conductivity increase, with greater response occurring at low conductivity, which makes it difficult to pinpoint the maximum conductivity measurable, see Figure 6.2.1 below. The final reflected voltage quickly becomes less than the initial voltage and the value for the relative voltage changes from a positive to a negative.

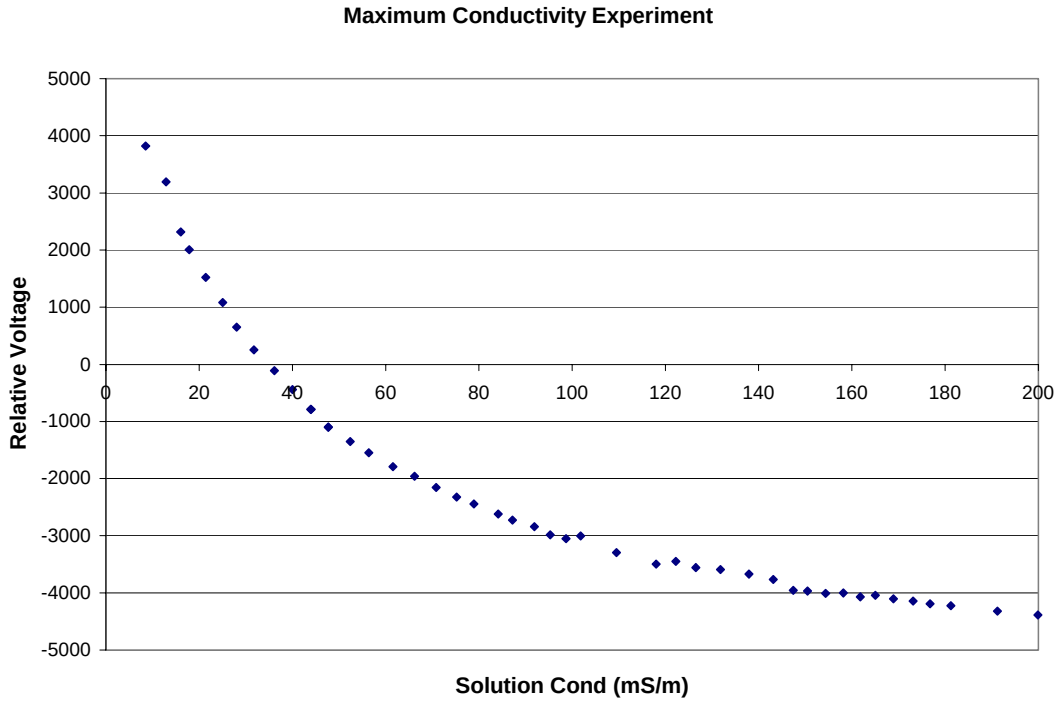


**Figure 6.2.1: As the solution becomes more conductive the final reflected voltage decreases and quickly becomes smaller than the initial voltage, leading to a negative value for the relative voltage.**

A column experiment was designed to test the variability in response between probes in different soil types. The column experiment was initially conducted on 11/14/01 and then again on 1/29/02. The same experiment was conducted several months apart to test the repeatability of the findings. The experiment conducted 11/19/01 was conducted in a laboratory using clean reverse osmosis treated water. The experiment conducted in January was preformed at the field site using the same water that is used for infiltration. Three solutions ranging in conductivity from 15 to 300 mS $m^{-1}$ were pumped through the columns during the 11/14/01 experiment. Four solutions ranging between 65 and 275 mS $m^{-1}$ were pumped through the columns during the repeatability experiment. Data was collected every ten minutes as the solutions were applied, and as the columns

drained after the last solution. For this experiment all three columns are filled with different soil samples gathered from the site.

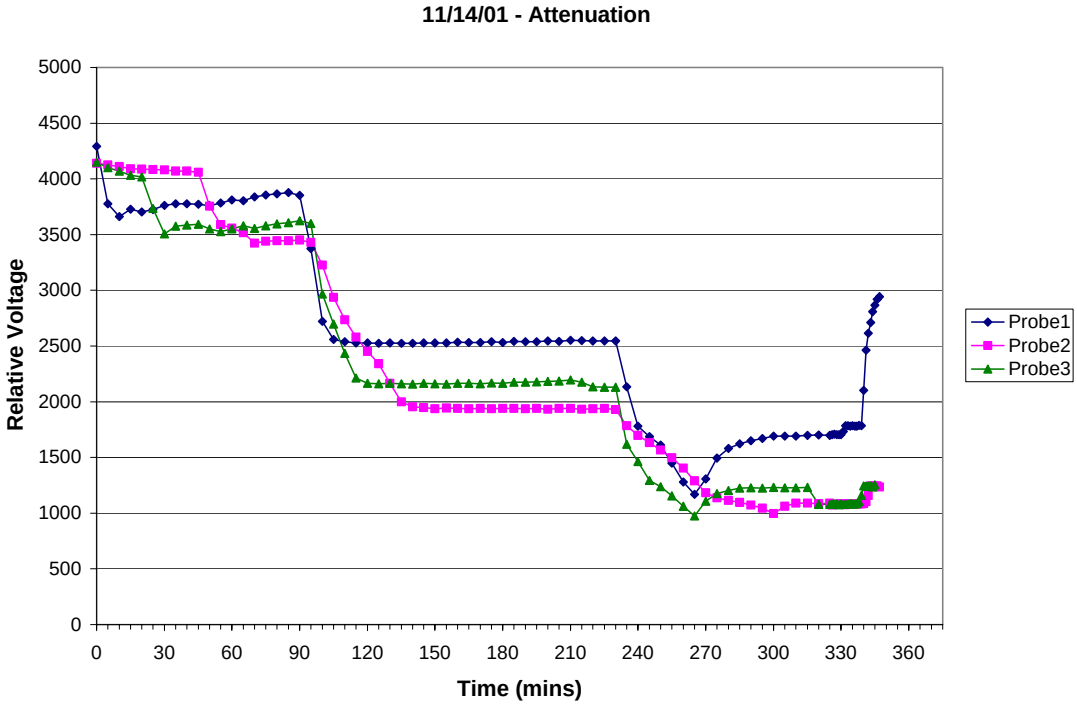


**Figure 6.2.2: An example of the relative voltage calculation during the column experiment.**

Figure 6.2.2 shows the decrease in the final reflected voltage as the soil salinity increases. Data is plotted as relative voltage, which is the final reflected voltage minus the initial voltage to correct for inconsistencies in the input voltage. The relative voltage jumps down with the addition of each higher concentration solution and then stabilizes as all of the pores become filled with the solution. The increase in voltage at the end of the experiment shows the decrease in conductivity as the column drains.

Unlike the conditions measure by the field probes, the experiments were conducted at saturated conditions. The problem of negative conductivity calculations using the method of Dalton (1984) and others quickly disappeared as the soils became

sufficiently moist. Due to a fairly uniform grain size distribution in most samples analyzed (Baker, 2001) it was difficult to run the experiment at different soil water contents. A different experimental set-up would have been necessary to test flow rates sufficiently low to sustain low soil water contents. Figures 6.2.3 and 6.2.4 are the results of the calculations of ECa using Eq. [6.3], for column experiments conducted on 11/14/01 and 1/29/02.

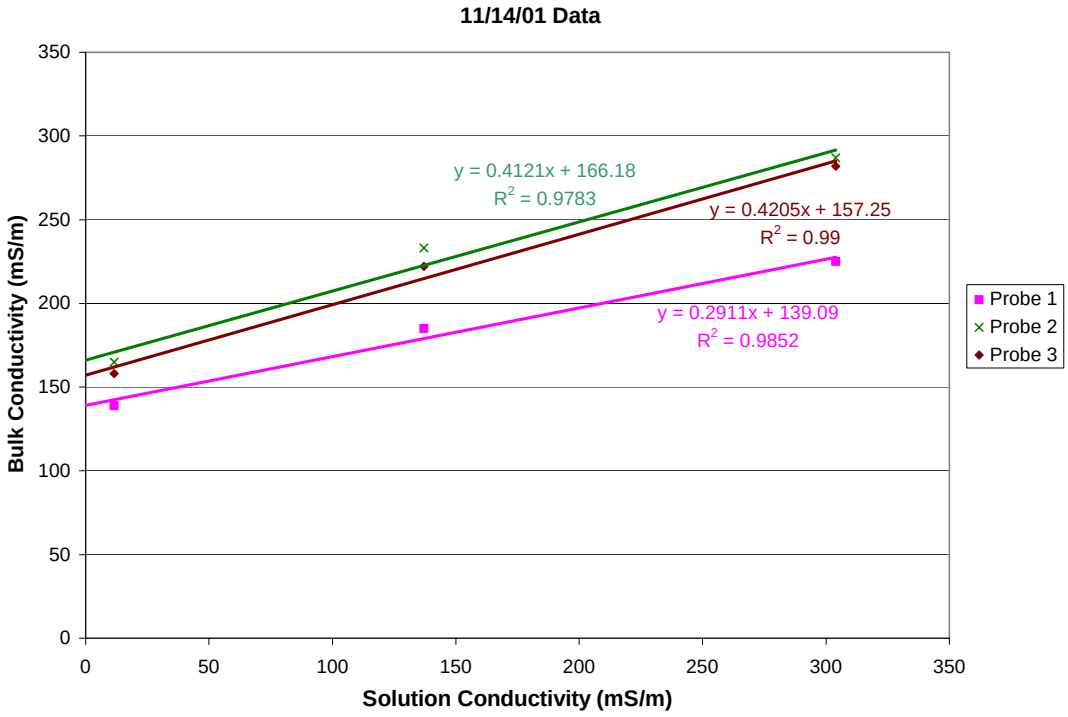


**Figure 6.2.3: Bulk conductivity calculations from the column experiment conducted on 11/14/01. The three data points for each probe are calculated from average values of relative voltage for each of the solutions.**

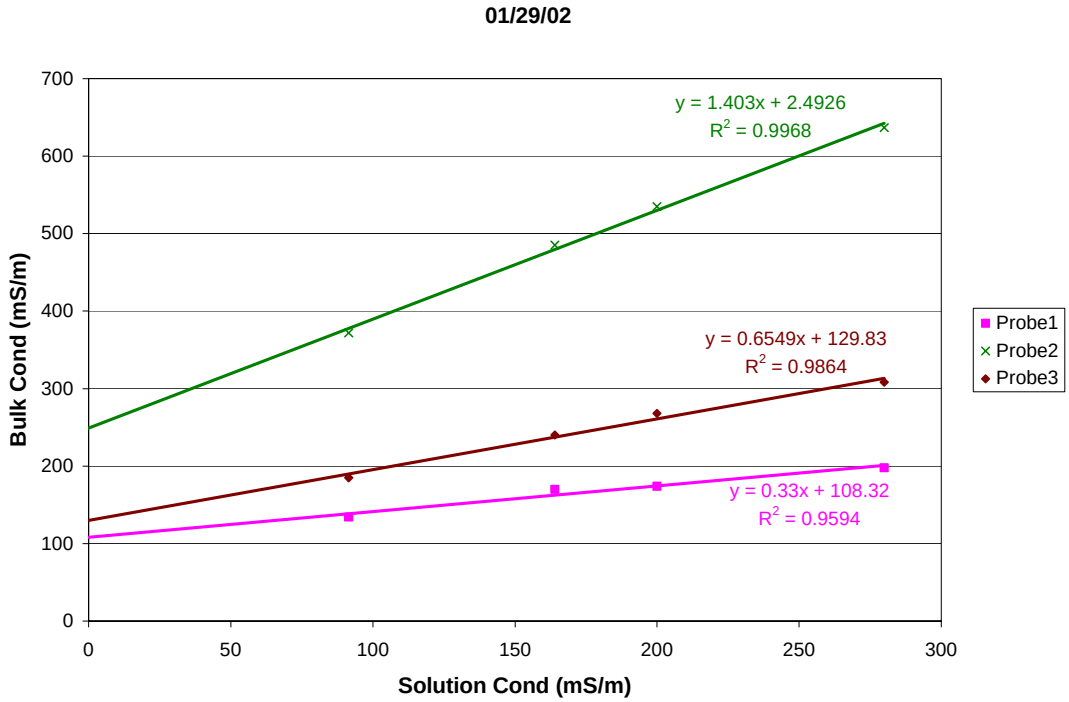


**Figure 6.2.4: Bulk conductivity calculations from the column experiment conducted on 1/29/02. The three data points for each probe are calculated from average values of relative voltage for each of the solutions.**

The average temperature of the solutions used on 1/29/02 were very cold, approximately 10ºC, while temperatures for the first experiment were closer to 25ºC. Figures 6.2.5 and 6.2.6 show the effect of temperature correcting the data, using Eq [14].

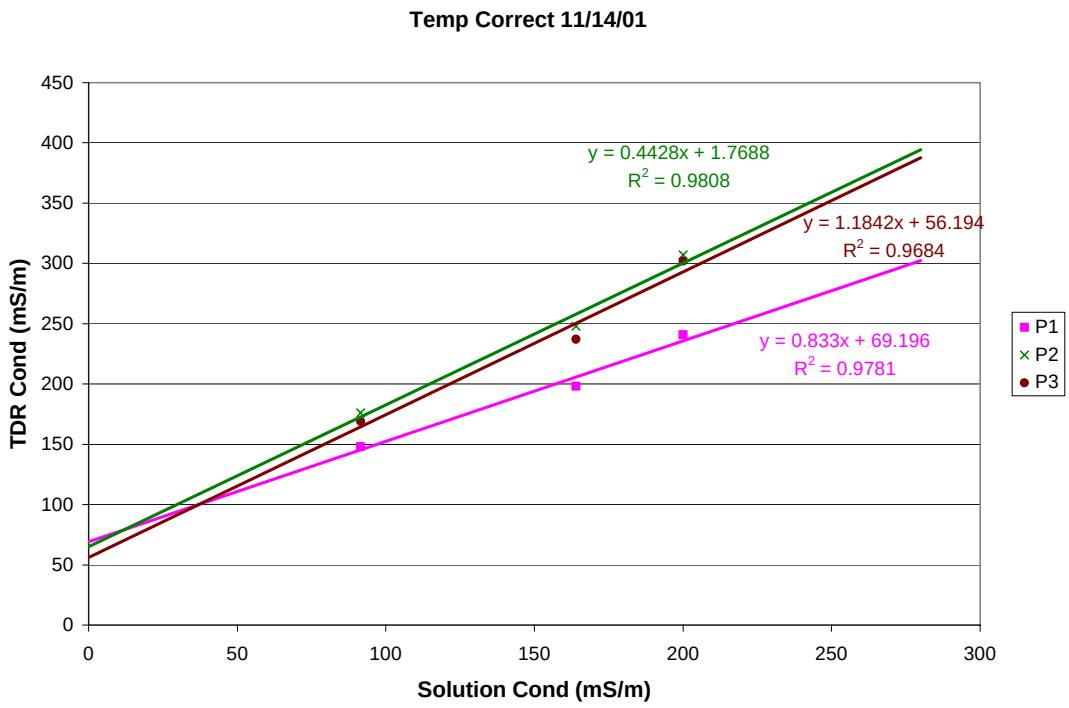


**Figure 6.2.5: Temperature corrected data from the 11/14/01 experiment.**

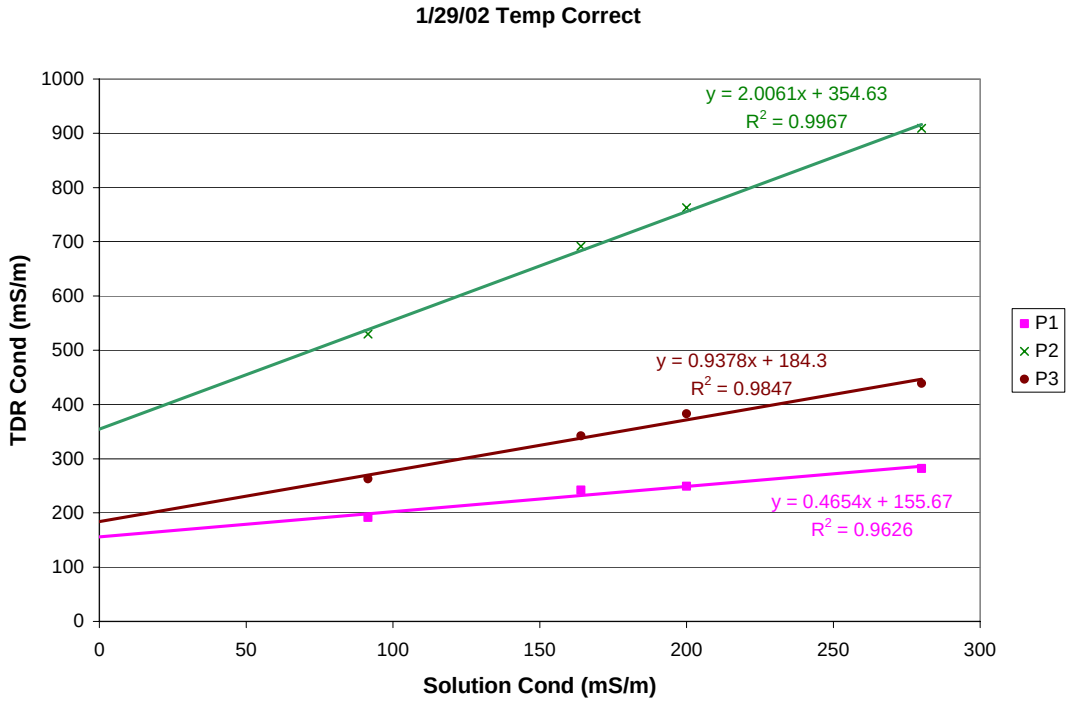


**Figure 6.2.6: Temperature corrected data from the 1/29/02 experiment.**

The results of these lab experiments show that the apparent soil electrical conductivity calculations outlined by Dalton and others is possible with our TDR instrumentation once the soil becomes significantly saturated. Unfortunately, the repeatability of the measurements was not strong between the two experiments, even after temperature correction. Further experiments would be necessary to define the reasons for the differences.

## 6.3 Instrumentation and Data Collection

The 24 time domain reflectometery probes used for this project were built at Sandia National Labs and they all have nearly identical dimensions, see Figure 6.3.1. The probes comprise of 30 meters of 50-ohm coaxial cable, terminated at one end with three metal prongs, each approximately 150 mm long. The prongs are held in place with two polycarbonate plates each roughly 20 mm thick. Between the polycarbonate plates the coaxial cable is in contact with the ends of the prongs.

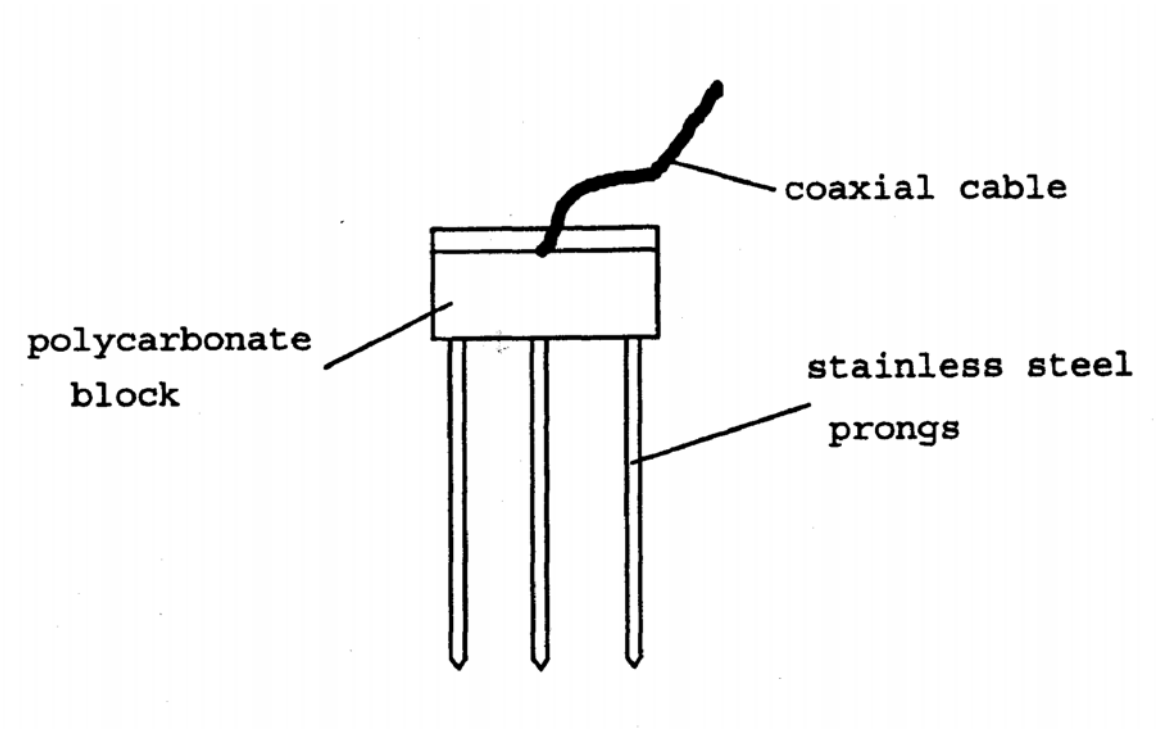


**Figure 7.3.1: Diagram of TDR probe (Ropeke, 1995).**

Suction lysimeters and TDR probes are nested together at 24 locations at the STVZ field site, see Figure 6.3.2. Sixteen of the probes are installed around the infiltrometer at 8 meters depth, an additional eight are nested at 3.5 and 6 meters depth near the four corners of the infiltrometer.

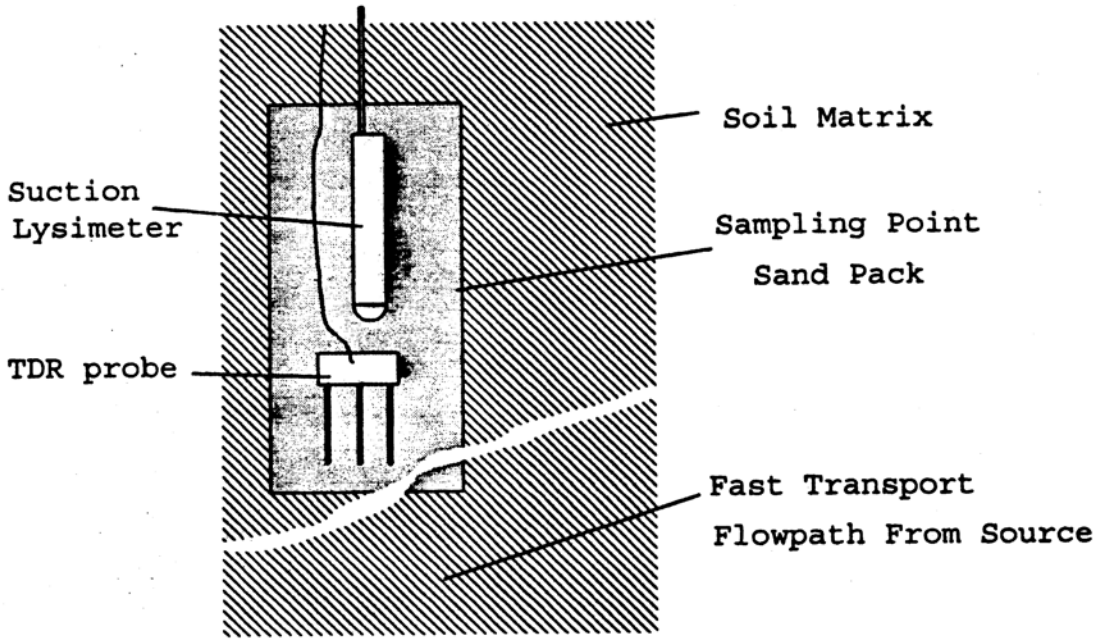


**Figure 6.3.2: Diagram showing approximate placement of TDR and suction lysimeter probes (Ropeke, 1995).**

The data acquisition system used at the STVZ site consisted of a Tektronix 1502B signal generator and receiver, an automated 24-port coaxial cable switch and a laptop. The entire TDR system was powered with a 12 V battery attached to 2-amp battery charger. A FORTRAN computer program was written to gather information about both volumetric water content and electrical conductivity.

Although data collection with the TDR began before the start of the first salt pulse, a change was made in the data collection settings (the signal was amplified) approximately 30 days after the pulse start. The data analyzed and presented here is only the amplified data (June 2001 through August 2002). The cable for the SWOB probe was too short to reach the multiplexer, so data was not collected from this probe.

## 6.4 Data Processing

To process the data collected from the field probes, a program was written in LabView that creates one summary file with the averages of the output values from the FORTRAN program for each probe. The calculations performed by the FORTRAN program include the dielectric constant, the water content, the final and initial voltage and the standard deviation of each of the voltage readings. The LabView program additionally calculated a standardized final voltage reading, as a measure of relative soil salinity, by subtracting the initial voltage from the final voltage.

## 6.5 Results

Most of the TDR probes did not detect the injection of either salt tracer and showed only minor changes in relative soil salinity during the year of data collection. The water content measurements are also very stable, with an average standard deviation of 0.003, or 0.03% volumetrically from all of the probes. The low variability of the water content suggests the shape of the wetted area is very stable and that the suction lysimeters are not significantly altering the flow field.

Since the soils at the site are so resistive, calculations of soil salinity could not be made as discussed earlier. Figure 7.5.1 shows the relative change in soil salinity during the infiltration of both pulses, from the 18 probes with measurable traces. Data is calculated as relative change from the first reading taken, unfortunately the first data set was only collected 40 days after the start of the first salt pulse, so this day probably does not represent a good background value. Figure 7.5.2 shows the relative change in soil salinity just due to the second salt pulse. Data is presented as change from the

measurements taken the day the second pulse started. A positive value is a relative increase in soil salinity and a negative number is a relative decrease from background. The relative change in soil salinity is much larger at the ED probe in both Figures 7.5.1 and 7.5.2. Figure 7.5.3 shows the relative change from the second pulse with the ED removed. In Figure 7.5.3 it is clear that an increase in soil salinity is observed at SD, NWIA, SWOB, and WS. A decrease in soil salinity is seen at ND and ED.

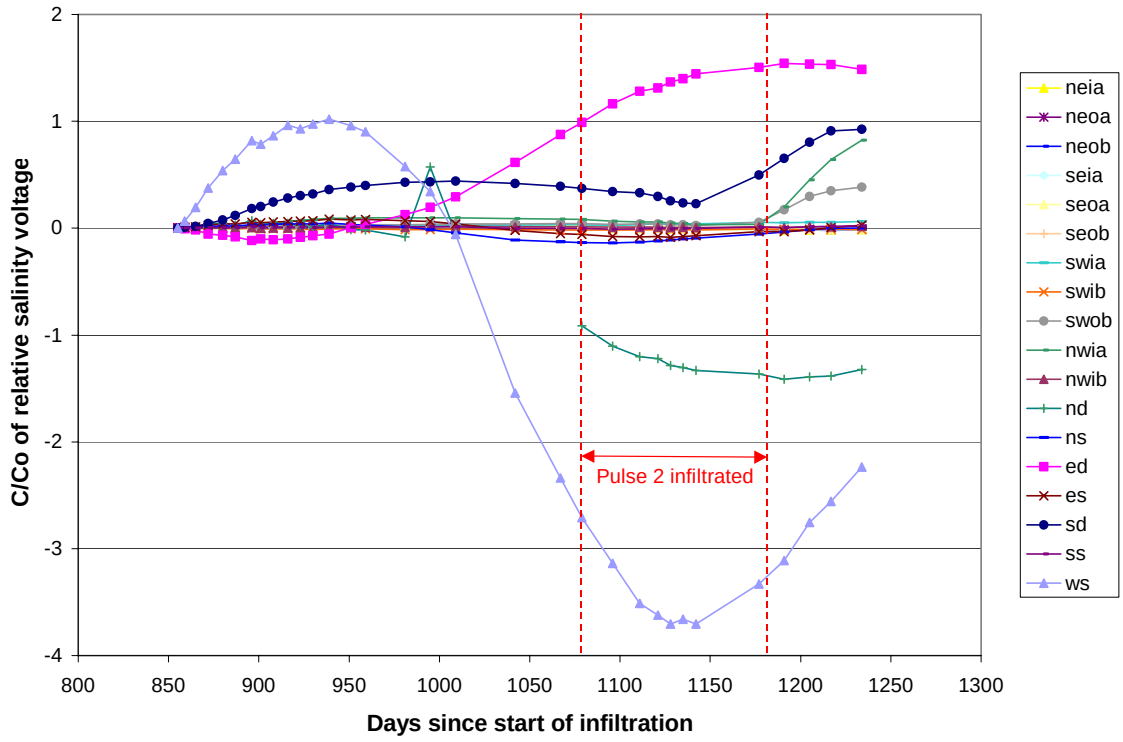


**Figure 6.5.1: Relative change in soil salinity for all the working probes.**

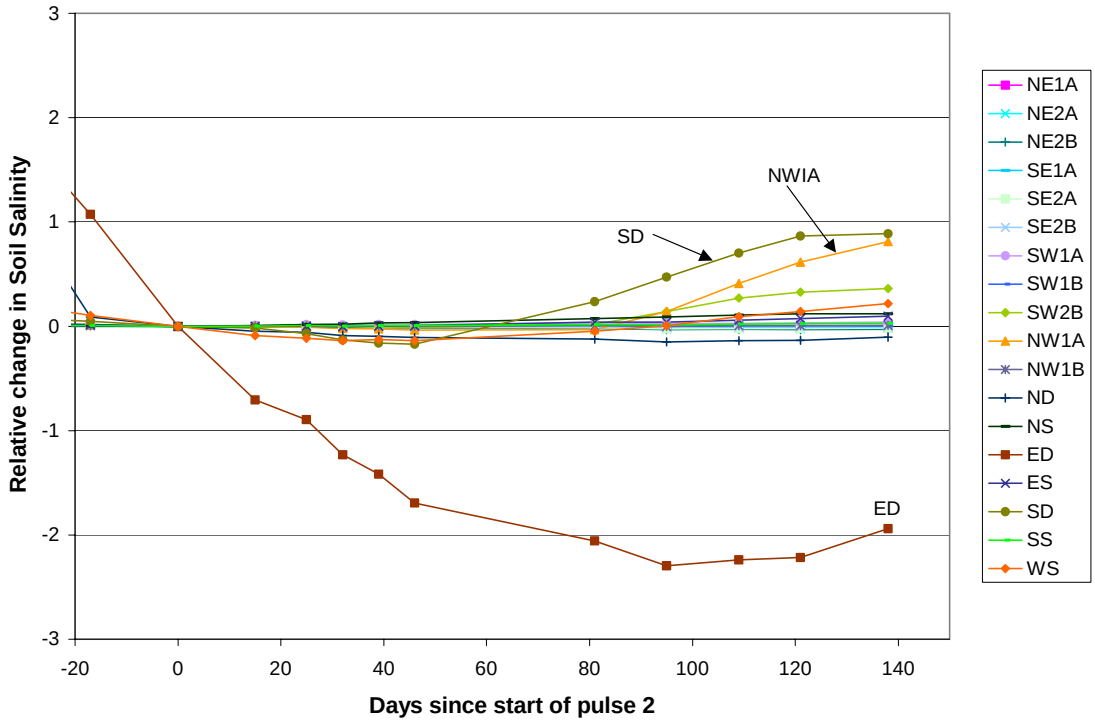


**Figure 6.5.2: Relative change in soil salinity after the infiltration of the second pulse.**

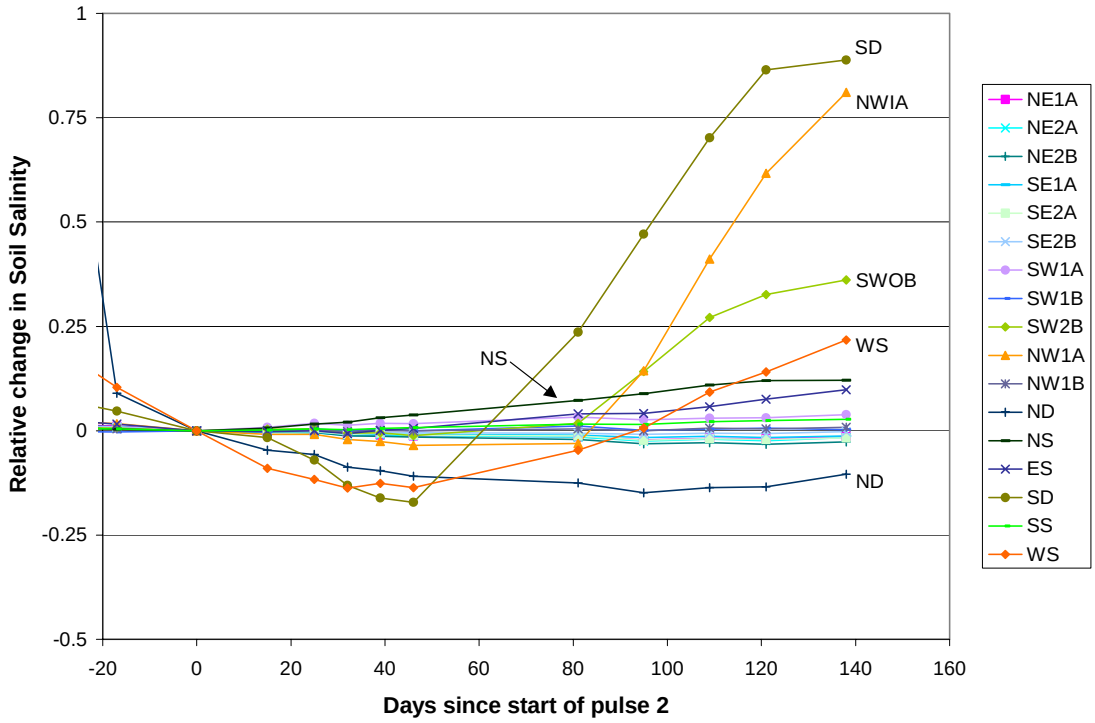


**Figure 6.5.3: Close up of data shown in Figure 7.5.2 with the ED data removed.**

Figures 6.5.5 through 6.5.6 show samples of unusual traces recorded from probes located at WD, SEIB, NWOA, and NWOB. The end of the probe tines was not detectable in these traces, which makes water content measurements impossible. These traces are most likely due to soils that are so dry the signal terminates as soon it enters the wave-guides. The very high resistivity of the soil could be due to air gaps around the wave-guides or very low water content. Another, less likely, explanation is that the probes were broken during installation and there is no longer good contact between the end of the cable and the wave-guides.

The limited response of the TDR probes agrees well with data from suction lysimeters nested at the same locations. Neutron probe data shows that most of the probes are installed outside of the zones of higher water content, so tracer detection would not be expected at most of the probes. The TDR data is presented in a series of graphs showing sample traces and water content measurements for each probe. The water content data is very consistent at each probe over the year sampling period. The average deviation in water content was only 0.003 over all data sets.

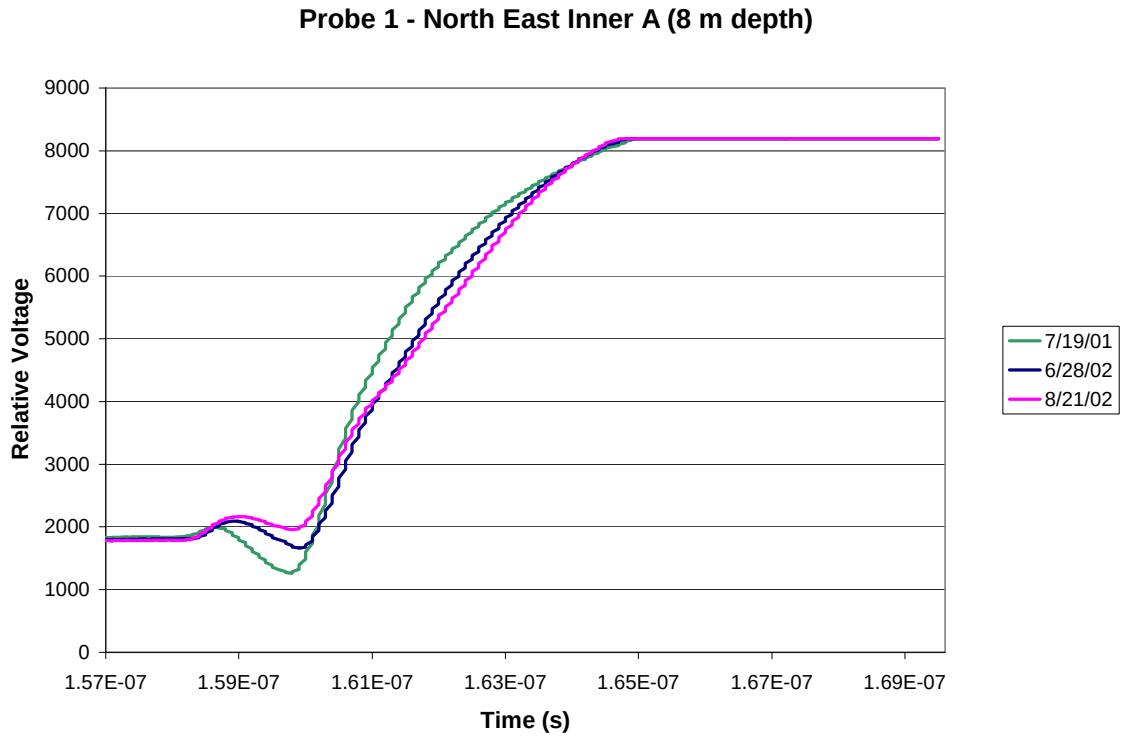


**Figure 6.5.4: North East Inner A, 8 m depth, sample traces.**

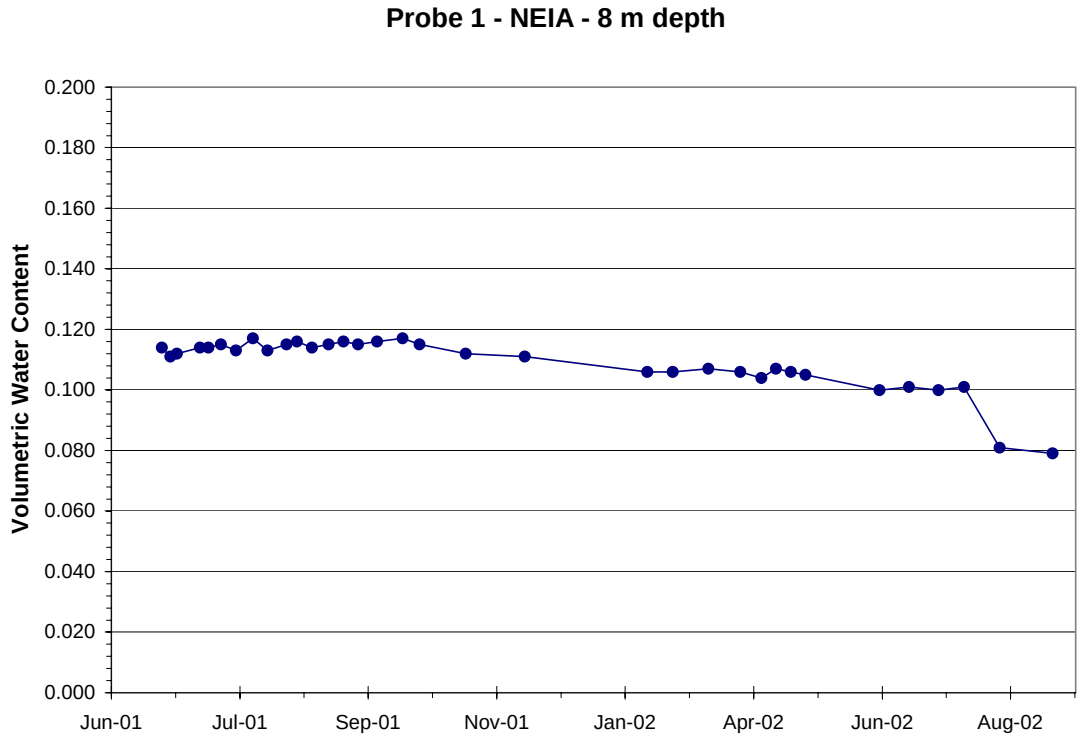


**Figure 6.5.5: North East Inner A, 8m depth – Change in water content with time**

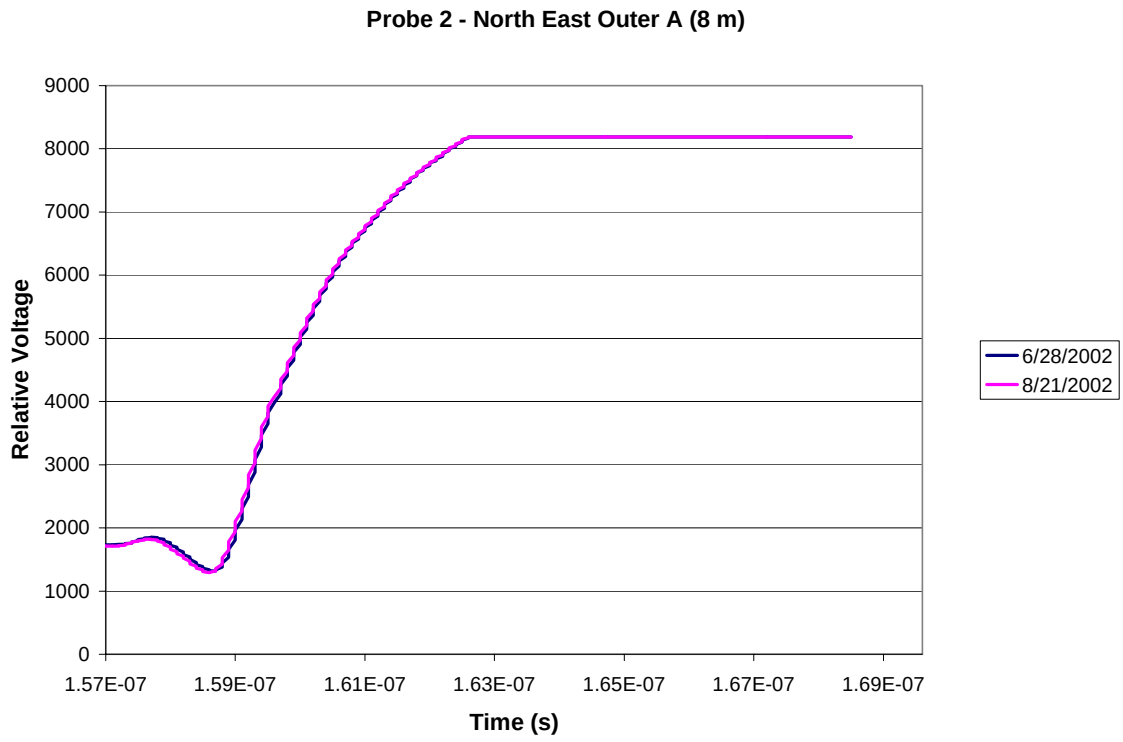


**Figure 6.5.6: North East Outer A, 8m depth, sample traces.**

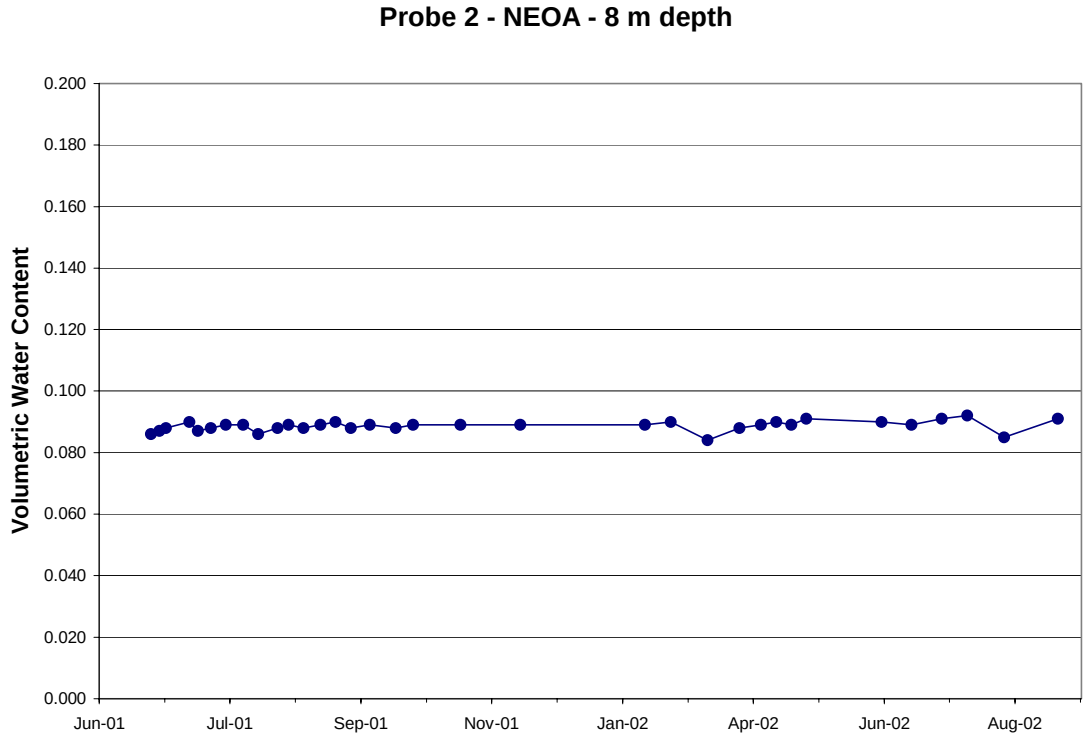


**Figure 6.5.7: North East Outer A, 8m depth, change in water content with time**

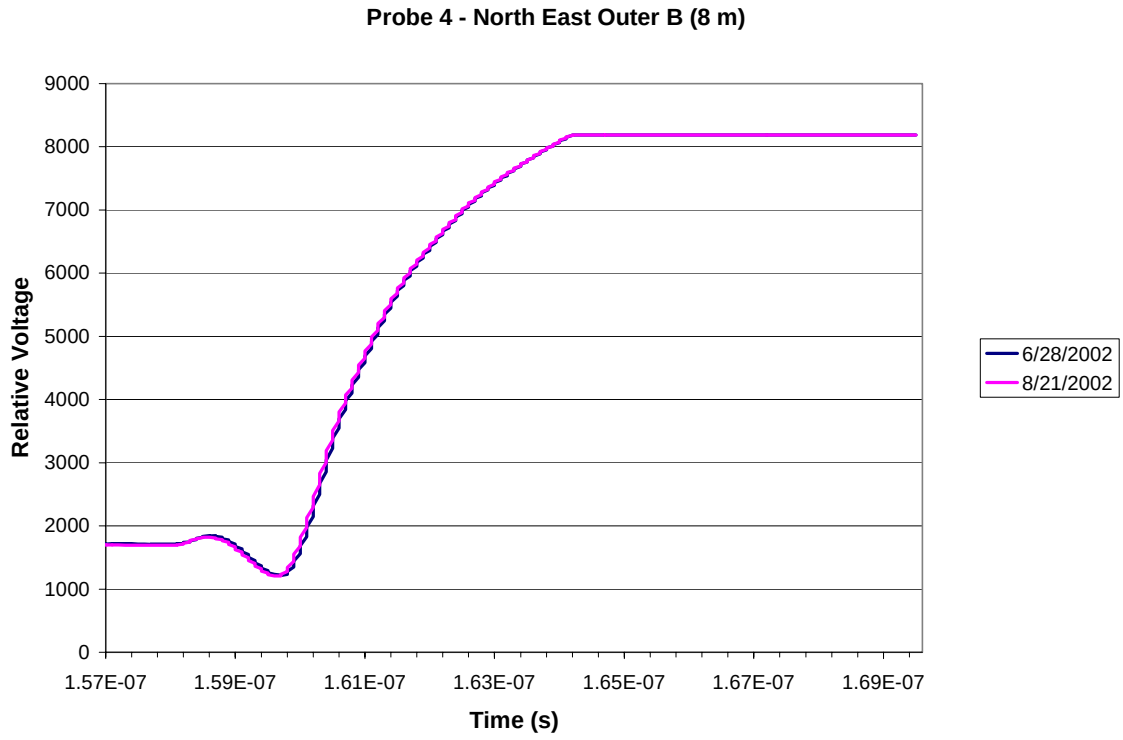


**Figure 6.5.8: North East Outer B, 8m depth, sample traces.**

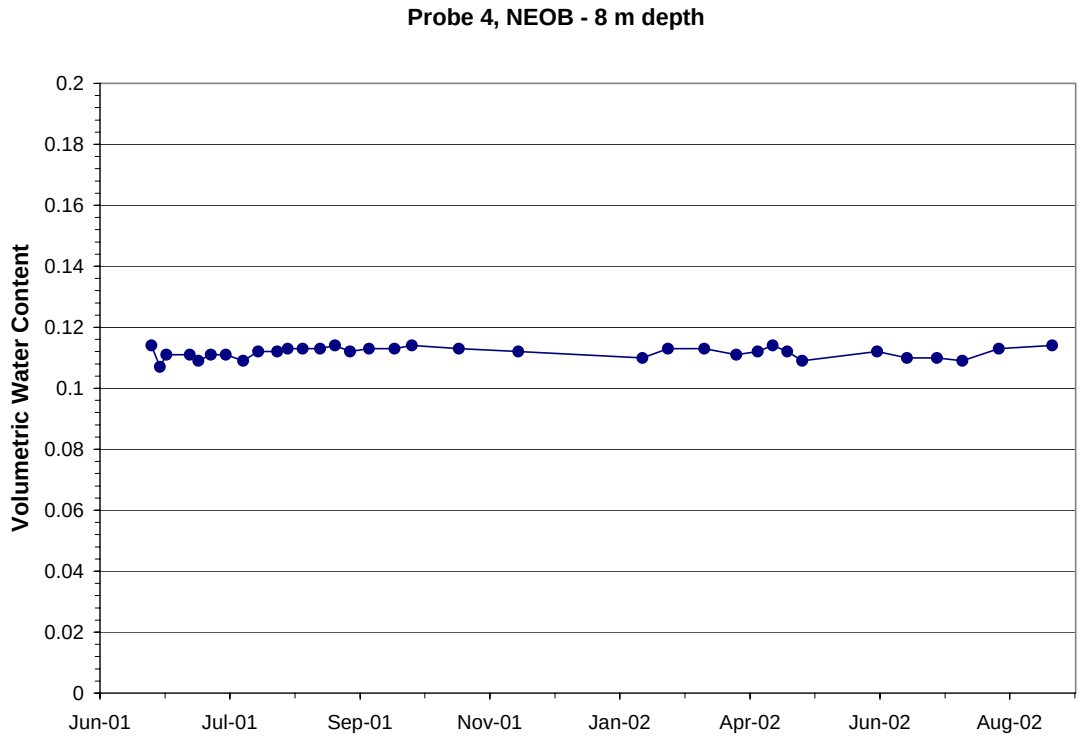


**Figure 6.5.9: North East Outer B, 8m depth, change in water content with time.**


**Figure 6.5.10: South East Inner A, 8m depth, sample traces reflected from probe.**

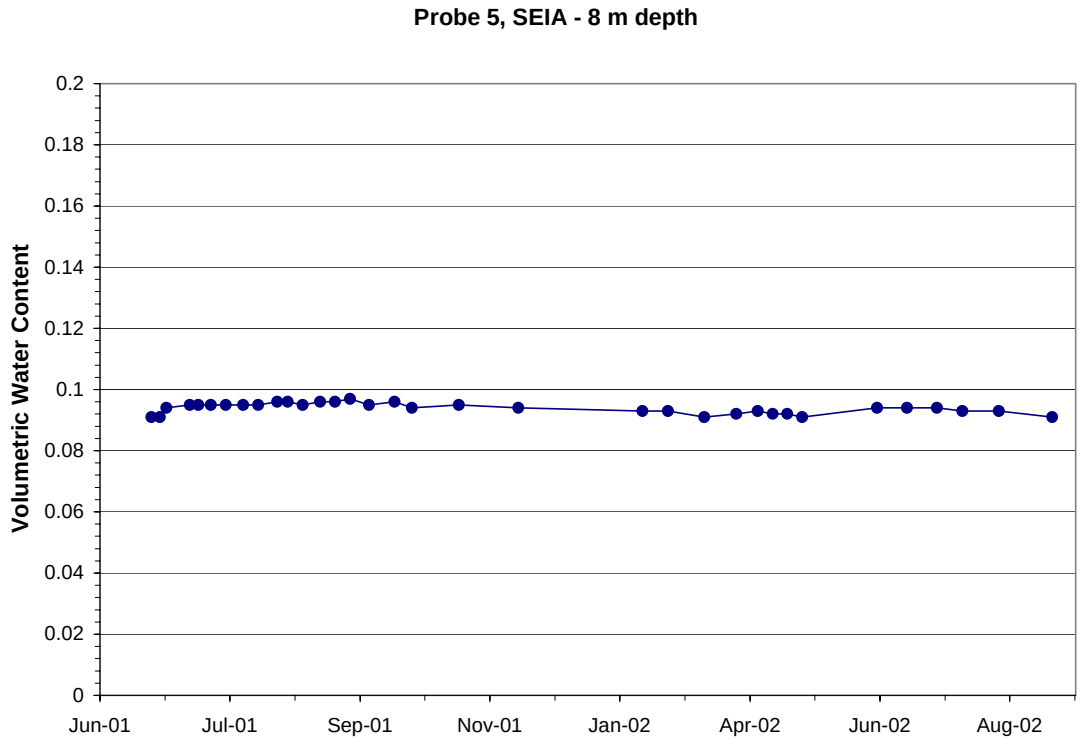


**Figure 6.5.11: South East Inner A, 8 m depth, volumetric water content with time.**

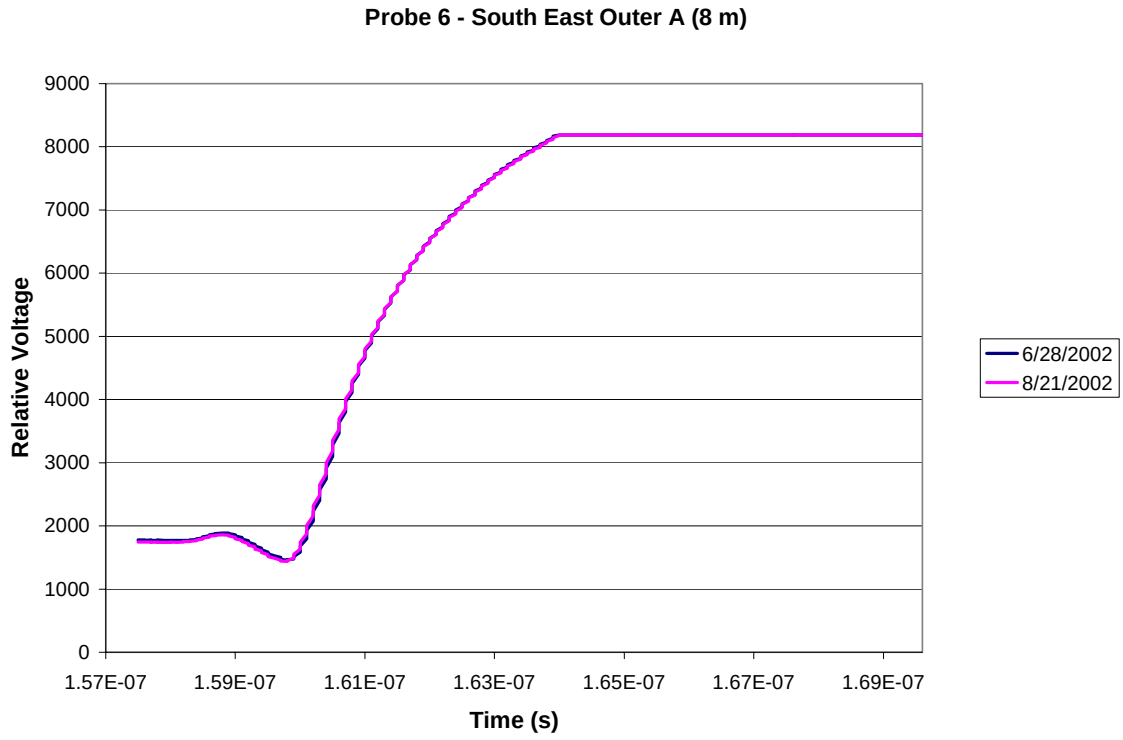


**Figure 6.5.12: South East Outer A, 8 m depth, sample traces reflected from probe.**

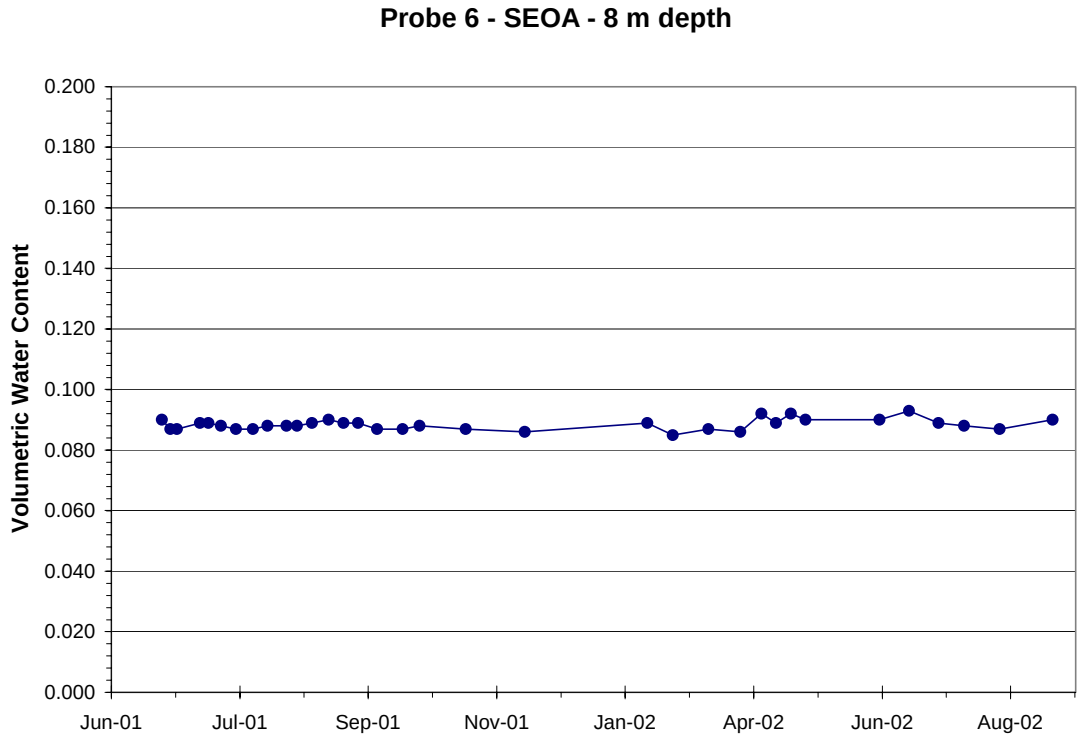


**Figure 6.5.13: South East Outer A, 8 m depth, volumetric water content with time.**

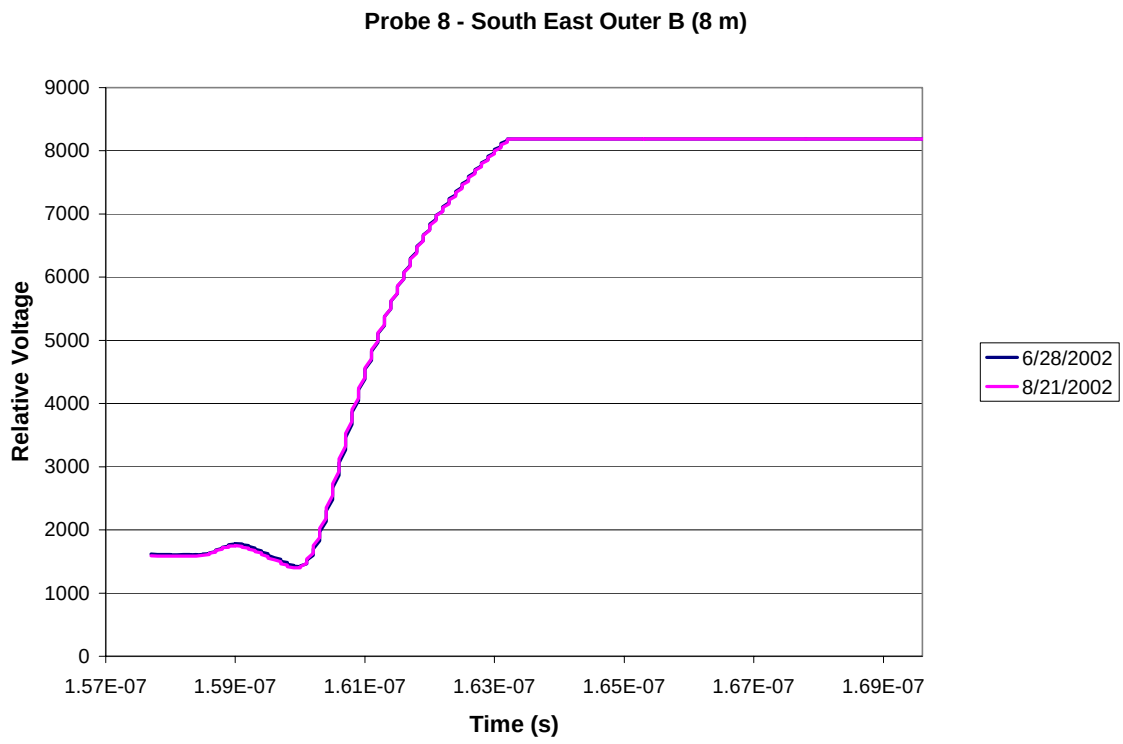


**Figure 6.5.14: South East Outer B, 8 m depth, sample traces reflected from probe.**

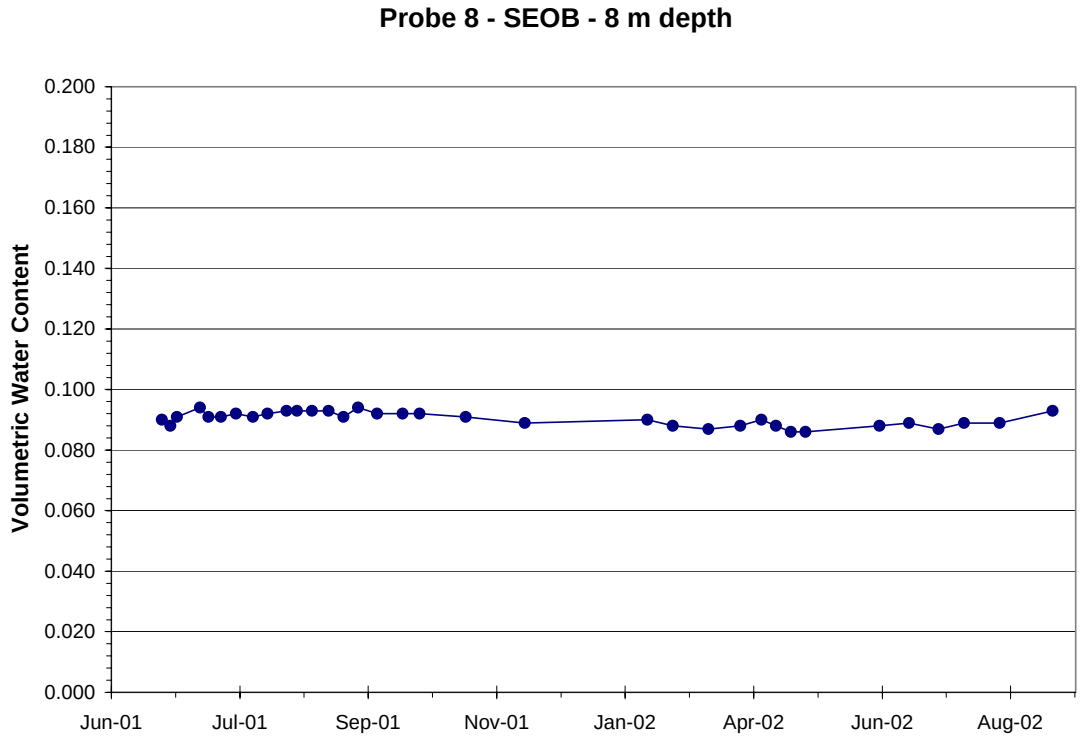


**Figure 6.5.15: South East Outer B, 8 m depth, volumetric water content with time.**

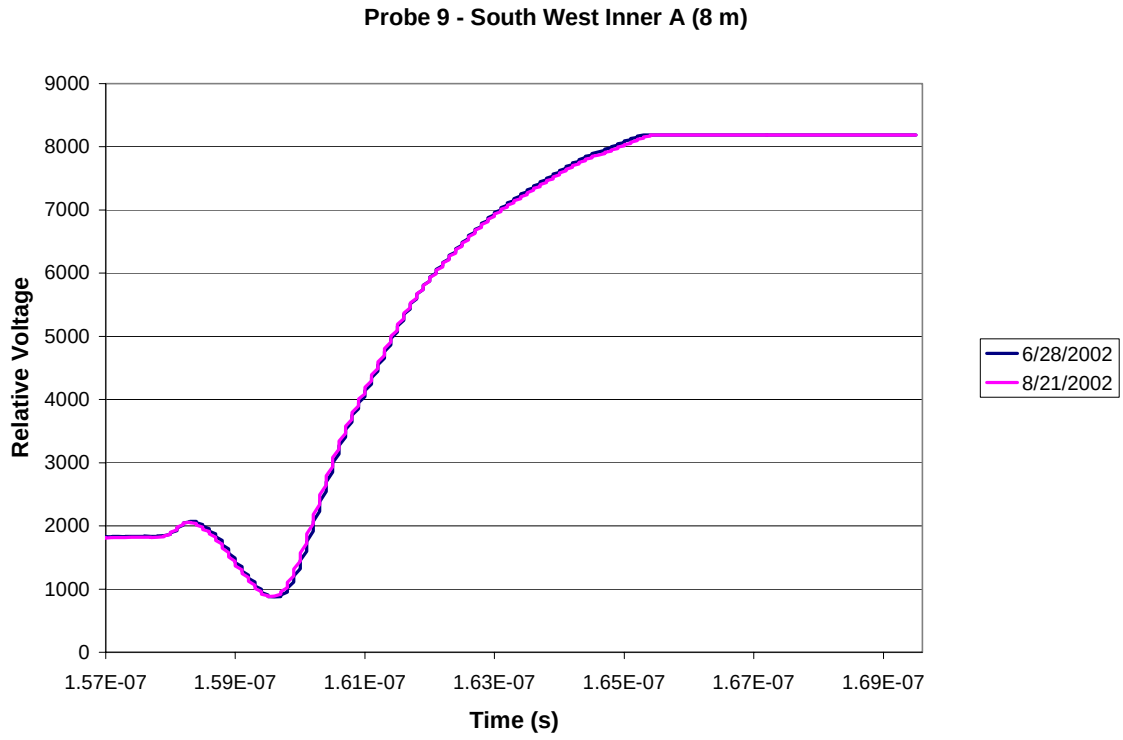


**Figure 6.5.18: South West Inner A, 8 m depth, sample traces reflected from probe.**

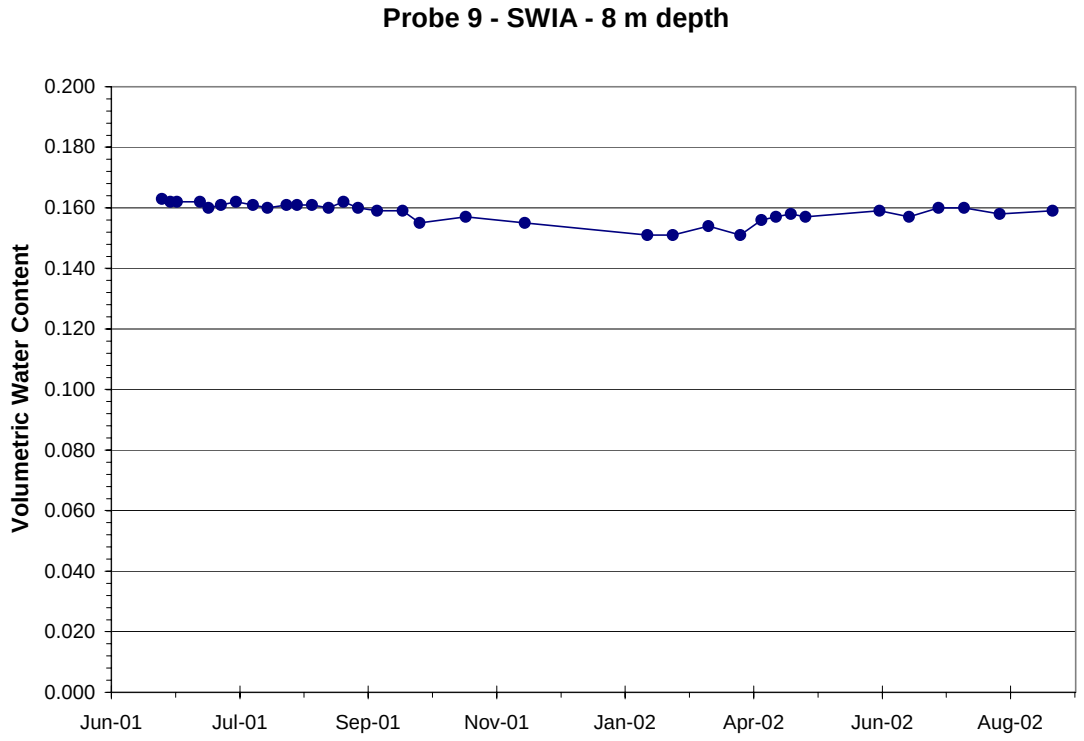


**Figure 6.5.19: South West Inner A, 8 m depth, volumetric water content with time.**

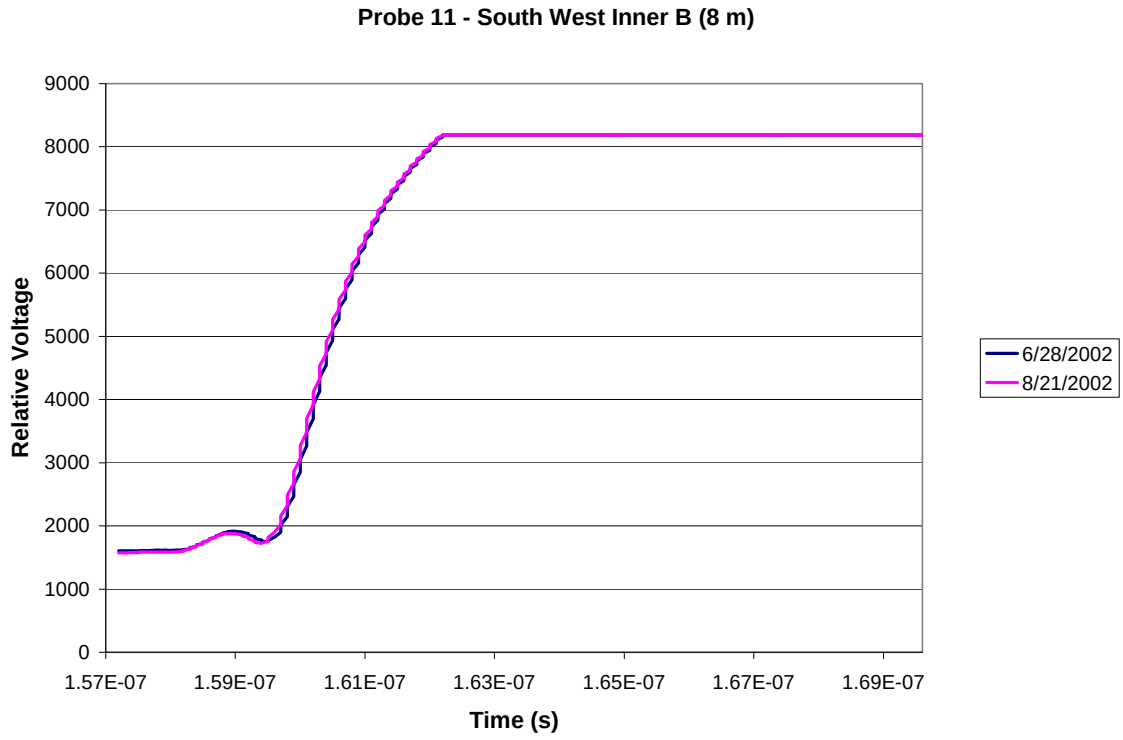


**Figure 6.5.20: South West Inner B, 8 m depth, sample traces reflected from probe.**

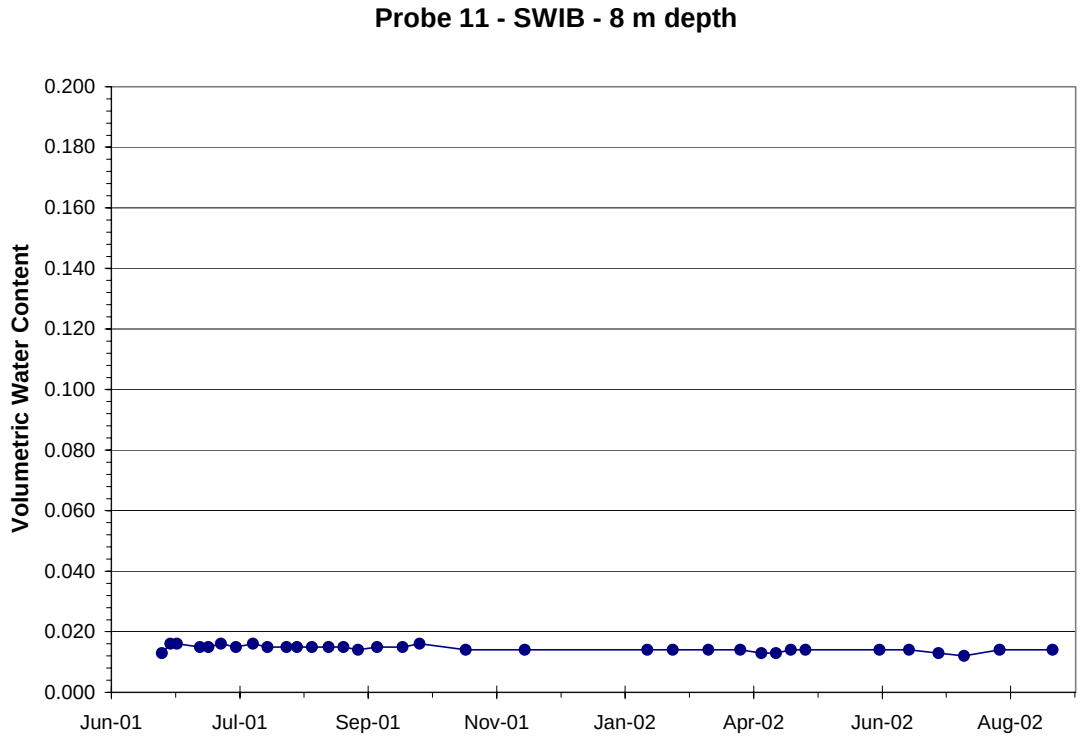


**Figure 6.5.21: South West Inner B, 8 m depth, volumetric water content with time.**

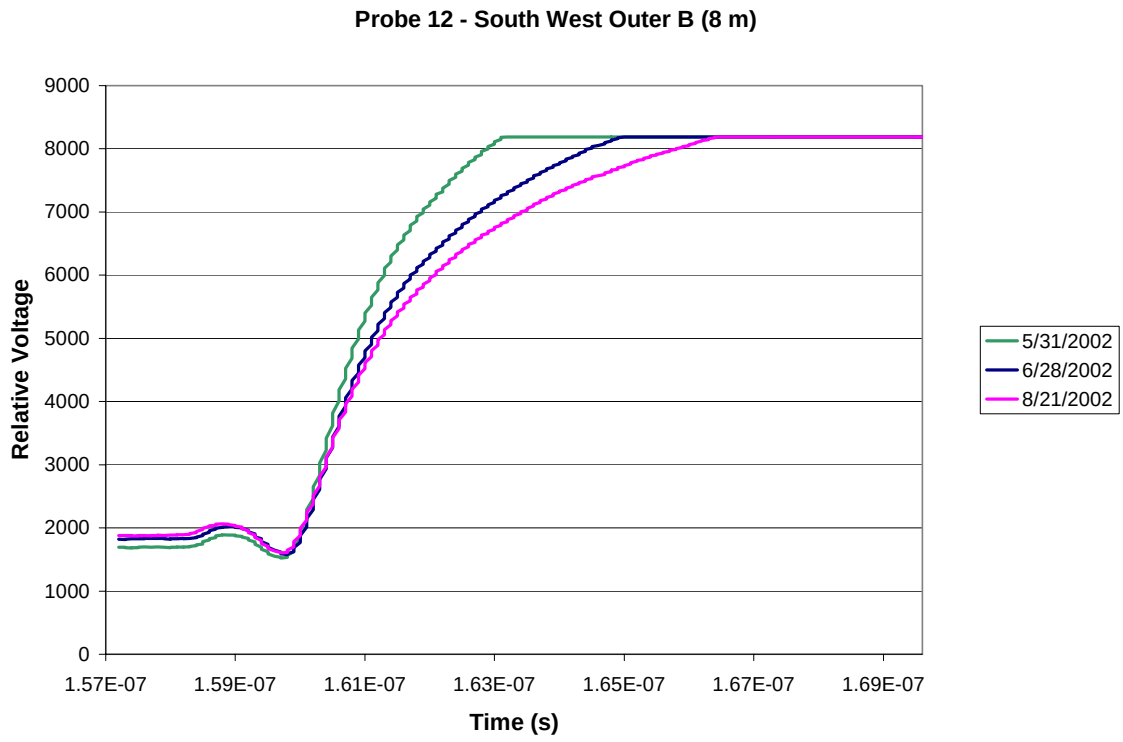


**Figure 6.5.22: South West Outer B, 8 m depth, sample traces reflected from probe.**

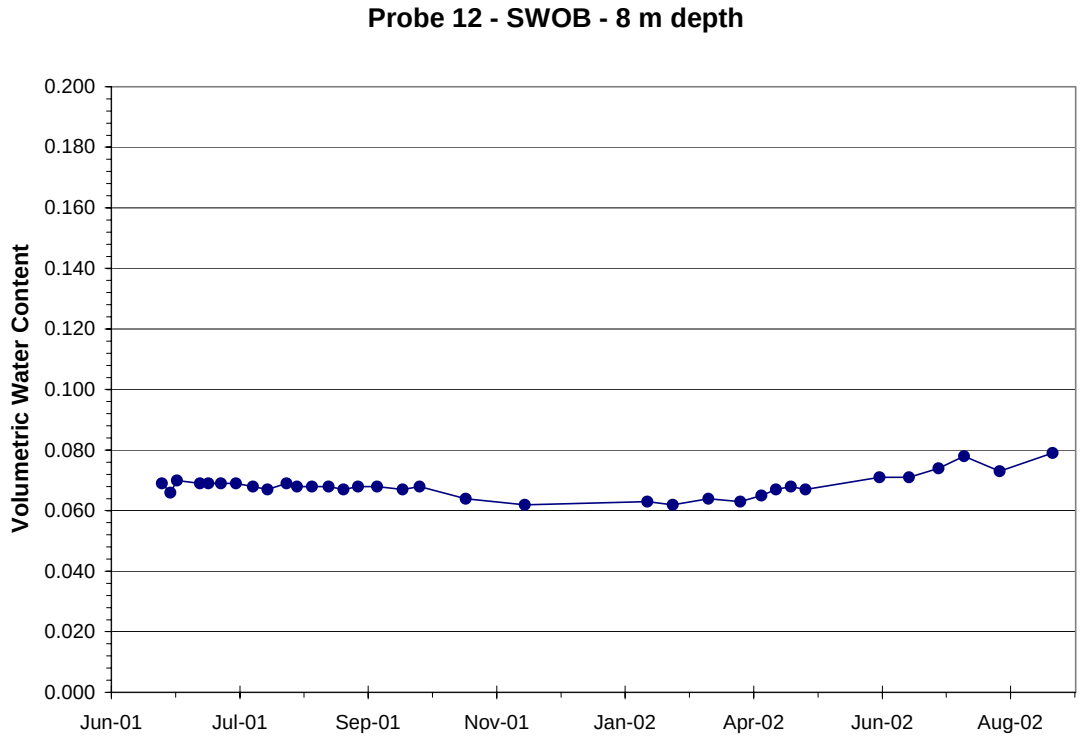


**Figure 6.5.23: South West Outer B, 8 m depth, volumetric water content with time.**

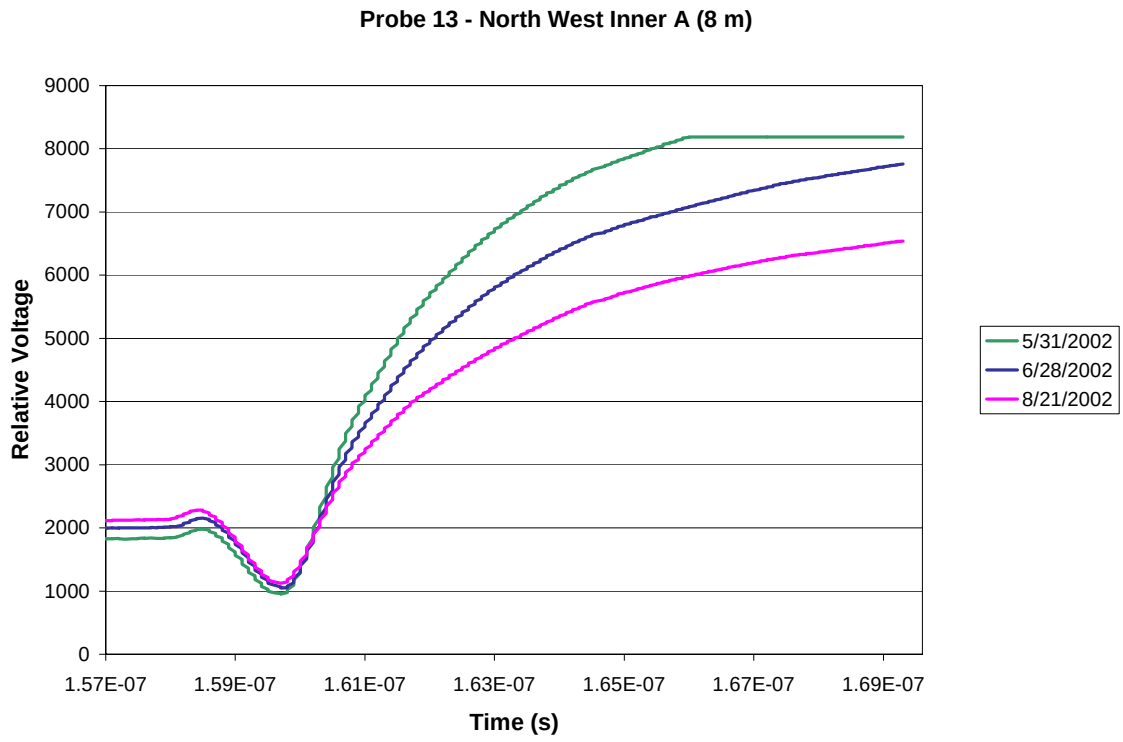


**Figure 6.5.24: North West Inner A, 8 m depth, sample traces reflected from probe.**

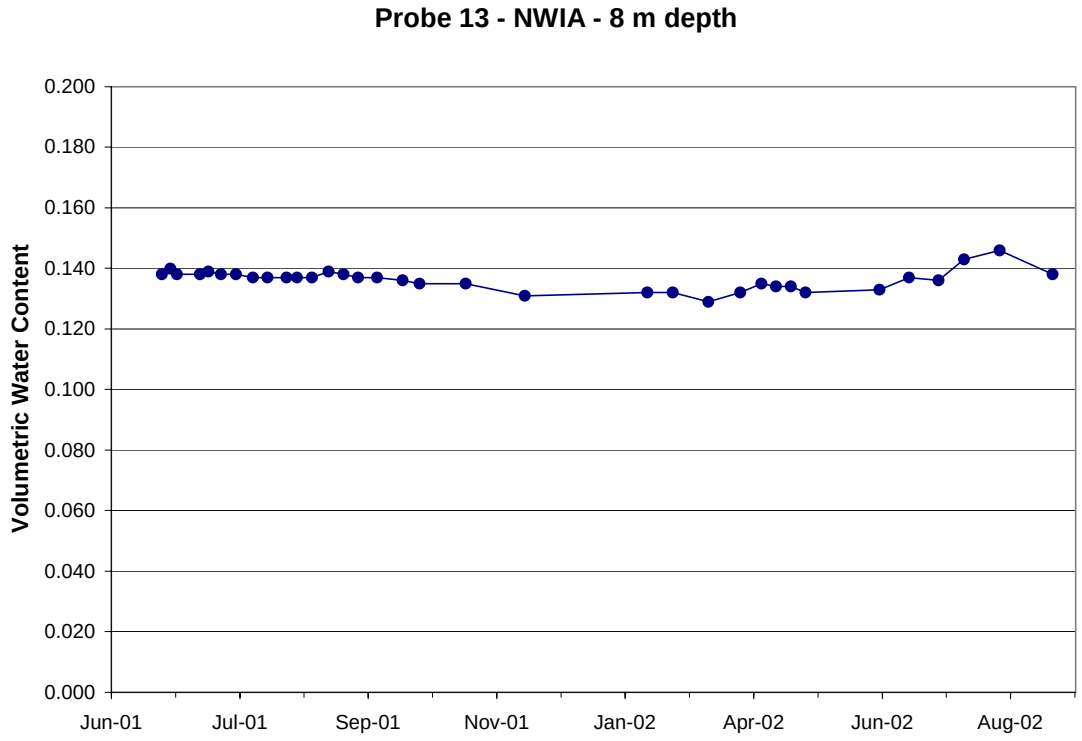


**Figure 6.5.25: North West Inner A, 8 m depth, volumetric water content with time.**

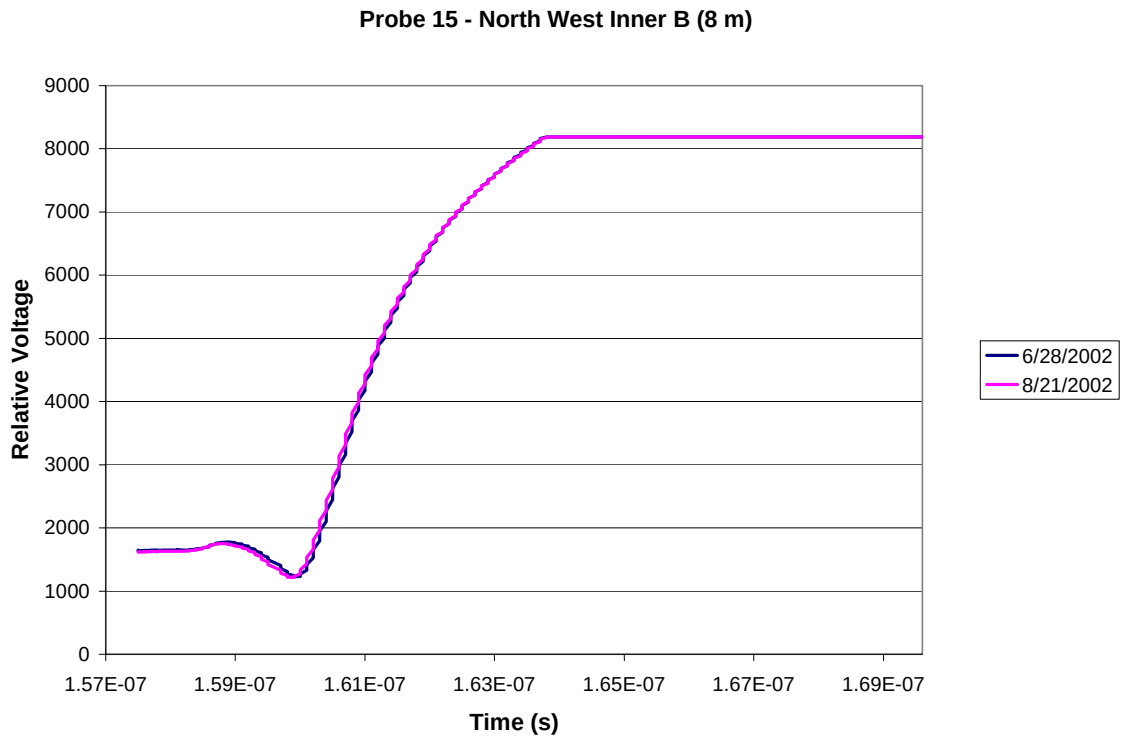


**Figure 6.5.26: North West Inner B, 8 m depth, sample traces reflected from probe.**

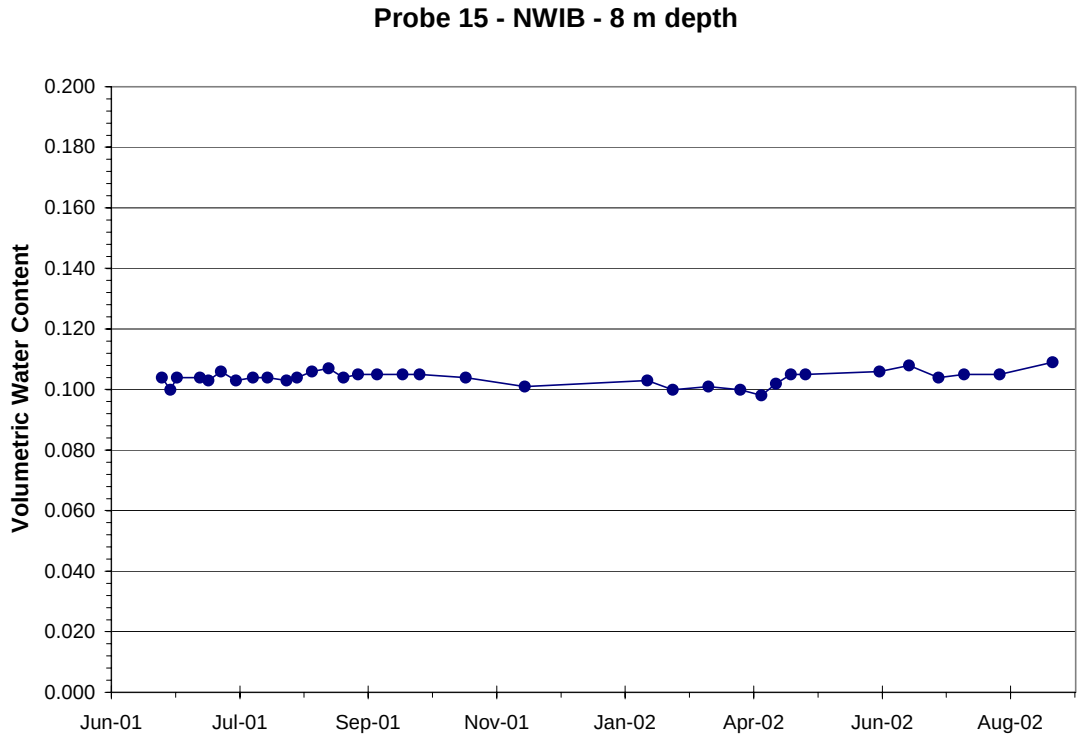


**Figure 6.5.27: North West Inner B, 8 m depth, volumetric water content with time.**

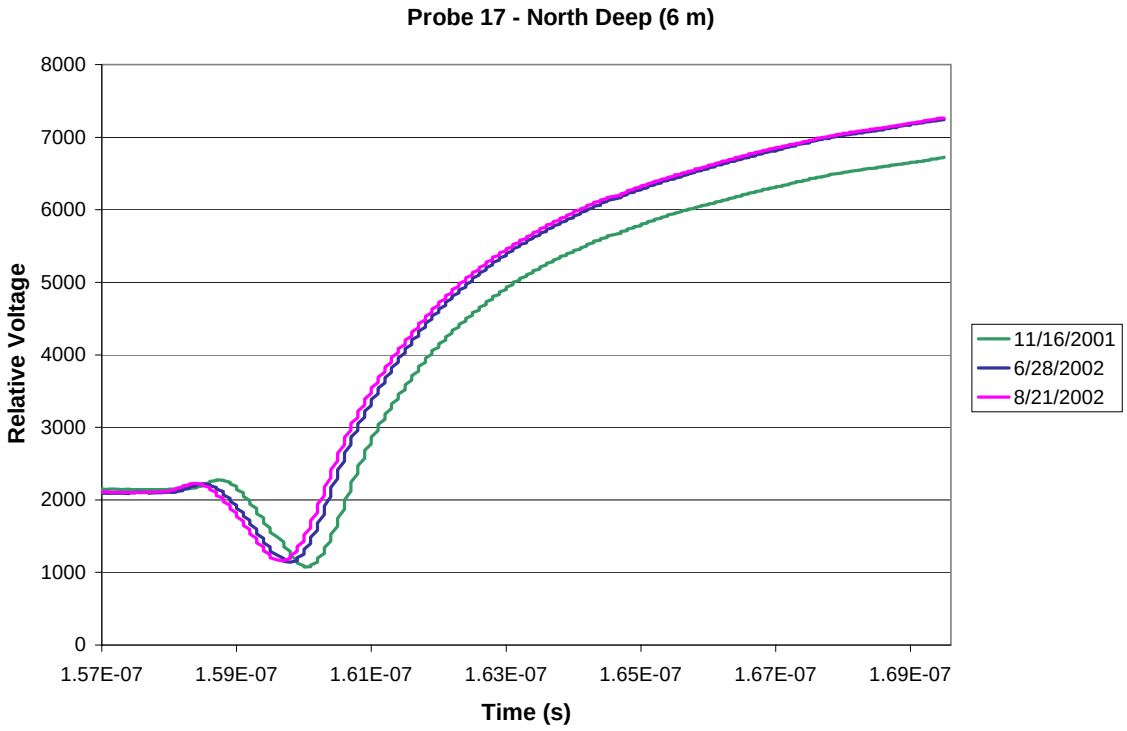


**Figure 6.5.28: North Deep, 6 m depth, sample traces reflected from probe.**

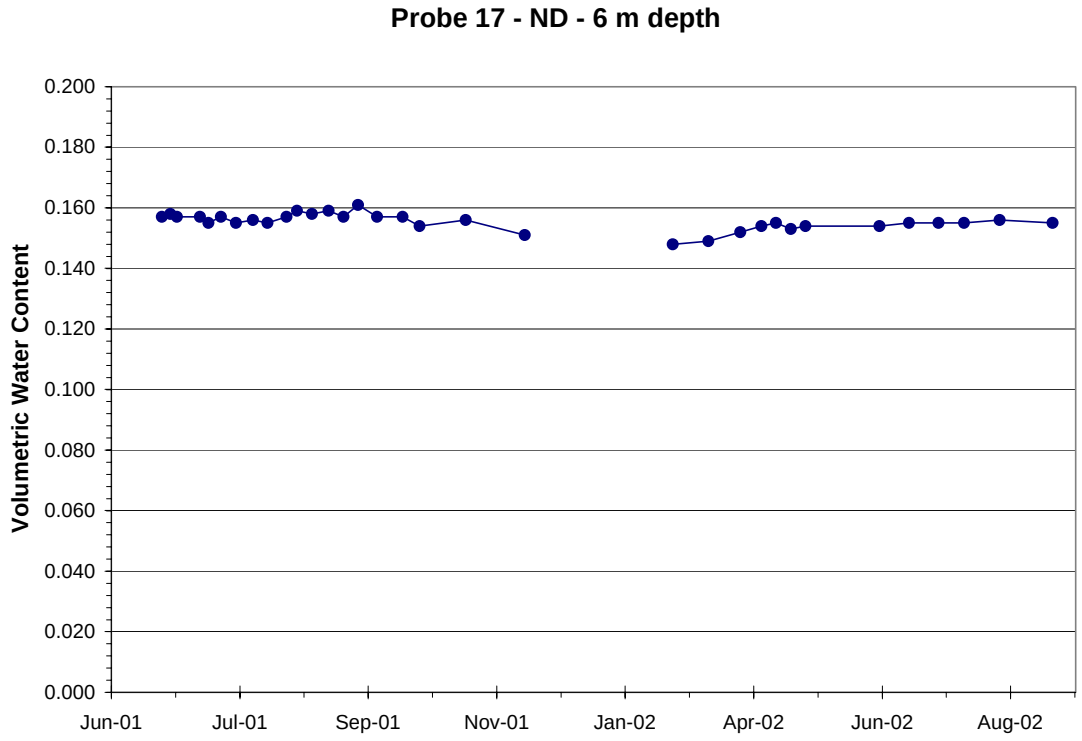


**Figure 6.5.29: North Deep, 6 m depth, volumetric water content with time.**

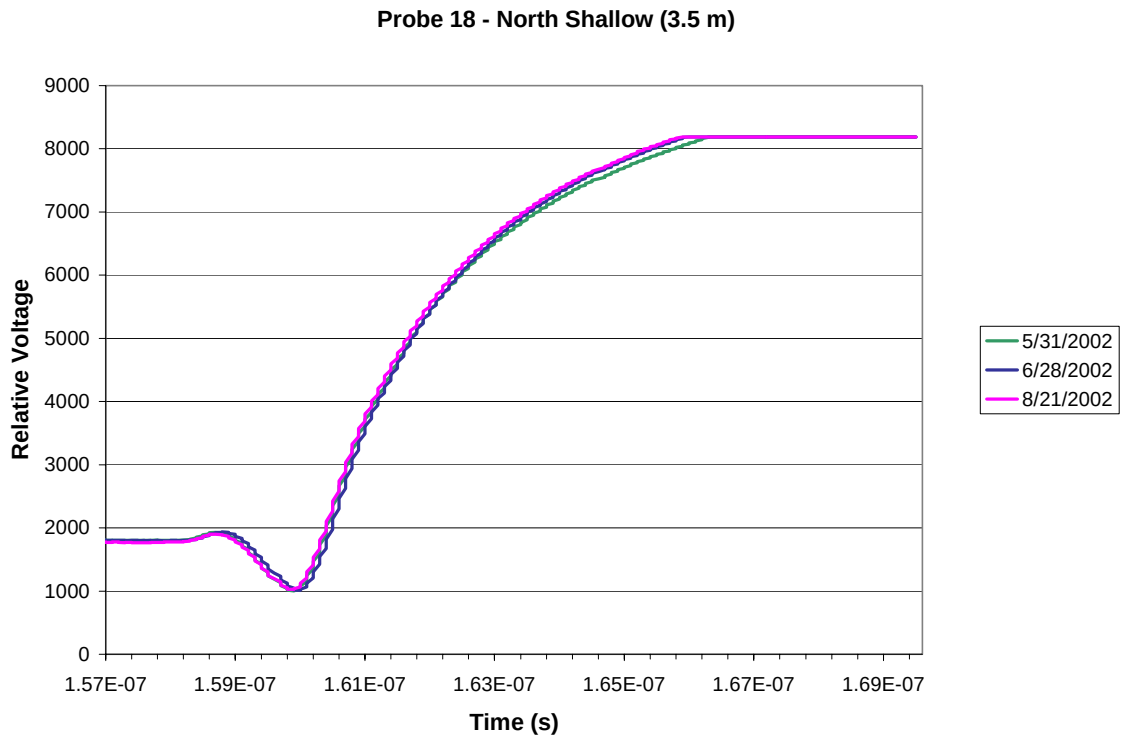


**Figure 6.5.30: North Shallow, 3.5 m depth, sample traces reflected from probe.**

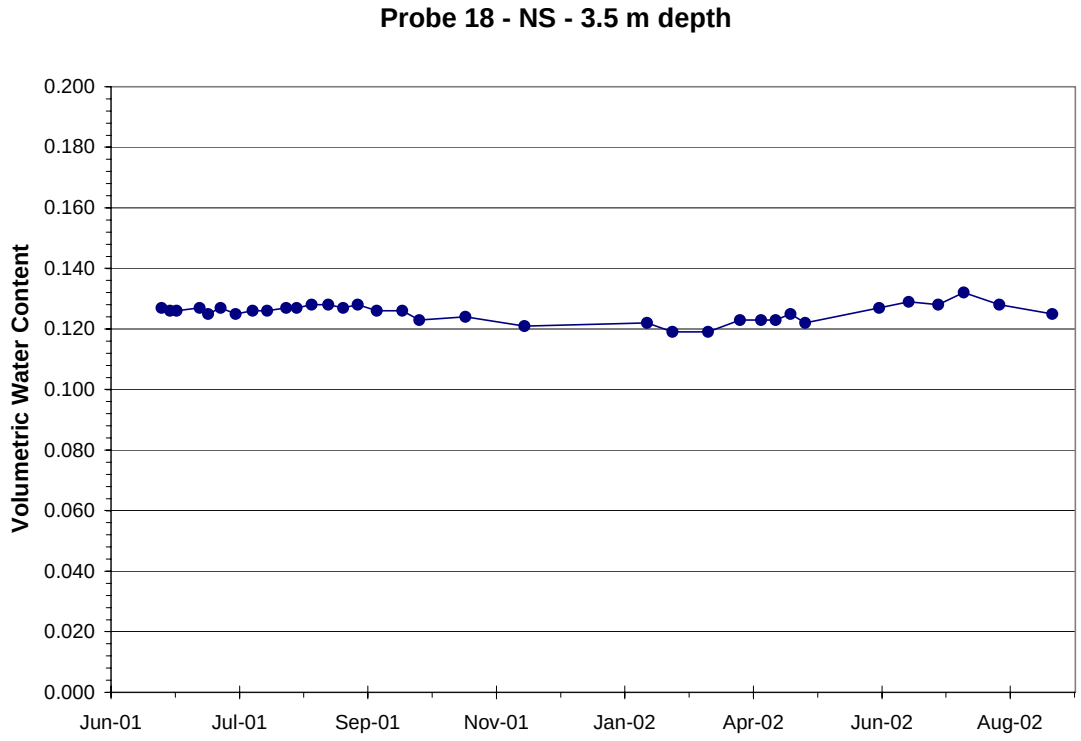


**Figure 6.5.31: North Shallow, 3.5 m depth, volumetric water content with time.**

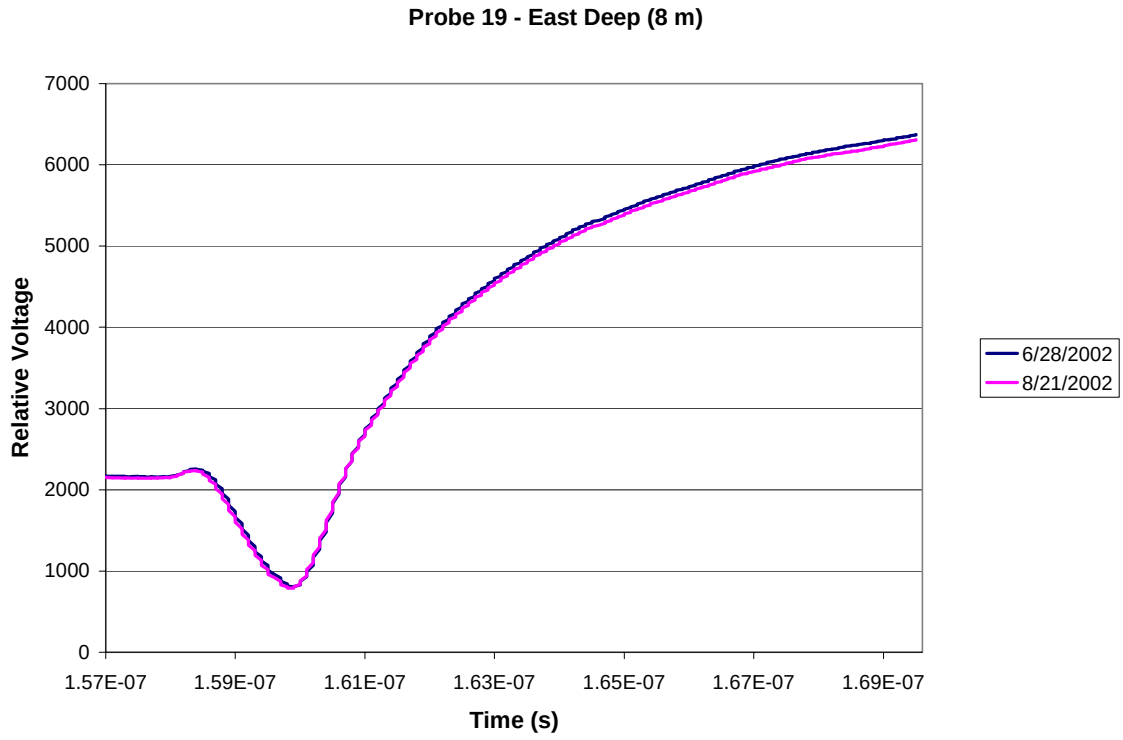


**Figure 6.5.32: East Deep, 6 m depth, sample traces reflected from probe.**

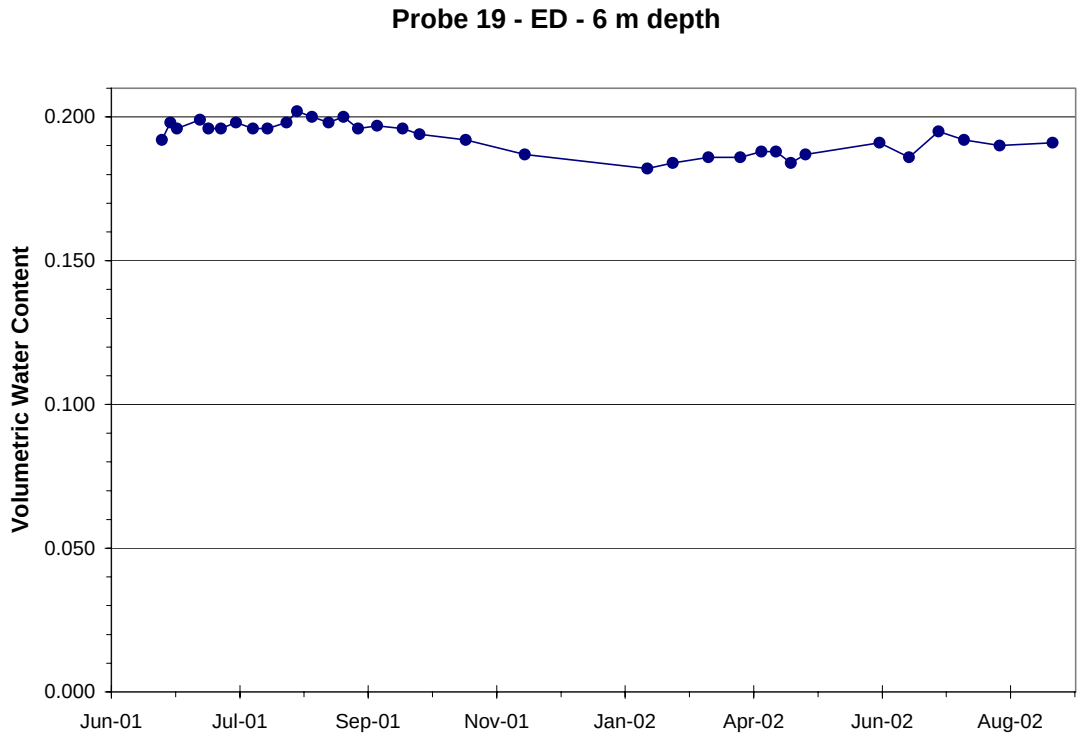


**Figure 6.5.33: East Deep, 6m depth, volumetric water content with time.**

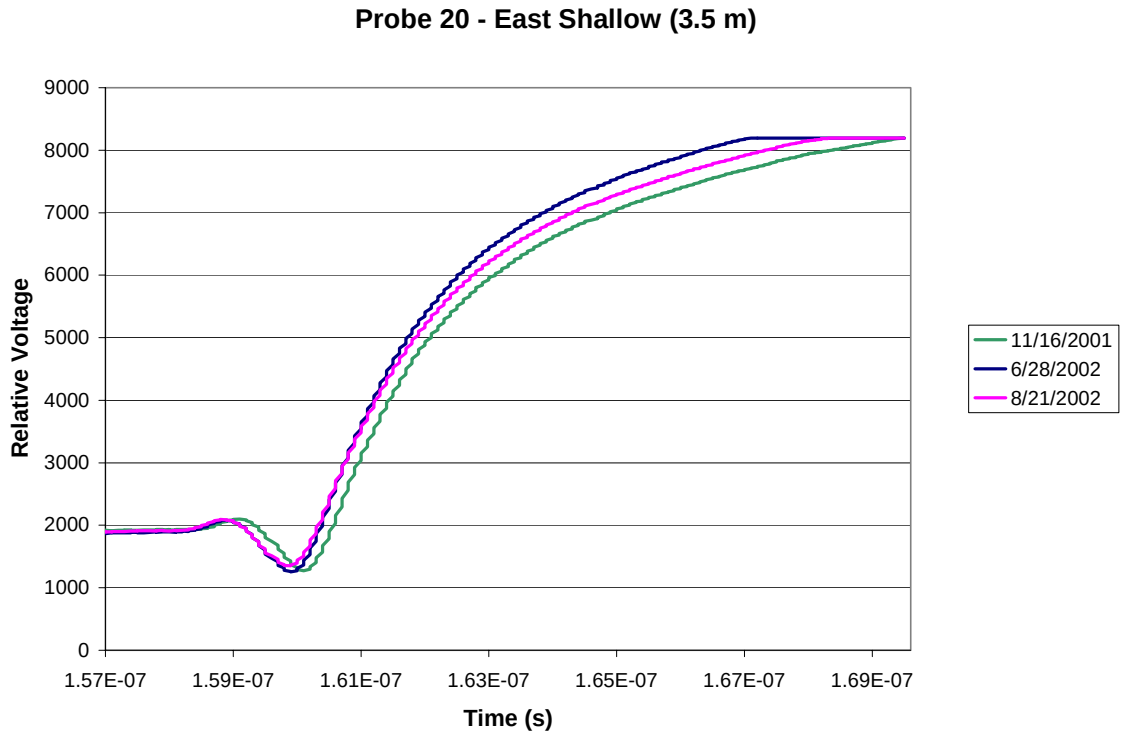


**Figure 6.5.34: East Shallow, 3.5m depth, sample traces reflected from probe.**

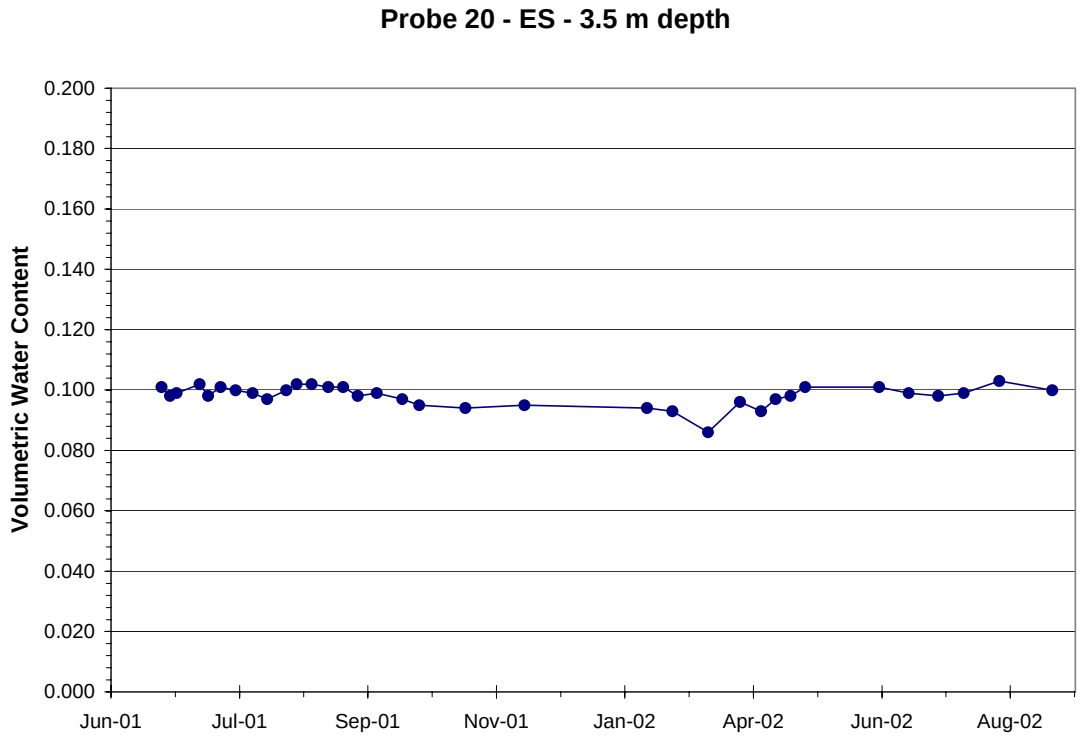


**Figure 6.5.35: East Shallow, 3.5m depth, volumetric water content with time.**

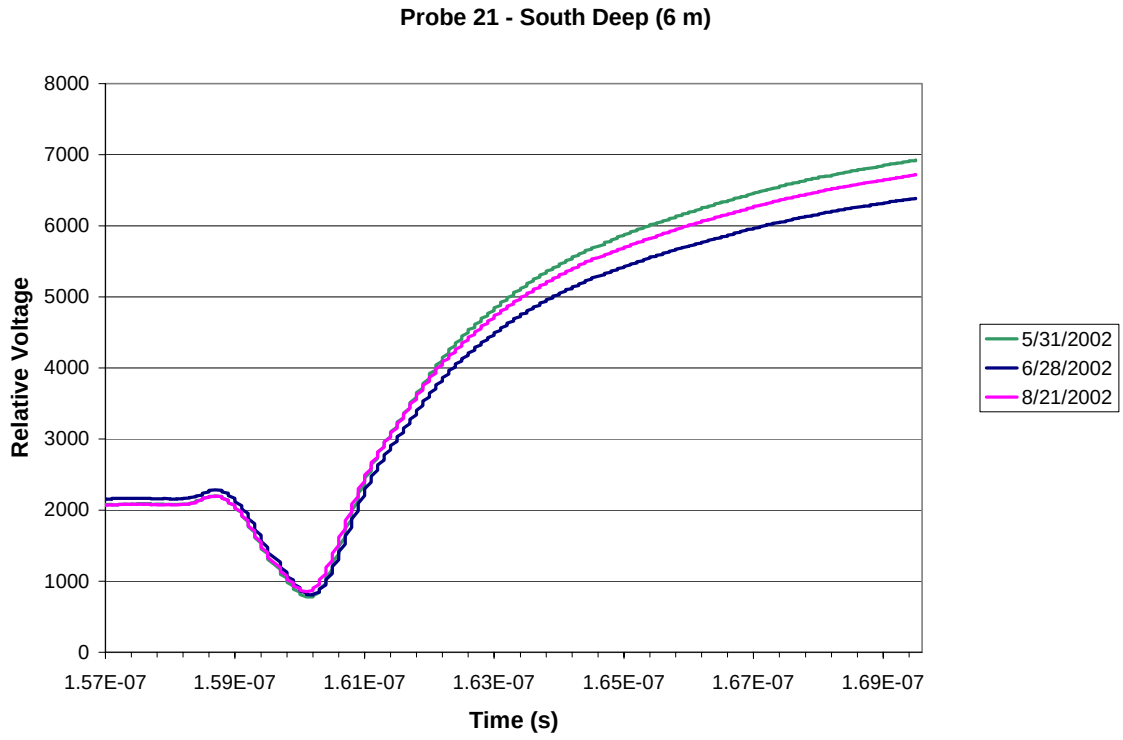


**Figure 6.5.36: South Deep, 6m depth, sample traces reflected from probe.**

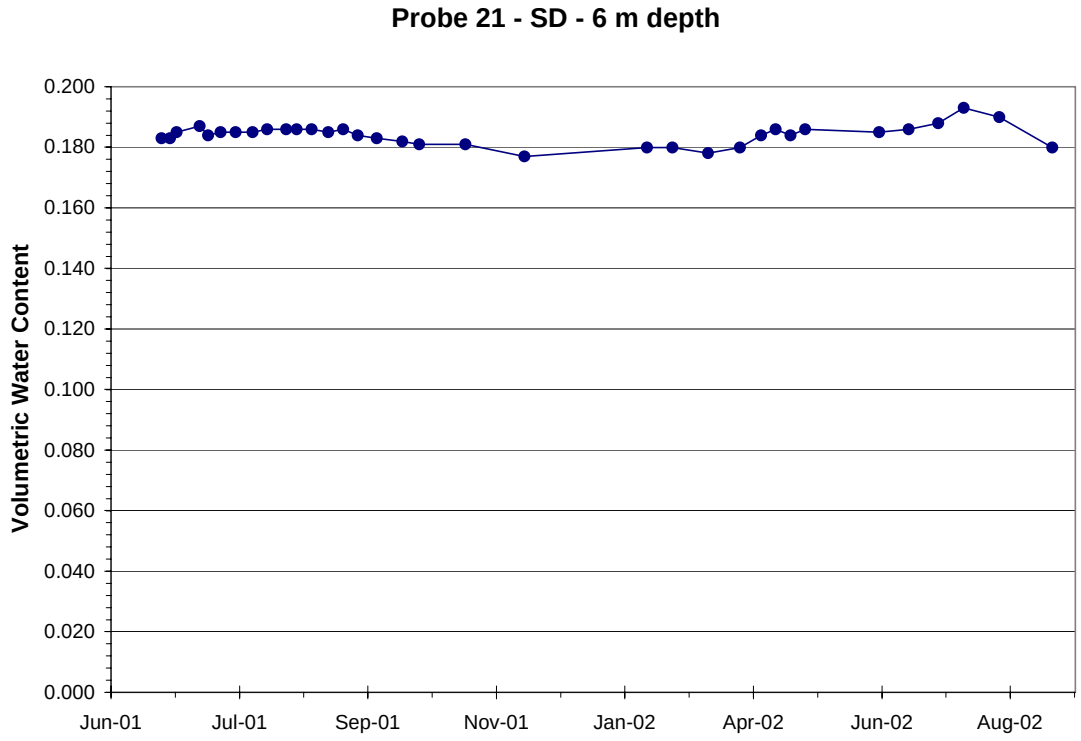


**Figure 6.5.37: South Deep, 6m depth, volumetric water content with time.**

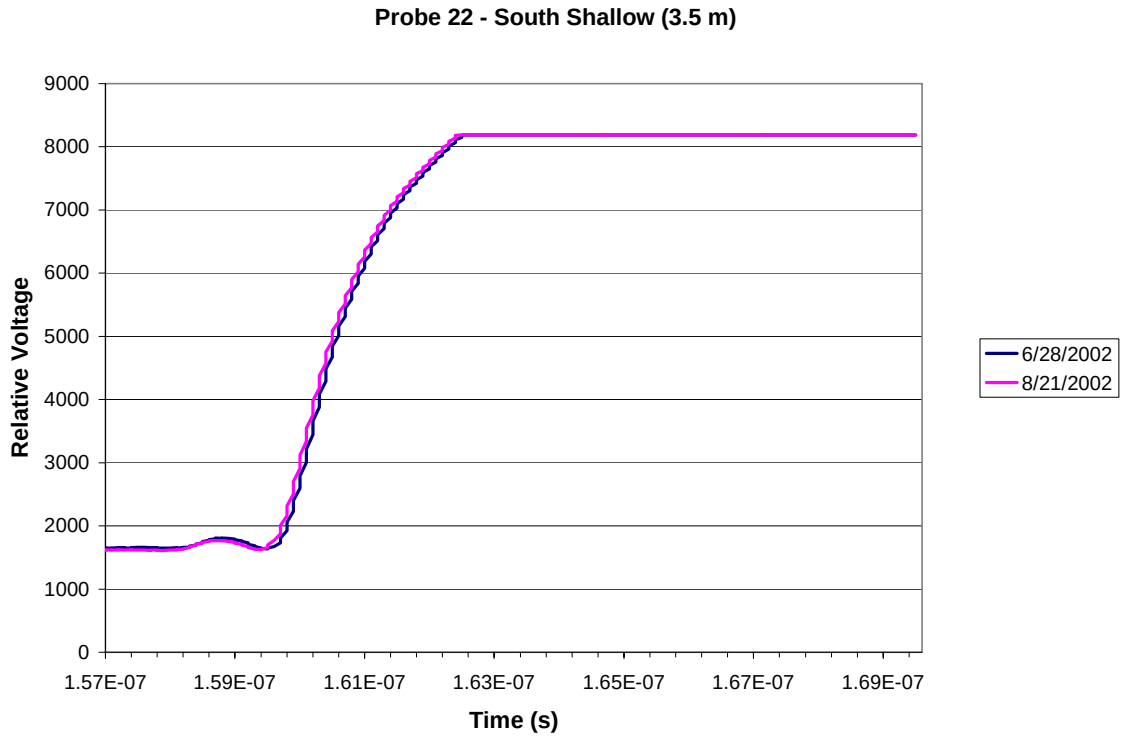


**Figure 6.5.38: South Shallow, 3.5m depth, sample traces reflected from probe.**

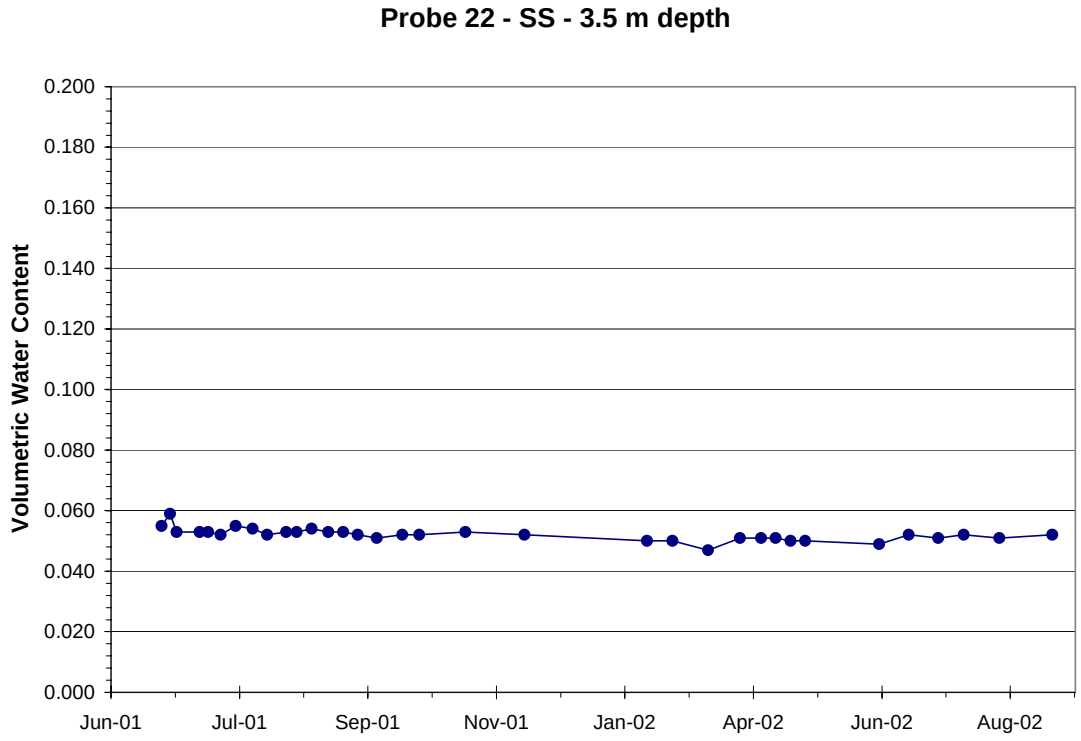


**Figure 6.5.39: South Shallow, 3.5m depth, volumetric water content with time.**

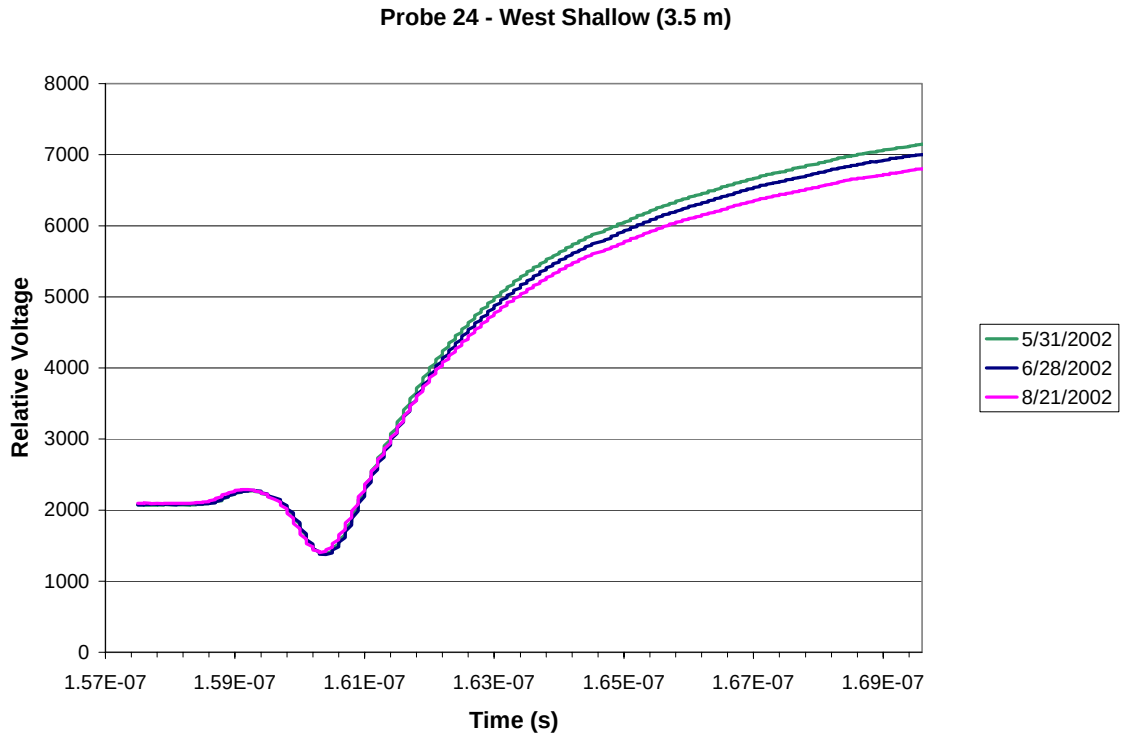


**Figure 6.5.40: West Shallow, 3.5m depth, sample traces reflected from probe.**

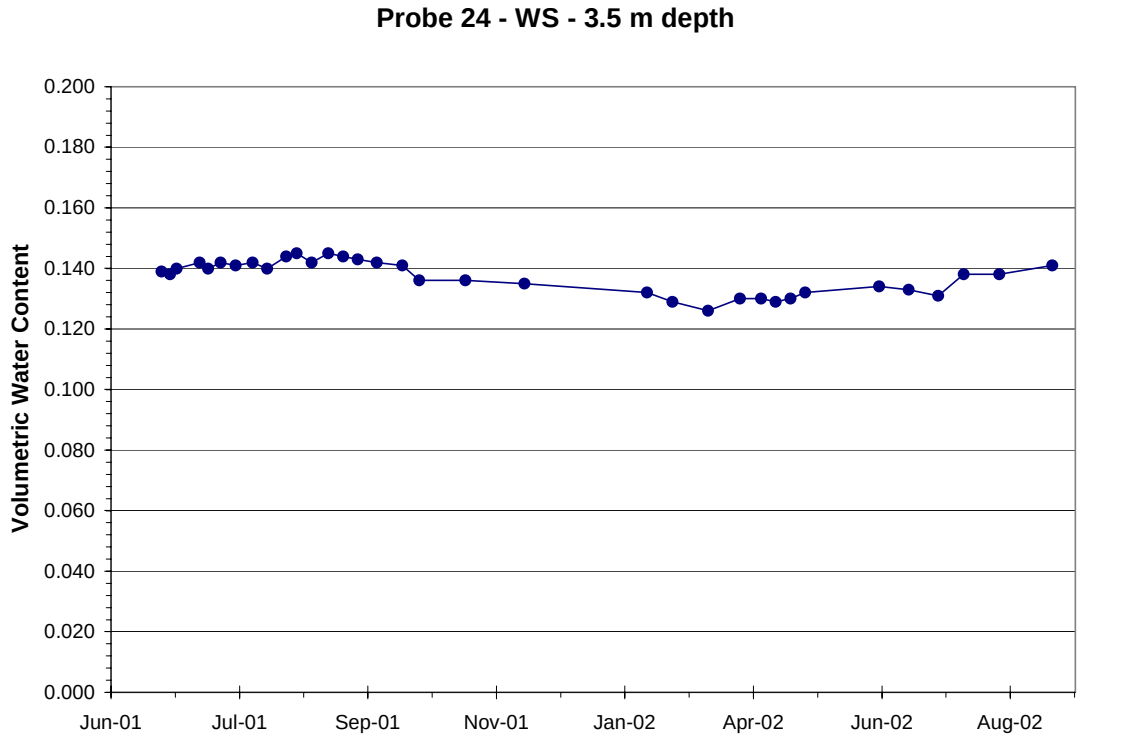


**Figure 6.5.41: West Shallow, 3.5m depth, volumetric water content with time.**

The following four figures are representative traces from the probes which were not able to measure soil water content. The start or end of the probe tines are not recognizable in these traces, and as such, travel time calculations could not be preformed. The sharp increase in relative voltage is most likely due to a very dry and very resistive soil surrounding the probe, which essentially shorts out the signal.

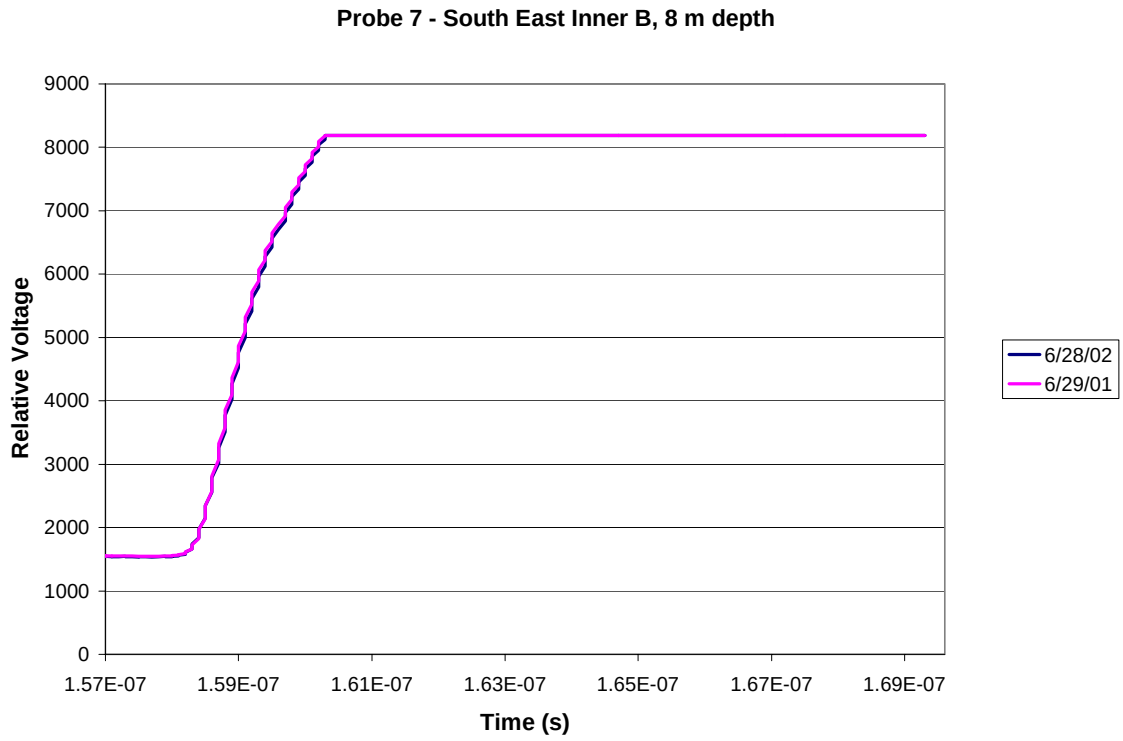


**Figure 6.5.42: South East Inner B, 8m depth, sample traces reflected from probe.**

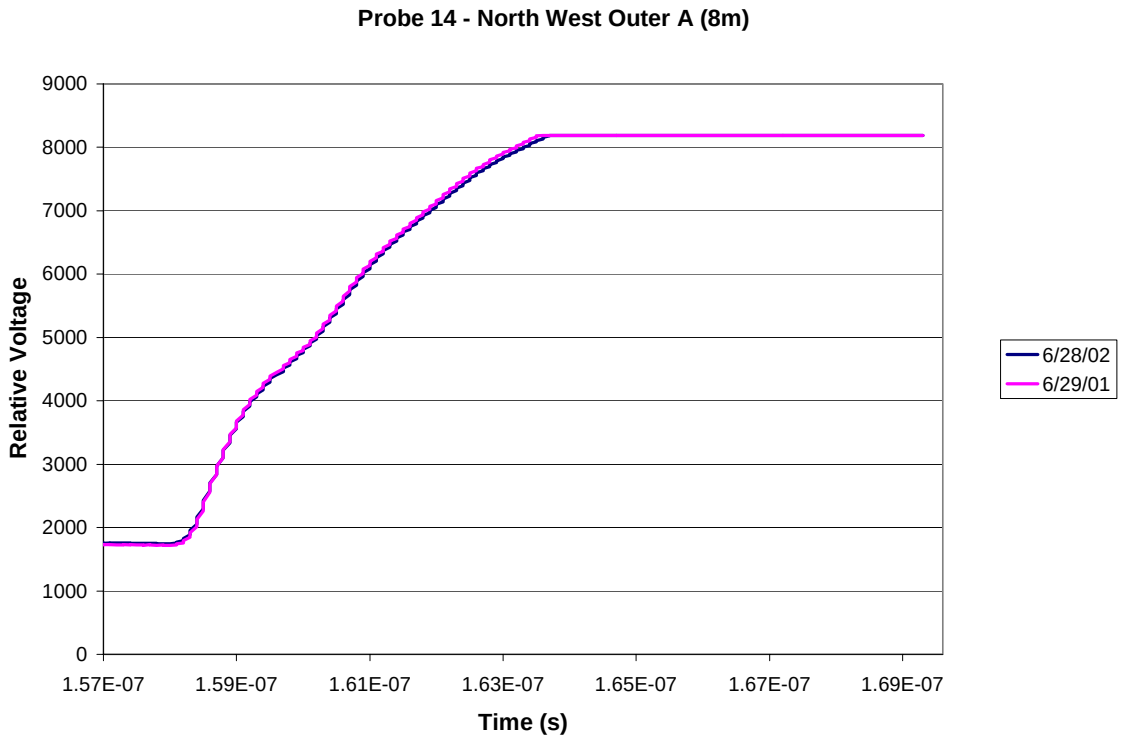


**Figure 6.5.43: North West Outer A, 8m depth, sample traces reflected from probe.**

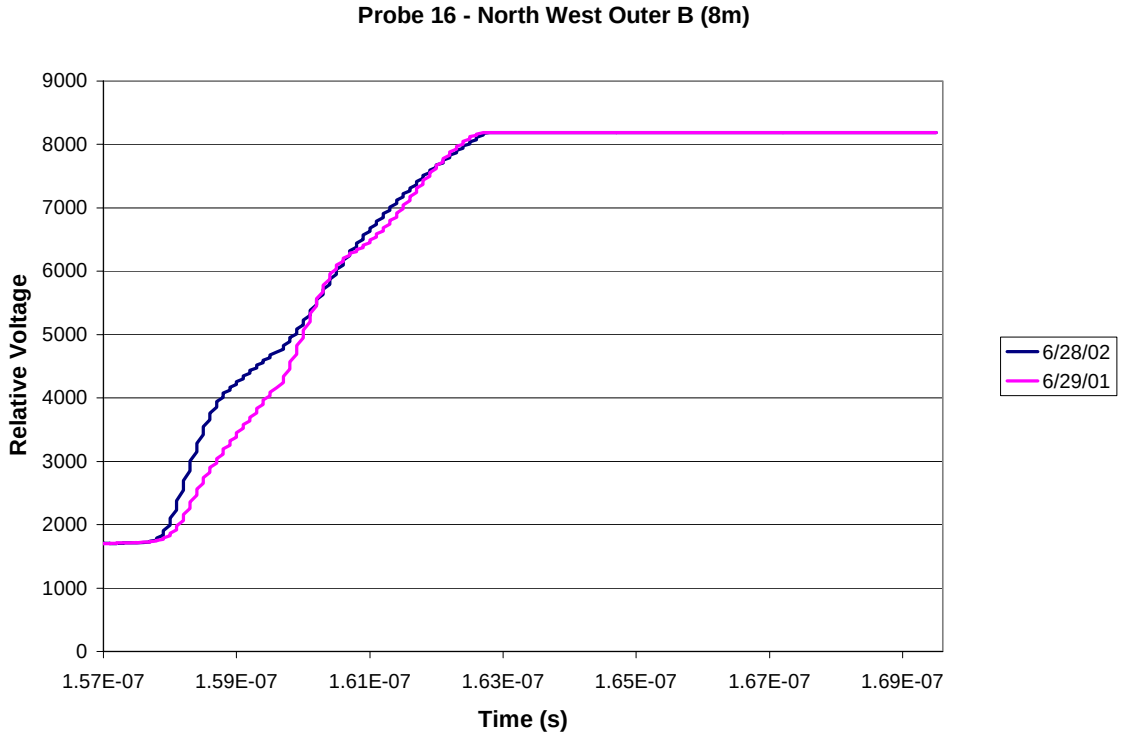


**Figure 6.5.44: North West Outer B, 8m depth, sample traces reflected from probe.**

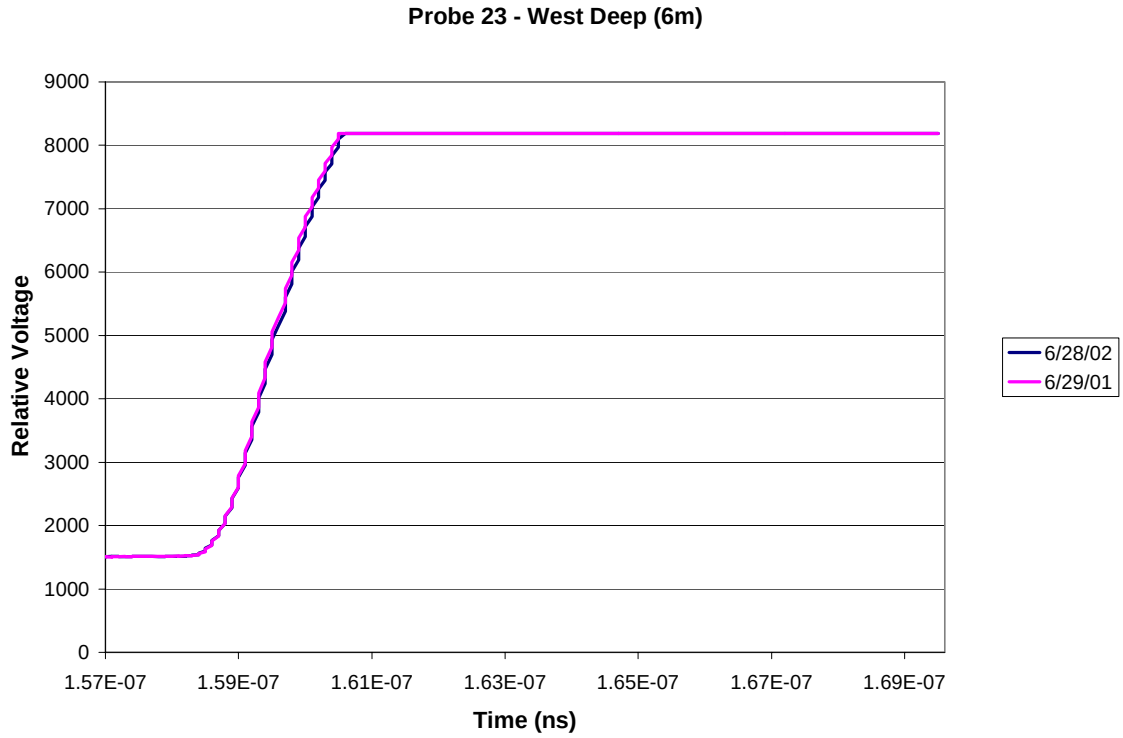


**Figure 6.5.45: West Deep, 6m depth, sample traces reflected from probe.**

## 6.6 Conclusions

The analysis of the TDR data was initially hindered by several unknowns such as the lack of a calibration before the probes were installed, and a lack of data for the initial conditions at the site. These problems became less important as it became obvious that most of the probes had no measurable response to either of the two salt pulses. Unfortunately, the majority of the probes were installed at 8 m depth, which appears to be directly below a clay layer, and where conditions remained virtually unchanged throughout the year they were monitored. Imaging with the EM39, GPR and neutron probe suggest that the clay layer prevented most of the water and salt solution from ever reaching below about 7 m depth in the instrumented area. While we do not have initial data from the TDR probes to verify if a wetting front ever reached those depths, the extremely low water contents measured 3 years after constant infiltration, would support this assumption. In the few probes that did measure a change in relative voltage, the probes at 6.5 m depth tended to respond quicker than those at 3 m depth. This may be due to water moving laterally at this depth, which is approximately at or above the clay layer.

The calculations of bulk conductivity as outlined by Dalton and others, work for the soil column experiments, but not for the field probes. Although this problem of impossible negative conductivity values is not discussed in the literature, it is most likely due to the highly resistive conditions of the soil surrounding the probes at our site. Most of the experiments reported in the literature are conducted in agricultural soils, which retain more water and have a higher bulk conductivity than coarse sands. The column experiments were conducted under saturated conditions, while the field probes were

usually at 10% volumetric water content. The six probes that did not produce recognizable waves could have been broken during installation, but also could represent soils that are too resistive for these probes to measure. Essentially the soil is so dry in some locations that signal shorts out, or becomes infinitely resistive, as soon as it enters the wave-guides. The EM39 data confirms that the soil at the site has very low conductivity, even after 3 years of infiltration.

Following the approach of Ropeke (1995), a calculation of the relative change in soil conductivity was made instead of an actual conductivity calculation. The timing of the salt pulse arrival using this approach agrees well with the suction lysimeter data.

The water content data shows almost no change throughout the year data was collected, confirming that the shape of the wetted area is very stable. The average standard deviation of water content from all the data sets is only 0.003 or 0.03% volumetrically. The repeatability of this data also suggests that temperature changes did not significantly affect the data.

## 6.7 TDR Operating Procedures

### 6.7.1 TDR length of cables

Follow instructions to set up display using the tdr.exe program.
Because each TDR has a unique cable length, you need to determine cable length for each probe.
(in the tdr.exe program after you have already established a connection with the multiplexer and have changed the units to meters etc.)

1. alt TDR → send manual command → resume manual mode
2. alt multiplexer → probe 1 → settings
3. on the Techtronics machine, turn the position knobs until you find trace. This is best if probe is submerged in bucket of water to make it easier to find the "bath tub"
4. set the x-position at the beginning of the trace.
5. enter the location that is shown on the Techtronics machine, in probe parameters settings.
6. dist/div = 2 (this stands for .1m/div)
7. probe gain = 70
8. vertical position is the hardest to find. Since there is no type of scale on the y-axis, you have to just enter a number, guess between 0-16383, this will be an iterative process until when you collect data you see the bathtub in the middle of the screen.
9. probe gain = 100. This affects the resolution of your data and once again needs to be adjusted after you see your trace in the window.
10. velocity of propagation = 66
11. length of probe assembly = cable length
12. length of probe tines = 160 TDR units
13. hit OK
14. alt file → save as new name
15. alt gather → settings
16. trace delay mult = interval in minutes
17. stopping port = 1 probe if you have only one that you are finding the length of at a time.

18. alt gather → autogather
19. watch the screen on the Techtronics machine and see where your trace is in relation to where it is that you want it to be, make notes so that you remember what to change in the settings.
20. alt gather → stop autogather
21. exit the program. (this program will not let you go back and make changes and start collecting again, if you do this it will hang up and you have to shut the whole computer down before you can connect to the multiplexer successfully)
22. go into file manager and delete the .dat file that you just created (the program does not know how to append and will hang up if you forget this step!)
23. re-enter the program and follow the same steps, filling in your corrected new trial values.
24. continue this process until you are satisfied with the trace you see in the window of the Techtronics machine. Don't forget to save this file and you can use it for that same probe for the rest of its life.

# References


Anderholm, Scott K., 1983. Hydrogeology of the Socorro and La Jencia Basins, Socorro County, New Mexico. New Mexico Geological Society Guidebook, 34th Field Conference, Socorro Region II, pp. 344.

Brainard, J. R., R. J. Glass, D. L. Alumbaugh, L. Paprocki, D. J. La Brecque, X. Yang, T.-C. J. Yeh, K. E. Baker and C. A. Rautman, 2002, The Sandia-Tech Vadose Zone Facility; Experimental Design and Data Report of a Constant Flux Infiltration Experiment.

Baker, Kristine. 2001. Investigation of Direct and Indirect Hydraulic Property Laboratory Characterization Methods for Heterogeneous Alluvial Deposits: Application to the Sandia-Tech Vadose Zone Infiltration Test Site. New Mexico Institute of Mining and Technology unpublished MS thesis.

Dalton, F.N., W.N. Herkelwrath, D.S. Rawlins, and J.D. Rhoades. 1984. Time Domain Reflectometry: Simultaneous Assessment of the Soil Water Content and Electrical Conductivity with a Single Probe. Science. 224:989-990.

Dasberg, S. and F.N. Dalton. 1985. Time Domain Reflectometry field measurements of Soil Water Content and Electrical Conductivity. Soil Sci. Soc. Am. J. 49:293-297.

McNeill, J. D., Bosnar, M., Snelgrove, F. 1990. Resolution of an Electromagnetic Borehole Conductivity Logger for Geotechnical and Ground Water Applications. Geonics Limited Technical Note TN-25.

Nadler, A., S. Dasberg, and I. Lapid. 1991. Time Domain Reflectometry Measurements of Water Content and Electrical Conductivity of Layered Soil Columns. Soil Sci. Soc. Am. J. 55:938-943.

Paprocki, Lee. 2000. Characterization of Vadose Zone In-Situ Moisture Content and an Advancing Wetting Front using Cross-Borehole Ground Penetrating Radar. New Mexico Institute of Mining and Technology unpublished MS thesis.

Persson, M. and R. Berndtsson. 1998. Textural and Electrical Effects on Temperature Dependency in Time Domain Reflectometry. Soil Sci. Soc. Am. J. 62:887-893.

Rhoades, J.D., N.A. Manteghi, P.J.Shouse, and W.J. Alves. 1989. Soil Electrical Conductivity and Soil Salinity: New Formulations and Calibrations. Soil Sci. Soc. Am.J. 53:433-439.

Rhoades, J.D., P.A.C. Raats, and R.J. Prather. 1976. Effects of Liquid-phase Electrical Conductivity, Water Content, and Surface Conductivity on Bulk Soil Electrical Conductivity. Soil Sci. Soc. Am. J., 40:651-655.

Rhoades, J.D., P.J. Shouse, W.J. Alves, N.A. Manteghi, and S.M. Lesch. 1990. Determining Soil Salinity from Electrical Conductivity Using Different Models and Estimates. Soil Sci. Soc. Am. J. 54:46-54.

Rhoades, J.D., B.L. Waggoner, P.J. Shouse, and W.J. Alves. 1988. Determining soil salinity from soil and soil-paste electrical conductivities: Sensitivity analysis of models. Soil Sci. Am. J. 53: 1368-1374.

Ropeke, Craig. 1995. Identification of Flow and Transport Process and Their Controls in the Near Surface Vadose Zone of a Clayey Glacial Till. New Mexico Institute of Mining and Technology unpublished MS thesis.

Shainberg, I., J.D. Rhoades, and R.J. Prather. 1980. Effect of Exchangeable Sodium Percentage, Cation Capacity, and Soil Solution Concentration on Soil Electrical Conductivity. Soil Sci. Soc. Am. J. 44:469-473.

Sheets, K.R., and J.M.H. Hendrickx. 1995. Noninvasive Soil Water Content Measurement Using Electromagnetic Induction. Water Resour. Res. 31:2401-2409.

Topp, G.C., J.L. Davis, and P. Annan. 1980. Electromagnetic Determination of Soil Water Content Measurement in Coaxial Transmission Lines. Water Resour. Res. 16:574-582.

U.S. Department of Agriculture. 1954. Diagnosis and Improvement of Saline and Alkaline Soils. U.S.D.A Agricultural Handbook 60, edited by L.A. Richards, U.S. Govt. Print Off., Washington D.C..